Universitat Politècnica de Catalunya
Barcelona Tech

Escola Tècnica Superior d'Enginyers de Camins, Canals i Ports de Barcelona
Departament d'Eginyeria Hidràulica, Marítima i Ambiental
Laboratori d'Enginyeria Marítima

Programa de Doctorat en Enginyeria Civil

Effects of climate change on wave climate and consequent coastal impacts

Application to the Catalan coast (NW Mediterranean Sea)

PhD Thesis presented by

Mercè Casas–Prat

for the degree of DOCTOR

Supervisor:

Dr. Joan Pau Sierra

Barcelona, November, 2013

The scientific contributions of this thesis can be totally or partially used or developed, in an indirect or direct way, as long as it is neither for military purposes nor for any other use which is against human rights, animal rights or the environment.

Thesis written in LaTeX

Als meus pares, Núria i Esteve

To my parents, Núria and Esteve

"Caminant, no hi ha camí, es fa el camí al caminar"

"Caminante, no hay camino, se hace el camino al andar"

"Wanderer, there is no road, the road is made by walking"

Antonio Machado (1875–1939)

Contents

Abstract

Climate change is a hot research topic due to the consequent impacts on our environment in the near future. Apart from the widely known sea-level-rise, the resulting changes in the atmospheric patterns will likely have several effects on the wave climate, which are far from being well-understood. Actually, the last report of the International Panel on Climate Change—the leading international body for assessment of climate change—highlights a lack of information on the potential changes in the wave climate and, consequently, in their coastal impacts. The problem is largely complicated because wave forcing is affected by a number of uncertainty factors, being the choice of the climate model one of the most relevant.

The main purpose of this thesis is to provide a better understanding of the future wave climate in the area of interest: the Catalan coast, which is located in the NW part of the Mediterranean Sea, a basin particularly exposed to climate change. Based on previous studies, three methodological approaches are explored to address this issue: trend analysis, dynamical modelling and statistical modelling. Trend analysis simply assesses the possible changes in the wave climate by means of evaluating the tendencies of long-term time series of wave data. Both dynamical and statistical modelling make use of future atmospheric projections to obtain the corresponding wave climate. The former uses wave numerical models based on the spectral energy balance equation whereas the latter employs an empirical relationship. Therefore, statistical modelling considerably reduces the associated computational cost but it might not be able to correctly reproduce complex wave patterns. The thesis work results in the generation and analysis, for the first time in this area, of a high temporal and spatial resolution database of future wave projections. The use in this thesis of atmospheric projections obtained by five combinations of regional-global climate models enables the study of the inter-model variability in terms of wave parameters. The results illustrate, for the winter season, the large variability associated to the parent global circulation model (particularly for the wave direction, a wave variable that seems to be especially affected by climate change in this area). In most of the domain, wave height and wave period tend to generally decrease for both mean and stormy conditions but extremes are associated to larger uncertainty (in some cases showing an increase in the northern Catalan coast). As expected, these changes are closely related to those of the (wave forcing) surface wind speed but fetch also plays an important role. For favourable fetch conditions (waves coming from east) wave climate changes are more accentuated and the percentage of mixed sea states tends to increase.

The second important contribution of this thesis is related with the methodology. New approaches of trend analysis that take into consideration the nature of the data are

presented. For example, the evolution of the wave direction distribution is investigated using the annual frequencies associated to directional sectors, which are previously transformed according to their compositional nature. Also, especial emphasis is given to the uncertainty analysis in order to detect statistically significant changes. In this regard, bootstrapping is shown to be a simple but effective method if adequately modified. Nevertheless, the most significant methodological contribution is perhaps the development of a new statistical method to model wave heights, that greatly improves the model performance at near-shore areas. The frequency and directional dispersion theory of wave propagation is used to explicitly model swell waves, making use of the principal component analysis to simplify the forcing into a set of representative atmospheric patterns.

Finally, a preliminary assessment of the wave-driven coastal impacts is performed. Without being case-specific and from an engineering perspective, this thesis reviews and quantifies the main physical impacts that changes in ocean wave patterns can have on coastal areas. It is found that mild variations of forcing wave conditions can greatly affect coastal processes, due to their non-linear relation. For example, longshore sediment transport can vary at a rate higher than 100% caused by a rotation of the mean wave direction of only 10°. Getting into more detail, a couple of case studies analyse the affectation on the harbour agitation and the beach longshore sediment transport. These processes are related with problems that currently threaten the Catalan coast (reduction of harbour operability and beach erosion).

Resum

El canvi climàtic és una àrea de recerca d'extrema actualitat degut als impactes que pot tenir sobre el nostre medi en un futur no gaire llunyà. A part de la famosa pujada del nivell del mar, els canvis que es generaran en els patrons atmosfèrics afectaran molt probablement el clima d'onatge. Encara hi ha un gran desconeixement sobre aquesta afectació. De fet, l'últim informe del Panell Internacional sobre el Canvi Climàtic—l'organisme internacional que lidera la investigació del canvi climàtic—posa en evidència que hi ha una llacuna d'informació pel que fa als canvis potencials del clima d'onatge i, conseqüentment, en els seus impactes costaners. El problema es complica perquè els agents dinamitzants de l'onatge es veuen afectats per un seguit de factors d'incertesa, essent la tria del model climàtic un dels més rellevants.

El principal propòsit d'aquesta tesi és comprendre millor com serà el clima d'onatge futur a l'àrea d'interès: la costa catalana, que es troba a la part nord-oest del Mediterrani, un mar que està particularment exposat al canvi climàtic. Partint d'estudis previs, s'utilitzen tres metodologies per tal d'abordar aquesta problemàtica: l'anàlisi de tendències, la modelització dinàmica i la modelització estadística. L'anàlisi de tendències estudia de manera senzilla els possibles canvis que pot patir l'onatge a base d'avaluar les tendències de sèries temporals de llarg termini del clima d'onatge passat. Tant la modelització dinàmica com la estadística fan servir projeccions atmosfèriques futures per tal d'obtenir el clima d'onatge corresponent. La primera tècnica utilitza models numèrics d'onatge que es basen en l'equació de balanç d'energia espectral, mentre que la segona empra una relació empírica. Per tant, la modelització estadística redueix considerablement el cost computacional associat però pot no reproduir correctament certs patrons complexes d'onatge. El treball d'aquesta tesi resulta en la generació i l'anàlisi, per primer cop per a aquesta àrea d'estudi, d'una base de dades d'alta resolució temporal i espacial de projeccions futures d'onatge. A més, l'ús de projeccions atmosfèriques obtingudes a partir de cinc combinacions de models climàtics regionals i globals permet caracteritzar la variabilitat deguda als models en termes de paràmetres de l'onatge. Els resultats il·lustren, per a l'estació d'hivern, una gran variabilitat associada al model de circulació global (sobretot pel que fa a la direcció de l'onatge, una variable que sembla veure's especialment afectada pel canvi climàtic a aquesta àrea). A la majoria del domini, l'alçada i el període d'ona tendeixen a disminuir tant per a condicions de clima mig com de tempesta però els extrems estan associats a una incertesa considerable (en alguns casos es projecta un increment al nord de la costa catalana). Tal i com era d'esperar, aquests canvis estan íntimament lligats als que es produeixen pel clima de vent superficial (principal agent dinamitzador) però el *fetch* també té un rol important. Quan

les condicions de *fetch* són favorables (onatge provinent de l'est) els canvis en l'onatge són més accentuats i es tendeix a incrementar el percentatge d'estats de mar mixtos.

La segona contribució a destacar d'aquesta tesi està relacionada amb la metodologia emprada. Es presenta una nova metodologia d'anàlisi de tendències que té en compte la naturalesa de les dades. Per exemple, s'investiga l'evolució de la distribució de la direcció d'ona en base a freqüències anuals d'ocurrència associades a sectors direccionals, que són prèviament tractades com a dades composicionals. També es fa especial èmfasi en l'anàlisi de l'incertesa per tal de detectar canvis estadísticament significants. En aquest sentit, s'observa com el *bootstrapping*, sempre i quan es modifiqui adequadament, és una tècnica simple però efectiva. No obstant, l'aportació metodològica més rellevant d'aquesta tesi és potser el desenvolupament d'un nou mètode de modelització estadística de l'alçada d'ona, que millora notablement la modelització en àrees properes a la línia de costa, en comparació amb estudis previs. En destaca la incorporació explícita del mar de fons basada en la teoria de la dispersió de freqüències i direccions de la propagació de les ones, que addicionalment fa servir l'anàlisi de components principals per a simplificar l'agent dinamitzant en un conjunt de patrons atmosfèrics representatius.

Finalment, es du a terme una valoració preliminar dels impactes costaners deguts a l'onatge. Amb una perspectiva enginyeril i sense especificar per a cap cas en concret, aquesta tesi revisa i quantifica els principals impactes físics que els canvis en els patrons d'onatge poden causar sobre les àrees costaneres. S'observa com una variació moderada de les condicions d'onatge pot afectar en gran mesura als processos costaners, degut a la relació no-lineal entre aquests. Per exemple, el transport longitudinal de sediments pot veure's afectat en més d'un 100% degut a una rotació de només 10° de la direcció mitjana de l'onatge. Entrant en més detall, s'analitzen un parell de casos d'estudi a la costa catalana que avaluen l'impacte sobre l'agitació portuària i el transport longitudinal de sediments a les platges. Aquests processos estan relacionats, respectivament, amb la inoperativitat portuària i l'erosió de les platges, problemàtiques ja presents avui dia a la costa catalana.

Acknowledgments

This thesis work has been funded: (i) by "Formació de Personal Investigador" (FPI) PhD fellowship from Universitat Politècnica de Catalunya (UPC), from November 2009 to December 2010, and (ii) by "Formación de Profesorado Universitario" (FPU) PhD fellowship from Ministerio de Educación, Cultura y Deporte (Spanish Ministry of Education), from January 2011 to October 2013. The Spanish Ministry of Education has also financed two international research stays through the FPU programme: (i) at Environment Canada – Climate Research Division, in Toronto (Canada), from October 2011 to January 2012 and (ii) at the Commonwealth Scientific and Industrial Research Organisation (CSIRO) – Centre for Marine and Atmospheric Research, in Aspendale (Australia), from January 2013 to April 2013. The Col·legi d'Enginyers de Camins, Canals i Ports (Civil Engineering Association in Catalonia) has also economically supported this thesis work during the first three years. Additional funding to attend and participate in international conferences and workshops has been obtained through the collaboration: (i) in "Climate change and impact research: the Mediterranean Environment" CIRCE project (2007-2010) from European Comission's Sixth Framework Programme and (ii) in "Vulnerabilidad, impactos y adaptación al cambio climático: estudio integrado sobre la agricultura, recursos hídricos y costas" ARCO project (2008-2011) from Ministerio de Medio Ambiente y Medio Rural y Marino (Spanish Ministry of Environment).

Certainly, this thesis would not have been possible without the used data. The following people, institutions and projects are thus sincerely acknowledged for having generated and/or provided the corresponding datasets: (i) Puertos del Estado (Spanish Port Authority) for supplying the needed data from the HIPOCAS project, (ii) the following research centres and institutions for freely providing their atmospheric wave-forcing projections: Danmarks Meteorologiske Institut (DMI, Denmark) — special thanks to Dr. Ole B. Christensen, Dr. Neil Mackellar and Dr. Fredrik Boberg; Koninklijk Nederlands Meteorologisch Instituut (KNMI, The Netherlands) — special thanks to Dr. Erik van Meijgaard; Max-Planck-Insitut für Meterologie (MPI, Germany) — special thanks to Dr. Daniela Jacob and Dr. Alberto Elizalde; Sveriges Meteorologiska och Hydrologiska Institut (SMHI, Sweden) — special thanks to Dr. Erik Kjellström and Dr. Barry Broman, (iii) the GEneral Bathymetric Chart of the Oceans (GEBCO) for easily providing global bathymetry datasets for the world's oceans, available at their public website for free download (`www.gebco.net`, accessed September 2013), (iv) Laboratori d'Enginyeria Marítima (LIM) for supplying the data related to the harbour configuration, and (v) Centre d'Investigació dels Recursos Costaners (CIIRC) for providing the beach geomorphology data obtained within the context of the "Llibre verd" project.

Apart from the personal effort, the success of a thesis also depends on the professional contribution of many others. I take this opportunity to express my gratitude to the people who have guided or assisted me on the road towards this goal.

First of all, I want to acknowledge my thesis supervisor: Dr. Joan Pau Sierra (UPC). Thanks for offering me the possibility to carry out this PhD, dealing with the interesting subject of climate change. It has been a really motivating and gratifying challenge that has involved not only purely marine engineering issues (more familiar to me due to my academic background) but also environmental and climate science aspects. But especially thanks for all the dedication and both professional and personal support throughout the thesis.

I also want to highlight the academic input of Dr. Juan José Egozcue (UPC). Thanks to his lectures on probability and statistics (in the Postgraduate and in the Master of Civil Engineering), I acquired a solid statistical background that has facilitated the further development of the data analysis approaches introduced in this thesis, particularly related to the trend analysis. I also acknowledge Maribel Ortego (UPC) and my colleague Dr. Raimon Tolosana-Delgado (UPC[1]) for their useful advice with respect to the interesting but complex world of statistics. Also in the academic context, I want to emphasize the indirect contribution of Dr. Leo H. Holthuijsen (Technische Universiteit Delft, TU Delft, The Netherlands), who gave me some lectures on physical oceanography and wave physics and was my minor thesis external supervisor during my ERASMUS stay in TU Delft (2007-2008). I think that his legacy has contributed to make me do this thesis. In addition, I take this opportunity to recommend his book "Waves in oceanic and coastal areas" [Holthuijsen, 2007], which I have consulted many times during this thesis, resulting very useful to clarify or get insight into some wave-related issues.

With respect to informatics and numerical modelling, I want to deeply acknowledge Federico Jérez (UPC) for always being willing to help with any kind of computer-related issue. I am also grateful to Josep Maria Jordana (UPC) for his good guidance and assistance in using the intensive computing facilities of the Faculty of Civil Engineering. Finally, I want to express my gratitude to Dr. Marcel Zijlema (TU Delft, The Netherlands), who I met also during my ERASMUS stay. He has always been very kind and quick in replying to my emails concerning any question related to the use and implementation of the SWAN wave model.

As a result of the previously mentioned doctoral research stays, I have had the opportunity to get in touch and work in two international leading research centres. This has significantly enriched not only the content of this thesis but also my professional scientific career. From my stay at Environment Canada, I especially want to express my

[1]Now at Helmholtz-Zentrum Dresden-Rossendorf (Germany)

gratitude to Dr. Xiaolan L. Wang. Thanks Xiaolan for all the interest and enthusiasm you have put in our collaborative work, which has resulted in the new statistical modelling method proposed in this thesis. During my stay at CSIRO, I had the pleasure to work with Dr. Kathleen MckInnes and Dr. Mark A. Hemer. Thanks for sharing interesting discussions that yielded deeper insights into the coastal impact analysis and for giving me the possibility to attend a conference and a workshop while I was in Australia.

For their review and comments of the final thesis dissertation, I want to acknowledge Dr. Sofia Caires (Deltares, The Netherlands) and Dr. Mark A. Hemer (CSIRO), who gently agreed on short notice to act as external referees. Also, many thanks to Dr. Tiago Castro (UPC[2]), for their suggestions to improve some formal aspects of the final text.

At this point, I want to outline that this thesis has been not only a long and hard intellectual process but also a very intense emotional and personal experience, full of ups and downs. Luckily, I can say that I have been accompanied by many people that have helped to make this journey a bit easier, in one way or another. In this regard, I owe the following acknowledgements, which are written in a more informal manner. And forgive me if I forget any Dr. title, I know for sure that more will come soon.

First, I want to thank all the staff of Laboratori d'Enginyeria Marítima (LIM) at UPC, for their warm welcome and for making the everyday work a pleasant task. Also, I thank the administrative staff for their help in the (sometimes excessive) bureaucracy. But, especially, I'm glad to have spent so many hours with my office-mates in such a good work environment (well, sometimes a bit noisy!). Eva Bosom, Cari Ballesteros, Mónica Valeria, Marcela Cunha, Dr. Tiago Castro, Dr. Marta Alomar, Dr. Raimon Tolosana, Dr. Manel Grifoll, Jordi Cateura, Joan Puigdefàbregas, Dr. Dago Alvarado, Dr. Tona Mendoza, Federico Jérez, Claudia Guilovança, Dr. Jacqueline Albino, Checco Sole, Dr. Eduard Ariza ... thanks for the shared coffees, for the lunches in good company, for the chocolate croissants at 5 p.m., for the *xampanyeries*, for the multicultural pot-luck dinners, for the future knitting sessions, for the interesting exchanging of intellectual thoughts, for the laughs and (really necessary) anti-stress relaxing moments ... Long story short, thanks for the good feeling! Particularly, special gratitude is extended to Eva. We arrived to this house at the same moment so we've got to share almost the whole PhD experience. Eva, thanks for your complicity, for your optimism, for the rock'n'roll moments but, especially, for your friendship.

Of course, I don't forget to say a word of thanks to my other colleagues from the *Barceloneta*, the wave flume, the rest of the Department and the university campus in general: Elena Pallarès, Pablo Cerralbo, Arnel German, Andrea Marzeddu, Dr. Corrado

[2]Now at Universidade Federal do Espírito Santo (Brasil)

Altomare, Marina Arbat, Dr. Sole Estrella, Dr. Niels van den Berg ... Italian guys (Andrea, Corrado and Checco), thanks for showing me how to have a proper coffee. And on the subject of coffee, thanks Marina and Sole for the relaxing cups of *café con leche* in your office (yeah, this thesis has unfortunately contributed to increase my daily dose of caffeine). Marina, also thanks for the shared musical moments that made us escape from our personal and professional headaches.

A special mention is also required for Ali González. Thanks for having been such an awesome flatmate (for more than 2 years!) but, most especially, thanks for your friendship, helping me to get through some critical moments. A long list of mythical evenings now come to my mind, like when you used to explained to me the historical context of a TV show or a film (I've got to say it's a pleasure to have an historian friend!) or like when waiting with impatience for the next episode of Game of Thrones.

Special thanks are also due to my close friend from school Ester Roquet, for always reminding me never to give up. I'm glad to have been enjoying your friendship since we were so little.

To my friends from uni (Elena Pallarès, Marta Miralpeix, Susana Anacleto, Carlos Saborido, Dani Molina, David Abadias, etc.), thanks for our meetings, remembering funny (and freak!) uni memories but also for sharing our respective ways, in which we try to follow our slogan: "Do not adapt to the road, build it!".

Also, thanks to the people I've got to know most recently that have added interesting perspectives to my life: Sílvia Servat, Marta Cayetano, Emily McBride, Dr. Víctor Pascual ... and a bunch of very promising musicians. People who know me know that music has been (is!) quite important in my life. Despite being terrible for remembering the name of bands and songs (I'm sorry!), I consider myself a major "music user", because music makes me enjoy good moments more and helps me to get over those not-so-good.

When living abroad far from your beloved ones, loneliness and homesickness make social bonds even more precious. In this regard, the following acknowledgements are due. For the lovely lunch times at work during my stay at Environment Canada, I want to thank Dr. Paula Camus, Maria Carney, Lina Fontana, Rose Iantorno, Lori Abougalala, Alvin Godin and Dr. Murray MacKay. Also, I'm grateful to my friend Zofia Koniakowska and my Canadian flatmate Deanna MacDonald. Moreover, thanks go to the Catalan Association in Toronto, who made me feel like home during my Canadian Adventure. Specially, I thank Anna Jover, Martí Faura, Anna Terrades, Rat Colomer, Cristina Mate, Emma Molina, David Cabedo, Tati Guevara. With respect to my stay in down-under, I'm glad to have met a group of very nice and sociable people: Hoang Anh

Cat, Dr. Peter Hoffmann, Dr. Jack Katzfey, Dr. John McGregor, Brenda Lin, Brendan, Dr. Jonas Bhend, Helen, Usman Zuberi, Mariam Mukaty, Dr. Elodie Charles, Rob, Martin, Russell, etc. With them I ended up enjoying several activities like daily VB, BQs, Friday drinks, concerts, Scottish dancing, etc. Especially, I want to express my gratitude to Cat and Peter, who became friends from the very beginning.

In fact, I have to admit that, even when staying in Catalonia, this thesis has given me the opportunity to meet many people from around the world. I'm really happy for this enriching experience that has stimulated my curiosity to keep exploring the world.

Coming to the end of this section, I want to express my most sincere gratitude to my close family: my grandparents, my aunty, my little cousin, my sister and my parents. We are few but very united! Special thanks go to my favourite sister, Maria, for being there whenever I've needed her. And a huge THANKS go undoubtedly to my parents, Núria and Esteve, you are my two pillars of strength. This achievement is largely thanks to you. Thanks not only for your unconditional love and support but also for being a good example of perseverance and talent. I need to confess that I've always admired my dad's intelligence and his passion for science (always asking himself "why?") and my mum's creativity and ingenuity.

And my last but very special thanks are dedicated to someone that has become crucial. Alan, thanks for your long wait and for having a family that has warmly welcomed me from the beginning. But, especially, thanks for having added magic (and more music!) to my life.

Agraïments

Aquesta tesi ha estat finançada per: (i) la beca doctoral de "Formació de Personal Investigador" (FPI) de la Universitat Politècnica de Catalunya (UPC), des del novembre de 2009 al desembre de 2010, i (ii) la beca doctoral de "Formación de Profesorado Universitario" (FPU) del Ministerio de Educación, Cultura y Deporte, des del gener de 2011 a l'octubre de 2013. El Ministerio de Educación, Cultura y Deporte també ha finançat dues estades de recerca internacionals a través del programa FPU: (i) a Environment Canada — Climate Research Division (a Toronto, Canadà), des de l'octubre de 2011 al gener de 2012, i (ii) a la Commonwealth Scientific and Industrial Research Organisation (CSIRO) — Centre for Marine and Atmospheric Research (a Aspendale, Austràlia), des del gener a l'abril de 2013. Durant els tres primers anys, aquesta tesi també ha rebut suport econòmic del Col·legi d'Enginyers de Camins, Canals i Ports. A més a més, s'ha pogut assistir i participar a conferències i seminaris internacionals gràcies al finançament adicional obtingut a través de la col·laboració en: (i) el Projecte CIRCE "Climate change and impact research: the Mediterranean Environment" (2007-2010) de la European Commission's Sixth Framework Programme i (ii) el Projecte ARCO "Vulnerabilidad, impactos y adaptación al cambio climático: estudio integrado sobre la agricultura, recursos hídricos y costas" (2008-2011) del Ministerio de Medio Ambiente y Medio Rural y Marino.

Certament, aquesta tesi no hagués estat possible sense la disponibilitat de les dades utilitzades. Així doncs, un fort agraïment va dirigit a les persones, institucions i projectes que es detallen a continuació, per haver generat i/o subministrat els conjunts de dades corresponents: (i) a Puertos del Estado per proporcinar les dades necessàries del projecte HIPOCAS, (ii) als centres i institucions de recerca següents per proporcionar lliurement i desinteressadament les seves projeccions atmosfèriques: Danmarks Meteorologiske Institut (DMI, Dinamarca) — un especial agraïment al Dr. Ole B. Christensen, al Dr. Neil Mackellar i al Dr. Fredrik Boberg; Koninklijk Nederlands Meteorologisch Instituut (KNMI, Països Baixos) — un especial agraïment al Dr. Erik van Meijgaard; Max-Planck-Insitut für Meterologie (MPI, Alemanya) — un especial agraïment a la Dra. Daniela Jacob i al Dr. Alberto Elizalde; Sveriges Meteorologiska och Hydrologiska Institut (SMHI, Suècia) — un especial agraïment al Dr. Erik Kjellström i al Dr. Barry Broman, (iii) a GEneral Bathymetric Chart of the Oceans (GEBCO) posar a l'abast públic les dades batimètriques del oceans, que es poden descarregar gratuïtament a `www.gebco.net` (accés el setembre de 2013), (iv) al Laboratori d'Enginyeria Marítima (LIM) per subministrar les dades relacionades amb la configuració dels ports i (v) al Centre d'Investigació dels Recursos Costaners (CIIRC) per proporcionar les dades geomorfològiques de les platges, obtingudes en el marc del projecte "Llibre verd".

A part de l'esforç personal, l'èxit de qualsevol tesi també depèn de la contribució professional d'altres persones. Aprofito, doncs, per expressar a continuació el meu agraïment a tothom que, en aquest sentit, m'ha assessorat i ajudat al llarg d'aquest camí.

En primer lloc, vull donar les gràcies al meu director de tesi: el Dr. Joan Pau Sierra (UPC). Primerament, gràcies per haver-me ofert la posssibilitat per dur a terme aquest doctorat, sobre el captivant tema del canvi climàtic. Ha estat tot un repte, engrescador i gratificant que m'ha portat a tractar no només aspectes purament d'enginyeria marítima (que m'eren més familiars degut a la meva experiència acadèmica) sinó també aspectes medi ambientals i relacionats amb el clima. Però, sobretot, gràcies per tota la dedicació i el recolzament rebuts al llarg de la tesi, tant a nivell professional com personal.

També vull destacar l'aportació acadèmica del Dr. Juan José Egozcue. Gràcies a les classes que em va impartir a la carrera d'Enginyeria de Camins, Canals i Ports i al període de formació del Doctorat, vaig assolir una base prou sòlida en probabilitat i estadística, que m'ha facilitat el desenvolupament de les metodologies d'anàlisi de dades introduïdes en aquesta tesi, particularment relacionades amb l'anàlisi de tendències. També agraeixo a la Maribel Ortego i al Dr. Raimon Tolosana-Delgado (UPC[3]) el seu assessorament en relació al món complex, però interessant, de l'estadística. També dins l'àmbit acadèmic, vull ressaltar la contribució indirecta del Dr. Leo H. Holthuijsen (TU Delft, Països Baixos), que va ser tutor extern de la meva tesina final de carrera i em va impartir algunes classes relacionades amb l'oceanografia i l'onatge durant la meva estada ERASMUS a TU Delft (2007-2008). Suposo que el seu llegat m'ha portat també a fer aquesta tesi. A més, aprofito per recomanar el seu llibre "Waves in oceanic and coastal waters" [Holthuijsen, 2007], que he consultat un gran nombre de vegades durant la realització de la tesi, éssent molt útil per aclarir i aprofundir en qüestions relacionades amb l'onatge.

Pel que fa a aspectes informàtics i relacionats amb l'ús de models numèrics, vull agraïr profundament a en Federico Jérez (UPC) que sempre s'hagi mostrat disposat a ajudar front a qualsevol problema que incumbís els (punyeters) ordinadors. Gràcies també a en Josep Maria Jordana (UPC) pel seu bon assessorament a l'hora d'utilitzar les instal·lacions de càlcul intensiu de l'Escola d'Enginyers de Camins, Canals i Ports de Barcelona de la UPC. Per acabar, també vull expressar el meu agraïment al Dr. Marcel Zijlema (TU Delft, Països Baixos), que vaig conèixer també durant la meva estada ERASMUS. Durant la tesi, ha estat sempre molt amable i ràpid a l'hora de respondre via email els meus dubtes pel que fa a l'ús i la implementació del model d'onatge SWAN.

[3]Ara a Helmholtz-Zentrum Dresden-Rossendorf (Alemanya)

Fruit de les estades de recerca doctorals, he tingut la oportunitat de conèixer i treballar en dos centres de recerca internacionals capdavanters. Això ha enriquit significantivament no només el contingut d'aquesta tesi sinó també la meva carrera professional científica. De la meva estada a Environment Canada (Canadà), en especial vull mostrar el meu agraïment a la Dra. Xiaolan L. Wang. Gràcies Xiaolan per l'interès i l'entusiasme que has mostrat en el nostre treball en col·laboració, que ha resultat en el desenvolupament del nou mètode de modelatge estadístic proposat en aquesta tesi. D'altra banda, durant la meva estada a CSIRO (Austràlia), vaig tenir el plaer de treballar amb la Dra. Kathleen McInnes i el Dr. Mark A. Hemer, amb els que vaig discutir idees interessants de la tesi, aprofundint en l'anàlisi dels impactes costaners. Gràcies també per donar-me la possibilitat d'assistir a una conferència i a un seminari mentre era a Austràlia.

Agraeixo també la revisió i els comentaris sobre el document final de la tesi de la Dra. Sofia Caires (Deltares, Països Baixos) i del Dr. Mark A. Hemer (CSIRO), que van acceptar ser revisors externs sense gaire antelació prèvia. També li vull agrair al Dr. Tiago Castro (UPC[4]), els seus suggeriments per tal de millorar alguns aspectes formals del text final.

Arribat aquest punt, vull recalcar que aquesta tesi no només ha estat un procés llarg i dur a nivell intel·lectual sinó que també ha sigut una experiència emocional i personal molt intensa, plena d'alts i baixos. He tingut la sort, però, d'estar envoltada d'un seguit de persones que m'han ajudat, d'una manera o d'una altra, a recórrer aquest camí més fàcilment. En aquest sentit, em sento amb el deure de dedicar els següents agraïments, que estan escrits d'una manera més informal. Per cert, demano disculpes per avançat si em deixo algun títol de Dr./Dra., sé del cert que n'hi haurà uns quants més ben aviat.

Primerament, vull agrair a tot el personal del Laboratori d'Enginyeria Marítima (LIM) de la UPC la seva càlida acollida, fent que la rutina de treball diària fos una tasca agradable. També gràcies a l'equip administratiu per a fer que els tràmits burocràtics, sovint excessius, fossin una mica menys feixucs. Però especialment, m'alegro d'haver compartit tantes hores amb els meus companys de despatx en un bon ambient de treball (bé, potser a vegades una mica sorollós!). Eva Bosom, Cari Ballesteros, Mónica Valeria, Marcela Cunha, Dr. Tiago Castro, Dra. Marta Alomar, Dr. Raimon Tolosana, Dr. Manel Grifoll, Jordi Cateura, Joan Puigdefàbregas, Dr. Dago Alvarado, Dr. Tona Mendoza, Federico Jérez, Claudia Guilovança, Dra. Jacqueline Albino, Checco Sole, Dr. Eduard Ariza ... gràcies pels cafès, pels dinars en bona companyia, pels croissants de xocolata de les 5h, per les xampanyeries, pels sopars multiculturals, per les futures sessions de ganxet, per les interessants elucubracions intel·lectuals, per les rialles i les teràpies de relax anti-estrès (sovint hiper necessàries) ... En poques paraules, gràcies pel caliu!

[4] Ara a la Universidade Federal do Espírito Santo (Brasil)

I un agraïment especial és per l'Eva. Entrant a aquesta casa pràcticament al mateix moment, hem arribat a compartir moltes de les vivències del doctorat. Gràcies per la teva complicitat, pel teu optimisme i pels moments de rock'n'roll, però, sobretot, gràcies per la teva amistat.

Per suposat, no m'oblido de dedicar unes paraules als meus altres companys, de la Barceloneta, del canal, de la resta del Departament i del campus en general: Elena Pallarès, Pablo Cerralbo, Arnel German, Andrea Marzeddu, Dr. Corrado Altomare, Marina Arbat, Dra. Sole Estrella, Dr. Niels van den Berg... A la colla d'italians (Andrea, Corrado and Checco), gràcies per ensenyar-me com prendre un cafè com cal. I parlant de cafè, gràcies Marina i Sole per les *relaxing cups of café con leche* (no ho he pogut evitar!) a la vostra oficina (sí, aquest docorat ha contribuit malauradament a incrementar la meva dosi de cafeïna diària). Marina, gràcies també pels grans moments musicals que hem compartit, que han ajudat a evadir-nos dels entrebancs personals i professionals.

Així mateix, vull fer un esment a l'Ali González. Gràcies per haver estat una companya de pis fantàstica (durant més de dos anys!) però, sobretot, gràcies per la teva amistat, ajudant-me a superar alguns tràngols. Una llarga llista de vespres mítics em venen al cap, com quan a vegades m'explicaves el context històric d'una sèrie o pel·lícula (és un plaer tenir una amiga historiadora!) o quan esperàvem amb impaciència el proper capítol de Game of Thrones.

També vull donar les gràcies a la meva millor amiga del cole, l'Ester Roquet, per sempre recordar-me que no tiri mai la tovallola, i que, per si de cas, me la lligui ben lligada! M'alegro d'haver gaudit de la teva amistat des que erem ben petites.

Als "camineros" (l'Elena Pallarès, la Marta Miralpeix, la Susana Anacleto, el Carlos Saborido, el Dani Molina, el David Abadias, etc.), gràcies per les nostres trobades, recordant mítics moments friquis de la uni però també compartint els nostres camins respectius, en què intentem seguir el nostre lema "No t'adaptis a la carretera, construeix-la!"

També, gràcies a la gent que he tingut el plaer de conèixer els darrers temps i que ha afegit perspectives interessants a la meva vida: la Sílvia Servat, la Marta Cayetano, l'Emily McBride, el Dr. Víctor Pascual... així com un grapat de músics molt prometedors. Els que em coneixen saben que la música ha estat, i és, bastant important per mi. De fet, tot i que sigui un desastre per recordar els noms dels grups i de les cançons, em considero una gran usuària de la música. Ella fa que gaudeixi més dels bons moments així com m'ajuda a atravessar els no tant bons.

Quan es viu l'estranger, lluny de la gent que t'estimes, la solitud i l'enyorança fan que les emocions encara estiguin més a flor de pell i els vincles socials siguin més preuats.

En aquest sentit, segueixen els següents agraïments. Pels agradables dinars en bona companyia a Environment Canada, vull donar les gràcies a la Dra. Paula Camus, la Maria Carney, la Lina Fontana, la Rose Iantorno, la Lori Abougalala, l'Alvin Godin i el Dr. Murray MacKay. Així mateix, gràcies a la meva amiga Zofia Koniakowska a la meva companya de pis canadenca Deanna MacDonald. També gràcies al Casal Català de Toronto, per fer-me sentir com a casa durant la meva aventura canadenca; en especial, gràcies a l'Anna Jover, a en Martí Faura, a l'Anna Terrades, a la Rat Colomer, a la Cristina Mate, a l'Emma Molina, al David Cabedo, a la Tati Guevara. Pel que fa a la meva estada a Austràlia, m'alegro d'haver coincidit amb un grup de gent molt agradable i sociable: la Hoang Anh Cat, el Dr. Peter Hoffmann, el Dr. Jack Katzfey, el Dr. John McGregor, la Brenda Lin, Brendan, el Dr. Jonas Bhend, la Helen, l'Usman Zuberi, la Mariam Mukaty, la Dra. Elodie Charles, en Rob, en Martin, en Russell, etc.. Amb ells/elles vaig gaudir de varies activitats com ara: voleibol diari, barbacoes, birres el divendres, concerts, dança escocesa, etc. Particularment, vull agraïr a la Cat i al Peter que, des d'un bon inici, es convertissin en els meus amics.

De fet, cal dir que, fins i tot quan he estat a Catalunya, aquesta tesi m'ha permès conèixer molta gent d'arreu del món. Això ha estat realment una experiència molt enriquidora, que ha estimulat la meva curiositat per seguir explorant el món.

Arribant cap al final dels agraïments, vull expressar la meva més sincera gratitud a la meva família més propera: els meus avis, la meva tieta, la meva cosineta, la meva germana i els meus pares. Perquè som pocs però fem pinya! En especial, gràcies a la meva germana, Maria, per ser-hi sempre que t'he necessitat. I unes GRÀCIES enormes són sens cap dubte pels meus pares: sou els meus dos grans puntals! L'assoliment d'aquesta meta és en bona part gràcies a vosaltres. Gràcies no només pel vostre recolzament i estimació incondicional, sinó també per ser uns grans exemples de perseverància i de talent. He de confessar que sempre he admirat la intel·ligencia i la passió per la ciència del meu pare (sempre qüestionant-se el perquè de tot) així com la creativitat i l'enginy de la meva mare.

I, per últim, dedico un agraïment molt especial a algú que ha esdevingut crucial. Alan, gràcies per la teva llarga espera i per tenir una família que des d'un bon inici m'ha acollit amb caliu. Però, sobretot, gràcies per haver posar màgia (i més música!) a la meva vida.

THESIS BODY

1 Introduction

1.1 Motivation

Climate change has become a major focus of attention for the scientific community due to the potential impacts on our environment in the near future. One of the best-known consequences is the sea-level-rise, mainly caused by melting of ice sheets and thermal volume expansion [Cazenave et al., 2008]. However, this is not the only problem of concern caused by global warming for coastal communities [Hemer et al., 2011b].

The Intergovernmental Panel on Climate Change (IPCC) is the leading international body for the assessment of climate change that, since 1988, provide the world with a scientific view on the current state of knowledge in climate change and its potential environmental and socio-economic impacts. Based on assumptions of economic, technological, environmental and demographic trends, the IPCC has defined future hypothetical greenhouse gas scenarios that have been used to force climate models to project a range of possible changes in the ocean-atmosphere system. The last IPCC assessment report is the Fourth Assessment Report (AR4), presented in 2007 (AR5 is being released in four parts between September 2013 and November 2014, see `http://www.ipcc.ch/`, accessed September 2013). Regarding the oceans, AR4 mainly focused on the sea-level-rise but highlighted a *lack of information on the potential changes in the wave climate*. In spite of the large uncertainty, AR4 states that climate change is likely to affect wave climate. The main reason is that global warming is not meant to be homogeneous over the atmosphere, provoking changes in the meridional temperature gradients that have direct consequences on the pressure and wave-forcing wind patterns, affecting the location, frequency and intensity of storms [Weisse and Von Storch, 2010].

Owing to the *lack of a clear guideline of how to asses wave climate changes*, in the last few years several researchers have started to face the problem using different methodological approaches, which can be roughly split into: (i) trend analysis of long-term measured or reconstructed wave data and (ii) future wave projections driven by atmospheric projections obtained by climate models. The latter can be further divided into dynamical and statistical modelling depending on the method employed to relate atmospheric to wave data. Each of these methodologies has its own limitations. For example, trend analysis is limited to the trend assumption. Compared to dynamical modelling, the statistical technique has the advantage of being computationally inexpensive but may present difficulties to correctly reproduce the complex wave patterns due to the simplification of the physical processes involved. Indeed, the choice of the method used to model waves represents an additional source of uncertainty [Hemer et al., 2013] that

has to be added to the chain of *uncertainty factors* associated with the wave drivers: greenhouse gas scenario, climate model and climate variability [Déqué et al., 2007].

In turn, waves are one of the main forcing drivers that shape our coastlines and therefore, potential climate change-driven impacts on the coastal zone must consider potential future changes in wave conditions [Hemer et al., 2012]. The previously mentioned insufficient understanding of the future wave climate translates into a *lack of a proper evaluation of the consequent coastal impacts*. The AR4 just describes qualitatively and in a generic way how the coastal system can be affected by changes in the wave climate. It is therefore necessary to review and quantify all wave-driven coastal effects, especially taking into account that the coast is a focus for growing population and economies [Nicholls et al., 2008] and that in some cases it is already facing problems related to safety, operational and/or recreational issues.

In relation to the aforementioned general needs, the following aspects have added extra motivation to select the study area of this thesis: the Catalan coast. It is located in the NW part of the Mediterranean sea, which is a basin particularly exposed to climate change [Ulbrich et al., 2009]. Previous to this thesis, just the wave climate projections of Lionello and Galati [2008] were available for this area. They were forced by atmospheric data generated by one climate model and two greenhouse gas scenarios at a 6 h and 50 km resolution (for the whole Mediterranean). Therefore, *the study of the future wave climate and the consequent coastal impacts in this area is especially needed.* In this regard, a larger fraction of the uncertainty range should be explored (for example using more climate models). Also, a higher time and spatial resolution is necessary to adequately resolve the complex regional wave features [Sánchez-Arcilla et al., 2008] and obtain a wave dataset suitable to conduct a proper coastal impact assessment.

1.2 Research objectives

Given the previously identified needs, the main objective of this thesis is **(1) to better understand the future wave climate** in the Catalan coast. The shortcomings encountered in the frequently used methods have led to the formulation of the second objective: **(2) to improve methodological aspects** for obtaining and analysing wave data, especially regarding the uncertainty analysis. Finally, to address the consequent impacts on the coastal system, the third objective follows: **(3) to assess the wave-driven coastal impacts**. The goal is to perform a preliminary assessment to identify and quantify the order of magnitude of these impacts and to address in more detail some of them in the study area.

Despite focusing on the Catalan coast, this thesis has been conceived to provide general tools, ideas and conclusions that in many cases can be directly applied or extrapolated to the assessment of other regions.

1.3 Outline

This thesis is structured in two parts. First, the **Thesis body** summarises the thesis work. Second, the **Compendium of papers** provides the details of the study.

The rest of the Thesis Body is structured as follows. The *background* information is given in Section 2. Section 3 describes the main datasets used in this thesis. Sections 4–6 briefly describe the methods developed and employed, as well as the results obtained using, respectively, the three existing approaches mentioned in the Introduction: *trend analysis*, *dynamical modelling* and *statistical modelling*. A preliminary assessment of the wave-driven *coastal impacts* is included in Section 7. At the end of each main section (4–7), a synthesis of the most significant contributions is highlighted in relation with the thesis objectives. The *summary and conclusions* of this thesis are presented in Section 8. Finally, in Section 9, ideas for *future work* are proposed.

The Compendium of papers is composed by a total of five papers, three of them being already published in international peer-reviewed journals. The third has been accepted for publication and the remaining one has been submitted for publication and it is currently under review. All of them are listed below (and enclosed after the Thesis Body):

Paper A Trend analysis of wave storminess: wave direction and its impact on harbour agitation. *Natural Hazards and Earth System Sciences*, *10*, 2327–2340, 2010.

[Casas-Prat and Sierra, 2010]

Paper B Trend analysis of wave direction and associated impacts on the Catalan coast. *Climatic Change*, *115*, 667–691, 2012.

[Casas-Prat and Sierra, 2012]

Paper C Projected future wave climate in the NW Mediterranean Sea. *Journal of Geophysical Research: Oceans*, *118* (7), 3548–3568, 2013.

[Casas-Prat and Sierra, 2013]

Paper D A physical-based statistical method for modeling ocean wave heights, *Ocean Modelling*, doi: http://dx.doi.org/10.1016/j.ocemod.2013.10.008, 2013.

[Casas-Prat et al., in press]

Paper E Analysis of potential impacts on coastal areas due to changes in wave conditions. Submitted to *Climatic Change*.

1.4 Symbols and abbreviations

Symbols and abbreviations are correspondingly defined throughout the thesis. However, in order to facilitate the reading, the mostly used symbols and abbreviations in the thesis body[5] are listed below:

H_s	Significant wave height
θ_m	Mean wave direction
T_p	Peak wave period
w_{10}	10-m (surface) wind speed
RCM	**R**egional **C**irculation **M**odel
GCM	**G**eneral **C**irculation **M**odel
N	**N**orth
NE	**N**orth-**E**ast
E	**E**ast
SE	**S**outh-**E**ast
S	**S**outh
SW	**S**outh-**W**est
W	**W**est
NW	**N**orth-**W**est

Unless stated otherwise, both wave and wind direction follow the nautical convention. Therefore, E waves, for instance, denote waves coming from east.

[5]Please note that some symbols might differ in the papers that make up the Compendium of papers

2 Background

Owing to the complexity of the climate change phenomenon, an intense and interdisciplinary literature review has been carried out. It has covered different areas, from physical issues, such as climate dynamics, to methodological aspects, such as data analysis. This literature review has been carried out not only at the beginning but also throughout the thesis development because climate change is a hot topic of current research and, consequently, the corresponding state-of-the-art is constantly being updated.

In this section, the background of the thesis work is expounded. First, Section 2.1 explains how (atmospheric) climate projections have been performed in the last years. Section 2.2 gives an overview of the present and future wave-forcing wind patterns in the NW Mediterranean Sea, where the Catalan coast is located. In Section 2.3, the three main existing approaches for analysing future changes in the wave climate are explained. Centred in the Catalan coast, Section 2.4 describes the main characteristics of the present wave climate and the coastal receptor as well as the current coastal impacts.

2.1 Climate change projections

To quantify the effect of climate change in our environment, climate models forced by different greenhouse gas concentrations have been used to project possible scenarios of the future climate. In 2000, the IPCC published the Special Report on Emissions Scenarios that established a set of greenhouse gas emission scenarios (the SRES scenarios) that updated the previous set established in 1992 (IS92). The SRES scenarios can be classified in four groups: A1, A2, B1 and B2. Generally speaking, "A" scenarios assume a development focused on the economy whereas environmental issues are better taken into account in the "B" group. Meanwhile, those classified with "1" tend to a more (integrated) globalised world, whereas the others ("2") consider a world more divided with regional emphasis. The A1 group is further divided into three (sub)scenarios as a function of the type of energy sources used: A1FI and A1T scenarios make emphasis on fossil and non-fossil energy sources, respectively. In between, the increasingly used A1B midline scenario considers a balance of all energy sources. The AR5 (expected to be completed by 2014) will adopt the Representative Concentration Pathways (RCPs) [van Vuuren et al., 2011] that will substitute the SRES scenarios. They describe four possible climate futures (RCP2.6, RCP4.5, RCP6, RCP8.5), which are named according to the radiative forcing target level for 2100 (e.g. 2.6 W/m^2). The word "representative" signifies that each of the RCPs represents a large set of scenarios in the literature. The

use of the word "concentration" instead of "emissions" emphasizes that concentrations are used as the primary product of RCPs. Finally, the word "pathway" reflects the fact that the RCPs are not the final new, fully integrated scenarios, but instead are internally consistent sets of projections for the components of radiative forcing that are used in subsequent phases [van Vuuren et al., 2011].

The first models that were used to approximate the future climate were the Atmospheric-Ocean Circulation Models (AOGCMs). Considering the interaction between the ocean and the atmosphere, AOGCMs use a compendium of differential equations to describe the fluid dynamics at a global scale. At the outset, the (horizontal) spatial resolution achieved by AOGCMs was at most 300 km [IPCC, 1990] owing to their huge computational demand (AOGCMs need to be run for several decades [Weisse and Von Storch, 2010]). As a consequence, their use and development was limited to few leading research centres in the world. To be able to increase the resolution and make the models more affordable, the (Atmospheric) Global Circulation Models (GCMs) were introduced, initially achieving a resolution around 150 km. GCMs do not account for the ocean-atmosphere feedback, being the influence of the ocean just incorporated with the sea surface temperature as an additional forcing. The resolution of GCMs, however, was still insufficient to undertake regional climate studies, specially in areas like the Mediterranean area, that has a very irregular topography. That problem lead to the appearance of the Regional Circulation Models (RCMs): limited area models whose boundaries are specified with atmospheric output from GCMs. Figure 1 compares the representation of the topography over Europe at 300 km and 50 km resolution, values that could correspond to AOGCMs and RCMs, respectively. Clearly, the complex orography features (which greatly affect the regional atmospheric patterns) are not well captured with the spatial resolution of 300 km. Obviously, the continuous increase of computational resources due to technological innovation, allows to constantly increase the resolution of any model. For example, although the RCMs are presently run on spatial grid sizes between about 10 km and 50 km [Weisse and Von Storch, 2010], Bengtsson et al. [2009] used a GCM with a resolution of 63 km. Therefore, in the following years, all models are expected to provide output data at much higher spatial resolution than nowadays.

At European scale, the PRUDENCE project (2001–2004, [Christensen et al., 2007]) unified all the results from different RCMs (forced by different GCMs) developed in (and for) Europe. Climate projections were performed for two periods of 30 years using the A2 and B2 SRES scenarios, with a spatial resolution of 50 km. Just a few years later, a similar work was done in the frame of the ENSEMBLES project (2004–2009, [van der Linden and Mitchell, 2009], `http://www.ensembles-eu.org/`, accessed September 2013). In this case, simulations were forced by the increasingly used A1B scenario at a higher spatial resolution (25 km) and covered the time period 1951–2050 (or even

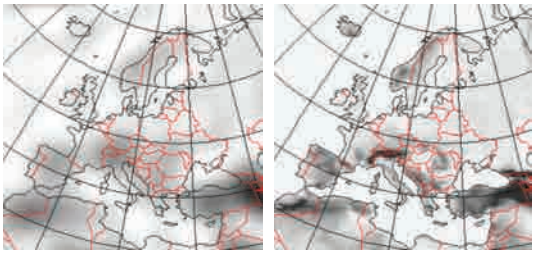

FIGURE 1: Representation of topography over Europe at 300 km (left) and 50 km (right) resolution (from PRUDENCE project [Christensen et al., 2007]). Dark grey qualitatively denote elevation.

1951–2100). For these projects, a database of the daily output was available on a public server but some research centres locally stored the corresponding sub-daily resolution data.

As explained by Déqué et al. [2007], the greenhouse gas concentration of each emission scenario is just the initial source in the causal chain of combinations. Formulations, resolutions and parametrisations used in the different RCMs (as well as the boundary conditions derived from the respective GCMs) contribute to additional uncertainty, and, lastly, the problem is further complicated because of the internal natural variability of simulated, as well as actual, climate.

As illustrated in Figure 2, just considering the existence of several SRES scenarios, GCMs and RCMs, leads to a large amount of combinations (e.g. 25 for the ENSEMBLES project), from which just an affordable selection can usually be explored (marked in red in Figure 2). In this regard, it is interesting to know which of these factors has a greater contribution to the total uncertainty. Paradoxically, it has been found that climate models produce more variability than greenhouse gas scenarios [Déqué et al., 2007]. At the European scale, Kjellström et al. [2011] concluded that RCMs and GCMs contribute in a different way depending on the output variable and the season studied. For example, the uncertainty associated with RCM tends to be higher during summer whereas uncertainty associated with GCM is higher in winter [Kjellström et al., 2011].

2.2 Present and future wind climate in the NW Mediterranean Sea

Extra-tropical cyclones are the dominant (synophtic) feature of midlatitudes [Ulbrich et al., 2009], where the Mediterranean basin is located, being their main forcing mechanism the meridional temperature gradient. They mainly grow via baroclinic instability, with the available potential energy being proportional to the variance of temperature in the troposphere [Bengtsson et al., 2009], which is highest during the winter season. In

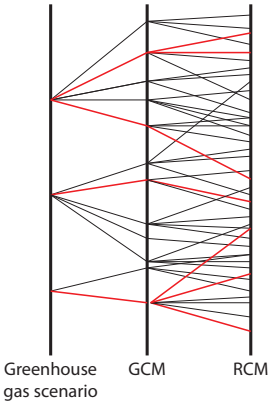

FIGURE 2: Sketch to illustrate the uncertainty derived from the following factors: greenhouse gas scenario, global and regional circulation models (GCMs and RCMs). Red line: affordable selection (adapted from Hemer et al. [2011a]).

the Mediterranean Sea, there is a maxima in the annual number of cyclones in the Gulf of Genoa (see Figure 3).

Compared to northern Europe, Mediterranean events are normally shorter and less intense and many subregional and mesoscale events take place producing a large spatial and seasonal variability. The reduced scale, along with the peculiar features of the basin (complex orography, veering winds, sharp gradients, etc.), makes the Mediterranean climate more difficult to predict. It is therefore necessary to work at a higher spatial and temporal scale compared to, for instance, the Atlantic Ocean [Lionello et al., 2006]. One example of a local feature is the Mistral wind (called *Mestral* in Catalonia), which consists of an intense and persistent NW wind often caused by a cyclone over the Gulf of Genoa, which is then channelled and intensified through the valleys between mountain ranges in the north side of the NW Mediterranean Sea (see Figure 3). At the Catalan coast, it is also common to have east winds in stormy conditions (*Llevant* events), which are caused by either and anticyclone over northern Europe or a low-pressure area over Balearic Islands. Indeed, the predominant wind directions (NE, E, SW and NW) vary along this coast, showing a significant topographic control [Sánchez-Arcilla et al., 2008].

During summer, thermal and orographic effects play a greater role in the genesis and maintenance of cyclones. In the NW Mediterranean, apart from the Gulf of Genoa there is a another maxima in the number of cyclone centres located over the Iberian Peninsula. It is caused by temperature contrasts between land and sea [Campins et al., 2000]. Spring and autumn can be considered as transitional periods between winter and summer contrasting patterns [Campins et al., 2000].

The uncertainty in the future wind patterns arise from the complex interaction of a number of competing processes produced by the anthropogenic warming. Global warming

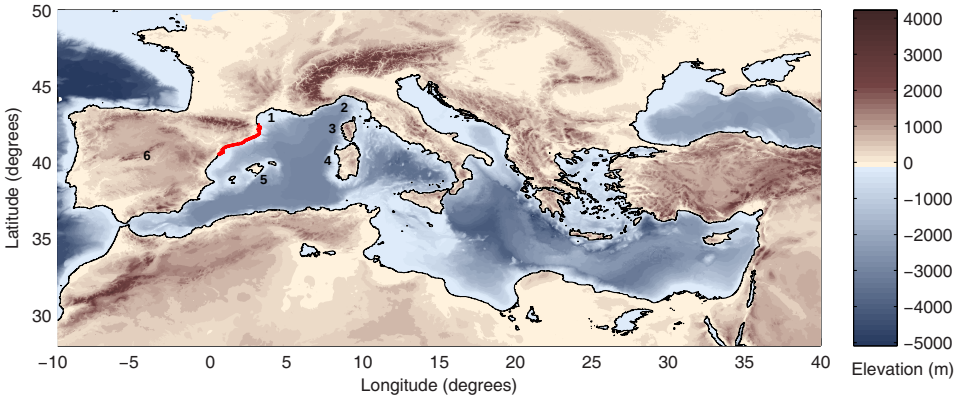

FIGURE 3: Situation of the Catalan coast (red) in the Mediterranean Sea. Numbers denote some relevant orographic elements close to the study area: Gulf of Lion (1), Gulf of Genoa (2), Corsica (3), Sardinia (4), Balearic Islands (5), Iberian Peninsula (6).

is not expected to be homogeneous in either latitude or altitude. In the lower troposphere, stronger warming is expected to occur in polar regions, whereas in the higher troposphere it is expected at lower latitudes. This involves a decrease(increase) of such gradient in the lower(upper) troposphere [Weisse and Von Storch, 2010]. Depending on the spatial extension of such temperature variations, the location of more unstable vertical stratification, linked to the preferred storm locations, will vary [Weisse and Von Storch, 2010]. Many studies have found a consistent poleward shift of such location [Ulbrich et al., 2009] which, at the European scale, would be translated into enhanced wind speeds over northern Europe, and a decrease in southern Europe [Lionello et al., 2002] where the study area is located. Actually, Nikulin et al. [2011] found a 45°-latitude limit between areas of increased and decreased storm intensity. In addition, the problem is further complicated since the position, activity and intensity of the storms is also affected by the sea surface temperature gradients and the concentration of water vapour in the atmosphere. For example, the increase in the amount of water vapour may contribute to stronger development of extra-tropical storms [Weisse and Von Storch, 2010].

As a result of these factors, AR4 concur that there will be a decrease in the number of Mediterranean cyclones [IPCC, 2007]; however, there is a lack of consensus on whether the number of intense cyclones will increase or decrease [Lionello et al., 2002], as summarised in the AR4. The variation of the wind direction remains even more uncertain. At a European scale, Donat et al. [2010] analysed changes in the circulation weather types associated to the (winter) storminess and found that the predominant westerly flow over Europe will be significantly enhanced. However, there was a GCM that exhibit a contrasting pattern, increasing the east component. Such uncertainties make difficult to predict the future wind climate, particularly at the regional scale needed for

the Catalan coast assessment.

2.3 Existing approaches to analyse changes in the wave climate

To investigate how wave climate can react to climate change, three main approaches have been followed in the last years: trend analysis, dynamical modelling and statistical modelling.

Based on the trend analysis of long-term measured or reconstructed wave data, some studies have assessed the possible changes in the wave climate without the need to involve future atmospheric climate projections [e.g. Hemer et al., 2008, Wang and Swail, 2002]. Compared to other wave variables (such as the wave height), the wave direction has been relatively little studied, probably due to the additional complexity of the trend analysis of this circular variable. In addition, there is a generalised use of standard tests that assume Normal distributed data (e.g. Student's t-test), which is not the case of most of the variables that are used to characterise the wave fields.

Trend analysis can definitely serve to have a first overview of the magnitude and direction of the wave changes without much computational effort but the tendencies thus obtained are limited to the trend assumption. Moreover, the increase of greenhouse gas emissions is not explicitly accounted for and therefore even statistically significant changes cannot be directly related to the climate change phenomenon (the attribution problem, as stated by Weisse and Von Storch [2010]).

In order to account explicitly for the rise in the greenhouse gas concentration, the other two remaining approaches (dynamical and statistical modelling) consist in simulating the future wave climate using the atmospheric projections obtained from climate models forced by the greenhouse gas emission scenarios described in Section 2.1.

Dynamical modelling makes use of third generation wave (numerical) models, which are forced by the 10-m wind fields and are governed by the spectral energy balance equation. In the absence of currents, the change of energy of a certain cell is given by the sum of the net energy input (wave propagation: refraction, shoaling and diffraction) and the local energy generation (wave generation by wind, non-linear interactions and energy dissipation). This approach is denoted as dynamical modelling because wave dynamics are explicitly involved, based on the principle that ocean waves are generated by air-pressure fluctuations, which are almost entirely caused by surface winds [Holthuijsen, 2007].

However, contrary to the case of atmospheric data, a public dataset of future wave climate projections driven by several RCM-GCM combinations does not exist for the time

being (like those developed in the PRUDENCE and ENSEMBLES, see Section 2.1). In Europe, some regional studies have investigated independently the affectation of specific areas like the Mediterranean Sea [Lionello et al., 2008], the North Sea [Grabemann and Weisse, 2008], the Bay of Biscay [Charles et al., 2012], etc., considering a limited number of combinations of the uncertainty factors (see Section 2.1). Owing to the high computational effort, global scale wave climate studies are mostly concentrated in the last few years [Hemer et al., 2012, 2013, Mori et al., 2010, Semedo et al., 2011]. Indeed, in the *WCRP-JCOMM Workshop on Coordinated Global Wave Climate Projections* (held in Geneva in 2011), the wave research community manifested the need to perform and combine different wave projections at a global scale to better understand the changes in the wave climate.

As an alternative to dynamical modelling, statistical methods have been developed to obtain wave climate projections without significant computational effort [e.g. Caires et al., 2006, Wang et al., 2012, Wang and Swail, 2006]. Basically, they establish an empirical relationship between atmospheric data (predictors) and wave data (predictands) which is calibrated for the present and assumed valid in the future. This approach has two main advantages. First, it has a low computational cost and therefore facilitates the exploration of a large number of combinations of the uncertainty chain (see Section 2.1). Second, predictors apparently more "reliable" than the surface wind field can be used, such as the sea level pressure (wind fields are typically more affected by model climate and variability biases [McInnes et al., 2011]). However, statistical modelling has some shortcomings due to the simplification of the complex physical processes in terms of "simple" empirical relationships and the assumption that this relation remains the same for the future. For example, it has typically presented difficulties to correctly reproduce the swell component of waves due to the non-direct relation with local winds.

For both dynamical and statistical modelling, modelled future scenarios are normally compared to a reference situation. It is important to account for the internal variability of the data to determine whether the projected changes are statistically significant. In this regard, in the literature this variability is not always considered or simply estimated with standard methods that assume a Gaussian distribution (e.g. confidence intervals obtained by classical linear regression analysis).

2.4 The Catalan coast: forcing and receptor

The Catalan coast stretches about 580 km, but when measured at higher definition, it is found to be approximately 780 km long. It is located at the latitude 40°45' N to 42°25' N and longitude 0°45' E to 3°º15' E (see Figure 3). It is characterised by a micro-tidal

environment with storm surges of limited extend, with an average number of positive moderate (surface elevation $\eta > 15$ cm) and strong ($\eta > 25$ cm) surges close to 3 and 1, respectively [Marcos et al., 2011]. Therefore, waves (the coastal driver considered in this thesis) are one of the most important drivers affecting this coastal environment.

To better understand the future changes in the wave conditions along the Catalan coast and their consequent impacts, it is important to first be acquainted with the present wave climate and the coastal impacts that this coast is currently facing. Moreover, wave-driven coastal impacts are determined not only by the forcing driver (i.e. wave action) but also by the coastal response which depends on the coastal geomorphology and configuration.

This section describes the current state of the wave climate (Section 2.4.1) and the coastal receptor (Section 2.4.2) of the study area.

2.4.1 Wave climate

The Catalan coast is a region dominated by low-to-medium winds with occasional strong events (maximum wind recorded is about 25 m/s, [Bolaños et al., 2009]) which translates into mild wave conditions with sporadic wave storms. Owing to the large temporal and spatial variability of wind fields, where the orography exhibits a significant control, the resulting wave climate can be characterised as "torrential": wave storms are impulsive and comparatively much more energetic than adjacent (more frequent) calm periods [Sánchez-Arcilla et al., 2008]. The mean wave climate is characterised by a significant wave height (H_s) lower than 1 m but extreme waves can reach much higher values. For example, H_s associated to a 50-year return period is around 6–7.5 m (larger as going northward along the coast) [Sánchez-Arcilla et al., 2008]. The mean duration of wave storms (defined with a threshold of 2 m) is estimated to be below 24 h [Bolaños et al., 2009].

The directional distribution of the wave field is obviously conditioned by that of the wind field, which has four predominant directions: NE, E, SW and NW (see Section 2.2). However, it is also affected by the fetch configuration because fetch modulates the effectiveness of storms in generating waves, making some storms more effective in producing waves [Lionello and Sanna, 2005]. In that respect, the frequent and energetic Mistral (NW) wind (see Section 2.2) does not contribute to generate high waves along the Catalan coast because it is a fetch-limited wind (it blows from land to sea). Instead, there is a predominance of high waves coming from the east sector where the stronger winds and larger fetches coincide (maximum fetch about 600 km since Corsica and Sardinia islands can be considered as a barrier from swell waves, see Figure 3) [Sánchez-Arcilla

et al., 2008]. At the Northern Catalan coast, N events are the most frequent although the maximum storm energy content is in general associated with the E direction.

Even though the relatively short fetches of the study area (compared to the ocean), swell waves are often present but usually combined with wind-sea states (mixed sea states), resulting in a large occurrence of bimodal sea states [Alomar, 2012]. Bear in mind that swell waves (propagating waves being remotely generated) usually travel at a lower frequency than the locally generated waves (wind-sea waves) and therefore produce a second peak in the frequency-energy spectrum.

More complexity is added to the wave fields in this region due to: the shadow effects caused by the Balearic Islands, the complex bathymetry with deep canyons close to the coast (specially in the Northern Catalan coast) [Sánchez-Arcilla et al., 2008] and the variable-width continental shelf, from very narrow at the North to very wide at the South [Bolaños et al., 2009].

2.4.2 Coastal receptor

The Catalan coast presents a large geo-diversity of coastal types [Jiménez et al., 2012], that spatially can be roughly divided into two parts. The northern part (Costa Brava, see location in Figure 4) mostly consists of beaches nestled between cliffs. The rest of the coast is mainly composed by low-lying beaches (with the exception of deltas and occasional abrupt cliffs), which in turn can be divided between narrow coarse sand beaches with relatively high slopes (Maresme, see Figure 4) and wide find sand beaches with soft slopes (Costa Daurada, see Figure 4). The sediment grain of these two types of low-lying beaches has a median size of 0.7 mm and 0.4 mm, originating in the coastal mountains and pre-coastal depression, respectively [CIIRC, 2010].

The Ebre Delta is a special feature of the Catalan shelf, located in the southern part of this coast (see Figure 4). This area of high ecological and economical value covers about 32,000 ha, with half ot that area lying at an altitude of less than 0.5 m. It is one of the largest deltas in the Mediterranean, after the Nile and Rhone deltas, that was build by the surplus of sediment discharge, but it is currently in a critical situation because both sediment input and river discharge have decreased drastically [Alvarado-Aguilar, 2009].

Currently, the Catalan coast is an area highly exposed to coastal erosion, as concluded by the EUROSION project (2002–2004, see `http://www.eurosion.org/`, accessed September 2013) (see Figure 4). The study also revealed that a considerable portion of the land under the influence of coastal erosion is urbanised, industrial and/or of high ecological value, which enhances the risk of a possible erosion event. Compounding the risk, it is

important to emphasize that 40% of the Catalan population (about 3 million people) live in coastal municipalities.

Actually, during the last 50 years, erosion has been the dominant reported damage in the Catalan beaches [Jiménez et al., 2012], being some coastal stretches currently exposed to high levels of vulnerability to erosion and inundation [Bosom and Jiménez, 2011]. Besides, some Catalan beaches do not only suffer from protection problems but also from recreational malfunctioning [Jiménez et al., 2011].

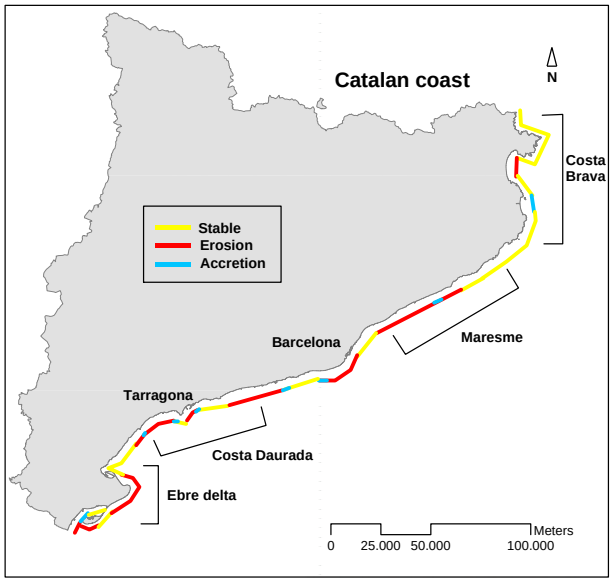

FIGURE 4: Trend erosion on the Catalan coast (adapted from EUROSION project).

Together with inundation, destruction of infrastructures is the second most reported damage [Jiménez et al., 2012] which has a broad repercussion since most of the Catalan coast is highly engineered, with the presence of many coastal structures. In this regard, it is important to highlight that Catatonia has a total of 47 harbours. Barcelona and Tarragona (see Figure 4) have the largest ports, combining commercial, fishing and leisure uses. From the 45 remaining, 22 are leisure ports, 1 is exclusively for fishing and 22 are mixed. According to the Catalan Government Port's plan (2007-2012) several operational problems are present in these harbours, mainly caused by excessive agitation, over-topping and/or siltation.

3 Datasets

The development of this thesis work has involved the use of several datasets. The most important are listed below along with a brief description of the main characteristics.

HIPOCAS data It consists of 44 years of hindcast data (1958–2001) from the European HIPOCAS project (HIndcast of dynamic Processes of the Ocean and Coastal AreaS of Europe, 2002–2004) [Guedes Soares et al., 2002], funded by the Energy, Environment and Sustainable Development Programme of the European Commission. This simulated dataset—available for the entire Mediterranean basin—used the regional atmospheric model REMO (see `http://www.remo-rcm.de`, accessed March 2012) forced by the global reanalysis of the National Center for Environmental Prediction (NCEP, [Kalnay et al., 1996]). The atmospheric dataset resulting from that simulation was in turn the input data of the HAMSOM [Backhaus, 1985] and WAM [The WAMDI group, 1988] models to simulate, respectively, the residual sea level and the wave climate. The atmospheric data (e.g. sea level pressure, surface wind speed, etc.) have a resolution of 0.5° and 1 hour. For the wave data (e.g. significant wave height, mean wave direction, etc.), the spatial resolution is 0.125° near-shore and 0.5° offshore, and the temporal resolution is 3 hours.

The HIPOCAS data have been widely used [e.g. Álvarez Ellacuria et al., 2009, Gomis et al., 2008, Marcos and Tsimplis, 2008, Mösso et al., 2009] and extensively validated in terms of wind speed and direction, significant wave height, wave direction and residual sea level parameters in the Mediterranean Sea [Musić and Nicković, 2008, Ratsimandresy et al., 2008, Sotillo et al., 2005]. It has some limitations in terms of properly reproducing certain storm events which might be attributable to numerical inertia, like most simulations. However, Ortego et al. [2012] did not find statistical evidence of wave storm magnitude bias compared to buoy observations in the southern Catalan coast. Meanwhile, Ratsimandresy et al. [2008] found that it generally reproduces mean values quite well. Although real measurements (e.g. buoy records) are usually more reliable, they do not have enough spatial and temporal coverage for climate studies and might suffer from inhomogeneities.

This thesis uses HIPOCAS data corresponding to the NW Mediterranean Sea (longitude from -1° to 9° and latitude from 36° to 44°), which was provided by Puertos del Estado (Spanish Port Authority). The wave data (significant wave height H_s, mean wave period T_m, mean wave direction θ_m) are employed to undertake the trend analysis (see Section 4), to validate the wave projections for the present situation (see Sections 5 and 6) and to generate the reference state of the sediment transport patterns along the

Catalan coast (see Section 7). With both the significant wave height and the sea level pressure the statistical method developed in Section 6 is calibrated and validated.

TABLE 1: Subsets of atmospheric projections and their (output) temporal (Δt) and spatial (Δx) resolution.* denotes that the average over the corresponding (computational) time/spatial step is considered, instead of the instantaneous/punctual value in time/space.

Acronym	Institute	RCM	GCM	Δt(h)	Δx(km)
HIR_E	DMI	HIRHAM5	ECHAM5	1	25
RAC_E	KNMI	RACMO2	ECHAM5	3	25
REM_E	MPI	REMO	ECHAM5	1*	25
RCA_E	SMHI	RCA3	ECHAM5	3	25*
RCA_H	SMHI	RCA3	HadCM3Q3	3	25*

Atmospheric projections They are composed by high spatial-resolution (25 km), regional 10-m wind and sea level pressure projections that were developed within the context of the European ENSEMBLES project (2004–2009, see `http://ensembles-eu.metoffice.com/`, accessed June 2013), supported by the European Commission's 6$^{\text{th}}$ Framework Programme. These projections were mainly forced by the mid-line A1B emission scenario. Mean and maximum daily data are publicly available at `http://www.ensembles-eu.org` (accessed June 2013) but the hourly time-resolution version of those simulations is stored locally. For this thesis, four European research institutes freely provided their corresponding projections for the NW Mediterranean Sea domain (same as selected for hindcast data), forced by the following RCMs: HIRHAM5 (from Danmarks Meteorologiske Institut — DMI, see Christensen et al. [2007]), RACMO2 (from Koninklijk Nederlands Meteorologisch Instituut — KNMI, see van Meijgaard et al. [2008]), REMO (from Max-Planck-Institut für Meteorologie — MPI, see `http://www.remo-rcm.de`, accessed March 2012) and RCA3 (from Sveriges Meteorologiska och Hydrologiska Institut — SMHI, see Samuelsson et al. [2011]). All projections were forced by the ECHAM5 general circulation model [Roeckner et al., 2003], and, for the RCA3 RCM, the configuration using HadCM3Q3 GCM [Collins et al., 2001] was also provided. Therefore, there is a total of five combinations of RCM-GCM realisations (see Table 1 and Section 2.1), which are respectively denoted in this thesis as: HIR_E, RAC_E, REM_E, RCA_E and RCA_H (see Table 1). Output time resolution is 3 h for RAC_E, RCA_E and RCA_H, vs. 1 h for HIR_E and REM_E. In all cases, the output is instantaneous except for REM_E, for which it is time averaged. Actually, despite some models having the same (output) time resolution, every model has a slightly different (internal) computational time step (usually between 10 and 30 min). With regards to the spatial resolution, all models have a resolution of 25 km but in the cases of RCA_E

and RCA_H, a spatial average is carried out in the computation, which might lead to a certain underestimation of extremes [Kriezi and Broman, 2008].

For each RCM-GCM combination, two 30 year time slices are selected (as recommended by Hemer et al. [2011b]) to project wave climate changes (using two methodologies, see Sections 5 and 6): "present" (1971–2000) and "future" (2071–2100); except for REM_E data, for which the first period is 1981–2010 (due to data availability).

Bathymetry The GEBCO One Minute Grid is used, which is a gridded bathymetry dataset at a spatial resolution of 1/60° available from the General Bathymetric Charts of the Oceans. GEBCO is an international group of experts who provides global bathymetry sets for the worlds' ocean that are freely available to download at `http://gebco.net`. The GEBCO One Minute Grid was released in 2003 and updated in 2008 being largely based on the most recent set of bathymetric contours contained within the GEBCO Digital Atlas (GDA). GDA includes a global set of digital bathymetric contours, coastlines and trackline control information.

The bathymetry database used in this thesis was downloaded from the aforementioned website and corresponds to the NW Mediterranean Sea domain (as in the case of HIPOCAS data and atmospheric projections). It is basically employed for the dynamical modelling (see Section 5).

Harbour configuration This thesis evaluates the impact of climate change on harbour agitation inside three Catalan harbours located in: Blanes, Fòrum and Tarragona (one of them presented in Section 7.2.1, the remaining can be found in Paper B). To carry out this analysis the data relative to the port configurations were necessary.

For Fòrum and Blanes, AutoCAD maps were obtained from, respectively, Ajuntament de Barcelona (Barcelona City Council) and TYPSA company. It was in the context of two local studies that aimed to analyse and reduce the excessive harbour agitation inside them. They were undertaken, respectively, by Centre Internacional d'Investigació dels Recursos Costaners CIIRC2011 and Laboratori d'Enginyeria Marítima [LIM, 1999].

In the case of Tarragona port, digital contour data at a variable resolution (∼5–20 m) have been obtained from Puertos del Estado (Spanish Port Authority) in the context of the Spanish project "Desarrollo de un programa de control de la calidad del agua en zonas portuarias mediante simulación numérica y observaciones" (2010), which was carried out in collaboration with Laboratori d'Enginyeria Marítima.

Beach geomorphology An extensive characterisation of the Catalan coast has been carried out by Centre Internacional d'Investigació dels Recursos Costaners [CIIRC, 2010] within the context of "Llibre verd" (in Catalan), a project funded by Generalitat de Catalunya (Catalan Government). In this study, the current state and the evolution of the Catalan coast were evaluated in order to better understand the coastal system and identify current/future conflicts towards an optimised coastal management and planning. For each (sandy) beach, a complete list of parameters is publicly available including morphodynamic, hydrodynamic, environmental and functional aspects.

As part of the impact assessment (see Section 7), the affectation on the coastal sediment transport is investigated using the following parameters corresponding to a total of 300 beaches approx: beach longitude, beach orientation and beach sediment grain size. Beach longitude and orientation were obtained from ortophoto maps at 1:5,000 scale that were provided by Institut Cartogràfic de Catalunya (Cartographic Institute of Catalonia). The longitude was taken as the distance between the beach extremes measured along half the beach width and following the coast orientation. To characterise the sediment, a sample was collected close to the shoreline in the middle of the beach and then filtered to obtain statistical parameters such as the median of the grain size.

4 Trend analysis

The temporal evolution of wave conditions at near-shore areas of the Catalan coast has been studied. In this section, a synthesis of the followed methodology is presented as well as a summary of the representative results, making special emphasis on the methodological contributions which are mostly related to the analysis of the wave direction. Many studies have omitted the investigation of this variable or have just analysed the mean wave direction without exploring what is happening to the wave direction distribution.

Based on 44 years of hindcast wave data (1958–2001) (HIPOCAS data, see Section 3) of 40 nodes located close to the coast (see Figure 5), the trend analysis is separately analysed for extreme and mean conditions (Sections 4.1 and 4.2, respectively). Refer to Papers A and B for further details.

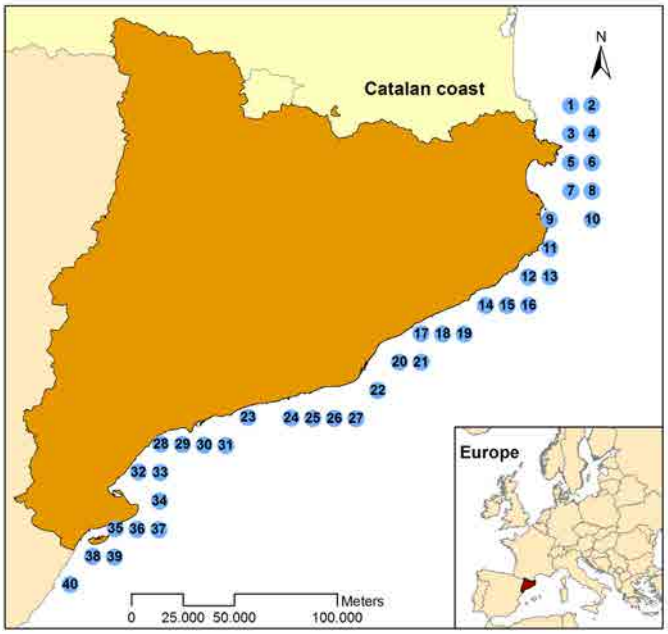

FIGURE 5: Location of the considered nodes of the HIPOCAS database along the Catalan coast for the trend analysis.

4.1 Extreme wave climate

When assessing any kind of impact, one normally thinks of extreme events first. Having in mind the third objective of this thesis (see Section 1.2), the trend analysis is firstly undertaken for the extreme wave climate. A parameter related with the beach erosion potential is used: the wave storminess (E_s), which integrates the significant wave height (H_s) over the storm duration [Mendoza and Jiménez, 2006]. As in the study of Mendoza and Jiménez [2006], storms are defined with the peak over threshold method using a

threshold of 2 m and certain duration requirements to select independent storms. The analysis is made in terms of both the annual mean and maximum values of E_s for all the detected events, first, and afterwards just for storms coming from a certain direction.

A trend analysis methodology has been developed for E_s that could be extrapolated to other variables such as the maximum H_s of a storm. The procedure is divided into two steps: trend detection and trend quantification. The trend detection makes use of the Mann-Kendall (MK) test [Kendall, 1975, Mann, 1945], which is a non-parametric test recommended by Van Gelder et al. [2008] that does not assume either a trend shape or a probability distribution, and is little sensitive to outliers. Figure 6 shows the results obtained for the mean and maximum E_s in the case of considering all storms, and those coming just from north (N) and south (S), respectively. When all waves are considered, the temporal trends are null or even negative (in a few offshore locations of the northern Catalan coast). These negative trends are probably related to the tendency of N events to decrease (in the northern coast, N waves are very frequent, see Section 2.4.1). For all nodes, the trend associated to events coming from east (E), the most energetic direction, is not statistically significant (not shown). In contrast, for some locations, increasing energy is expected for storms coming from south (S), as illustrated with blue dots in Figure 6. These results demonstrate the importance of discretizing the trend analysis in directions to appreciate important variations that are not captured in an overall analysis.

To assess the relevance of the tendencies detected by MK test, the trend quantification follows, which consists of a combination of (i) the linear regression analysis to estimate the trend and (ii) the bootstrap technique to assess the uncertainty related to the data variability. A linear trend is assumed rather than a more complex function according to the parsimony principle and the scope of the trend analysis (to provide a preliminary assessment).

The classical regression analysis assumes that residuals are normally distributed, which implies that the regressed variable needs to be free to range from $-\infty$ to ∞. By definition, E_s is generally a positive variable, i.e lower bounded, and therefore it does not fulfil this basic assumption. In order to be consistent, E_s is previously log-transformed, as similarly done by Ortego et al. [2012] when fitting an extreme probability density function to $\ln H_s$. The log-transformation implies that the relation obtained by linear regression analysis between E_s and time t becomes exponential.

Note that the positive nature of E_s is subjected to the annual presence of storms and that a year without storms would lead to the problematic $\ln(0)$. To avoid that, the absolute "zero" can be substituted by a very low energy threshold value. However, this approach leads to a distortion of the results when there are many years without storms (e.g. when analysing wave storms associated to low energetic directions). In

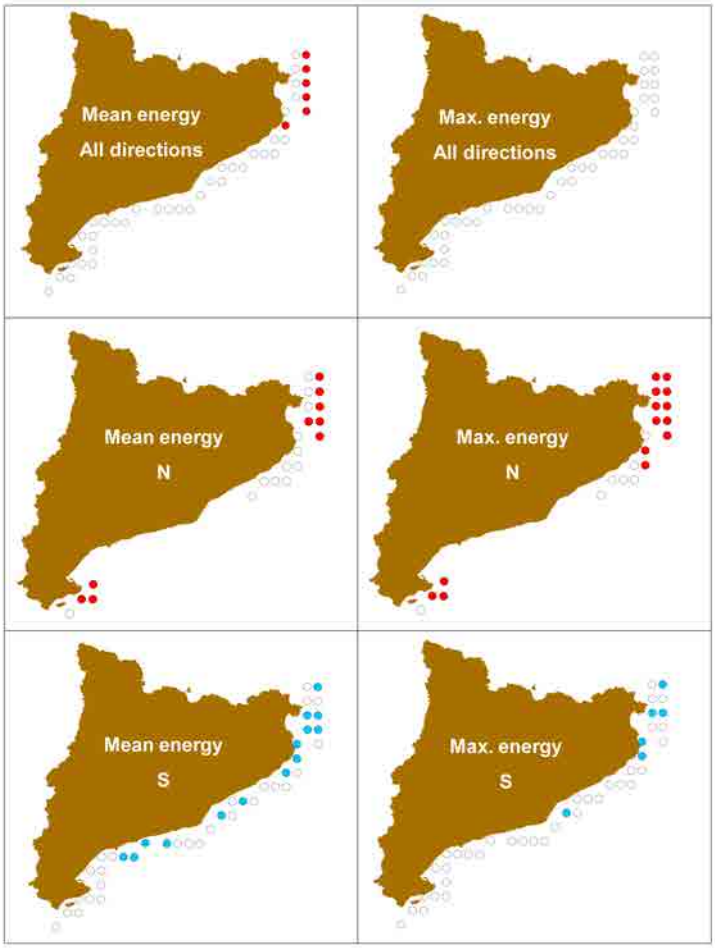

FIGURE 6: Trend detection of wave storminess, E_s, for some directions (left: annual mean, right: annual maximum). Red: negative trend. Blank: no significant trend. Blue: positive trend.

that case, the probability of storm occurrence (p_s) is introduced. The zero values of E_s associated to years without storms are simply removed from the time series and the temporal trend of $E_s(t|\text{storm})$ (E_s conditioned to storm occurrence) is obtained as $\ln(\hat{E}_s(t|\text{storm})) = \hat{a}_E t + \hat{b}_E$ (a_E, b_E are the regression coefficients and $\hat{}$ stands for "predicted"). Separately, $\hat{p}_s(t)$ is obtained by binomial logistic regression and, finally, the temporal evolution of E_s, $\hat{E}_s$, is estimated as the product:

$$\hat{E}_s(t) = \hat{p}_s(t) \exp(\hat{a}_E t + \hat{b}_E) \tag{1}$$

Eq. 1 is applied not only to the original time series $\{t, E_s(t)\}$ but also to the bootstrapped samples, whose pairs of values $\{t^*, E_s^*(t^*)\}$ (* means bootstrapped) are obtained by random selection from the original time series allowing for repetition. For each year t, a sample of $\hat{E}_s^*(t)$ is therefore obtained and the corresponding $\alpha/2$ and $1-\alpha/2$ percentiles (with confidence level α) can be interpreted as the confidence intervals of $\hat{E}_s(t)$. As an

example, Figure 7 shows the trend quantification for events coming from S corresponding to a node with previously detected positive trend with MK test (node 2, see Figure 5 and 6). The trends of both $\hat{E}_s(t)$ (solid red line) and $\hat{E}_s(t|\text{storm})$ (dashed red line) are shown, as well as those corresponding to the bootstrapped samples, $\hat{E}_s^*(t)$ (1000 in total as recommended by Park et al. [2001], yellow lines) and their confidence intervals (with α=0.05, doted black lines). In 2001, $\hat{E}_s(t)$ is about four times higher than for 1958 and this is caused by an increase of both $E_s(t|\text{storm})$ and $\hat{p}_s(t)$ (note that $\hat{E}_s(t)$ increases more rapidly than $\hat{E}_s(t|\text{storm})$). These results suggest that, for some locations, a larger fraction of S waves will correspond to stormy conditions, which, in turn, will be more energetic.

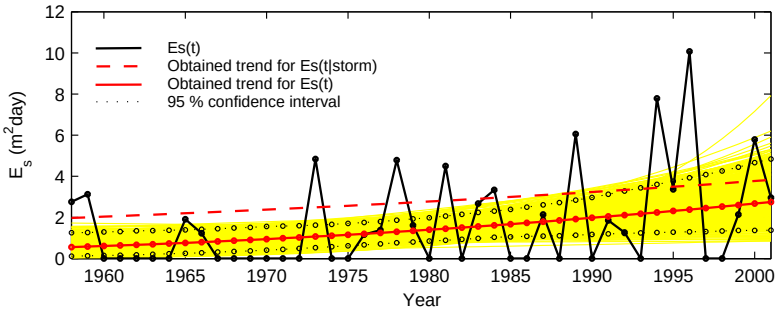

FIGURE 7: Example of trend quantification of the annual mean $E_s(t)$ associated to events coming from S (node 2, see Figure 5). Yellow lines are the bootstrapped samples.

To get insight into the changes in the mean wave direction θ_m, the evolution of the distribution of θ_m for storm events is investigated. The proposed method consists of analysing the evolution of the annual frequency of k directional sectors. In this study $k = 8$, which corresponds to the eight 45°-directional sectors centred in the cardinal and ordinals directions: north (N), northeast (NE), east (E), southeast(SE), south (S), southwest (SW), west (W), northwest (NW), north (N). As for E_s, the trend is estimated by linear regression analysis and the uncertainty is bounded by bootstrapping. However, in this case another transformation is needed, as explained below.

Frequencies are compositional data: the sum is a constant value and therefore they are defined in a simplex space. This inter-relation produces spurious effects in the calculation of, for instance, the covariance matrix [Pawlowsky-Glahn, 1984]. As a consequence, a previous conversion is needed before applying the regression analysis (which makes use of the covariance matrix). This thesis proposes to apply the isometric log-ratio (ilr) transformation [Egozcue et al., 2003], whose application has been mainly focused so far on the analysis of compositional data in the field of geochemistry and sedimentology [e.g. Tolosana-Delgado, 2012]. In this case, the ilr transformation translates the k directional frequencies $\{f_1, ..., f_k\}$ into $k-1$ coordinates $\{y_1, ..., y_{k-1}\}$ on an orthonormal basis in a real vector space $\mathbb{R}^{k-1}$, obtained from sequential binary partition (R_i, S_i). The

conversion can be expressed as the geometric mean of each partition $(g(f_{\in R_i}), g(f_{\in S_i}))$, multiplied by a normalising factor $a(r_i, s_i)$.

$$y_i = a(r_i, s_i) \ln\left(\frac{g(f_{\in R_i})}{g(f_{\in S_i})}\right), \quad a(r_i, s_i) = \sqrt{\frac{r_i s_i}{r_i + s_i}} \tag{2}$$

for $i = 1, ..., k-1$, where r_i and s_i are the number of elements of each partition. After some basic algebraic transformations and taking into account that frequencies are a function of each year t, this expression can be rewritten as:

$$\mathbf{y}(t) = \mathbf{M} \ln(\mathbf{f}(t)) \tag{3}$$

where $\mathbf{y} = [y_1, ..., y_{k-1}]^T$, $\mathbf{f} = [f_1, ..., f_k]^T$ and $\mathbf{M}$ is a $(k-1) \times (k)$ matrix of known coefficients. The regression analysis is therefore applied to $\mathbf{y}(t)$ (and the corresponding bootstrapped samples) obtaining the regression coefficients $\hat{\mathbf{a}}$ and $\hat{\mathbf{b}}$ (and the corresponding $\hat{\mathbf{a}}^*$ and $\hat{\mathbf{b}}^*$). Inverting Eq. 3, the estimated temporal trend of $\mathbf{f}$, $\hat{\mathbf{f}}$, can be expressed as follows:

$$\hat{\mathbf{f}}(t) = C \exp(\mathbf{M}^T(\hat{\mathbf{a}}t + \hat{\mathbf{b}})) \tag{4}$$

in which C is the closure operation to fit the relationship $\sum_i f_i = 1$. To better interpret the obtained tendencies, instead of using the coefficients $\hat{\mathbf{a}}$ and $\hat{\mathbf{b}}$, which are expressed in terms of the (artificial) coordinates $\mathbf{y}$, the future distribution of the wave direction is extrapolated giving a value to the variable t. Certainly, this extrapolation has some limitations because the same trend shape for the current climate is assumed valid in the future. To reduce the level of speculation, a mid-term future projection is chosen (t=2050) rather than a long-term projection as with the methodologies used in Sections 5 and 6. The goal is not to get a precise picture of the future wave climate but to find out how wave climate is expected to evolve.

Figure 8 illustrates the projections for 2010 and 2050 corresponding to a couple of nodes located respectively at the northern and southern part of the Catalan coast. The marginal confidence bounds (green and blue dots) are complemented with the (1000) bootstrapped samples (yellow lines) to visually integrate the interaction of the uncertainty between directions. The tendencies observed in the frequencies are similar to those of E_s (except for some locations that exhibit a reduction of the frequency of E events whereas the corresponding energy remained unchanged). However, the variations are not statistically significant—confidence intervals of 2050 projections are large and include the 2010 situation—which makes difficult to draw a robust conclusion. The large uncertainty can be explained by the large inter-annual variability and the implicit reduction in the data as in any extreme analysis.

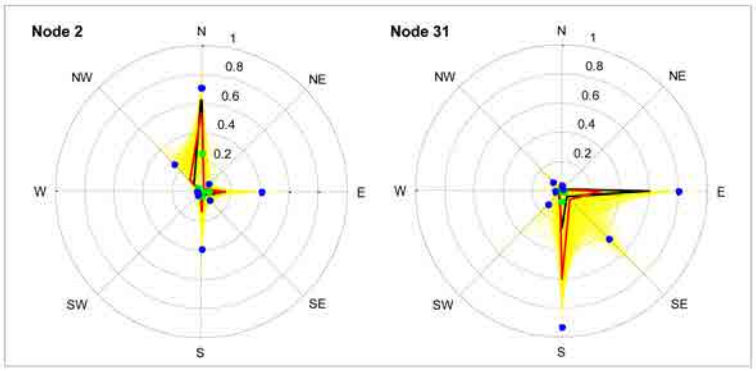

FIGURE 8: Comparison between 2010 and 2050 projections (nodes 2 and 31, see Figure 5). Black: $\hat{\mathbf{f}}(t = 2010)$. Red: $\hat{\mathbf{f}}(t = 2050)$. Yellow: $\hat{\mathbf{f}}^*(t = 2050)$. Green and blue dots: 95% marginal confidence intervals of $\hat{\mathbf{f}}(t = 2050)$ (α=0.05).

4.2 Mean wave climate

Extending the procedure used to evaluate the tendencies of the wave directional distribution in stormy conditions (see Section 4.1), a methodology of trend analysis and extrapolation for mean wave climate is developed in terms of a typical wave rose, which is a wave graphic tool with several engineering and scientific applications. Figure 9 illustrates an example of a wave rose, where the wave climate is discretised in five groups of H_s ([0–1, 1–2, 2–3, 3–4, >4] m) and eight directional sectors of 45° each, as those used in Section 4.1. The directions of the rose with the longest spoke show the wave direction with the greatest frequency (N in the example of Figure 9).

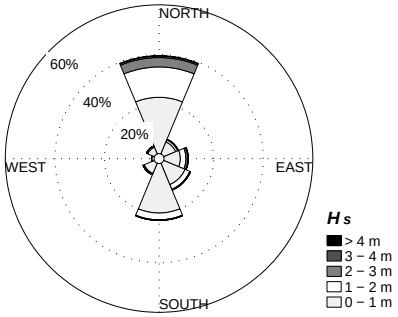

FIGURE 9: Example of a wave rose (node 6, see Figure 5) for the period 1958–2001.

As similarly done for the extreme analysis, the future mean wave climate is extrapolated in terms of the (annual) frequencies associated to each θ_m and H_s bin. After ilr-transforming them, the linear regression method complemented by bootstrapping is applied. The procedure is first undertaken for $\{f_1, ..., f_{k_\theta}\}$ corresponding to the eight θ_m sectors (Eqs. 2-4 with $k = k_\theta = 8$) and afterwards for $\{f_1, ..., f_{k_H}\}$ associated to the groups of H_s for each θ_m (eight times Eqs. 2-4 with $k = k_H = 5$) (see Paper B for further details).

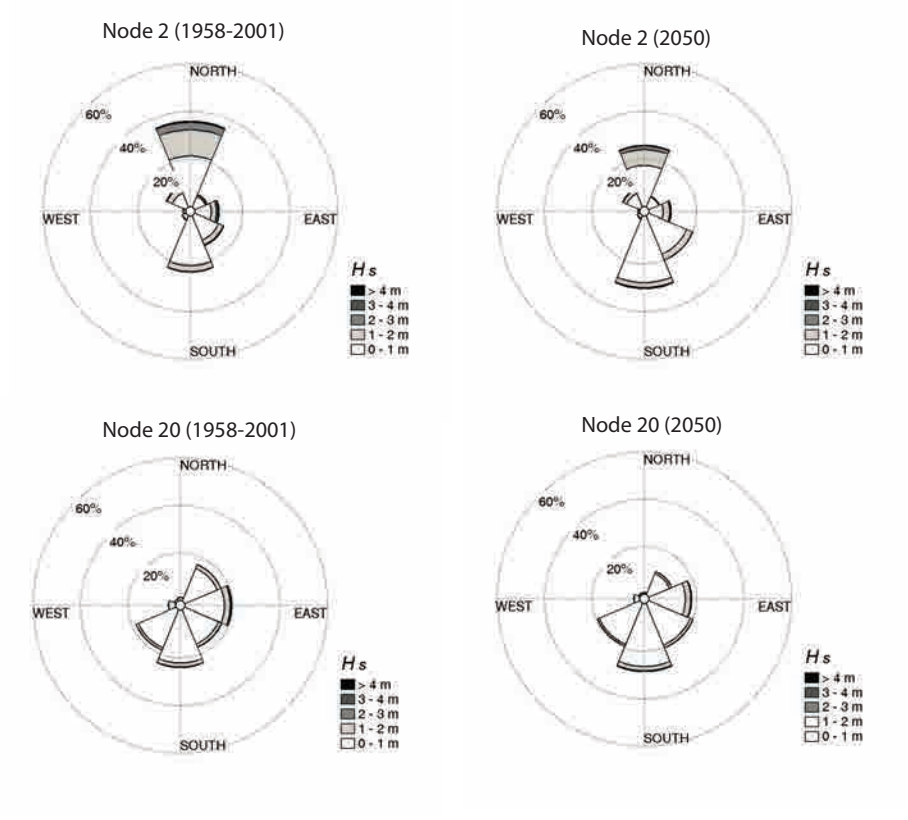

FIGURE 10: Examples of wave roses for the period 1958–2001 and the future extrapolation for 2050.

As an example, Figure 10 compares the wave roses corresponding to the whole period 1958–2001 and to the future extrapolation (2050) for two locations. In general, the results seems to indicate that the total amount of annual wave energy will not suffer from large alterations since the distribution of H_s does not seem to vary significantly (although there is a certain tendency to decrease). Contrary, remarkable differences are observed in the θ_m distribution. Similar to that obtained for the extreme wave climate, the frequencies of N and NE waves tend to decrease whereas an increase is found for SE, S and SW but in this case the average uncertainty is lower (see Paper B). This reduction of uncertainty can be probably explained by the fact that the whole dataset is considered here instead of a sub-sample of extreme events. In Figure 11, the marginal evolution of S frequency alone is plotted for four locations with the 80% and 90% confidence intervals (α=0.10 and α=0.05). For all cases shown in this figure, the extrapolated frequency for 2050 is expected to be larger than the average value for the 44 years of data (with 80% confidence).

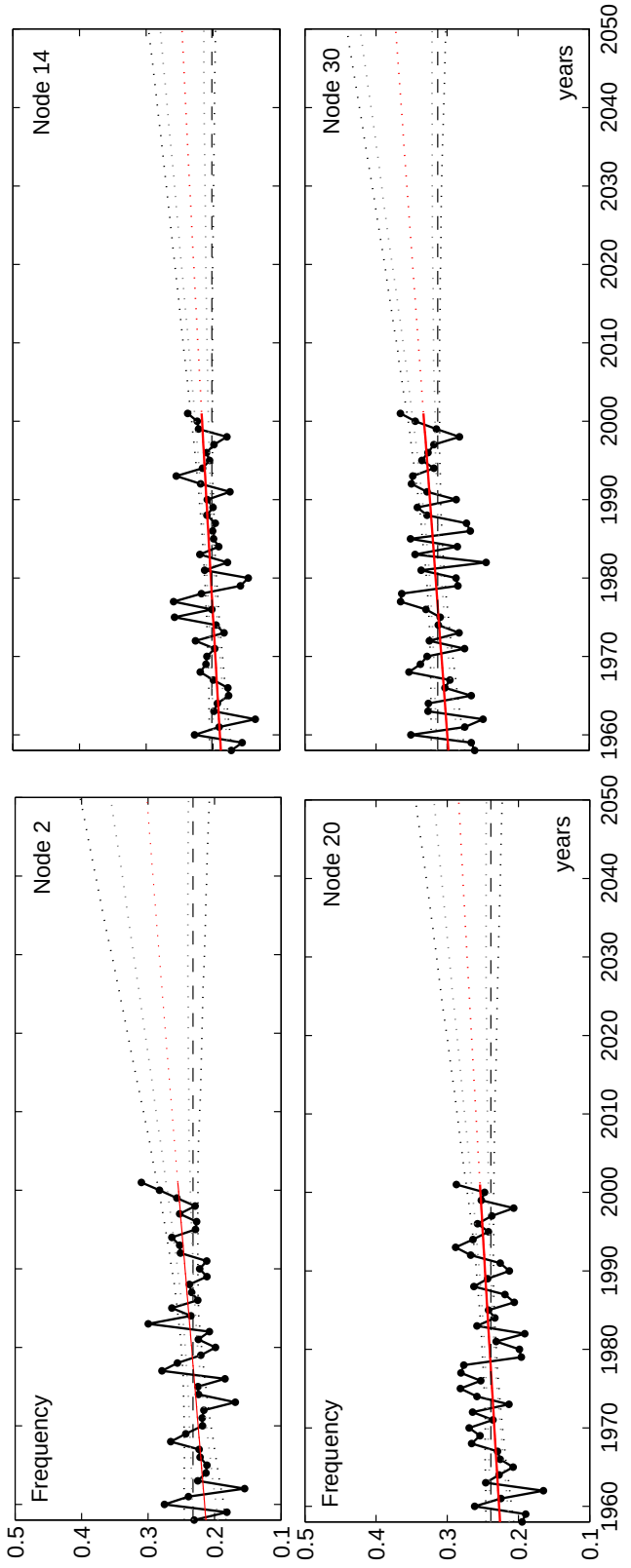

FIGURE 11: Examples of the evolution of S frequency (in red the fitted trend and in black the original time series) including the 80% (grey doted line) and 95% (black dotted line) marginal confidence intervals and the mean frequency value during the period 1958–2001 for reference (in dashed line).

Trend analysis - Contributions

(1) Understanding the future wave climate

- Provide a first assessment of wave climate changes at near-shore areas of the Catalan coast, which highlights the relevance of the variations of the wave direction in this area.

(2) Improving methodological aspects

- Development of a trend analysis methodology to study the evolution of the magnitude of an extreme wave event (e.g. wave storminess). It has two steps: trend detection (Mann-Kendall test) and trend quantification (linear regression analysis). The (positive) data are previously log-transformed and the uncertainty is assessed by bootstrapping. In the case of non-frequent events (e.g. storms coming from S), the binomial logistic regression is involved to evaluate the evolution of the storm occurrence.

- Development of a trend analysis methodology to estimate the evolution of the wave direction distribution. It considers the annual frequency of a given number of directional sectors and evaluates their trend by linear regression analysis. The data are previously ilr-transformed to take into account the compositional character. Confidence intervals are obtained by bootstrapping.

- Extension of the previous methodology to extrapolate future wave conditions in terms of a wave rose, a graphic tool with many engineering applications that integrates wave height and wave direction information.

5 Dynamical modelling

The trend analysis presented in Section 4 has served to provide a first assessment of the possible future changes in the wave conditions approaching the Catalan coast. However, the underlying limitations, as for example the assumption of a certain trend shape, make necessary to go one step further and project the future wave climate directly accounting for the greenhouse effect.

Section 5.1 explains how the dynamical technique is performed to generate a high spatial and temporal resolution (3h and 0.125°) wave dataset suitable to properly reproduce the regional wave features. The parameters used to characterise the wave climate are described in Section 5.2. To determine the significance of the (multivariate) climate change signals a methodology based on bootstrapping is proposed. It jointly implements two existing methods in order to: (i) account for the time dependency of the wave data [Cai and Davies, 2012] and (ii) improve the correct reproduction of extremes [Pandey et al., 2003, 2004]. Finally, in Section 5.4, the obtained wave projections are studied. Special focus is given to the wave direction, since the trend analysis revealed that this variable seems to be especially affected by climate change in this area.

In accordance with the thesis outline (Section 1.3), this Section is just a summary of the thesis work related with dynamical modelling. More information about methods and results can be found in Paper C.

5.1 Wave modelling

Wave climate projections are computed with the SWAN wave model [Booij et al., 1999] in parallel mode and following a downscaling-nesting procedure with two computational grids, as illustrated in Figure 12. The larger domain considers most of the areas where waves can be remotely generated and then propagated towards the Catalan coast in the form of swell waves. SWAN is forced by surface (10-m) wind fields corresponding to two 30-year time slices (1971–2000 for the "present"[6] and 2071–2100 for the "'future") that were driven by the most recently used greenhouse scenario A1B (see Section 3), using, respectively, five combinations of regional and global atmospheric models (four RCMs and two GCMs, see Table 1). This allows the investigation of the inter-model variability in terms of wave climate, which is one of the most important factors of uncertainty with regards to atmospheric climate (see Section 2.1). The SWAN wave output consists of typical spectrum variables: significant wave height H_s, peak wave period T_p and mean wave direction θ_m.

[6]Except for one RCM for which the period is 1981–2010 (see Section 3)

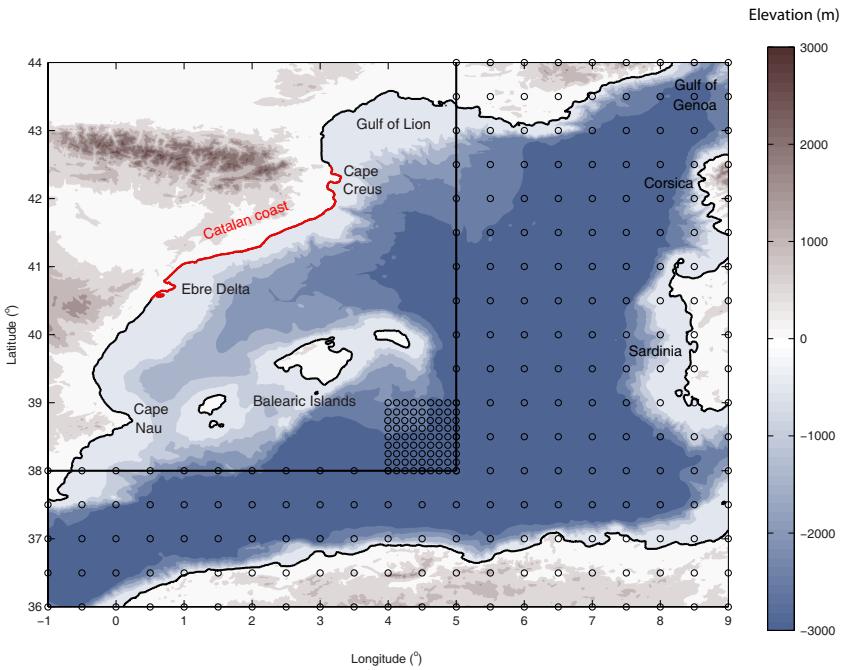

FIGURE 12: Domains used for the nesting procedure with the SWAN wave model (distance between circles indicate the spatial resolution of each grid).

5.2 Characterisation of the wave climate

The mean wave climate is first characterised by the median of H_s and T_p, which is a robust measure little affected by outliers. As in the trend analysis, the distribution of the wave direction is analysed by means of the frequency of the eight (45°) directional sectors: N, NE, E, SE, S, SW, W, NW. Additionally, the wind-sea/swell distribution is investigated using the occurrence of the types of sea states as determined with the inverse wave age A^{-1}, like in the work of Charles et al. [2012]. This parameter compares the wind velocity w_{10} with the wave (deep water) celerity C_p ($C_p = 1.56T_p$) and also evaluates the difference between the wind and wave direction ($\Delta\Theta$, see Eq. 5). A value of A^{-1} closer to unity ($A^{-1} > 0.83$) is therefore related with a wind-sea state, i.e. waves locally generated by wind. On the contrary, a low value of A^{-1} ($A^{-1} < 0.15$) implies that wind and waves are fairly independent which is the case of swell waves, waves that are travelling after being remotely generated. The two types of waves are often combined, which is classified as mixed sea states ($0.15 \leq A^{-1} \leq 0.83$).

$$A^{-1} = \frac{\mathrm{w}_{10} \cos \Delta\Theta}{C_p} \tag{5}$$

To inspect the extremes, the 50-year return period of H_s (z_{50}) is used (see Eq. 6). This parameter is derived from the same General Pareto Distribution (GPD) involved in

the last stage of the uncertainty analysis (see Section 5.3). Instead of selecting independent storms, which would entail a (slow) storm-by-storm checking, z_{50} is computed making use of all exceedances above the selected threshold u (95^{th} percentile of H_s), reducing considerably the associated computational cost. The error thus introduced—GPD assumes independence between storms—is counteracted with the extremal index β [Fawcett and Walshaw, 2012], as shown in Eq 6:

$$z_r = u + \frac{\hat{\sigma}}{\hat{\xi}} \left[\left(\lambda_u^{-1} \left\{ 1 - \left[1 - \frac{1}{r n_y} \right]^{\beta^{-1}} \right\} \right)^{-\hat{\xi}} - 1 \right] \tag{6}$$

where $\hat{\xi}$ and $\hat{\sigma}$ are the fitted GPD parameters, n_y is the number of observations per year (estimated as the total number of observations divided by the number of years), $\lambda_u = 1 - F_E(u)$ (see Eq. 7) and r the return period ($r = 50$ years).

5.3 Uncertainty analysis

In this section, a methodology is proposed to assess the significance of the differences between the present and future situation which takes into account the uncertainty introduced by the data variability. It consists of a modified bootstrap method that combines (i) the method of Cai and Davies [2012] and the (ii) semi-parametric approach of Pandey et al. [2003, 2004].

Cai and Davies [2012] developed a model-free method adapted to time series, which are typically characterised by being autocorrelated. This autocorrelation is particularly relevant for high-temporal resolution data (like the 3 hourly wave dataset generated in this thesis). Basically, instead of re-sampling individually each data item $x(t_i)$ ($i = 1, ..., T$, where T is the time length) like in the classical bootstrapping, Cai and Davies [2012] proposed to re-sample in segments of data that correspond to the same percentile bin as illustrated in Figure 13 (being the number of bins previously defined according to a sensitivity analysis). The bootstrap samples are therefore constructed by randomly reproducing the same distribution of those percentiles over time, which maintains the (temporal) autocorrelation structure. To replicate a coherent spatial correlation (same variable, different location) and cross-correlation (same location, different variable, e.g. H_s and T_p) the permutations are jointly implemented as follows. First, the method of Cai and Davies [2012] is applied only to a "representative" H_s time series: the spatial-average on the entire set of wave grid points. Second, for each grid point and studied variable (H_s, θ_m and T_p), the corresponding bootstrapped samples (H_s^*, θ_m^* and T_p^*) are obtained using the same beginning and ending indexes of the permutations corresponding to the aforementioned representative time series. This multivariate procedure is based on

[Wilks, 1997]'s conclusion that the simultaneous application of univariate re-sampling methods yields to a powerful multivariate method.

The approach of Pandey et al. [2003, 2004] serves to overcome the deficiencies of bootstrapping as regards to the correct estimation of extremes. They proposed that the final cumulative distribution of the bootstrapped variable $F_B(x^*)$ can be approximated with the expression of Eq. 7. Essentially, they consider that the bootstrapped sample x^* cannot be fully trusted above a certain threshold u and therefore the (empirical) probability density function for $x^* > u$ is substituted by a General Pareto distribution (GPD) (see Figure 13).

$$F_B(x^*|u) = \begin{cases} [1 - F_E(u)]F_P(y) + F_E(u) & \text{for } x^* > u \\ F_E(x^*) & \text{for } x^* \leq u \end{cases} \tag{7}$$

where F_E is the preliminary empirical cumulative density function of x^*, in this case obtained with the simultaneous application of Cai and Davies [2012] method, and F_P is the GPD fitted to all extreme events above u (see Section 5.2).

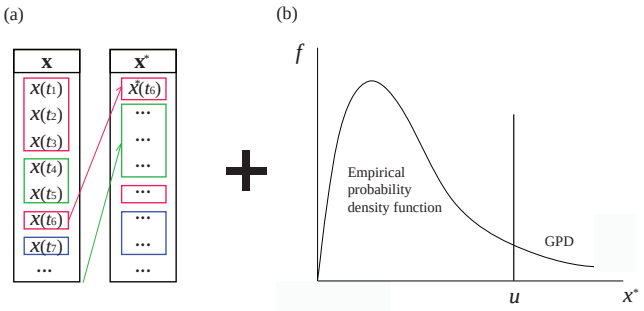

FIGURE 13: Sketch of the proposed modified bootstrap method combining the methods of (a) Cai and Davies [2012] and (b) Pandey et al. [2003, 2004]. First, the bootstrapped sample x^* is obtained from the original time series x reproducing the temporal distribution of percentiles (illustrated with colours as an example) and then its probability density function is modified for $x^* > u$ (see main text).

From both the original and bootstrapped samples, the parameters specified in Section 5.2 to characterise the wave climate are computed. The projected changes associated to those parameters are considered (statistically) significant if the null hypothesis of no change is rejected, in other words, if the confidence intervals of the (bootstrapped) projected changes do not include the zero.

5.4 Wave projections

To gain insight into the understanding of the atmosphere-wave climate system, the projected variations in the wave climate are not merely described but also discussed in

relation to the forcing wind climate. Winter and summer seasons (defined as December-January-February and June-July-August, respectively) are analysed separately because they are typically associated to different atmospheric features, as explained in Section 2.2. In Section 5.4.1, the simulation of the present climate is qualitatively validated and in Section 5.4.2, the evaluation of the climate change signals is presented. Not all the results explained in this section are supported by the corresponding figures. Please refer to Paper C for further information.

5.4.1 Present climate

The five model combinations used in this thesis simulate a similar spatial pattern for the present value of the median H_s which is similar to that of the median T_p (not shown). In winter, the larger values of the median H_s are situated offshore in the NE corner of the domain (see Figure 14) which is in agreement with the nearby Gulf of Genoa-cyclogenesis area (see Figure 12). However, the magnitude of the median H_s varies among models. The model biases are closely related with those of the (median of the) forcing wind speed w_{10}. A similar bias pattern (but with accentuated magnitudes) is obtained for z_{50} (see Figure 15) which can be explained by the nonlinear relation between H_s and w_{10}. HIR_E model results largely overestimates both the median H_s and z_{50} which seems to be related with an over-representation of the NW component. That, in turn, leads to an erroneous seaward mean θ_m close to the Catalan coast (see Figure 14).

The regional Mistral wind pattern seems to be well resolved by all models since all simulations have a notable occurrence of NW waves in the Gulf of Lion and, to a lesser extent, close to the Ebre Delta. Actually, all models simulate a fairly similar distribution of all directions. However, local differences are observed. For example, in RCA_H case, there is a greater frequency of E waves along some coastal stretches that face E. As explained in Section 5.4.2, this discrepancy is related with the use of the parent GCM and it is largely accentuated for the future wave climate. For the present climate, the hardly noticed difference in the wave direction distribution is better reflected in the wind-sea/swell distribution: E waves contribute to swell formation along the Catalan coast, in detriment of wind-sea states.

In summer, apart from the expected lower median H_s, the spatial pattern is different in comparison to winter: there are two focus of wave energy (larger values of the median H_s). The first is in the Gulf of Genoa, as in winter, and the second is located in the southern part of the domain. The latter might be related with the cyclogenesis area over the Iberian Peninsula caused by thermal contrasts which are typical during summer (see

Section 2.2). Compared to winter, there is a lower occurrence of wind-sea states which can be explained by the milder wind (and wave) conditions.

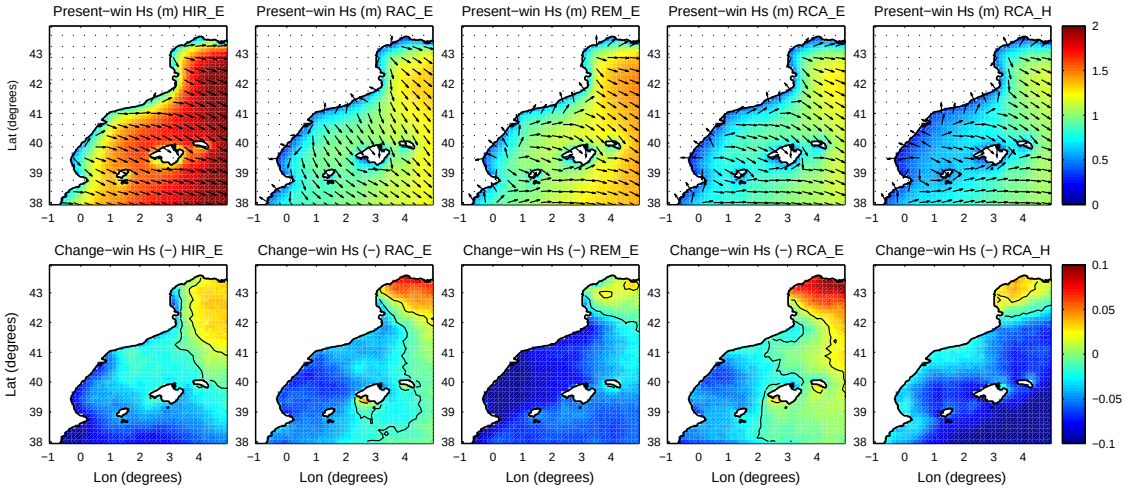

FIGURE 14: Estimated present (upper rows) and projected relative change (lower rows) of the median H_s (color maps) for winter, forced by the five RCM-GCM wind datasets. Arrows show the mean θ_m, and thin black lines delimit areas of significant change.

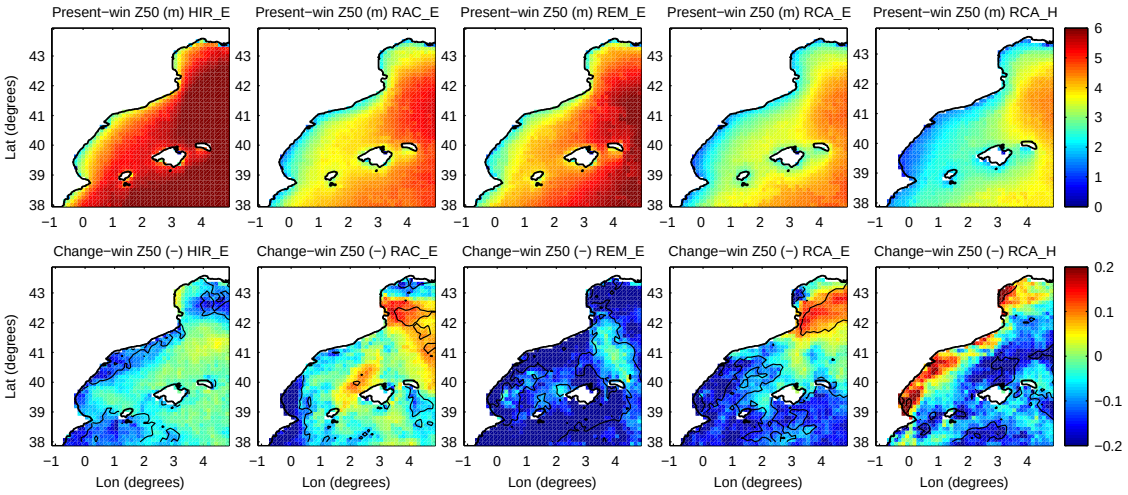

FIGURE 15: Estimated present (upper rows) and projected relative change (lower rows) of z_{50} (color maps) for winter, forced by the five RCM-GCM wind datasets. Thin black lines delimit areas of significant change.

5.4.2 Climate change signals

Figure 14 shows a general pattern of moderate reduction of the median H_s during winter which could be explained by the general weakening of Mediterraenan storms (see Section 2.2). However, results also illustrate an increase of wind and wave intensity in the area of the domain close to the Gulf of Genoa (RCA_H and REM_E to a

lesser extent), which could be related with the 45°-latitude limit between areas of increased/decreased storm intensity (encountered by Nikulin et al. [2011]). Both negative and positive changes are statistically significant in most of the domain.

Comparing the rate of change of the median H_s (around ±10%) with that of the corresponding forcing w_{10}, one realizes that H_s does not vary in proportion to w_{10}^2, which would be the case in a pure (fully-developed) wind-sea state. That confirms the complexity of the wave climate in this area: some wave directions are fetch-limited and others facilitate the swell formation. Note that for pure swell waves, H_s is independent of the local w_{10}. Regarding the extremes, the range of variation of z_{50} is larger (around ±20%). This can be explained by the fact that storm events are usually controlled by wind-sea states (although not necessarily being fully-developed), for which there is a stronger (non-lineal) relation between H_s and w_{10}.

Just with some exceptions, the pattern of predicted changes of the median T_p is similar to that of H_s but has a lower rate of increase/decrease, around ±5% (while around ±10% for the median H_s). Despite the aforementioned complexity of the wave climate, in most cases the theory of fetch limited wave growth seems to be applicable to relate H_s and T_p ($H_s \propto \sqrt{T_p}$). Note that this might not be the case for large oceans, where swell waves are a predominant feature [Hemer et al., 2013].

The decomposition of the wave climate in directional bins is very useful to realize that the evolution of the wave direction distribution greatly varies depending on the parent GCM (see Figure 16). ECHAM5-driven projections (HIR_E, RAC_E, REM_E, RCA_E) show a remarkable increase of the S-SW-W-NW frequencies for some locations whereas HadCM3Q3-driven projection (RCA_H) show a significant increase of the whole E sector (NE-E-SE, but only E affects the Catalan coast). Results obtained by trend analysis showed variations qualitatively in agreement with the ECHAM5-driven projections. Maximum absolute differences are about 5% but they can reach values over 100% in relative terms. Such opposite responses imply discrepancies in the wind-sea/swell distribution (Figure 17) and in the variations of extreme waves (Figure 15). The rise of the frequency of E waves associated to RCA_H produces an increase of both the occurrence of mixed sea states and z_{50} along most of the coastal stretches that face E. However, in the later case, changes are not statistically significant as similarly obtained by Lionello et al. [2008] when studying extremes. Moreover, contrary to what happens for the mean wave climate, there are important discrepancies between simulations using the same GCM but different RCMs (e.g. REM_E vs. RCA_E).

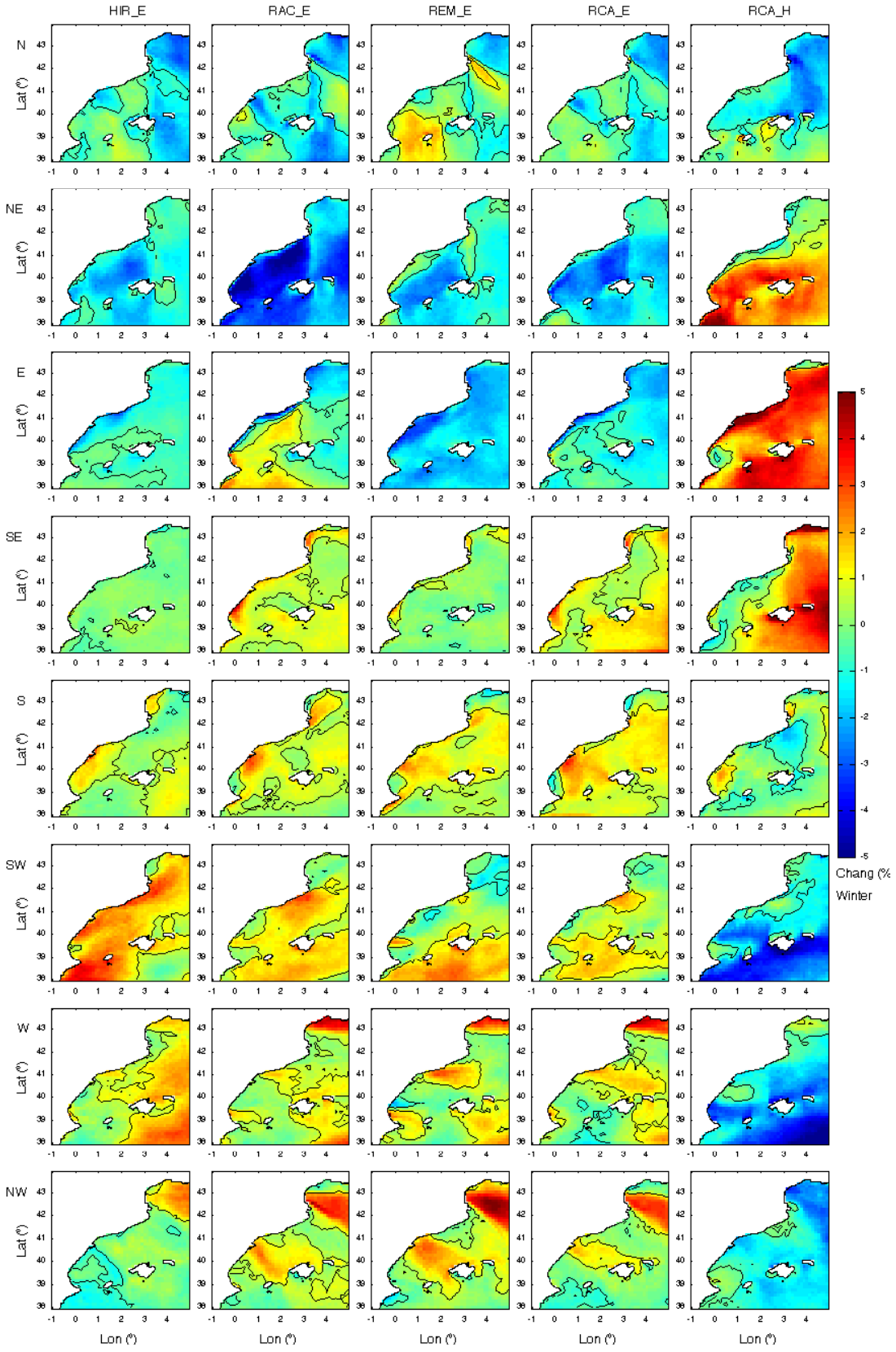

FIGURE 16: Projected absolute change of the frequencies associated to each directional sector, forced by the five RCM-GCM wind datasets (for winter). Thin black lines delimit areas of significance change.

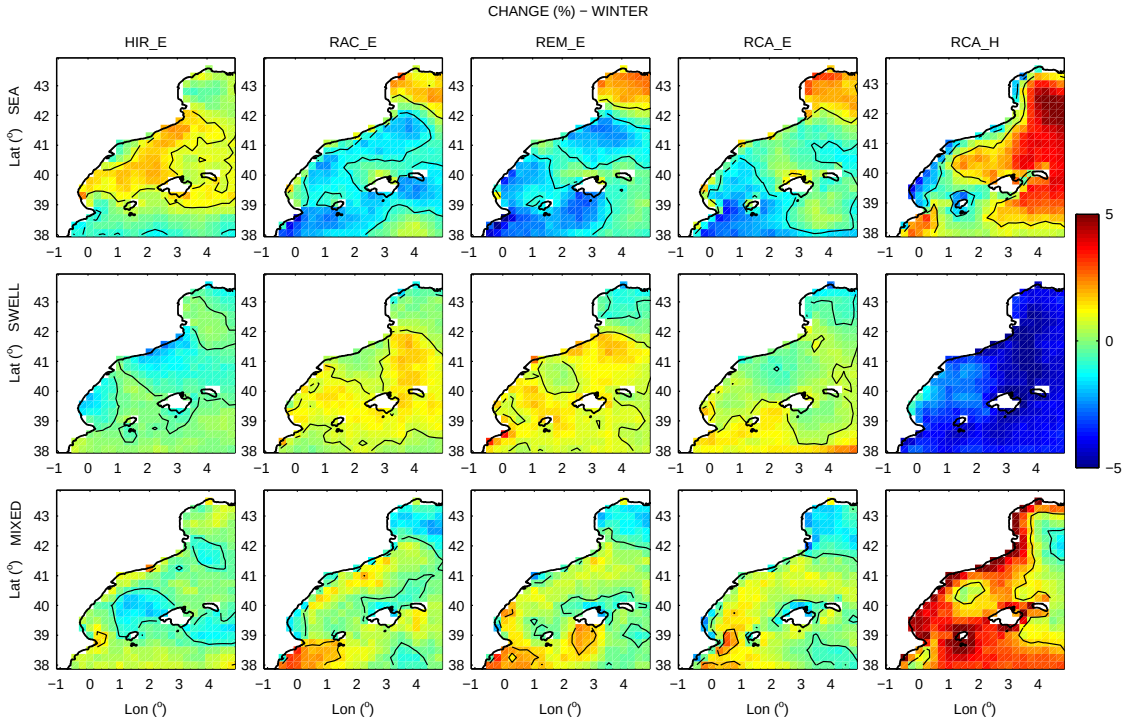

FIGURE 17: Projected absolute change of wind-sea, swell and mixed sea states occurrence for winter. Thin black lines delimit areas of singificance change.

The disagreement between the realisations corresponding to the two GCMs are consistent with the findings of Donat et al. [2010]. Among other GCMs, they analysed atmospheric patterns obtained by ECHAM5 and another model similar to HadCM3Q3 and realised that these models differ in the projected tendency for the W-E flow. However, it is hard to determine which GCM is more reliable in terms of the projected changes in wind climate and, consequently, in wave climate. Donat et al. [2010] found that they both reproduce the current characteristic climatological pressure patterns that are relevant for central Europe better than other GCMs. Other studies [Bengtsson et al., 2006, Ulbrich et al., 2008] have tested ECHAM5 model results in a single basis or comparing with other models (but not with the HadCM3Q3 model) resulting in a reasonably well representation of the present climate by ECHAM5. However, owing to the lack of a proper comparison between the two GCMs considered in this thesis, both ECHAM5 and HadCM3Q3 (driven projections) should be considered equally feasible.

Some studies [e.g. Donat et al., 2010] have suggested that an ensemble mean is better than a single model. This thesis results points out that such an ensemble has to be done with caution, in order not to cancel out contrasting patterns and obtain a fictitious climate change signal. This thesis results show that differences in the winter atmospheric patterns produced by GCMs can be intensified in terms of the wave climate (depending on the fetch configuration). Therefore, winter wave projections should be at least separated between those corresponding to different GCMs.

In summer, climate change signals are completely different from those of winter. The median H_s increases in the SW part of the domain, which is closely related to the increase of the median w_{10} in the same area. Such increase seems to be explained by the larger frequency of NE waves, which, in turn, is translated into a rise of the mixed sea states in the coastal stretches that are favoured by this configuration. Apart from a rise in the occurrence of NE (and E) waves, the directional analysis shows a decrease of the frequency of NW waves, with a lower median H_s (and w_{10}) projected in the NE corner of the domain. S waves tend to be less frequent which could be associated with a lower thermal difference between land and sea in the Iberian Peninsula. In contrast to the winter season, a reasonable degree of agreement is obtained for the wave direction distribution among all model realisations, being the inter-model variability due to both RCMs and GCMs. This is a plausible result since global models typically control synoptic-scale atmospheric patterns, which have more influence during winter. Finally, regarding the extreme wave climate, results indicate that z_{50} will vary at a higher rate than the median H_s (20% vs. 10% approx.) but with a larger uncertainty (as it occurred for winter). Except for RCA_H, the rest of the models project significant increases in some segments of the Catalan coast.

Dynamical modelling - Contributions

(1) Understanding the future wave climate

- For the first time, provide the Catalan coast with future wave climate projections (wave height, wave period and wave direction) at high spatial (0.125°) and temporal (3 h) resolution, which is a potential source of data for several impact assessment studies.
- Get insight into the atmosphere-wave climate system, that has helped to better understand the changes in the wave patterns. Determine the relative influence of the local forcing wind and the swell component.
- For the first time in this area, explore the inter-model variability at a regional scale in terms of wave parameters.

(2) Improving methodological aspects

- Develop a bootstrap-based methodology to assess the significance of a multivariate climate change signal, that better represent the extremes and accounts for the time-autocorrelation present in the high temporal-resolution data.

6 Statistical modelling

Dynamical modelling has been successfully used to provide high temporal and spatial resolution wave projections for the NW Mediterranean Sea (where the Catalan coast is located, see Section 5). However, owing to the high computational cost, this method is not suitable to address a sufficient number of combinations (of climate models and forcings) to estimate the full range of uncertainty (see Figure 2). This is a general problem that becomes more critical when coastal regions have larger fetches for which a larger computational domain is needed. As a low computational cost alternative to dynamical modelling, in the last years statistical methods have been developed to model ocean waves [Caires et al., 2006, Camus et al., 2013, Gunaydin, 2008, Laugel et al., 2013, Wang et al., 2012, Wang and Swail, 2006, Wang et al., 2010]. These approaches obtain wave parameter(s), i.e. predictand(s), from atmospheric parameter(s), i.e. predictor(s). Although the method is based on an empirical relation, wave physics can be indirectly considered in the selection of the appropriate predictors. Also, the selection of these predictors is rather flexible, wave conditions do not need to be obtained from surface wind fields (like in dynamical modelling), which are usually more affected by climate model biases than other atmospheric variables [McInnes et al., 2011].

This thesis proposes a method for modelling (high temporal and spatial-resolution) ocean wave heights based on the method of Wang and Swail [2006]. Wang and Swail [2006] developed a method based on multiple linear regression analysis to predict the significant wave height (H_s, the predictand) from predictors derived from the sea level pressure (SLP) field (present-day climate models tend to represent atmospheric fields (such as SLP) much better than the surface wind [Wang et al., 2010]). Specifically, the anomalies of the local SLP and its squared spatial gradients were used. This is based on the fact that the SLP spatial gradient represents the geostrophic wind at the surface level, and H_s is proportional to the squared surface wind speed in a fully developed sea state. Wang and Swail [2006] and Wang et al. [2010] obtained reasonable good results in simulating seasonal mean and 12-hourly H_s for the global and North Atlantic scales, respectively, with a resolution of 2°. However, this model mainly accounted for local wave generation and failed to properly simulate H_s where the swell component is important. Recently, with 6-hourly wave data Wang et al. [2012] extended the set of predictors adding (1) their (scalar) principal components to account for the swell component of waves and (2) lagged values of the predictand H_s to account for its time dependence.

The basic features of the method proposed in this thesis are described in Section 6.1. Section 6.2 explains the calibration and validation processes showing a good model performance. The calibrated model is finally applied to project wave climate scenarios for the study area using the atmospheric projections driven by the same five RCM-GCM model combinations that were used with dynamical modelling. The results corresponding to the winter season (defined as December-January-February) are presented in Section 6.3. Please refer to Paper D for further information about methodology and results.

6.1 The proposed method

A multivariate regression model is proposed to obtain H_s at a relatively high spatial (0.125°) and temporal (3h) resolution (the same resolution as for dynamical modelling, see Section 5):

$$\hat{H}_s(t,m) = \hat{a}(m) + \hat{a}_P(m)\, P(t,m) + \hat{a}_G(m)\, G(t,m) + \Delta_{\mathrm{sw}}(t,m) + \Delta_t(t,m) \qquad (8)$$

where the terms $\Delta_{\mathrm{sw}}(t,m)$ and $\Delta_t(t,m)$ have been added to the regression model developed by Wang and Swail [2006]. They account for swell waves ($\Delta_{\mathrm{sw}}(t,m)$) and time dependence of H_s ($\Delta_t(t,m)$). P and G are, respectively, the anomalies of SLP and of squared gradients of SLP (the baseline mean climates are subtracted). As in the trend analysis (see Section 4), $\hat{}$ stands for "predicted". m and t are, respectively, the location and time index ($t = 1, ..., T$ and $m = 1, ..., M$, where T is the time length and M the total number of wave grid points). $\hat{a}$, $\hat{a}_P$ and $\hat{a}_G$ are the estimated regression coefficients (which are fitted together with those included in the terms $\Delta_{\mathrm{sw}}(t,m)$ and $\Delta_t(t,m)$, see Eqs. 11 and 13).

The proposed model aims to improve the performance in modelling H_s at near-shore areas, where good representation of the swell component is found to be particularly important. Therefore, special focus has been given to develop the term $\Delta_{\mathrm{sw}}(t,m)$ taking into account the physics of wave propagation. Basically, this term is based on the frequency/directional dispersion theory of waves and makes use of the lagged (directional) principal components of the SLP gradients representing the remotely generated waves. Below a more detailed explanation is included.

Owing to the frequency and directional dispersion, the initially random wave field generated in a storm propagates while disintegrating in several more regular waves—swell trains—characterised respectively by a predominant frequency and direction (Holthuijsen [2007], see Figure 18). Low-frequency waves travel faster than high-frequency ones (frequency dispersion) and propagate around the predominant direction (directional dispersion). Swell waves are therefore much lower than those initially generated in the

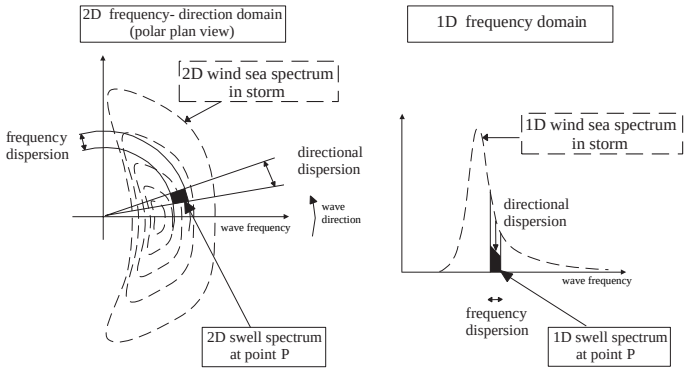

FIGURE 18: The transformation by frequency and directional dispersion of a wind-sea spectrum into a swell spectrum within a frequency and directional bin at a geographic location P (courtesy of Leo H. Holthuijsen, from Holthuijsen [2007]).

storm: the swell spectrum is just a narrow portion of the initially generated (wind-sea) wave spectrum (indicated with black shadow in Figure 18). The wave height corresponding to a swell train (H_{sw}) at a certain location m_P and time t can thus be expressed as a fraction of the wave height at the location of generation m_0 and time $t - \delta$ (H_0):

$$H_{\mathrm{sw}}(t, m_P) = \sqrt{K} \cdot H_0(t - \delta, m_0) \tag{9}$$

K is the proportion between the integral of the swell train spectrum (with a certain predominant frequency and direction) and that of the original wind-sea spectrum (see Figure 18). The square root of K is explained by the proportionality of H_s and the squared root of the integral of the wave spectrum. δ is the time needed by the swell wave train to travel the distance from m_0 to m_P, which also depends on the frequency of such waves (the lower the frequency, the larger the wave celerity, the shorter δ). No explicit energy dissipation is taken into account due to the short fetches of the study area but only the typical swell frequencies [Sánchez-Arcilla et al., 2008] are used as specified below. The total swell height (H^c_{sw}) at point m_P can therefore be approximated as the contribution of all swell trains. They are associated to all "possible" frequencies (7–12 s) and directions (± 90° around the wind direction), which are discretised in $n_f = 4$ frequencies and 5 directional bins (see Table 2):

$$H^c_{\mathrm{sw}}(t, m_P) = \sum_{l=1}^{n_0} \sum_{k=1}^{n_f} \sqrt{K^{k,l}} \cdot H_0(t - \delta^{k,l}, m_0^l) \tag{10}$$

n_0 is the total number of points of influence m_0. K is computed as $K = K_f K_\theta$ (see Table 2) taking into account the shape of the original wind-sea spectrum that can be parametrised as the product of a JONSWAP (1D) frequency spectrum multiplied by a directional spreading function (the expression of Denis and Pierson [1953] is used).

TABLE 2: Frequency and directional bins and their associated coefficients of reduction K_f and K_θ. The frequency bin is expressed in terms of the relative frequency f/f_{peak} (f_{peak} = 10 s being the peak frequency) and the directional bins in terms of the difference between wave and wind direction.

a. Frequency bin	K_f
(0.72,0.83)	0.04
(0.83,1)	0.29
(1,1.25)	0.40
(1.25,1.67)	0.17

b. Directional bin	K_θ
(-90°, -54°)	0.05
(-54°, -18°)	0.26
(-18°, 18°)	0.38
(18°, 54°)	0.26
(54°, 90°)	0.05

Considering the proportionality between H_s and the squared SLP gradients for fully-developed wind-sea states, Eq. 10 is expressed in terms of G^0 (^{0} denotes the original variable before calculating the anomaly). However, it is not evident to determine all possible m_0 from which swell trains might come and affect waves at point m_P. This depends on the topography of the region (i.e. land obstacles) and the direction of surface winds (which constantly varies in time). In that respect, the following method is proposed to find the points of influence.

Firstly, the principal component analysis is used to obtain the first N leading principal components of the SLP gradient fields ($N = 30$), namely, a small number of important subspaces that contain most of the dynamics of the SLP gradient fields [von Storch and Zwiers, 2002]. In order to retain both the information of the wind direction—important to know towards where waves propagate—and the magnitude of the squared wind—which directly influence the magnitude of H_s— the principal component analysis is performed for $G_{xy} = [G_x, G_y]$, where $G_x^0 = G^0 \cos(\theta_w)$ and $G_y^0 = G^0 \sin(\theta_w)$. θ_w is the geostrophic wind direction, i.e. the direction of $\sqrt{G^0}$. The resulting ith leading PC (PC_i) represents the temporal evolution of the ith spatial pattern of G_{xy} (EOF_i). Each EOF is a vector of length $2M$, with the first(second) half describing the x(y) components of such pattern. Note that the directions of the winds associated with each EOF are "constant" over time. Constant is written between quotes because depending on the phase of each pattern (PC>0 or PC<0), the direction may vary 180°. To account for these variations, PCs are further divided into its positive and negative phase.

Secondly, for each chosen leading pattern EOF_i and each phase, the set of n_0 points of influence are calculated according to the following procedure. Essentially, for each target point m_P, a point m is considered as m_0 if the imaginary straight line between points m_P and m is within the sector comprising ± 90°around the direction defined by EOF_i at point m (wind direction) and it is not interfered by any land obstacle. Obviously, this method simplifies the real world situation, in which wave direction can be further modified by local phenomena like diffraction. Figure 19 shows an example of the n_0

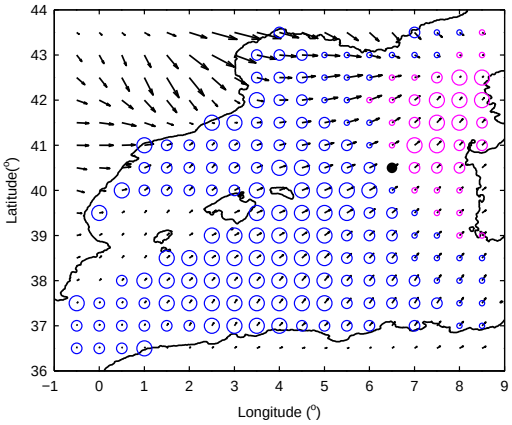

FIGURE 19: Example of the n_0 selected points of influence (circles) of a random target wave grid point m_P (black dot) corresponding to the positive (in blue) and negative (in purple) phase of the first atmospheric pattern EOF_1. Arrows illustrate the corresponding gradient field associated to the positive phase of EOF_1 (i.e. when $\mathrm{PC}_1 > 0$). The circle size denotes the directional dispersion associated to each point m_0, making use of the 5 directional bins (see Table 2) but joining those with the same absolute value.

selected points of influence for a random target wave grid point m_P and for the first leading pattern EOF_1, that could be related to a Mistral event (see Section 2.2).

With the aforementioned decomposition procedures the term Δ_{sw} in Eq. 8 is of the form:

$$\begin{aligned}\Delta_{\mathrm{sw}}(t,m) &= \sum_{i=1}^{N} \hat{a}^{+,i}_{\mathrm{EOF}}(m) \underbrace{\sum_{l=1}^{n_0^i}\sum_{k=1}^{n_f} \sqrt{K^{k,l,i}}\,\mathrm{PC}_i^{+}(t-\delta^{k,l}) G_{\mathrm{EOF}i}(m_0^l)}_{[*]} + \\ &+ \sum_{i=1}^{N} \hat{a}^{-,i}_{\mathrm{EOF}}(m) \underbrace{\sum_{l=1}^{n_0^i}\sum_{k=1}^{n_f} \sqrt{K^{k,l,i}}\,\mathrm{PC}_i^{-}(t-\delta^{k,l}) G_{\mathrm{EOF}i}(m_0^l)}_{[*]}, \end{aligned} \tag{11}$$

where $G_{\mathrm{EOF}i}$, the gradient field associated with the pattern $\mathrm{EOF_i}$, is defined as:

$$G_{\mathrm{EOF}i}(m) = \sqrt{\mathrm{EOF}_i{}^2(m) + \mathrm{EOF}_i{}^2(m+M)} \tag{12}$$

For each t, m and i, the term $[*]$ of Eq. 11 is a known value. Therefore, just the $2N$ coefficients $\hat{a}^{+}_{\mathrm{EOF}}(m,i)$ and $\hat{a}^{-}_{\mathrm{EOF}}(m,i)$ have to be estimated, along with coefficients $\hat{a}$, $\hat{a}_P$ and $\hat{a}_G$ of Eq. 8 (first $\Delta t = 0$ is considered). To select the optimal set of predictors, for each wave grid point m the F test is applied as similarly done by Wang and Swail [2006].

The second contribution to improve the statistical model (Eq. 8) is the term Δ_t, which takes into consideration that ocean wave generation is not an instantaneous process. Even when having a constant blowing wind, H_s gradually increases over a certain period

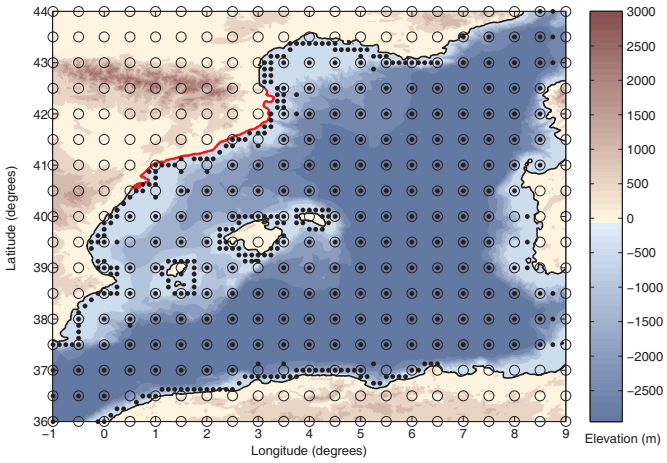

FIGURE 20: Study area (in red contour line the Catalan coast) and datasets (dots: H_s grid, circles: SLP grid).

of time until a fully developed wave field is formed. In a real case, in which wind speed constantly varies in magnitude and direction, a fully developed wave field is not always achieved. Therefore, H_s generally depends on both the forcing wind and the previous sea state conditions. This becomes specially relevant when simulating high-temporal resolution data, like in this thesis (3 h) and explains why the 3 hourly time series of H_s is a highly autocorrelated variable. Being different from Wang et al. [2012], only the one time step lagged H_s is included as an additional predictor (see Eq. 13), that can be interpreted as a discretisation of the first order time derivative of the wave action density balance governing equation:

$$\Delta_t(t, m) = \hat{\alpha} H_s(t-1, m) \tag{13}$$

The regression coefficient $\hat{\alpha}$ is estimated iteratively after the selection of the set of optimal predictors with the F test.

6.2 Calibration and validation

The method has been calibrated and validated for the study area using the hindcast data of the HIPOCAS project (see Section 3). Figure 20 illustrates the selected domain and the spatial resolution of, respectively, the SLP and H_s data. The domain coincides with that of the first (coarse) grid used for dynamical modelling, which includes most of the possible areas of wave generation responsible of swell waves approaching the Catalan coast. Despite the method being adapted and calibrated to the features of the study area, it could be tuned and applied to project the future wave climate of other regions.

HIPOCAS data are divided in two non-overlapping periods. The period 1971–2001 is employed to obtain the regression coefficients of Eq. 8 (calibration) whereas the remaining available period (1958-1970) is used to validate the model. The validation is made in three steps. First, the correlation coefficient map between H_s and $\hat{H}_s$ is employed to assess the spatial distribution of the model performance. Second, the Pierce skill score (PSS) and frequency bias index (FBI) [Lin and Wang, 2011] are used to evaluate the model prediction skill as a function of a range of H_s quantiles. The larger the PSS and the FBI closer to one, the more skilful the model is. Third, focusing on the Catalan coast, the relative error (RE) of $\hat{H}_s$ associated to three percentiles (50^{th}, 95^{th}, 99^{th}) is computed at the 40 nearest-coastal locations (see Figure 5 in Section 4).

Figure 21 shows the correlation coefficient maps obtained with (i) the method of Wang and Swail [2006] (left panel), i.e. with $\Delta_{\text{sw}} = \Delta_t = 0$ (Eq 8), and (ii) the proposed method in this thesis. With the model of Wang and Swail [2006], reasonable good results are achieved offshore (the correlation is around 0.8) but the performance is notably reduced near the coast (down to 0.5). By adding the terms Δ_{sw} and Δ_t, the correlation largely increases almost everywhere (achieving values around 0.9). This improvement in model performance is captured by the other skill measures. For example, Figure 22 illustrates the PSS and FBI scores associated to a wave grid point close to Barcelona (41.38° N, 2.18° E). In general, medium waves (around 60^{th} percentile) are the best predicted, which is reflected in a maximum in the PSS function and the FBI values getting closer to one. Lower waves tend to be overestimated whereas the opposite for higher waves. The proposed method (red line) maintains the bias pattern but significantly reduces the rate of over(under)estimation.

To investigate which factor contributes more to increase the model skill, several model configurations "in between" the model of Wang and Swail [2006] and the proposed method have been tested and inter-compared (eight settings in total). Especially, given the complexity of Δ_{sw}, simpler configurations to account for swell waves are investigated and the following conclusions are drawn. A large improvement is achieved by (i) just adding to the local predictors (P and G) the leading simultaneous PCs (considering neither a time lag nor involving the frequency/directional dispersion of waves) and (ii) adding the one-step lagged H_s to account for the temporal dependence (Δ_t term). By separating PCs into its positive and negative phase, the model skill increases but to a lesser extent. When including the swell representation with the full term Δ_{sw}, the model performs even better but the improvement is not very pronounced in general. This model response can be attributed to the short fetches of the study area and, possibly, a more significant improvement would be obtained when modelling H_s in near-shore areas affected by larger fetches (and therefore swell waves travelling longer distances). For the Catalan coast however, the improvement is more noticeable than for the rest of

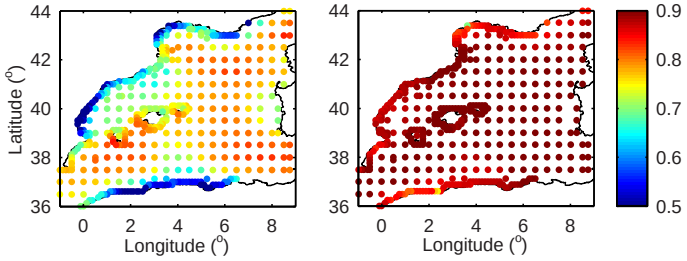

FIGURE 21: Correlation coefficient of all locations for the model of Wang and Swail [2006] (left), the proposed model (right).

the domain, being the average RE associated to the highest percentiles (95^{th} and 99^{th}) halved.

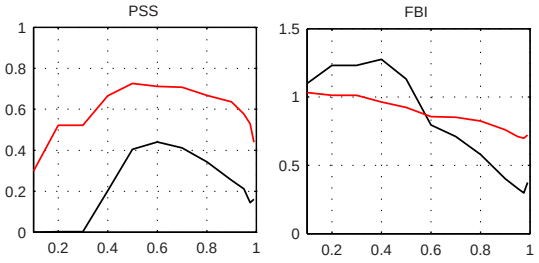

FIGURE 22: PSS(left) and FBI(right) close to Barcelona for: the model of Wang and Swail [2006] (black line) and the proposed model with (red line).

One important assumption in regression analysis is that residuals are Gaussian distributed. This assumption is likely violated here because H_s and most of predictors are non-negative data, which are obviously non-Gaussian. To evaluate the effect of the violation in the model performance, two options for transforming the data are explored: (i) the log-transformation and (ii) the Box-Cox transformation [Sakia, 1992]. The Box-Cox transformation, also used by Wang et al. [2012], involves a parameter λ that minimizes the deviation from the Gaussian distribution. For a positive variable X, the Box-Cox transformation is $(X^{\lambda} - 1)/\lambda$ except for $\lambda = 0$, that equals the log-transformation function.

The transformation of the predictand (H_s) alone worsens the model skill because it distorts the relationship between H_s and the squared SLP gradient fields. Applying the log-transformation to the predictand and the positive predictors (squared SLP gradients) is much better than transforming just H_s but it is generally not as good as without any transformation (in terms of the used performance skills). However, it is interesting to point out that the log-transformation (applied to all positive variables) improves the model performance for low-to-medium waves (up to 40^{th} percentile). This result is reasonable since the non-Gaussianity of H_s is more accentuated as getting closer to zero. Replacing the log-transformation with a Box-Cox transformation improves the prediction skill for medium-to-high waves but slightly worsens the skill for low waves.

Compared with the model without transformation, the Box-Cox transformation seems to improve the model performance offshore but substantially over-predicts large waves near the coast, as for example for the 99^{th} percentile of H_s along some stretches of the Catalan coast.

6.3 Wave projections

The calibrated proposed method (Eq. 8) is used to model present and future H_s scenarios using the 30-year SLP projections corresponding to the five combinations of RCM-GCM presented in Section 3 (the same as used for dynamical modelling, see Section 5). Despite having a few values $\hat{H}_s < 0$, the method without transformation is applied since this option presents the best skill for the Catalan coast area, the focus of this study. As for dynamical modelling, the median H_s is used to explore the changes in the mean wave fields and the 50-year return value of H_s (z_{50}) to investigate the extremes (see Section 5).

Figure 23 illustrates the projected median H_s. The upper rows show the present-day climatological values, whereas the lower rows show the projected relative changes in future climates, as similarly done in the presentation of the results obtained by dynamical modelling (see Section 5). HIR_E model has a clear positive bias (overestimation of projected H_s) whereas the other models show more similar present-day wave climates, with much smaller positive bias.

Results for the projected change of the median H_s are similar to those obtained by dynamical modelling but here the differences between GCMs are accentuated. For all RCMs driven by ECHAM5 (HIR_E, RAC_E, REM_E, RCA_E), the projected future changes share a common tendency for H_s to increase in the NE part of the domain (up to 10%). The increase is projected more offshore compared to dynamical modelling. In the SW part of the domain, H_s tends to decrease (up to 10%) but the extent of decrease varies between RCMs. HIR_E projects a more pronounced decrease; whereas the REM_E and RCA_E models project much more limited decreases.

In contrast, RCA_H (which is forced by HadCM3Q3 global model) projects a general decrease of the median H_s (up to 10%) over the entire domain (especially in the SE part). Close to the east-facing coasts, H_s reduction is smaller and in some stretches tends to remain the same or even to slightly increase. This spatial pattern of change is in qualitative agreement with the differences between the GCMs as presented in the study of Donat et al. [2010], which were highlighted in terms of the wave direction distribution (see dynamical modelling results, Section 5).

As similarly found by dynamical modelling, during winter the variability of H_s derived from using different RCMs is much lower than the one associated to GCMs. However, the differences among RCMs become larger for z_{50}, showing sometimes contrasting patterns of future changes (e.g. increase/decrease in the Northern part of the Catalan coast, not shown here). Differences among projections obtained by the two methods employed to project H_s (dynamical vs. statistical modelling) become larger when looking at the extremes, as would be expected, but still seem to be lower than the inter-model variability.

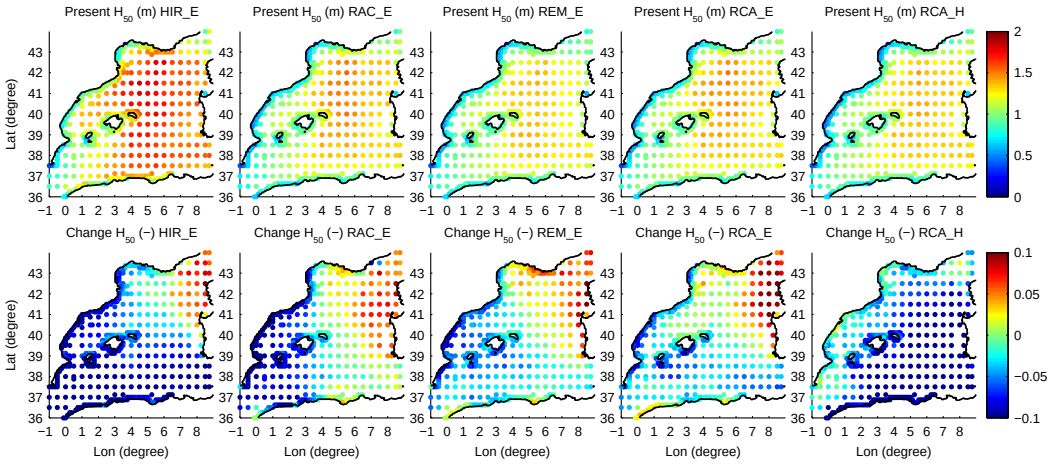

FIGURE 23: The present day-climate (upper panels) and future relative change (lower panels) of the median H_s using the proposed model without transformation.

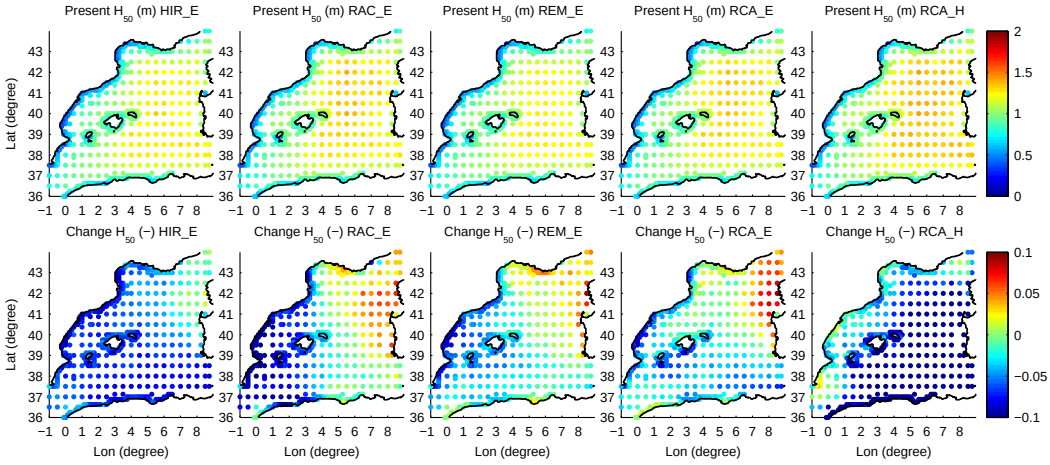

FIGURE 24: Same as Figure 23 but with the simulated SLP data being adjusted to the HIPOCAS baseline climate and variation scale.

To diminish the bias in the climate model simulations, another set of H_s projections has been carried out in which the SLP fields are adjusted to have the HIPOCAS baseline climate and variation scale. The corresponding results for the median H_s projections are shown in Figure 24.

After the simulated SLP data being adjusted, the bias for the present-day median H_s almost disappears completely, as would be expected. The adjustments also affect the projected changes in H_s; they attenuate the projected relative changes in general (especially for models driven by ECHAM5), although the pattern of change is maintained. The adjustment performed here is based on the mean climate but it would be interesting to see how other approaches (e.g quantile-matching adjustments) might affect the future projections. Note that statistical modelling is a flexible method thanks to the low computational cost, and can be used to easily perform additional simulations, for example, with various adjustment techniques.

Statistical modelling - Contributions

(1) Understanding the future wave climate

- Explore the variability of projected H_s as a function of the method to simulate wave climate.
- Find more robust climate change signals of H_s, i.e. when both dynamical and statistical modelling results agree.

(2) Improving methodological aspects

- Develop a (physical-based) statistical method to model H_s with high temporal and spatial resolution. Two terms are added to a multiple linear regression model of a previous study that mainly accounted for local wave generation. In the context of climate change, this computationally inexpensive tool can be very useful to analyse the uncertainty of future wave climate, as well as test the output of dynamical modelling.
- The first term involves swell waves by means of considering the frequency and directional dispersion of waves and makes use of the principal component analysis to simplify the forcing field in several patterns.
- The second term considers the serial correlation of H_s with the one-time step lagged H_s that is in agreement with the first order time derivative of the wave action density balance governing equation.

7 Coastal impact analysis

Waves are one of the climate change factors affecting coastal areas (see Figure 25), which are a focus for growing populations and economies [Nicholls and Kebede, 2012]. It is therefore important to assess the potential wave-driven coastal impacts in the context of climate change in order to design adaptation strategies to mitigate the associated negative effects.

In the last IPCC report (AR4) several impacts related with the sea-level-rise were addressed and quantified, such as beach retreat or inundation, but the effects produced by variations in the wave conditions were not properly evaluated. The AR4 concludes that changes in the wave climate are uncertain with a high regional variability and qualitatively explains the main consequent physical effects on coastal systems as follows: altered patterns of erosion and accretion, re-orientation of beach platform, enhanced high water levels and wave heights with risk of storm damage, episodic erosion, flooding and defence failure [Nicholls et al., 2007]. Recently, some studies have addressed some specific wave-driven impacts (mainly focusing on coastal erosion) for particular areas (but not for the Catalan coast) [eg. Adams et al., 2011, Coelho et al., 2009, Zacharioudaki and Reeve, 2011]. Hence, a study that appropriately covers all wave-driven impacts is needed in general but particularity for the study area of this thesis.

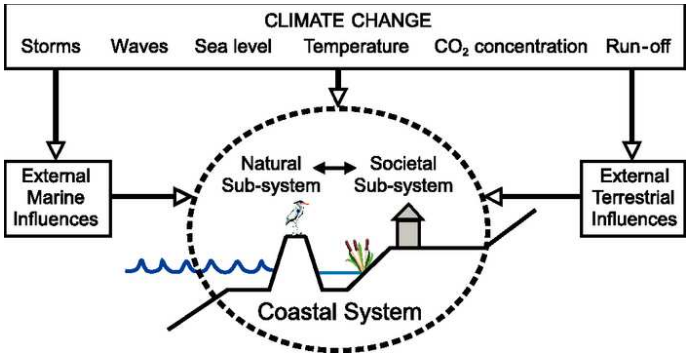

FIGURE 25: Climate change and the coastal system showing the major climate change factors [Nicholls et al., 2007].

Without being case-specific and from an engineering perspective, Section 7.1 provides an overview of the main (physical) impacts that changes in ocean wave patterns can have on coastal areas. Although they are analysed simply and generically, these impacts are quantified in order to give order of magnitudes of the degree of affectation that can serve as a guideline for further detailed local/regional coastal impact assessments. Details of this analysis can be found in Paper E.

Towards a first wave-driven coastal impact assessment for the Catalan coast (which is not meant to be completed in this thesis), Section 7.2 comprises the analysis of a

couple of case studies regarding the affectation of two types of coastal infrastructures: harbours and beaches. They deal with problems that currently threaten the Catalan coast (see Section 2.4.2) and that are very sensitive to changes in the wave direction, one of the wave parameters found to be more affected by climate change in this area (see Sections 4 and 5). First, the impact on harbour agitation of a commercial harbour is presented and, second, the effect on the long-shore sediment transport, that is directly related with the long term beach erosion/accretion, is analysed for the Catalan (sandy) beaches. Details of the first case study can be found in Paper B (including the analysis of two other harbours). A paper covering the second case study is under preparation in collaboration with Dr. Kathleen McInnes and Dr. Mark Hemer (from CSIRO). However, a similar (but simpler) study can also be found in Paper B, at a coarser scale and using a different wave forcing dataset.

7.1 Wave-driven coastal impacts

Table 3 presents the wave-induced processes and consequent coastal impacts identified in this thesis that are relevant for coastal and port engineering. They are grouped in three categories according to whether they affect (sandy) beaches, harbours or coastal structures in general. Their relationship with mean and extreme wave climates is qualitatively indicated as high (H), low (L) or none (N).

Beaches are mainly affected by the following wave-induced processes: long-shore sediment transport (LST), cross-shore sediment transport (CST) and wave run-up. As waves approach the coast, they break and generate a long-shore current which moves beach material in parallel to the coast causing the LST. This process, driven by the mean wave climate, controls the long term beach dynamics and the patterns of erosion and accretion since the volume variation of sediment is results from the alongshore gradients in LST rates. At event or seasonal time scale, erosion/accretion can also occur due to CST, which governs the short term beach dynamics and encompasses both offshore and onshore transport. Finally, waves contribute to beach inundation due to the uprush of water from wave action which is the combination of the wave set-up and the wave swash (i.e. wave run-up) caused by waves breaking in the near-shore. Both CST and wave flooding are mainly forced by the extreme wave climate.

TABLE 3: Analysed processes, their impacts, the parameter estimated (and the method used for evaluation) and their relationship (H, high; L, low; N, none) to mean and extreme wave climates. (LWP: linear wave propagation, BM: Boussinesq-type numerical model)

System affected	Process	Impact	Parameter estimated	Formula/Method	Mean wave climate	Extreme wave climate
Beaches	Longshore sediment transport (LST)	Erosion/accretion	Volume variation	SPM [1984]	H	L
	Cross-shore sediment transport (CST)	Erosion/accretion	Erosion potential	Jiménez et al. [2012]	L	H
	Wave run-up	Flooding	Distance flooded	Mase [1989]	N	H
Harbours	Wave propagation within the harbour	Agitation	Wave height inside the harbour	LWP + BM	H	L
	Sediment transport close to the harbour	Siltation	Siltation rate	LWP + BM + Zhang et al. [2009]	H	L
Coastal structures	Wave action	Instability	Block weight needed	LWP + Hudson [1961]	N	H
		Overtopping	Discharge	LWP + Pullen et al. [2007]	L	H
		Scouring	Scour depth	LWP + Sumer and Fredsøe [2000]	L	H
	Wave reflection	Erosion/accretion, agitation	Reflected wave height	LWP + Sorensen and Thompson [2002]	H	H
	Wave transmission	Erosion/accretion, agitation	Transmitted wave height	LWP + D'Angremond et al. [1996]	H	H

Regarding coastal structures in general, changes in the wave climate can affect structure stability or induce overtopping, scouring, excessive wave reflection and/or wave transmission. The involved wave processes are typically controlled by the extreme wave climate, except for the last two, for which the mean wave climate is also relevant. Hydrodynamic forces produced by wave action can affect the stability of a typical rubble-mound structure and produce scouring at the toe, entailing a risk of structure failure. In addition, if wave run-up exceeds the structure freeboard, water flows over the structure producing a certain discharge that can affect the operability and safety behind or on top of the structure. Wave reflection and wave transmission are complemented wave processes that can result in areas of undesired excessive agitation and/or sediment erosion/deposition. After the impact of a wave train on a structure, wave reflection depends on the portion of wave energy that is diverted or propagated to another direction whereas wave transmission is related with those waves passing over and through the structure.

Ports are (singular) semi-enclosed coastal structures likely to be affected by changes in wave conditions. The effect on the wave patterns inside a harbour are of great importance because they directly affect its safety and operability. For example, certain port operations cannot be carried out when H_s at the harbour berth exceeds a certain threshold. Obtaining H_s inside the harbour is not straightforward because it results from the interaction of several wave processes: shoaling, refraction, diffraction and reflection. Meanwhile, changes in the incident wave conditions affect not only the agitation inside the port but also the (sediment) siltation rate at the harbour mouth, which can lead to obstruct shipping at the harbour entrance.

The aforementioned processes/impacts are assessed for the cases described in Table 4, which are based on the ranges of variation (at deep water) of typical wave parameters (H_s, T_p and θ_m) obtained by recent global-scale studies of climate change [Hemer et al., 2012, Mori et al., 2010]. Also, these studies are used to establish the range of their current values ($H_{s,P}$, $T_{p,P}$ and $\theta_{m,P}$). In general H_s and T_p vary together because they both depend on the wind speed w_{10} ($H_s \propto \mathrm{w}_{10}^2$ and $T_p \propto \mathrm{w}_{10}$ for fully-developed wind-sea states) resulting in $T_p \propto \sqrt{H_s}$ [Resio et al., 2002]. Owing the non-linear relation between H_s and w_{10}, the extreme wave climate is expected to suffer from more alterations than the mean wave climate (see Section 5). This is manifested in the employed values for case I. For coastal areas with prevailing swell waves (some coasts that bound a large ocean), T_p variations do not necessarily follow those of H_s, as seen by Hemer et al. [2012], because waves are no longer a direct function of the local wind speed. This situation of swell predominance is only studied for mean wave conditions (case II) since stormy (extreme) wave conditions are generally associated to wind-sea states. Changes in θ_m (case III) are investigated separately (although in a real case they might interact with changes in H_s and T_p) and only for the mean wave climate because wave impacts affected

by extreme wave conditions (e.g. structure failure) typically assume perpendicular waves (the most unfavourable wave incidence).

TABLE 4: Cases considered of changes in the wave conditions (subscripts P and F denote "present" and "future" situations, respectively).

Case	Mean wave climate	Extreme wave climate
I. Both H_s and T_p vary	$0.9H_{s,P} < H_{s,F} < 1.1H_{s,P}$ $0.95T_{p,P} < T_{p,F} < 1.15T_{p,P}$ $\theta_{m,F} = \theta_{m,P}$	$0.8H_{s,P} < H_{s,F} < 1.2H_{s,P}$ $0.9T_{p,P} < T_{p,F} < 1.1T_{p,P}$ $\theta_{m,F} = \theta_{m,P}$
II. Only T_p varies	$H_{s,F} = H_{s,P}$ $0.95T_{p,P} < T_{p,F} < 1.15T_{p,P}$ $\theta_{m,F} = \theta_{m,P}$	-
III. Only θ_m^1 varies	$H_{s,F} = H_{s,P}$ $T_{p,F} = T_{p,P}$ $\theta_{m,F} - 10\ ^\circ < \theta_{m,F} < \theta_{m,P} + 10\ ^\circ$	-

[1]In this section, θ_m is measured as the angle between the wave front and the shoreline or structure orientation.

The parameter estimated for each process/impact is indicated in Table 3 as well as the method used in this thesis for its evaluation. Given the objective of obtaining orders of magnitude, simple empirical formulas are employed (references included in Table 3) except when computing the wave patterns inside a harbour (for which a Boussinesq-type numerical model has been used, denoted as BM in Table 3). When necessary, linear wave propagation (denoted as LWP in Table 3) is additionally applied to convert wave parameters from deep water to shallow water (where some of the formulas used are defined). Also, some computations have required to make additional assumptions as, for example, the dimensioning of the structures (they are correspondingly detailed in Paper E).

Table 5 summarises the results obtained which are expressed as a percentage between the future and the present value of the corresponding parameter used to estimate each process/impact (Table 3). When necessary, results are separated between ports and coastal environments because the corresponding structures typically have different dimensions and are situated at different depths (e.g. harbour breakwater vs. coastal seawall) which affect the final results.

Table 5 illustrates that changes in H_s and T_p strongly affect overtopping discharge, stability and scouring and, to a lesser extent, siltation, wave transmission, LST and port agitation. Beach flooding and wave reflection vary at the same rate as H_s, while following a sub-linear function for CST case. Changes in T_p alone affect significantly port siltation, whereas the other processes vary at a lower rate than T_p.

Among the processes studied for θ_m changes (the same as for variations of T_p alone) the most affected process is clearly the LST, which can suffer from relative variations over

TABLE 5: Relative variation between present and future values of the parameters specified in Table 3, driven by the cases described in Table 4. In brackets values corresponding to extreme wave climate.

Process/Impact	Domain	Case I	Case II	Case III
LST	Coasts	-23% to +27%	-2.3% to +1.1%	-296.4% to 264.8%
CST	Coasts	[-5% to +5%]	-	-
Flooding	Coasts	[-20% to +20%]	-	-
Agitation	Ports	-13% to +12%	-3% to +2%	-22% to 20%
Siltation	Ports	-37% to +35%	-15% to +17%	-24% to 21%
Instability	Coasts	[-52% to +87%]	-	-
	Ports	[-48% to +72%]	-	-
Overtopping	Coasts	[-73% to +159%]	-	-
	Ports	[-83% to +249%]	-	-
Scouring	Coasts	[-38% to +47%]	-	-
	Ports	[-52% to +75%]	-	-
Wave reflection	Coasts	[-19% to +19%]	-1.8% to +1.9%	<0.2%
		-10% to +10%		
	[Ports	-19% to +19%]	-1.4% to +1.5%	<0.2%
		-10% to +10%		
Wave transmission	Coasts	[-30% to +33%]	-1.7% to +2%	0% to 1.4%
		-15% to +20%		
	Ports	[-33% to +39%]	-0.2% to +0.2%	0% to 1.4%
		-10% to +12%		

100%, depending on the incident wave direction. In Figure 26, the variation in LST is plotted as a function of the present θ_m and the difference between the future and present θ_m. For $\theta_{m,P} < 45°$ (low wave incidence angles), the smaller the value of $\theta_{m,P}$, the greater the changes in LST rates, and the contrary for $\theta_{m,P} > 45°$ (high wave incidence angles). The minimum relative changes are obtained for $\theta_{m,P} = 45°$ because this angle produces the highest present LST rate. Note that for $\theta_{m,P} = 90°/0°$ (parallel/perpendicular incidence to the shoreline), the present LST rate is zero, so the relative changes would be infinite.

The main general conclusion of this analysis is that plausible (moderate) changes in wave conditions can greatly affect coastal systems due to the nonlinear relation governing many of the processes studied. Therefore, it is necessary to raise awareness among coastal and port authorities and other stakeholders about the potential impacts of climate change on coastal areas.

In the case of harbours, increases in wave height could force port authorities to make large investments to reinforce breakwaters against instability or to increase their freeboard to limit overtopping discharge. In addition, major changes to port layout or the design of new structures could be necessary due to changes in wave direction in order to avoid excessive siltation or agitation. Coastal defence structures or new coastal planning

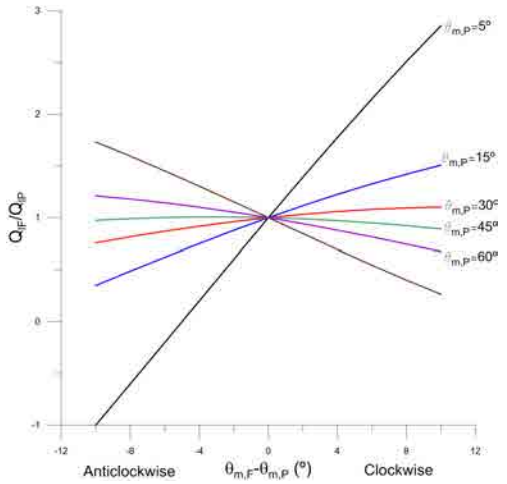

FIGURE 26: Relative variation of LST rate ($Q_{l,F}/Q_{l,P}$) as a function of $\theta_{m,P}$ and $\theta_{m,F} - \theta_{m,P}$.

measures can be necessary as well (or the modification of the existing ones) to prevent from significant variations in beach dynamics. All of these measures will obviously entail a considerable cost.

The next step for impact evaluation is an integrated assessment that takes into account socio-economic aspects [Nicholls et al., 2008] (see Section 9). This will facilitate the inter-comparison between different impacts (that in this study is limited to the physical parameters used for evaluation) and determine (and give priority to) the adaptation measures.

7.2 Case studies

7.2.1 Harbour agitation

According to the Catalan Government's 2007-2015 Port Plan, one of the most common problems affecting the functionality of Catalan ports is the high degree of agitation inside them. It is therefore necessary to study the possible intensification of this phenomenon caused by future changes in the wave climate. Almost all Catalan harbours have entrances oriented towards the SW because the current predominant storms in the Catalan coast are from E and NE. Thus, an increase of, for instance, S waves (projected in some cases by trend analysis and dynamical modelling, see Sections 4 and 5) will consequently increase the waves in port berths, which could affect the safety and comfort of moored vessels. As a function of the port activities, the Spanish Port Authority recommends a maximum value of H_s (among other climate variables) above which the port operations should be stopped. For instance, for leisure crafts the maximum value accepted for safe mooring is $H_s = 40$ cm with perpendicular incidence [Puertos del Estado].

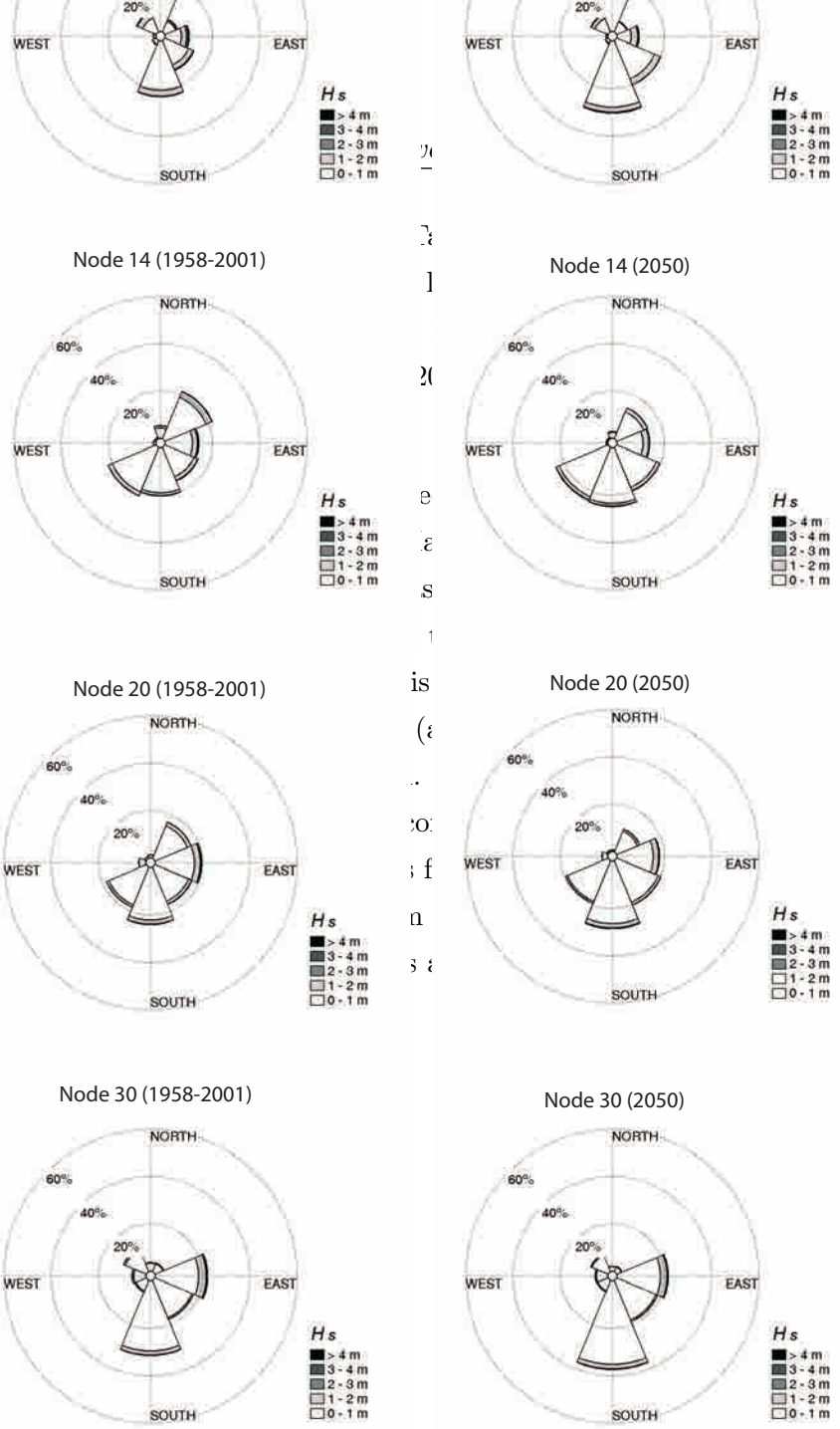

FIGURE 27: Wave roses for the "present" situation (left) and the future extrapolation (right) obtained by trend analysis for node 30 (see Section 4).

From the set of all wave conditions defined by the waves roses of Figure 27, just the waves capable of entering the harbour are considered, which correspond to the following directions: E, SE, S and SW (denoted as "effective" directions). For each of these effective wave directions, 5 values of H_s are considered (0.5, 1.5, 2.5, 3.5 and 5) m, as representative values of the 5 groups used to build the corresponding wave roses ([0–1], [1–2], [2–3], [3–4], > 4) m. T_p is computed as a function of H_s according to $T_p \propto \sqrt{H_s}$. Taking into account that the outer boundaries of the harbour domain correspond to

shallow/intermediate depths, the selected (deep water) wave conditions are propagated to this boundary by linear wave theory previous to the numerical simulations.

The numerical simulation provides, for each grid point inside the harbour(spatial resolution is 5 m), a value of H_s and the corresponding agitation coefficient k_a (the ratio between H_s inside and outside the harbour). Figure 28 illustrates, as an example, the results obtained for waves coming from E and S, respectively, forced by $H_s = 2.5$ m at deep water. As expected, agitation inside the harbour is clearly greater for waves coming from the south than for those coming from the east. For E waves, H_s is less than 20 cm in large areas of the harbour basin and does not exceed 40 cm at any interior point. For S waves, H_s is less than 20 cm at only few points, while in many areas the wave height exceeds 40 cm, even reaching 80 cm in some places.

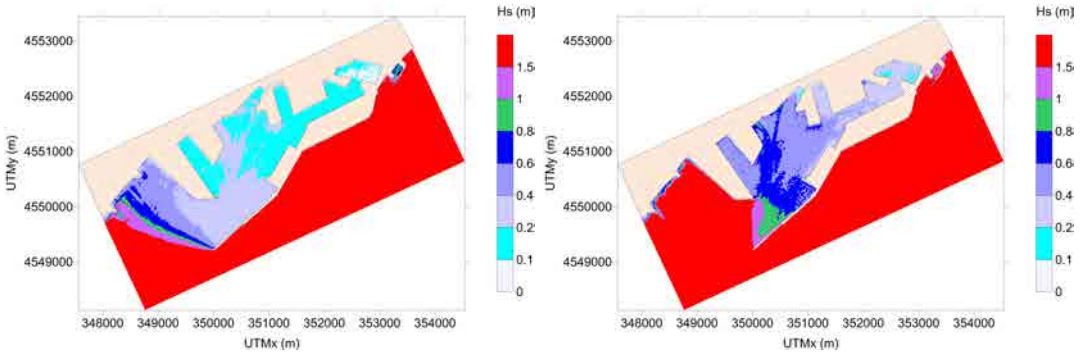

FIGURE 28: H_s obtained with numerical simulation at Tarragona port forced incident $H_s = 2.5$m at deep water. Left panel: waves from E. Right panel: waves from S.

In general, k_a is found to be larger for the group of lowest waves entering the harbour, tending to an asymptotic value of k_a between 0.1 and 0.3 as incident H_s increases (see Figure 29). This is an expected behaviour since lower waves have shorter periods and, as a consequence, they are shorter and diffract less in the harbour entrance. In other words, low waves are proportionally less damped than higher waves. On the contrary, for SW waves k_a surprisingly increases with H_s, which can probably be explained by the generation of reflected waves. This pattern is a bit worrying because large values of k_a coincide with large values of H_s. However, thanks to the fetch configuration, these high energetic wave conditions coming from SW have a low probability of occurrence (see Figure 27).

Involving the annual frequencies of the wave roses, the spatial-average of H_s in Tarragona harbour is: 0.11 m for the "present" and 0.13 m for the future, which entails a statistically significant relative increase of 11%. Taking into account the current activities undertaken at this harbour berths and the Spanish Port Authority recommendations [Puertos del Estado], the consequent reduction in the number of hours of operability per year is considerably low [Riba Monzó, 2010]. Anyway, in order to derive a robust

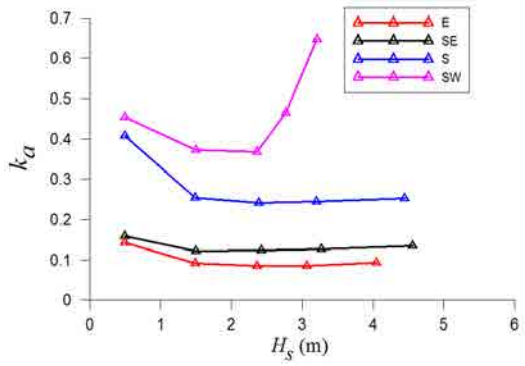

FIGURE 29: Spatial-averaged k_a for each effective direction as a function of H_s entering the port.

conclusion, a range of plausible future wave scenarios should be considered (e.g. those obtained by dynamical modelling). Note that k_a greatly varies as a function of the incoming wave direction (see Figure 29) which implies that Tarragona harbour agitation is very sensitive to changes in the wave direction, i.e., little variations of this parameter can induce large variations in k_a.

7.2.2 Longshore sediment transport

As mentioned in Section 2.4.2, erosion is a current problem of many Catalan beaches. This section assesses the effect of changes in wave climate on the beach longshore sediment transport (LST) along the Catalan coast, which is related with the long term patterns of beach erosion/accretion. The formula of Bayram et al. [2007] is employed, which takes into account not only the forcing wave climate but also the beach geomorphology. Bayram's formula is based on the well-known CERC formula in which the constant of proportionality between the long-shore wave energy flux and LST, denoted as K (see Eq. 14), is estimated as a function of wave and sediment properties (see Eq. 15).

$$Q = \frac{K\rho}{16(\rho_s - \rho)(1-a)} H_{s,b}^2 C_{g,b} \sin 2\alpha_b \tag{14}$$

$$K = f\left(\frac{H_{s,b}}{\mathrm{w}_s T_p}\right) \tag{15}$$

Q is the LST produced by the wave conditions at breaking (denoted with the subscript b) defined by: the significant wave height ($H_{s,b}$), the group velocity $C_{g,b}$ and the angle between the wave crest and the coastline (α_b). ρ is the density of water ($\rho = 1026$ kg/m^3), ρ_s is the density of sand ($\rho_s = 2650$ kg/m^3) and a is the porosity index ($a = 4$). w_s is the sediment settlement velocity which is estimated as a function of the median sediment grain size (d_{50}) using the formula of Jiménez and Madsen [2003].

The coastline orientation and the sediment grain size are obtained from CIIRC [2010] (see Section 3) and are assumed to remain constant in the future. In this case study, the wave forcing is obtained from the present/future wave projections performed by dynamical modelling (that were obtained from 5 combinations of RCM-GCM, see Section 5). The use of this forcing database allows: (1) to assess the future impact on LST at the Catalan coast involving explicitly the greenhouse effect (as done for the first time in this area) and (2) to evaluate how inter-model (atmospheric) climate variability and climate biases translate to coastal impacts through the wave driver (which has been little explored before).

To compute LST (Eq. 14), the wave climate is discretised in groups of H_s and θ_m (like for the wave roses generated in Section 4.2) and their representative wave conditions are propagated to the breaking point using the linear wave theory. The associated T_p is obtained after averaging all period values corresponding to each wave group. Finally, the annual (net) LST is computed using the mean frequency of occurrence of each 30-year period (present, 1971–2000[7], and future, 2071–2100)

Figure 30 illustrates the results of the present period for the 5 combinations of RCM-GCM: HIR_E, RAC_E, REM_E, RCA_E, RCA_H. Additionally, the LST generated by the wave climate of HIPOCAS project for the same period (see Section 3) is included as a reference situation in order to qualitatively estimate the climate model biases in terms of LST. Positive values (red colour) denote LST going from north to south (see arrow in Figure 30), whereas the opposite for negative values (in blue).

Except for the HIR_E case, all models are capable to reproduce the existing prevailing positive LST pattern [CIIRC, 2010]. Also, they correctly simulate the negative(positive) LSTs north(south) of the Ebre Delta. However, LST is in general not very accurate where the orography is very irregular, for example south of Cape Creus. This can be probably caused by the linear wave propagation method.

The RCA_E-driven wave climate produces the lowest values of LST, which is in agreement with the low values of the median H_s (see Figure 14 in Section 5.4.1). On the contrary, RCA_H is associated to the largest rates of LST even though the associated median H_s is similarly low too (see Figure 14 in Section 5). RCA_E and RCA_H were obtained with the same RCM, that tends to underestimate the forcing (extreme) wind field (see Section 3). However, the parent GCM is different which can explain why RCA_H (that simulates a larger fraction of E waves) contributes to larger values of (positive) LST.

[7]Except for REM_E for which it is 1981–2010 (see Section 3)

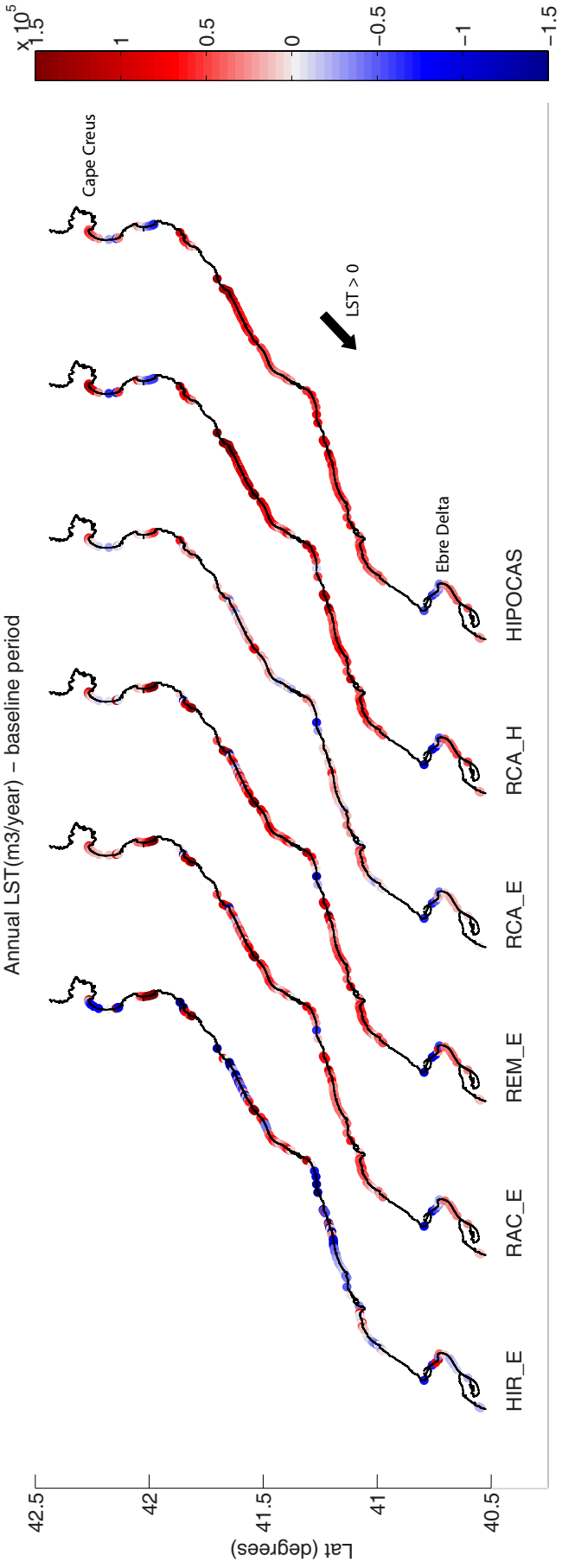

FIGURE 30: LST (in m^3/year) along the Catalan coast corresponding to the present period of HIPOCAS data and the 5 RCM-GCM-driven wave scenarios obtained by dynamical modelling.

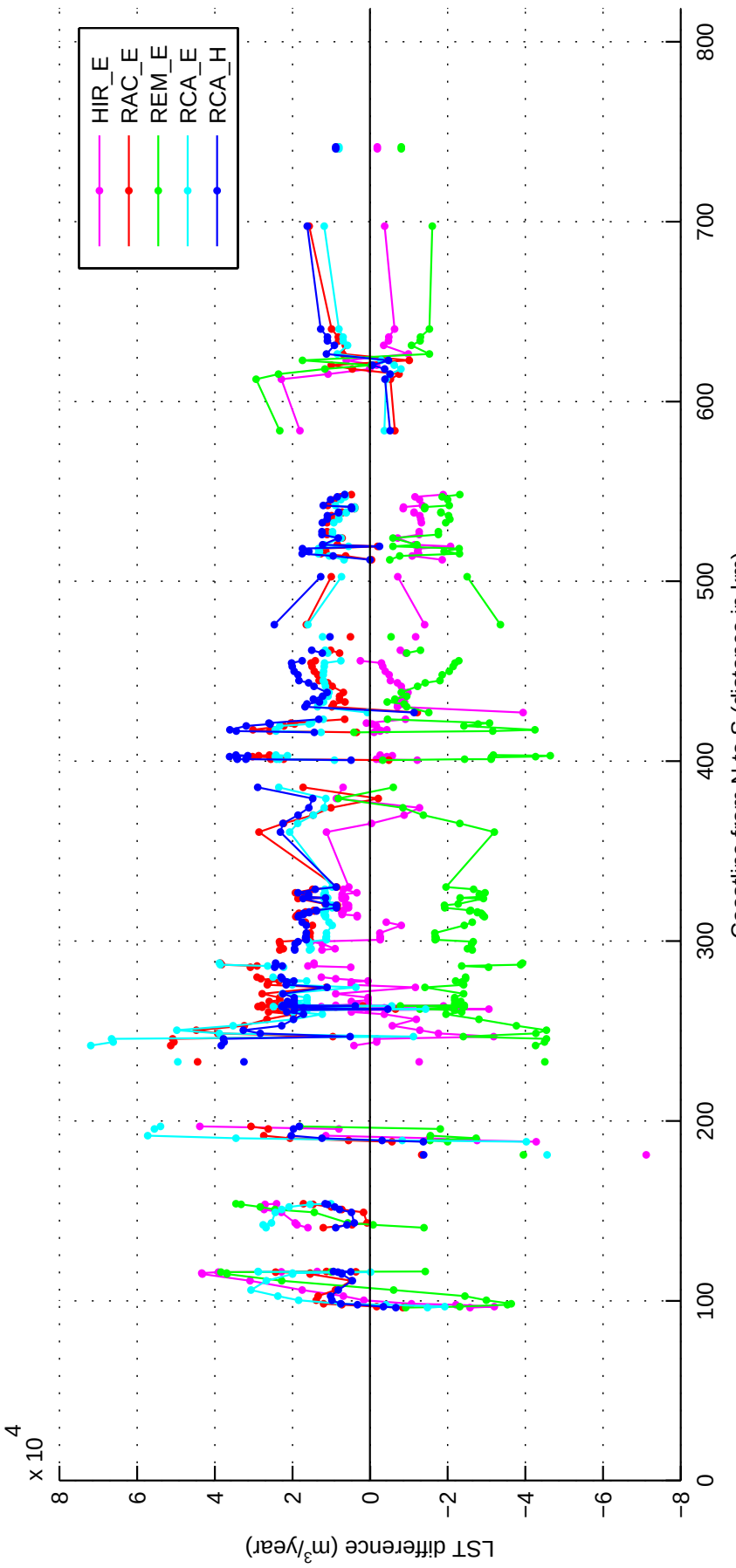

FIGURE 31: Projected absolute change in LST (in m^3/year) along the Catalan coast corresponding to the 5 RCM-GCM-driven wave scenarious obtained by dynamical modelling.

HIR_E-driven wave climate clearly reproduce an erroneous negative LST pattern for the baseline period. This suggest that discrepancies in the wave climate (that were not as accentuated as here) can be notably enhanced in terms of LST due to the non-linear relation between wave parameters and LST (see Eq. 14). Actually, integrating both H_s and θ_m information, LST can be understood as a parameter that indirectly check climate models capability to correctly reproduce the current (wave) climate.

Figure 31 illustrates absolute projected changes of LST as a function of the distance along the coastline (from N to S) projected onto the x-axis. Most of the simulations project a general rise in LST, in most cases around 10,000–20,000 m^3/year. A similar value, but with opposite sign, is found for the REM_E case (green line). For the majority of realisations, this corresponds with a relative variation of about 50%, except for RCA_E which, due to the lower current rates, presents considerable higher relative variations (>100%). Again, the non-linear LST equation (Eg. 14) explains why moderate changes of wave parameters can lead to large variations in LST.

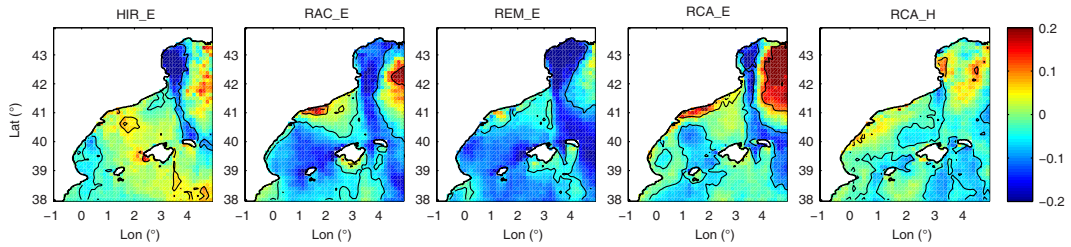

FIGURE 32: Projected relative change in the mean H_s for waves coming from NE during winter, associated to the 5 RCM-GCM models (using dynamical modelling).

At first sight, it is surprising to see how only REM_E is associated to a general future decrease of LST. During the (most energetic) winter season, RCA_E, RCA_E and REM_E models all projected a rise of the frequency of S-SW waves in detriment of NE-E waves (see Figure 5.4.2). That suggested a decrease in the LST, as obtained just for REM_E. It is necessary to analyse the wave projections in more detail to find the reason of these apparent discrepancies. Close to some Catalan coastal stretches, it is found that, for instance, H_s associated to waves coming from NE tends to increase for RAC_E and RCA_E models, despite the frequency of NE waves decreasing (see Figure 32). In other words, θ_m and H_s variations can produce competing LST changes (as pointed out by Charles et al. [2012]), being not trivial to anticipate the resulting net LST at first glance. In this case, H_s-driven LST variations prevail over those produced by changes in θ_m. Certainly, local scale response of coastline to broader scale changes in wave climate is a challenging problem, in this case reflected in the disparity of LST results.

Coastal impact analysis - Contributions

(3) Assessing wave-driven coastal impacts

- From an engineering perspective, review and quantify the potential wave-driven coastal impacts in order to determine the most affected coastal processes.
- For the first time, analyse the impact of changes in wave climate on harbour agitation, an operational problem already present in some Catalan ports.
- Study the climate biases and inter-model variability in terms of LST, a process closely related to coastal erosion, which is one of the most important problems currently threatening the Catalan beaches.

8 Summary and conclusions

This section presents the conclusions drawn from the thesis work as long as it summarises the main findings. It is structured in three parts responding to the three research objectives formulated in this thesis and presented in Section 1.2.

(1) Understanding the future wave climate

The possible future variations of wave conditions approaching the Catalan coast have been firstly assessed by trend analysis with especial emphasis on the wave direction θ_m. A novel methodology based on linear regression analysis and bootstrapping that takes into account the nature of the data have been developed and applied to 44-year time series of wave hindcast data. The results thus obtained can be summarised as follows:

- The total amount of wave energy seems to remain constant or even to decrease for both mean and extreme conditions.
- For some locations, the tendency associated to wave storminess E_s for particular directions differs from the total one. For example, E_s associated to N(S) waves tends to significantly decrease(increase).
- The wave direction distribution varies too. In general, the frequency of waves coming from N-NE is estimated to diminish whereas the opposite for the SE-S-SW sector. That occurs for both the mean and extreme climate but in the latter case the variations are not statistically significant due to the large uncertainty.

The previous results underscore the importance of involving the wave direction in the trend analysis. Regardless of what happen to the total wave energy, significant changes in the distribution of θ_m might occur which could entail important coastal impacts.

To overcome the limitations of the trend analysis (e.g. trend shape assumption) and to involve directly the greenhouse effect, high-resolution present/future wave climate scenarios have been simulated for the first time in the NW Mediterranean Sea. The SWAN wave model [Booij et al., 1999] (dynamical modelling) has been forced by surface wind fields obtained from 5 combinations of regional and global models RCM-GCM (allowing to study the inter-model variability) driven by the most recently used A1B greenhouse gas emission scenario. The generated wave output consists of the typical wave spectrum parameters (significant wave height H_s, peak wave period T_p and mean wave direction θ_m), which have been analysed

in relation to the forcing 10-m wind speed (w_{10}). The general concluding remarks are:

- Maximum rates of projected changes in H_s are around $\pm 10\%$ for mean conditions (50^{th} percentile of H_s) versus $\pm 20\%$ for extreme climate (50-year return value of H_s, z_{50}). The larger rise in the latter case can be explained by the larger presence of wind-sea states during stormy conditions (less influence of swell waves), for which the relationship $H_s \propto w_{10}^2$ is more applicable (although not strictly because waves might not be fully-developed)
- Patterns of H_s variations are similar to those of w_{10}, however, the magnitude of change is enhanced or attenuated depending on the fetch configuration (for the Catalan coast, waves coming from the NE-E-SE sector have favourable fetch conditions).
- Despite the presence of swell influencing the relationship between H_s and w_{10}, it does not seem to greatly affect the correlation between H_s and T_p. Contrary to what may happen in large oceans, T_p varies at a rate similar to that of $\sqrt{H_s}$.

To better understand how and why wave climate will react to climate change, the analysis of wave projections has been divided into seasons because they are typically controlled by different atmospheric patterns. For the (most energetic) winter season, the following conclusions can be drawn:

- Regarding the mean wave climate, a general moderate decrease of H_s is projected in agreement with the same tendency of w_{10}. By contrast, in the NE part of the domain (close to Genoa cyclogenesis area), both variables tend to increase. REM_E and RCA_H have a lower rate of increase (being the latter, the one forced by a different global model).
- The differences between the two GCMs are accentuated in terms of the wave direction distribution leading to opposite patterns of change. HadCM3Q3-driven wave climate (RCA_H) predicts a greater frequency of NE-E-SE waves, whereas the S-SW and NW components tend to rise when driven by ECHAM5. These discrepancies can be explained by the different generation of W-E wind (flow) of the respective GCMs, which is accentuated in terms of the wave climate when the fetch configuration is favourable.
- The discrepancy between GCMs is reflected in the changes in the wind-sea/swell distribution too. The GCM that simulates an increase in the E component (HadCM3Q3) is associated with an increase in the mixed sea states along the Catalan coast.

- The variations associated to stormy conditions have a larger uncertainty, being the inter-model variability not only due to GCMs but also RCMs. For the HadCM3Q3 model, z_{50} tends to rise along the Catalan coast probably due to the aforementioned increase of (fetch-favourable) E waves.
- The large disagreement between GCMs, specially in terms of the wave direction distribution, questions the (nowadays frequent) use of ensemble projections. This thesis results suggest that such an ensemble has to be done with care: at least wave projections should be separated as a function of the parent GCMs.

As expected, during summer wave climate is affected by climate change in a different manner because of the different atmospheric processes involved, like land-sea temperature gradients. In that respect, the following differences can be highlighted:

- For the mean wave climate, H_s tends to increase in the SW part of the domain which might be related with the centre of cyclones located in the Iberian peninsula during summer. The increase translates northwards as regards to the extreme wave climate.
- In general, a larger agreement is found among model realisations, both RCMs and GCMs contributing similarly to the inter-model variability.

Dynamical modelling is computationally expensive which results in a limited capacity to explore the full range of uncertainty associated to climate projections. In this regard, statistical modelling is a powerful alternative which, in addition, can avoid the use of (the usually more biased) wind fields. This thesis proposes an improved statistical method to model high-resolution H_s from the sea level pressure field (a more robust variable compared to wind speed). Special focus has been given to the swell component of waves, whose inaccurate resolution has typically limited the applicability of statistical methods. The method has been applied for the winter season forced by the aforementioned 5 combinations of RCM-GCM. The results thus obtained have been compared with those corresponding to dynamical modelling leading to the following conclusions:

- From a regional perspective, a large agreement between the two wave modelling techniques is obtained for the mean wave climate. The median H_s has a similar pattern of change with the same rate of variation ($\pm 10\%$). More discrepancies arise as reducing to local scale: the area of H_s increase is projected more offshore with the statistical model. Also, statistical modelling projects a larger difference between results obtained with the different two GCMs.

- With regards to extreme waves, the same range of variation of z_{50} is projected ($\pm 20\%$) but the simulated future climate is not necessarily consistent with that obtained by dynamical modelling (RAC_E and RCA_H are especially in disagreement). However, it is interesting to point out that the inter-model variability (including both RCMs and GCMs) is higher than the variability between the two wave modelling methods.

(2) Improving methodological aspects

This thesis has involved the generation and study of a large amount of climate data for which a rigorous data analysis has been carried out. If necessary, the use of "conventional" methodologies has been substituted by new approaches that are more appropriate since they take into consideration the nature of the data. In that respect, the following conclusions have been derived:

- Climate data (in particular wave data) are in general non-Gaussian distributed whereas many statistical methods assume a Normal distribution. Therefore, these methods should be used with care, previously transforming the data accordingly. At least, the effect of the violation of the Gaussian assumption has to be explored. In this thesis, a log-transformation or Box-Cox transformation is used for the positive data (e.g. H_s)
- The evolution of the magnitude of a non-frequent extreme event (e.g. E_s of S storms) has been successfully evaluated my means of involving the logistic regression to estimate the event occurrence.
- Wave direction is a variable little addressed in trend analysis studies, probably due to its circular (complex) character. This thesis proposes to analyse this variable by means of the occurrence of directional sectors. To operate with these (non-Gaussian distributed) frequencies (e.g. to perform a regression analysis) the use of ilr-transformation is proposed which avoid the spurious effects of these compositional data.
- The uncertainty (and evaluation of significant projected changes) has been assessed by bootstrap-based techniques. If adequately modified, bootstrapping is shown to be a simple but effective method to study the uncertainty. For example, in order to evaluate the variability of high-temporal resolution data, the method can be adapted to account for the time-autocorrelation and better reproduce the extremes.

In addition, a new method of statistical modelling has been proposed in order to improve the simulation of high-spatial and temporal resolution H_s. It is based on a previous study that uses multiple linear regression analysis to model H_s

from local conditions of sea level pressure (SLP) and the corresponding spatial gradients. The model development has specially focused on the performance at near-shore areas where is important to correctly reproduce the swell component of waves. Also, the H_s serial correlation has been considered which is an essential issue for high-temporal resolution H_s driven by highly variable wind conditions, as in the study area. The two major contributions are:

- Swells are taken into account with a complex term, which expression is based on the frequency-directional dispersion of waves, including lagged values of the principal components of the squared SLP gradient fields. Validation results show that just accounting for swell waves in a simpler manner (only using the simultaneous principal components) greatly improves the model performance near-shore. The use of the full term developed in this thesis additionally increases the model skill but to a lesser extent, probably due to the short fetches of the study area.
- Time-dependence of H_s is introduced by incorporating one additional predictor in the equation: the one time step lagged H_s which is conceptually in agreement with the first time derivative in the wave action density balance governing equation. This term significantly further improves the model skill.

(3) Assessing wave-driven coastal impacts

In the context of coastal and port engineering, a review and quantification of the most important wave-driven coastal impacts has been carried out. The identified wave-driven processes are: erosion/accretion caused by changes in the longshore and cross-shore sediment transport, flooding induced by wave run-up, harbour agitation and siltation, increase/decrease of structure stability, overtopping, scouring, wave reflection and wave transmission.

The quantification has been done simply and generically in order not to be case-specific and serve as a guideline for further local/regional coastal impact assessments. Simple cases of variations of wave parameters (H_s, T_p and θ_m) are considered taking into account the ranges obtained by state-of-the-art global-scale wave climate studies. The results conclude that:

- In spite of having mild variations of the forcing wave conditions, coastal processes can be greatly affected due to the non-linear character of the relationships governing the processes involved. This should raise awareness among coastal and ports authorities.
- For example, changes in H_s and T_p strongly affect processs impacting structures: overtopping discharge, stability and scouring. For changes in θ_m, the

longshore sediment transport seems to be the most affected process, which can suffer from relative variations over 100%, depending on the incident wave direction.

Towards a first assessment of the impacts in the Catalan coast, a couple of case studies (related to currently problematic issues) has been presented in this thesis. They cover, respectively, the harbour agitation and the longshore sediment transport.

- **Harbour agitation** of Tarragona port.
  Owing to the SW entrance orientation, as most Catalan harbours have, the agitation of this port is largely affected by S-SW waves. Using the extrapolated wave climate by trend analysis, for which there is a greater frequency of these wave directions, the agitation inside the harbour significantly increases but this does not entail an important reduction of the operability.
- **Longshore sediment transport** along Catalan beaches.
  Using the projected wave scenarios obtained by dynamical modelling, the effect on the long-shore sediment transport (LST) is assessed and, additionally, the inter-model variability is evaluated in terms of LST. Results show that variations(discrepancies) of(among) wave projections are accentuated in terms of LST and are difficult to anticipate. The reasons lay, respectively, in the non-linear relation between LST and wave parameters and the competing processes sometimes produced by changes in H_s and θ_m. Despite most of the models projecting a LST increase, it is difficult to derive a robust conclusion of a consistent variation.

9 Future work

The work carried out in this thesis leaves several open research lines for the future, some of which are suggested below. They are classified according to the general objectives of this thesis, being related with both general (poorly known) aspects and specific demands for the study area.

(1) Understanding the future wave climate

The wave database generated in this thesis is definitely a source of further data analysis to fully understand the future wave climate. In this regard, the following lines of investigation are proposed:

- Perform a more detailed extreme analysis, considering several return values and inter-annual (non-stationary) effects [e.g. Izaguirre et al., 2013].
- Get insight into the climate models performance using, for example, the FBI and PSS score skills [Lin and Wang, 2011] in an attempt to assign weights or to suggest a prioritisation of climate models.

Dynamical modelling is still an indispensable technique to reproduce most of the important wave parameters. Therefore, it would be interesting to improve its computational efficiency. One suggestion is to:

- Explore the use of the SWAN model (or other wave models) with unstructured meshes that allow a rise in the spatial resolution just where it is desired, as recently done by Laugel et al. [2013] with the TOMAWAC model.

With respect to statistical modelling, this thesis has mainly focused on the model performance leaving the deep study of its applicability for future work. Some recommendations are:

- To carry out wave projections taking into account more combinations of greenhouse gas emission scenarios, RCMs and GCMs to better evaluate the climate change uncertainty. The quantification of this uncertainty can be evaluated by using, for example, the ANOVA analysis [e.g. von Storch and Zwiers, 2002] as in Wang and Swail [2006].
- Involve the use of recent high-resolution GCMs to project future changes in wave climate and determine the necessity of using RCM models of a similar resolution.

Finally, wave projections will need to be updated with the implementation of the new greenhouse gas emission scenarios included in the Fifth Assessment IPCC

report (AR5, expected to be finished by 2014), that are based in Representative Concentration Pathways [van Vuuren et al., 2011]. Indeed, a comparison with the existing SRES scenarios would be interesting. In addition, it is necessary to study the combined effect of changes in wave climate and sea-level-rise. As pointed out by Atkinson [2013], a rise in the sea level not only implies an increase of the water level but also allows larger waves propagate into inland areas due to the larger water depth.

(2) Improving methodological aspects

One of the most relevant contributions of this thesis is the development of an improved statistical model to simulate H_s. In this regard, future lines of research could involve the extension of the method in order to obtain other wave variables such as T_p and θ_m. Preliminary ideas are suggested below, based on the relation with the forcing wind field w_{10} (for fully-developed wind-seas):

- The model could be easily adapted to simulate T_p taking into account the proportionality $T_p \propto \sqrt{G}$.
- Meanwhile, θ_m could be computed by relating $[H_s \cos(\theta_m), H_s \sin(\theta_m)]$ with $[G \cos(\theta_m), G \sin(\theta_m)]$, for instance.

Given the large-inter model variability obtained in many of the wave climate projections it is necessary to determine the best approach(es) of bias adjustment. A first step could be to:

- Compare the mean-and-variance bias adjustment used in this thesis with (a) other simple techniques, such as quantile-quantile adjustment, and (b) more complex techniques, such as involving Bayesian analysis with different bias assumptions [e.g. Buser et al., 2009].

(3) Assessing wave-driven coastal impacts

Given the considerable number of wave-driven processes and the geo-diversity and extension of the Catalan coast, a large amount of work is still necessary to properly evaluate all wave-driven coastal impacts. Below three interesting aspects for investigation are suggested which obviously does not mean to cover all the work needed:

- The use of a numerical model like Delft3D (`http://oss.deltares.nl/web/delft3d/home`, accessed June 2013) to evaluate more accurately the long-term beach morphological changes, such as LST (very susceptible to changes of θ_m). This work could serve not only to provide the Catalan coast with a more accurate assessment but also to investigate the use of the "morphological acceleration factor" [Lesser et al., 2004], that is implemented in these

numerical models to cope with the different time scales associated to the hydrodynamic and morphological processes involved.

- A limited number of studies have covered and quantified harbour siltation which reflects the fact that the physical processes involved are not well-known yet. It would be interesting to get insight into the proper evaluation of this phenomenon and, for example, use a morphological model to evaluate this complex coastal impact under different climate change scenarios.
- Structure-related impacts seem to be largely affected by changes in the wave climate. Therefore, these impacts (structure stability, overtopping and scouring) should be systematically checked out for all Catalan coastal structures. From the results thus obtained, it would be interesting to stablish a classification of the cases (say, unfavourable structure dimensions and/or materials in relation to wave conditions) that lead to larger impacts and will probably require more attention.

References

Adams, P N; Inman, D L, and Lovering, J L. Effects of climate change and wave direction on longshore sediment transport patterns in Southern California. *Climatic Change*, 109(Suppl 1):S211–S228, 2011.

Alomar, M. *Improving wave forecasting in variable wind conditions. The effect of resolution and growth rate for the Catalan Coast.* PhD thesis, Universitat Politècnica de Catalunya, Barcelona, 2012.

Alvarado-Aguilar, D. *Coastal flood hazard mapping at two scales. Application to the Ebro delta.* PhD thesis, Universitat Politècnica de Catalunya, Barcelona, 2009.

Álvarez Ellacuria, A; Orfila, A; Olabarrieta, M; Gómez-Pujol, L; Medina, R, and Tintoré, J. An alert system for beach hazard management in the Balearic Islands. *Coastal Management*, 37(6):569–584, 2009.

Atkinson, J; Mckee Smith, J; Bender, C. Sea-level rise effects on storm surge and nearshore waves on the Texas coast: influence of landscape and storm characteristics. *Journal of Waterway, Ports, Coastal and Ocean Engineering*, 139(2):98–117, 2013.

Backhaus, J O. A Three-Dimensional Model for Simulation of Shelf Sea Dynamics. *Deutsche Hydrografische Zeitschrift*, 38(6):164–187, 1985.

Bayram, A; Larson, M, and Hanson, H. A new formula for the total long-shore sediment transport rate. *Coastal Engineering*, 54:700–710, 2007.

Bengtsson, L; Hodges, K I, and Roeckner, E. Storm Tracks and Climate Change. *Journal of Climate*, 19(15):3518–3543, 2006.

Bengtsson, L; Hodges, K I, and Keenlyside, N. Will extratropical storms intensify in a warmer climate? *Journal of Climate*, 22(9):2276–2301, 2009.

Bolaños, R; Jordà, G; Cateura, Jordi; Lopez, J; Puigdefabregas, J; Gomez, J, and Espino, M. The XIOM: 20 years of a regional coastal observatory in the Spanish Catalan coast. *Journal of Marine Systems*, 77(3):237–260, 2009.

Booij, N; Ris, R C, and Holthuijsen, L H. A third-generation wave model for coastal regions 1. Model description and validation. *Journal of Geophysical Research: Oceans*, 104(C4):7649–7666, 1999.

Bosom, E and Jiménez, José A. Probabilistic coastal vulnerability assessment to storms at regional scale – application to Catalan beaches (NW Mediterranean). *Natural Hazards and Earth System Science*, 11(2):475–484, 2011.

Bringham, H B. An hybrid Boussinesq-panel method for predicting the motion of a moored ship. *Coastal Engineering*, 40:21–38, 2000.

Buser, C M; Künsch, H R; Lüthi, D; Wild, M, and Schär, C. Bayesian multi-model projection of climate: bias assumptions and interannual variability. *Climate Dynamics*, 33:849–868, 2009.

Cai, Y and Davies, N. A Simple Bootstrap method for time series. *Communications in Statistics - Simulation and Computation*, 41(5):621–631, 2012.

Caires, S; Swail, V R, and Wang, X L. Projection and analysis of extreme wave climate. *Journal of climate*, 19:5582–5605, 2006.

Campins, J; Genovés, A; Jansà, A; Guijarro, J A, and Ramis, C. A catalogue and a classification of surface cyclones for the Western Mediterranean. *International Journal of Climatology*, 20(9):969–984, 2000.

Camus, P; Cofiño, A S; Méndez, F J, and Medina, R. Multivariate wave climate using self-organizing maps. *Journal of Atmospheric and Oceanic Technology*, 28:1554–1568, 2011.

Camus, P; Mendez, F; Medina, R; Tomas, A, and Izaguirre, C. High resolution downscaled ocean waves (DOW reanlysis in coastal areas. *Coastal Engineering*, 72:56–68, 2013.

Casas-Prat, M and Sierra, J P. Trend analysis of wave storminess: wave direction and its impact on harbour agitation. *Natural Hazards and Earth System Sciences*, 10(11): 2327–2340, 2010.

Casas-Prat, M and Sierra, J P. Trend analysis of wave direction and associated impacts on the Catalan coast. *Climatic Change*, 115(3–4):667–691, 2012.

Casas-Prat, M and Sierra, J P. Projected future wave climate in the NW Mediterranean Sea. *Journal of Geophysical Research: Oceans*, 118(7):3548–3568, 2013.

Casas-Prat, M; Wang, X L, and Sierra, J P. A physical-based statistical method for modeling ocean wave heights. *Ocean Modelling*, doi: http://dx.doi.org/10.1016/j.ocemod.2013.10.008, 2013.

Cazenave, A; Lombard, A and Llovel, W. Present-day sea level rise: A synthesis. *C. R. Geoscience*, 340:761–770, 2008.

Charles, E; Idier, D; Delecluse, P; Déqué, M, and Cozannet, G. Climate change impact on waves in the Bay of Biscay, France. *Ocean Dynamics*, 62(6):831–848, 2012.

Christensen, J H; Carter, T R; Rummukainen, M, and Amanatidis, G. Evaluating the performance and utility of regional climate models: the PRUDENCE project. *Climatic Change*, 81(1):1–6, 2007.

CIIRC. Estat de la zona costanera a Catalunya (in Catalan). International Centre for Coastal Resources Research. Technical report, Barcelona, 2010.

CIIRC. Estudi de diferents solucions per a la reducció del fenomen d'agitació del Port Fòrum (in Catalan). Technical report, Barcelona, 2011.

Coelho, C; R, Silvam; Veloso-Gomes, F, and Taveira-Pinto, F. Potential effects of climate change on northwest Portuguese coastal zones. *Journal of Marine Science*, 66:1497–1507, 2009.

Collins, M; Tett, S F B, and Cooper, C. The internal climate variability of HadCM3, a version of the Hadley Centre coupled model without flux adjustments. *Climate Dynamics*, 17:61–81, 2001.

D'Angremond, K; van der Meer, J W, and Jong, R J. Wave transmission at low crested structures. In *Proceedings of the 25th International Conference on Coastal Engineering*, pages 2418–2427, Orlando, FL, USA, 1996.

Denis, M St and Pierson, W J. On the motions of ships in confused seas. *Society of Naval Architects and Marine Engineers*, 61:280–357, 1953.

Déqué, M; Rowell, D P; Lüthi, D; Giorgi, F; Christensen, J H; Rockel, B; Jacob, D; Kjellström, E; De Castro, M, and Van Den Hurk, B. An intercomparison of regional climate simulations for Europe: assessing uncertainties in model projections. *Climatic Change*, 81:53–70, 2007.

Donat, M G; Leckebusch, G; Pinto, J G, and Ulbrich, U. European storminess and associated circulation weather types: future changes deduced from a multi-model ensemble of GCM simulations. *Climate Research*, 42(1):27–43, 2010.

Egozcue, J J; Pawlowsky-Glahn, V; Mateu-Figueras, G, and Barceló-Vidal, C. Isometric logratio transformations for compositional data analysis. *Mathematical Geology*, 35 (3):279–300, 2003.

Fawcett, L and Walshaw, D. Estimating return levels from serially dependent extremes. *Environmetrics*, 23(3):272–283, 2012.

Gomis, D; Ruiz, S; Sotillo, M G; Álvarez Fanjul, E, and Terradas, J. Low frequency Mediterranean sea level variability: the contribution of atmospheric pressure and wind. *Global Planetary Change*, 63:215–229, 2008.

González-Marco, D; Sierra, J P; Fernández de Ybarra, O, and Sánchez-Arcilla, A. Implications of long waves of harbour management: the Gijón port case study. *Ocean and coastal management*, 51:180–201, 2008.

Grabemann, I and Weisse, R. Climate change impact on extreme wave conditions in the North Sea: an ensemble study. *Ocean Dynamics*, 58:199–212, August 2008.

Guedes Soares, C; Weisse, R; Carretero, J C, and Alvarez, E. A 40 years hindcast of wind, sea level and waves in European waters. In *Proceedings of OMAE 2002: 21st International Conference on Offshore Mechanics and Arctic Engineering*, number June, pages 669–675, Oslo, Norway, 2002.

Gunaydin, K. The estimation of monthly mean significant wave heights by using artificial neural network and regression methods. *Ocean Engineering*, 35:1406–1415, October 2008. ISSN 00298018.

Hemer, M A; Mcinnes, K; Church, J A; O'Grady, J, and Hunter, J R. *Variability and trends in the Australian wave climate and consequent coastal vulnerability.* Final Report for Department of Climate Change Surface Ocean Wave Variability Project, CSIRO, 2008.

Hemer, M A; Church, J; Swail, V; Wang, X L, and Weisse, R. Cowclip coordinated ocean wave climate projections: An introduction. Presented in the WCR-JCOMM Workshop on Coordinates Global Wave Climate Projections in Geneva, Switzerland, 2011a.

Hemer, M A; Wang, X L; Weisse, R, and the COWCLIP team. WCRP-JCOMM Workshop on Coordinated Global Wave Climate Projections. Technical report, Switzerland, 2011b.

Hemer, M A; Wang, X L; Weisse, R, and Swail, V R. Advancing Wind-Waves Climate Science. *Bulletin of the American Meteorological Society*, 93(6):791–796, 2012.

Hemer, M A; Fan, Y; Mori, N; Semedo, A, and Wang, X L. Projected change in wave climate from a multi-model ensemble. *Nature Climate Change*, 3(5):471–476, 2013.

Holthuijsen, L H. *Waves in oceanic and coastal waters.* Cambridge University Press, 2007.

Hudson, R Y. Laboratory investigation of rubble mound breakwaters. *American Society of Civil Engineers - Transactions*, 126:Pt IV, 1961.

IPCC. *Processes and Modelling.* Cambridge University Press, Cambridge, United Kingdom and New York, NY, USA, contribution of working group i to the first assessment report of the intergovernmental panel on climate change, 1990 edition, 1990.

IPCC. *The Physical Science Basis*. Cambridge University Press, Cambridge, United Kingdom and New York, NY, USA, contribution of working group i to the fourth assessment report of the intergovernmental panel on climate change, 2007 edition, 2007.

Izaguirre, C; Menéndez, M; Camus, P; Méndez, F J; Mínguez, R, and Losada, I J. Exploring the interannual variability of extreme wave climate in the Northeast Atlantic Ocean. *Ocean Modelling*, 59–60:31–40, 2013.

Jiménez, J A and Madsen, O S. A simple formula to estimate settling velocity of natural sediments. *Journal of waterway, ports, coastal and ocean egneering*, 129:70–78, 2003.

Jiménez, J A; Gracia, V; Valdemoro, H I; Mendoza, E T, and Sánchez-Arcilla, A. Managing eriosion-induced problems in NW Mediterranean urban beaches. *Ocean and Coastal Management*, 54:907–918, 2011.

Jiménez, J A; Sancho-García, A; Bosom, E; Valdemoro, H I, and Guillén, J. Storm-induced damages along the Catalan coast (NW Mediterranean) during the period 1958–2008. *Geomorphology*, 143–144:24–33, 2012.

Kalnay, E; Kanamitsu, M; Cistler, R; Collins, W; Deaven, D; Gandin, L; Iredell, M; Saha, S; White, G; Woollen, J; Zhu, Z; Chelliah, M; Ebisuzaki, W; Higgins, W; Janowiak, J; Mo, KC; Ropelewski, C; Wang, J; Leetma, A; Reynolds, R; Jenne, R, and Joseph, D. The NCEP/NCAR Reanalysis Project. *Bulletin of the American Meteorological Society*, 77:437–471, 1996.

Karambas, T W and Koutitas, C. Resonant response of harbours to short-wave group. *Maritime Engineering*, 40:163–170, 2000.

Kendall, M G. *Rank correlation methods*. Griffin, London, 1975.

Kjellström, E; Nikulin, G; Hansson, U; Strandberg, G, and Ullerstig, A. 21st century changes in the European climate: uncertainties derived from an ensemble of regional climate model simulations. *Tellus A*, 63(1):24–40, 2011.

Kriezi, E E and Broman, B. Past and future wave climate in the Baltic Sea produced by the SWAN model with forcing from the regional climate model RCA of the Rossby Centre. In *US/EU-Baltic International Symposium*, pages 1–7, Tallin, Estonia, 2008.

Laugel, A; Menendez, M; Benoit, M; Mattarolo, G, and Mendez, F. A comparison of dynamical and statistical downscaling methods for regional wave climate projections along french coastlines. Presented at the European Geosiences Union General Assembly 2013, Vienna, Austria, 2013.

Lesser, G R; Roelvink, J A; van Kester, J A T M, and Stelling, G S. Development and validation of a three-dimensional morphological model. *Coastal Engineering*, 51(8–9): 883–915, 2004.

LIM. Estudio mediante modelado numérico para la reducción de la agitación en el interior del puerto de Blanes (in Spanish). Technical report, 1999.

Lin, A and Wang, X L. An algorithm for blending multiple satellite precipitation estimates with in situ precipitation measurements in Canada. *Journal of Geophysical Research: Atmospheres*, 116(D21111):1–19, 2011.

Lionello, P and Galati, M B. Links of the significant wave height distribution in the Mediterranean sea with the Northern Hemisphere teleconnection patterns. *Advances in Geosciences*, 17:13–18, 2008.

Lionello, P and Sanna, A. Mediterranean wave climate variability and its links with NAO and Indian Monsoon. *Climate Dynamics*, 25(6):611–623, 2005.

Lionello, P; Dalan, F, and Elvini, E. Cyclones in the Mediterranean region: the present and the doubled CO2 climate scenarios. *Climate Research*, 22:147–159, 2002.

Lionello, P; Malanotte-Rizzoli, P, and Boscolo, R. *Mediterranean Climate Variability*. Elsevier, 2006.

Lionello, P; Cogo, S; Galati, M B, and Sanna, A. The Mediterranean surface wave climate inferred from future scenario simulations. *Global and Planetary Change*, 63: 152–162, 2008.

Mann, H B. Nonparametric test against trend. *Econometrica*, 13:245–259, 1945.

Marcos, M and Tsimplis, M. Coastal sea level trends in Southern Europe. *Geophysical Journal International*, 175:70–82, 2008.

Marcos, M; Jordà, G; Gomis, D, and Pérez, B. Changes in storm surges in southern Europe from a regional model under climate change scenarios. *Global and Planetary Change*, 77:116–128, 2011.

Mase, H. Random wave runup height on gentle slope. *Journal of Waterways, ports, coastal and ocean engineering*, 115:642–661, 1989.

McInnes, K L; Erwin, T A, and Bathols, M. Global climate model projected changes in 10 m wind speed and direction due to anthropogenic climate change. *Atmospheric science letters*, 12:325–333, 2011.

Mendoza, E T and Jiménez, J A. Storm-Induced Beach Erosion Potential on the Catalonian Coast. *Journal of Coastal Research*, SI 48(SI 48):81–88, 2006.

Mestres, M; Sierra, J P; Mösso, C, and Sánchez-Arcilla, A. Sources of contamination and modelled pollutant trajectories in a Mediterranean harbour (Tarragona, Spain). *Marine Pollution Bulletin*, 60:898–907, 2010.

Mori, N; Yasuda, T; Mase, H; Tom, T, and Oku, Y. Projection of Extreme Wave Climate Change under Global Warming. *Hydrological Research Letters*, 4:15–19, 2010.

Mösso, C; Mestres, M; Sierra, J P; Sánchez-Arcilla, A, and Goodess, C. Waves and surges in the Valencia Gulf. Variability rather than climate change. *Journal of Coastal Research*, Special Issue 56:243–247, 2009.

Musić, S and Nicković, S. 44-year wave hindcast for the Eastern Mediterranean. *Coastal Engineering*, 55:872–880, 2008.

Nadaoka, K and Raveenthiran, K. A phase-averaged Boussinesq model with effective description of carrier wave group and associated long wave evolution. *Ocean Engineering*, 29:21–37, 2002.

Nicholls, R J and Kebede, A S. Indirect impacts of coastal climate change and sea-level-rise: the UK example. *Climate Policy*, 12(sup01):S28–S52, 2012.

Nicholls, R J; Wong, V R; Burkett, J O; Codignotto, J E; Hay, R F; McLean, S; Ragoonaden, S, and Woodroffe, C D. Coastal systems and low-lying areas. Climate Change 2007: Impacts, Adaptation and Vulnerability. Contribution of Working Group II to the Fourth Assessment Report of the Intergovernmental Panel on Climate Change, M.L. Parry, O.F. Canziani, J.P. Palutikof, P.J. van der Linden and C.E. Hanson, Eds., Cambridge University Press, Cambridge, UK, 315-356. 2007.

Nicholls, R J; Wong, P P; Burkett, V; Woodroffe, C D, and Hay, J. Climate change and coastal vulnerability assessment: scenarios for integrated assessment. *Sustainability Science*, 3(1):89–102, 2008.

Nikulin, G; Kjellström, E; Hansson, U; Strandberg, G, and Ullerstig, A. Evaluation and future projections of temperature, precipitation and wind extremes over Europe in an ensemble of regional climate simulations. *Tellus A*, 63(1):41–55, 2011.

Ortego, M I; Tolosana-Delgado, R; Gibergans-Báguena, J; Egozcue, J J, and Sánchez-Arcilla, A. Assessing wavestorm hazard evolution in the NW Mediterranean with hindcast and buoy data. *Climatic Change*, 113:713–731, 2012.

Pandey, M D; Van Gelder, P H A J M, and Vrijling, J K. Bootstrap simulations for evaluating the uncertainty associated with peaks-over-threshold estimates of extreme wind velocity. *Environmetrics*, 14(1):27–43, 2003.

Pandey, M D; Van Gelder, P H A J M, and Vrijling, J K. Dutch case studies of the estimation of extreme quantiles and associated uncertainty by bootstrap simulations. *Environmetrics*, 15(7):687–699, 2004.

Park, D S; Kim, Y B; Shin, K I, and Willemain, T R. Simulation output analysis using the threshold bootstrap. *European Journal of Operational Research*, 134(1):17–28, 2001.

Pawlowsky-Glahn, V. On spurious spatial covariance between variables of constant sum. *Science de la Terre*, 21:107–113, 1984.

Puertos del Estado. Technical report, Madrid.

Pullen, T; Allsop, N W H; Bruce, T; Kortenhaus, A; Scüttrump, H, and van der Meer, J W. Eurotop wave overtopping of sea defences and related structures—Assessment Manual. Technical report, 2007.

Ratsimandresy, A W; Sotillo, M G; Alvarez-Fanjul, E; Carretero-Albiach, J; Perez-Gomez, B, and Hajji, H. A 44-year (1958–2001) sea level residual hindcast over the Mediterranean Basin. *Physics and Chemistry of the Earth*, 33:250–259, 2008.

Resio, R; Bratos, S M, and Thompson, E F. Meteorology and wave climate, in Coastal Engineering Manual, Part II, Chapter 2, 72 p. Technical report, 2002.

Riba Monzó, O. Effectes potencials del canvi climàtic sobre l'operativitat del port de tarragon (in catalan). Master's thesis, Universitat Politècnica de Catalunya, Barcelona, 2010.

Roeckner, E; Bäuml, G; Bonaventura, L; Brokopf, R; Esch, M; Giorgetta, M; Hagemann, S; Kirchner, I; Kornblueh, L; Manzini, E; Rhodin, A; Schlese, U; Schulzweida, U, and Tompkins, A. The atmospheric general circulation model ECHAM5. Model description. Technical Report 349, Hamburg, 2003.

Sakia, R M. The Box-Cox transformation: a review. *The Statistician*, 41:169–178, 1992.

Samuelsson, P; Jones, C G; Willén, U; Ullerstig, A; Gollvik, S; Hansson, U; Jansson, C; Kjellström, E; Nikulin, G, and Wyser, K. The Rossby Centre Regional Climate model RCA3: model description and performance. *Tellus A*, 63(1):4–23, January 2011. ISSN 02806495.

Sánchez-Arcilla, A; González-Marco, D, and Bolaños, R. A review of wave climate and prediction along the Spanish Mediterranean coast. *Natural Hazards and Earth System Science*, 8:1217–1228, 2008.

Semedo, A; Beherens, A; Bengtsson, L; Günther, H; Sterl, A, and Weisse, R. Impact of a Warmer Climate on the Global Wave Field. In *12th International Workshop on Wave Hindcasting and Forecasting and 3rd Coastal Hazards Symposium*, Khoala Coast, Hawaii, 2011.

Sorensen, R and Thompson, E F. Harbour hydrodynamics, in Coastal Engineering Manual, Part II, Chapter 7, 91 p. Technical report, 2002.

Sotillo, M G; A WRatsimandresy, Carretero J C; Bentamy, A; Valero, F, and González-Rouco, F. A high-resolution 44-year atmospheric hindcast for the Mediterranean Basin: contribution to the regional improvement of global reanalysis. *Climate Dynamics*, 25:219–236, 2005.

SPM. *Shore Protection Manual 4th ed, 2 Vol, US Army Engineer Waterways Experiment Station, US Government Printing Office*. Praxis Publishing, Washington, DC, USA, 1984.

Sumer, B M and Fredsøe, J. Experimental study of 2D scour and its protection at a rubble mound breakwater. *Coastal Engineering*, 40:59–87, 2000.

The WAMDI group. The WAM model—a third generation ocean wave prediction model. *Journal of Physical Oceanography*, 18:1775–1810, 1988.

Tolosana-Delgado, R. Uses and misuses of compositional data in Sedimentology. *Sedimentary Geology*, 280(1):60–79, 2012.

Ulbrich, U; Pinto, J G; Leckebusch, G C; Spangehl, T, and Reyers, M. Changing northern hemisphere storm tracks in an ensemble of IPCC climate change simulations. *Journal of Climate*, 21(1-2):1669–1679, 2008.

Ulbrich, U; Leckebusch, G C, and Pinto, J G. Extra-tropical cyclones in the present and future climate: a review. *Theoretical and Applied Climatology*, 96(1-2):117–131, 2009.

van der Linden, P and Mitchell, J F B. 2009: ENSEMBLES: Climate Change and its Impacts: Summary of research and results from the ENSEMBLES project. Met Office Hadley Centre, FitzRoy Road, Exeter EX1 3PB, UK. 160pp. Technical report, 2009.

Van Gelder, P; Mai, C; Wang, W; Shams, G; Rajabalinejad, M, and Burgmeijer, M. Data management of extreme marine and coastal hydro-meteorological events. *Journal of Hydraulic Research*, 46(919083124):191–210, 2008.

van Meijgaard, E; van Ulft, LH; van de Berg, WJ; Bosveld, FC; van den Hurk, BJJM; Lenderink, Geert, and Siebesma, AP. The KNMI regional atmospheric climate model RACMO, version 2.1. Technical Report 302, 2008.

van Vuuren, D P; Edmonds, J; Kainuma, M; Riahi, K; Thomson, A; Hibbard, K; Hurtt, G C; Krey, V; Lamarque, J-F; Masui, T; Meinsahusen, M; Nakicenovic, N; Smith, S J, and Rose, S K. The representative concentration pathways: an overview. *Climatic Change*, 109:5–31, 2011.

von Storch, H and Zwiers, F W. *Statistical analysis in climate research*. Cambridge University Press, 2002.

Wang, L; Feng, Y, and Swail, V R. North Atlantic wave height trends as reconstructed from the Twentieth Century Reanalysis. *Geophysical Research Letters*, 2012GL0533, 2012.

Wang, X L and Swail, V R. Trends of Atlantic Wave Extremes as Simulated in a 40-Yr Wave Hindcast Using Kinematically Reanalyzed Wind Fields. *Journal of Climate*, 15: 1020–1035, 2002.

Wang, X L and Swail, V R. Climate change signal and uncertainty in projections of ocean wave heights. *Climate Dynamics*, 26:109–126, 2006.

Wang, X L; Swail, V R, and Cox, A. Dynamical versus statistical downscaling methods for ocean wave heights. *International Journal of Climatology*, 30:317–332, 2010.

Weisse, R and Von Storch, H. *Marine Climate and Climate Change. Storms, wind waves and storm surges*. Praxis Publishing, Chicheste, UK, springer p edition, 2010.

Wilks, D K. Resampling Hypothesis Tests for Autocorrelated Fields. *American Meteorological Society*, 10:65–82, 1997.

Woo, S B and Liu, P L-F. Finite-element model for modified Boussinesq equations II: Applications to nonlinear harbour oscillations. *Journal of waterway, port, coastal and ocean engineering*, 130(1):17–28, 2002.

Zacharioudaki, A and Reeve, D E. Shoreline evolution under climate change wave scenarios. *Climatic Change*, 108:73–105, 2011.

Zhang, Q-E; Yan, B, and Wai, O W H. Fine sediment carrying capacity of combined wave and current flows. *International Journal of Sedimentology*, 24:425–438, 2009.

COMPENDIUM OF PAPERS

Paper A

Trend analysis of wave storminess: wave direction and its impact on harbour agitation

M. Casas-Prat and J.P. Sierra

Natural Hazards and Earth System Sciences, **10**, 2327–2340, 2010.

Nat. Hazards Earth Syst. Sci., 10, 2327–2340, 2010
www.nat-hazards-earth-syst-sci.net/10/2327/2010/
doi:10.5194/nhess-10-2327-2010
© Author(s) 2010. CC Attribution 3.0 License.

Natural Hazards and Earth System Sciences

Trend analysis of wave storminess: wave direction and its impact on harbour agitation

M. Casas-Prat and J. P. Sierra

Centre Internacional d'Investigació dels Recursos Costaners, Jordi Girona 1-3, Mòdul D1 Campus Nord, 08034 Barcelona, Spain

Laboratori d'Enginyeria Marítima, Universitat Politècnica de Catalunya, Jordi Girona 1-3, Mòdul D1 Campus Nord, 08034 Barcelona, Spain

Received: 7 June 2010 – Revised: 13 October 2010 – Accepted: 21 October 2010 – Published: 19 November 2010

Abstract. In the context of wave climate variability, long-term alterations in the wave storminess pattern of the Catalan coast (northwestern Mediterranean Sea) are analysed in terms of wave energy content and wave direction, on the basis of wave hindcast data (from 44-year time series). In general, no significant temporal trends are found for annual mean and maximum energy. However, the same analysis carried out separately for different wave directions reveals a remarkable increase in the storm energy of events from the south, which is partly due to a rise in the annual percentage of such storms. A case study of Tarragona Port (on the southern Catalan coast) highlights the importance of including changes in wave direction in the study of potential impacts of climate change. In particular, an increase in the frequency of storms from the south leads to greater agitation inside the Port.

1 Introduction

Climate change is an important area of current scientific research because of potential future hazards. The greenhouse effect is expected to lead to global warming. The resulting complex interactions in atmospheric processes may cause substantial modifications in near-surface wind and pressure patterns. This could affect typical mean and extreme wave conditions, leading to variations in coastal hydrodynamics. Stormy conditions are especially important because they are closely related to more hazardous events, including extremely high water levels that may be one of the main causes of extensive property damage in coastal areas (De Zolt et al., 2006; Soomere et al., 2008). Weisse and von Storch (2010) give a general overview of the state-of-the-art in the relation between anthropogenic climate change and marine climate. Processes such as changing temperature gradients, increasing amount of water vapour and variations in sea surface temperatures might modify the number, frequency and situation of mid-latitude ($30° - 60°$) storm tracks. However, due to incomplete understanding of the system and computer limitations, a wide range of possible changes have been described in the literature and some of them (especially in the case of regional projections) are still being disputed.

In addition, a high inter-annual and decadal variability in sea levels and wave patterns has been detected in the Mediterranean Sea for the second half of the 20th century (Musić and Nicković, 2008; Ratsimandresy et al., 2008b; Tsimplis et al., 2008) and could have an impact on coastal areas that is as great as that of climate change.

This study focuses on the Catalan coast (northwestern Mediterranean Sea), as shown in Fig. 1, and aims to identify and quantify possible trends in storm wave-related parameters. It is an extension of a previous study carried out by Casas-Prat and Sierra (2010) and is based on hindcast data covering the second half of the 20th century. Due to the nature of these data, some limitations may prevent us from properly detecting the real long-term variability. However, the use of this database is justified because, unlike wave measurements, it comprises a consistent data series that is long enough for climate studies (> 40 years).

We aim to increase knowledge of long-term variations in wave storminess in this semi-enclosed sea domain, in which the wave climate is complex and was defined as "torrential" by Sánchez-Arcilla et al. (2008). Although some strong events are controlled by larger-scale synoptic activity, local

Correspondence to: M. Casas-Prat (merce.casas@upc.edu)

Published by Copernicus Publications on behalf of the European Geosciences Union.

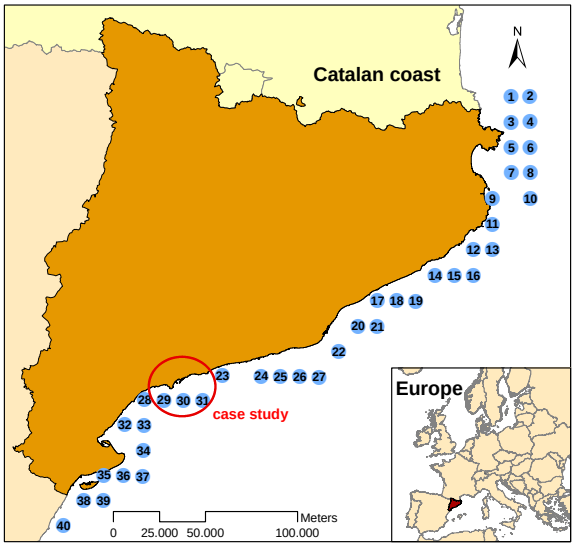

Fig. 1. Location of the Catalan coast and simulated nodes considered in this study.

topography has a significant impact on the wind climate and therefore on the wave field (Bertotti and Cavaleri, 2008). Waves are further modified by the irregular bathymetry of the zone (Sánchez-Arcilla et al., 2008). Hence, regional temporal trends may differ from the results of more general studies.

In this paper, special emphasis is placed on wave direction, an important factor that has been underestimated or simply ignored in previous studies of the area. Even in a situation of constant wave storminess magnitude, rotation of the mean wave direction may have severe consequences, since most beach and harbour defence structures are designed assuming a permanent directional distribution of waves. Liste et al. (2004) illustrated this fact with an example in which a rotation of only 2 degrees in the mean energy flux vector could produce a beach retreat of 20 m. A higher frequency of coastal storms in the same direction as the harbour mouth would influence port operations, as it could cause increased agitation and siltation. Since most Catalan ports and marinas are oriented to the south, they are extremely vulnerable to an increase in extreme events from this direction. The present study illustrates this possible impact by computing and comparing harbour agitation in current and future situations in a case study of Tarragona Port (see Fig. 1).

2 Data

In spite of the obvious advantages of in situ measurements, they are usually limited in spatial and temporal coverage. Temporal coverage is crucial in long-term analysis. In addition, in situ measurements are usually inhomogeneous, as their accuracy increases over time, which is not suitable for climate studies. Therefore, the present analysis is based on simulations: 44-year hindcast wave data (1958–2001) from the European HIPOCAS project (Guedes Soares et al., 2002). This simulated data set is available for several European coastal areas, including the entire Mediterranean basin. It used REMO, the regional atmospheric model, which was forced with NCEP and followed by the HAMSOM and WAM (WAMDI, 1988; Monbaliu et al., 2000) models to simulate the sea level and wave data, respectively. The HIPOCAS database is widely used (Gomis et al., 2008; Marcos and Tsimplis, 2008; Tsimplis, et al., 2008; Alvarez-Ellacuria et al., 2009; Mösso et al., 2009) and has been extensively validated for wind speed and direction, significant wave height, wave direction and residual sea level parameters in the Mediterranean Sea (Sotillo et al., 2005; Musiv and Nicković, 2008; Ratsimandresy et al., 2008a, b). Although some extreme events are underestimated, this database seems to be useful in the study of the long-term behaviour of these parameters. A calibrated data set has been computed to try to diminish the negative bias (Tomás et al., 2004). It was obtained by minimising the distance between the probability distributions of measurements and simulations, through the application of an exponential relation. In our study area, few storms are better captured by this calibrated sample. However, most of the observations are systematically overpredicted, as shown in the example in Fig. 2 (Tortosa buoy, 1993) that compares the absolute error of the two data sets for a certain location and time period. In general, the figure illustrates that the calibrated HIPOCAS data nearly always overestimate the buoy measurements, whereas an average error that is closer to zero is found for the uncalibrated data. In addition, larger differences (up to 2.83 m) are found for the calibrated data than for the uncalibrated data (up to 1.75 m). Figure 3 shows the mean ratio between the relative errors, in absolute value, of calibrated and uncalibrated data sets. This plot was obtained by comparing the hindcast data with buoy measurements at the same location as in Fig. 2, but considering the time period 1991–2001. The error ratio was computed for subsets of data with significant wave heights (H_s) above a certain value. For example, for $x = 3$ m, we find $y = 1.3$ m. This means that, on average, the relative error of calibrated data is 1.3 times that of uncalibrated data for all $H_s > 3$ m. Generally, this ratio is higher than 1 (in favour of uncalibrated data), particularly for all wave heights ($H_s > 0$ m) and for extreme wave heights ($H_s > 3$ m). Therefore, the original data set is used in this study because it performs better. Figure 1 illustrates the 40 selected nodes along the Catalan coast from which the significant wave height (H_s) and the mean wave direction (θ) were considered. The spatial resolution was about 12.5 km and the time step was 3 h.

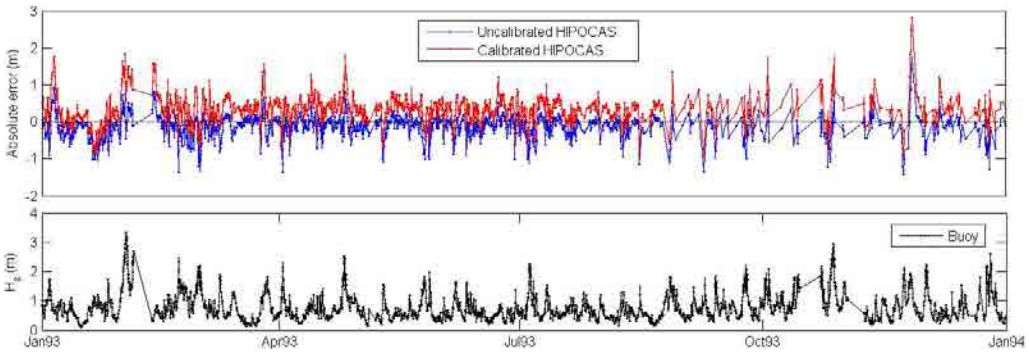

Fig. 2. Upper panel: differences between hindcast (calibrated and uncalibrated) data and buoy measurements during 1993 in Tortosa. Lower panel: H_S buoy time series (Tortosa buoy coordinates: 40°43.29′ N, 00°58.89′ E, from XIOM network).

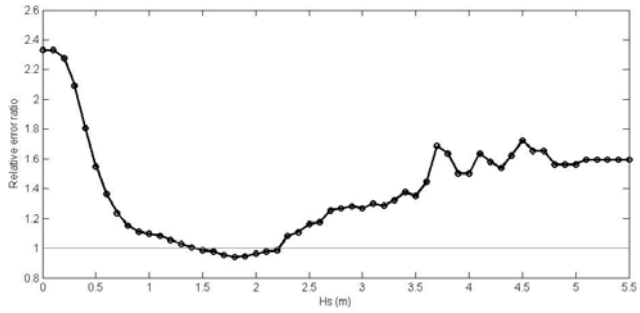

Fig. 3. Mean ratio between relative errors of calibrated and uncalibrated HIPOCAS data for subsets of time series of H_s greater than the values of x-axis (for the time period 1991–2001 from Tortosa buoy: 40°43.29′ N, 00°28.89′ E).

3 Methods

The methods are explained below in five subsections, in which the following aspects are covered:

1. Wave storminess characterisation: storm energy content and directional frequency.
2. Trend analysis of storm energy content.
3. Trend analysis of wave directional frequency.
4. Application to the case study.
5. The role of uncertainty.

3.1 Wave storminess characterisation

As the present analysis focuses on extreme conditions, first we must define a wave storm. The common peak over threshold (POT) method is used with a typical H_S threshold of 2 m (within the range of values recommended by the Spanish National Harbour Authority) and a minimum duration of 6 h. Additionally, a second hypothesis is formed in which only statistically independent storms are considered (Mendoza and Jiménez, 2006). In this case, a storm involving two extreme episodes with a maximum inter-event separation of 72 h and a period of wave heights under 1.5 m in less than 6 h is considered a single two-peaked storm.

To characterise wave storminess for each storm, we use the storm energy content (E_S) which combines both H_S and duration as the integral over time illustrated in Eq. (1) (Mendoza and Jiménez, 2004). In addition, wave storminess is classified depending on the incoming wave direction of the storm peak, according to the following eight sectors of 45°, which are centred in the four cardinal and four ordinal directions of a compass rose: north (N), northeast (NE), east (E), southeast (SE), south (S), southwest (SW), west (W), northwest (NW).

$$E_S = \int H_S^2 dt \tag{1}$$

To evaluate long-term trends rather than seasonal variability, the annual mean and maximum values of E_S are calculated for each sector and for all the storms in each year. Moreover, the same operation is carried out for the entire period of data (1958–2001) to obtain a general picture of the past-present situation and to identify the most energetic locations and directions. In addition, for the entire period of data as well, the circular correlation (Fisher and Lee, 1983; see Eq. 2) between wind and wave directions in stormy conditions is computed to gain an idea of the presence of sea and swell in each node.

$$r = \frac{\sum_{i=1}^{n-1}\sum_{j=i+1}^{n}\sin(\theta_i-\theta_j)\sin(\alpha_i-\alpha_j)}{\sqrt{\sum_{i=1}^{n-1}\sum_{j=i+1}^{n}\sin^2(\theta_i-\theta_j)\sum_{i=1}^{n-1}\sum_{j=i+1}^{n}\sin^2(\alpha_i-\alpha_j)}} \tag{2}$$

where n is the number of data items, θ the wave direction and α the wind direction. The aim of this classification is not to make a clear distinction between these two phenomena, but to illustrate the type of wave climate to which significant temporal changes are most closely related.

The second parameter used to characterise the wave storminess is the directional frequency in stormy conditions, in other words, the percentage of storms associated with each direction in a certain year. Casas-Prat and Sierra (2010) calculated these annual frequencies by Bayesian inference (Agresti, 2002; see Eq. 3), from which $p_i \neq 0$ because $p_i \geq 0.5 \cdot (n_{\text{total}} + 0.5k)^{-1}$. This property is useful in both theoretical and practical terms. Firstly, although the occurrence of a storm from a certain direction may be highly unlikely (e.g. offshore directions) and may not in fact have been simulated during the entire period, zero probability should not be assigned, as this means the negation of such an event. Secondly, as shown in Sect. 3.3, compositional data is log-ratio transformed, which results in the exclusion of zeros. However, when n_{total} is relatively small (a few annual storms), the probability of an absent event is exaggeratedly increased by using Eq. (3), which in turn is compensated by considerably lowering the value of higher percentages. This might cause some distortion in the results.

$$p_i = \frac{n_i + 0.5}{n_{\text{total}} + 0.5k}, \quad \text{for } i = 1, \ldots, k \tag{3}$$

where n_i and n_{total} are, respectively, the number of storms per sector and in total, and $k = 8$ is the number of classes.

To overcome the aforementioned disadvantage, we obtain the frequencies directly by computing $p_i^* = n_i / n_{\text{total}}$. Then, a multiplicative replacement strategy is applied to the zeros of the compositional data set (Martín-Fernández et al., 2003; see Eq. 4). In principle, Eq. (4) is defined for use with rounded zeros. However, owing to the theoretical and practical reasons explained above, this expression is extrapolated to this case of absolute zeros.

$$p_i = \begin{cases} \delta & \text{if} \quad p_i^* = 0 \\ (1 - n_Z \delta)\, p_i^* & \text{if} \quad p_i^* > 0 \end{cases}, \quad \text{for } i = 1, \ldots, k \tag{4}$$

where n_Z is the number of zeros and δ the imputed value for zeros ($\delta = 0.01$). As in the energy analysis, the frequencies for the entire period of data (1958–2001) are also calculated.

3.2 Trend analysis of storm energy content

Before the trend analysis, an adjustment should be made according to the data scale, since most standard techniques are designed to be used with data that are free to range from $-\infty$ to ∞. By definition, E_s is generally a positive variable and therefore its scale is relative. Therefore, E_s is log-transformed so that distorted distances are not measured when linear regression analysis (which assumes normally distributed data) is performed, for example. Note that this positive assumption is subject to the annual presence of storms. In situations in which most of the years have storms (e.g. when all directions are considered), one year without storms is associated with a very low energy threshold value, to avoid the problem of ln(0). However, when there are many years without storms (e.g. for the S direction) the probability of storm occurrence is introduced (see below in the trend quantification procedure).

A two-step method is used for the trend analysis of storm energy content: trend detection and trend quantification. As in Casas-Prat and Sierra (2010), the Mann-Kendall (MK) test (Mann, 1945; Kendall, 1975; see Eqs. 5, 6, 7 and 8) is performed for the trend detection for all the calculated annual mean and maximum time series of E_s, to detect the locations and directions in which major long-term changes can be expected in terms of energy. This nonparametric test is recommended by van Gelder et al. (2008) as it is less sensitive to outliers and does not assume any trend shape. This is a rank-based test that measures the strength of the monotonic relationship between two variables. Under the null hypothesis of no trend with a time series $\{x_1, x_2, \ldots, x_N\}$ from a population in which the random variables are independent and identically distributed, the MK test uses the z statistic, which is standard normally distributed:

$$z = \left\{ \begin{array}{lll} (S-1)/\sigma_S & \text{if} & S > 0 \\ 0 & \text{if} & S = 0 \\ (S+1)/\sigma_S & \text{if} & S < 0 \end{array} \right\} \sim N(0,1) \tag{5}$$

where S is calculated as follows:

$$S = \sum_{i=1}^{N-1} \sum_{j=i+1}^{N} \operatorname{sgn}\left(x_j - x_i\right) \tag{6}$$

in which $\operatorname{sgn}(x)$ is the sign function. The variance of S, σ_S^2 is calculated by Eq. (7), which accounts for the possibility of equal x values:

$$\sigma_S^2 = \frac{1}{18}\left[N(N-1)(2N+5) - \sum_{i=1}^{m} t_i (t_i - 1)(2t_i + 5) \right] \tag{7}$$

where m is the number of tied groups in the data set and t_i the number of data points in the i-th tied group. Regarding the basic assumption of independence of the MK test, von Storch (1995) noted that positive serial correlation in time increases the possibility of rejecting the null hypothesis of no trend. However, the annual time series of E_s can be assumed to be independent. The significance level used to perform the statistical test (see Eq. 8) is $\alpha_{\text{MK}} = 0.1$, which is slightly higher than the typical value of 0.05 so as not to miss any possible trends in the second step of the analysis.

$$\text{if} \begin{cases} z > \phi^{-1}\left(1 - \alpha_{\text{MK}}/2\right) & \Rightarrow \text{Positive trend} \\ z < \left| \phi^{-1}\left(1 - \alpha_{\text{MK}}/2\right) \right| & \Rightarrow \text{No trend} \\ z < -\phi^{-1}\left(1 - \alpha_{\text{MK}}/2\right) & \Rightarrow \text{Negative trend} \end{cases} \tag{8}$$

in which $\phi^{-1}(\cdot)$ is the inverse of the standard normal cumulative density function.

Secondly, in the trend quantification for interesting nodes with a previously detected trend, a classical linear regression analysis is carried out and complemented with the bootstrap technique (Efron, 1979) using 1000 simulated samples to capture the uncertainty in the temporal trend. Linear regression analysis is performed for $\ln(E_s)$, and therefore the relationship between E_s and time becomes exponential. As stated above, for wave directions that have had no storms for several years, the probability of storm occurrence (p_s) is introduced and the low energy threshold replacement strategy is not used, since its use and abuse may distort the results. In such cases, the values of E_s for years without storms are simply removed and the temporal trend of E_s, which is now conditioned to storm occurrence, is calculated by linear regression as explained above (to avoid the "zero" problem). Two coefficients are obtained for each node: a_E and b_E. Separately, the temporal trend of p_s is obtained by binomial logistic regression and, finally, the product of these two trends is the approximation of the temporal evolution of E_s (see Eq. 9). The same bootstrapping method is used to assess the uncertainty.

$$E_s(t) = p_s(t) \cdot \exp(a_E t + b_E) \tag{9}$$

3.3 Trend analysis of wave directional frequency

Wave directional frequencies are compositional data and require previous conversion, as there is a link between proportions (they are defined in the simplex space). If the data were not converted, the results of regression analysis, for instance, would be clouded by spurious effects (Pawlowsky-Glahn and Egozcue, 2006). The isometric log-ratio (ilr) transformation (Egozcue et al., 2003; see Eq. 10) is one of the best alternatives as it preserves the isometry. This transformation translates the $k = 8$ directional percentages $\{p_1, \ldots, p_8\}$ into 7 coordinates $\{y_1, \ldots, y_7\}$ on an orthonormal basis in a real vector space $\Re^7$, obtained from sequential binary partition (R_i, S_i). The conversion can be expressed as the log-ratio between the geometric mean of each partition $\left(g\left(p_{\in R_i}\right), g\left(p_{\in S_i}\right)\right)$, multiplied by a normalising factor $a(r_i, s_i)$.

$$y_i = a(r_i, s_i) \ln\left(\frac{g\left(p_{\in R_i}\right)}{g\left(p_{\in S_i}\right)}\right), \quad a(r_i, s_i) = \sqrt{\frac{r_i s_i}{r_i + s_i}},$$

$$\text{for } i = 1, \ldots, k-1 \tag{10}$$

where r_i and s_i are the number of elements in each partition. After some basic algebraic transformations, this expression can be rewritten as Eq. (11) for a certain year t:

$$\boldsymbol{y}(t) = \mathbf{M} \cdot \ln(\boldsymbol{p}(t)) \tag{11}$$

where $\boldsymbol{y} = [y_1, \ldots, y_7]^T$, $\boldsymbol{p} = [p_1, \ldots, p_8]^T$ and $\mathbf{M}$ is a certain matrix of known coefficients of 7×8 dimensions. The partition that is used is, in principle, arbitrary, especially if we are more interested in the final result in terms of the original percentages than in the interpretation of the coordinates obtained by the transformation.

Once the original values have been transformed for each year, we perform a classical linear regression analysis complemented with bootstrapping, which is similar to the storm energy content case explained in the previous subsection. Thus, we obtain a linear relation between the 7 coordinates and time, defined by two vectors of coefficients: $\boldsymbol{a}$ and $\boldsymbol{b}$. To obtain the expected $\left\{\hat{p}_1, \ldots, \hat{p}_8\right\}$ values (or 95% confidence intervals) for a certain time, the inversion conversion is carried out (Eq. 12).

$$\hat{\boldsymbol{p}}(t) = C \exp\left(\mathbf{M}^T \cdot (\boldsymbol{a}t + \boldsymbol{b})\right) \tag{12}$$

in which C is the closure operation to fit the relationship $\sum_{i=1}^{8} \hat{p}_i = 1$. To better interpret and discuss the results, instead of using the coefficients $\boldsymbol{a}$ and $\boldsymbol{b}$ from the complex expression of Eq. (12), two extrapolations are calculated: 2010 (for the present) and 2050 (for the future). In turn, these are used for the application study on harbour agitation (see Sect. 3.4). The extrapolation is performed as follows: the linear trends ($\boldsymbol{a}$ and $\boldsymbol{b}$) are used to calculate the extrapolated values $\boldsymbol{y}(t = 2010)$ and $\boldsymbol{y}(t = 2050)$. Subsequently, the inverse conversion (see Eq. 12) is performed to obtain $\hat{\boldsymbol{p}}(t = 2010)$ and $\hat{\boldsymbol{p}}(t = 2050)$. These projected percentages (and their 95% marginal confidence intervals) are named "projections". However, we must bear in mind the limitations of the methods, due to the underlying assumptions and the hindcast data that are used.

3.4 Harbour agitation modelling

A number of numerical models simulate wave propagation inside a harbour. These include Boussinesq-type models, which have been widely used as they can reproduce most of the physical processes involved in wave propagation. Boussinesq-type models (Peregrine, 1967) were originally developed to simulate the propagation of long waves. Various subsequent modifications (Sierra et al., 1988; Madsen et al., 1991; Nwogu, 1993; Chen and Liu, 1995) enabled these models to solve wind-wave propagation and low-frequency motion. Mutual interactions between short and long waves are inherent in these models. Therefore, they enable the study of nonlinear processes involved in the propagation, breaking and run-up of irregular wave trains (Karambas and Koutitas, 2004).

There are numerous examples of the application of such models to harbour agitation. Bingham (2000) used a Boussinesq model to predict the induced short- and long-wave motion of a restrained floating body in restricted water. Nadaoka and Raveenthiran (2002) developed a phase-averaged Boussinesq model to describe wave groups and the accompanying long-wave evolution. Karambas and

Koutitas (2004) employed a Boussinesq model to simulate low-frequency waves induced by short-wave groups. They found good agreement between their calculations and experimental data taken from the literature. Woo and Liu (2004) developed a finite element model for modified Boussinesq equations and applied it to the study of harbour resonance problems. González-Marco et al. (2008) used a Boussinesq-type model to analyse the propagation of short and long waves inside a Spanish harbour and their effect on port operations.

In this paper, a Boussinesq-type model (González-Marco et al., 2008) is applied to a harbour on the Catalan coast to illustrate the impact on harbour agitation of potential changes in wave storm direction. We study Tarragona Port, which is one of the most active in the Mediterranean area in terms of cargo (33.3 million tons per year) and vessel traffic (2700 arrivals per year) (Mestres et al., 2010). The port is located on the southern Catalan coast (41°0.5′ N; 1°14′ E). It is about 4.5 km long and 2 km wide and lies along a longitudinal axis with an approximate NE-SW orientation.

The following procedure is used to assess the potential changes in Tarragona port agitation. Wave propagation inside the harbour is simulated for the different possible directions entering the port and an average agitation coefficient (the ratio between the wave height at a point and the incident wave height) is computed for the entire harbour and for each direction. Taking into account the frequency of each of these directions in the present and future conditions (2010 and 2050 projections, see Sect. 3.3) according to the estimated trends, an overall agitation coefficient can be computed that considers all directions. This coefficient is subjected to the assumptions and used to assess expected temporal variations in agitation under storm conditions. To evaluate part of the uncertainty of these results (see Sect. 3.5), the 95% confidence intervals of these overall agitation coefficients are calculated using the bootstrap technique. In other words, for each time scenario (2010 and 2050), 1000 samples of the eight-directional percentages are obtained. For each sample, the agitation coefficient is calculated by considering only the directions that produce waves that affect the harbour (the other directions lead to null agitation). Finally, the quantiles of the obtained sample of overall agitation coefficients establish the confidence band that integrates the uncertainty between directions.

3.5 The role of uncertainty

A correct assessment of uncertainty is crucial in a long-term analysis, especially in the context of wave climate variability. In this study, we only consider the uncertainty associated with the inherent variability of the data. The bootstrap technique is used to bound the results, as explained frequently in different processes of trend quantification. In general, 1000 samples are simulated for each case to compute robust 95% confidence intervals as their quantiles, as a function of time or for a certain projection. Despite its simplicity, bootstrapping, which is computer intensive, has been proven to be a suitable method for this type of analysis, in combination with linear regression. Casas-Prat and Sierra (2010) compared the uncertainties thus obtained with a Bayesian model (with flat priors) and the results were very similar. This suggests that, in a general case with little a priori information, the combination of linear regression + bootstrapping is more suitable than the more complex Bayesian method. Nevertheless, if more prior knowledge were available, a Bayesian analysis with more informative priors might reduce the uncertainty.

Other sources of uncertainty, which are very difficult to quantify, are not accounted for in the present study and, therefore, the confidence bands represent a lower boundary of the total uncertainty. Two examples of such uncertainty are the intrinsic errors present in the data due to the modelling (as discussed in Sect. 2) or the chosen model for trend extrapolation, which is related to the evolution of the atmospheric patterns.

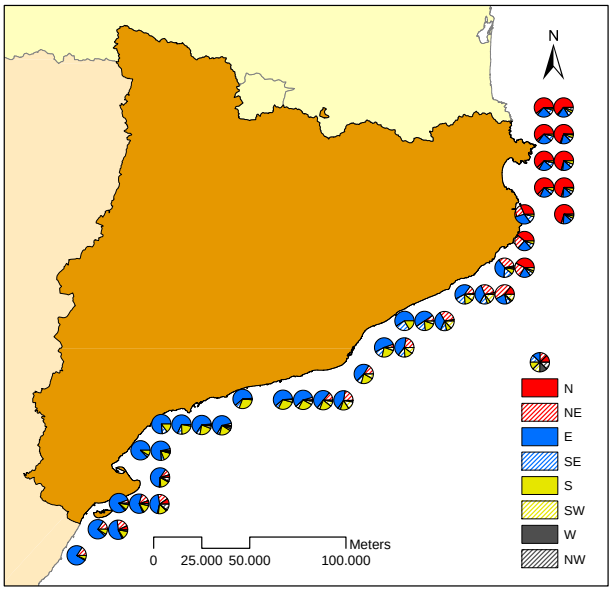

Fig. 4. Mean frequency for each direction for the data period 1958–2001 (sector areas proportional to the percentages).

4 Results and discussion

4.1 Wave storminess characterisation

To characterise wave storminess for the second half of the 20th century, in this subsection we present the storm energy content (E_s) and directional frequency (p_i) results for the entire data period of data (1958–2001). Figure 4 shows p_i as a pie chart for each location, in which the surface areas are proportional to the percentages. Figure 5 illustrates the mean and maximum values of E_s for each direction and location.

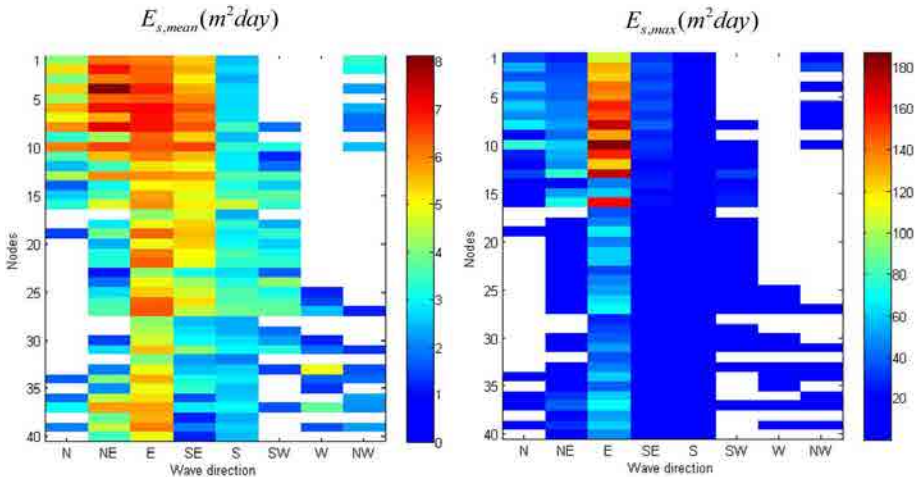

Fig. 5. Mean and maximum E_S for each direction and each node along the Catalan coast.

In terms of both frequency and intensity, the Catalan coast is clearly dominated by storm events coming from the E (see Figs. 4 and 5), in which larger fetches and stronger winds coincide (Sánchez-Arcilla et al., 2008). N events are the most frequent on the northern Catalan coast, although the maximum storm energy content is again associated with the E direction (see Figs. 4 and 5). S and SE events are generally remarkable, even though they are less intense due to the Balearic Islands and their associated shadow effects (see the location of the Catalan coast in Fig. 1). Locally, at the Ebre Delta (southern Catalan coast), there is a considerable presence of waves from the NW sector, due to the Mestral wind funnelled through the Ebre river valley. However, fewer extreme waves are developed near the coast as there is limited fetch.

As mentioned above, Fig. 5 illustrates the spatial E_S distribution among the different sectors along the Catalan coast. Blank squares mean a lack of storms during the entire data period (1958–2001). Note that for some locations, some combinations of node-direction (e.g. W) show calm situations without any storms. Therefore, a significant trend analysis of wave storminess cannot be carried out for such cases.

The mean storm energy oscillates between zero (indicating no storms) and 8 m^2 day. Values of up to 180 m^2 day are reached for the maximum variable (see Fig. 5). According to Mendoza and Jiménez (2006), these values correspond to storms classified as Moderate (II) and Extreme (V), respectively. If a simple triangular-shaped storm is assumed, Eq. (13) follows:

$$E = H_{s,peak}^2 d \Big/ 3 \quad (13)$$

where $H_{s,peak}$ is the significant wave height of the storm peak and d is the storm duration. Along the Catalan coast, d is generally less than 24 h (Sánchez-Arcilla et al., 2008). If a reasonable value of 20 h (similar to that found by Mösso et al., 2009) is considered and Eq. (13) is used, a mean wave storminess of 6 m^2 day corresponds to $H_{s,peak} = 4.6$ m.

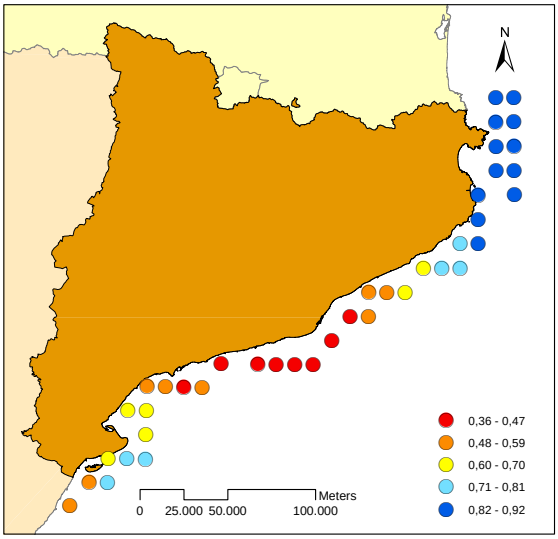

Fig. 6. Circular correlation between wind and wave direction in stormy conditions.

To roughly distinguish between sea and swell, the circular correlation (Fisher and Lee, 1983) between wind and wave directions is used, as illustrated in Fig. 6. As expected, it is found that northern locations (with most events coming from the N) are highly correlated (0.81–0.92), which can be explained by the lower N fetch and the greater presence of sea-type waves. Conversely, in the mid-southern part, E predominance is related to more mixed sea states, with poor correlations of 0.36–0.59. The correlation is higher in the area surrounding the Ebre Delta. This could be due to the relatively high presence of locally developed waves, caused by the aforementioned Mestral (NW) winds.

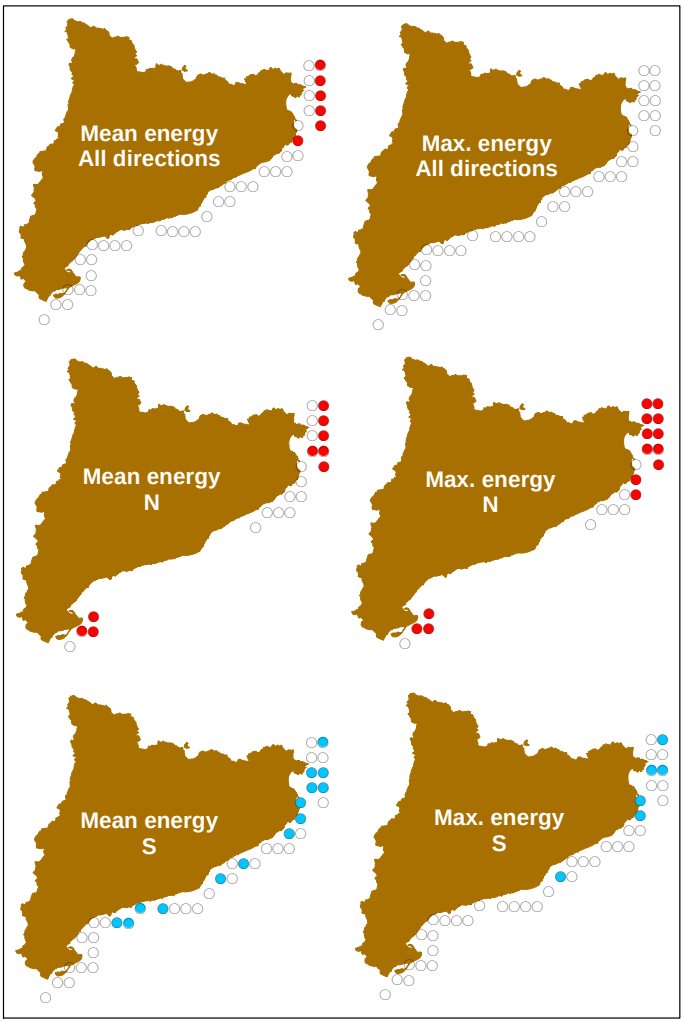

Fig. 7. Trend detection of E_S for some directions. Red: negative trend. Blank: no significant trend. Blue: positive trend (adapted from Casas-Prat and Sierra, 2010).

4.2 Trend analysis of storm energy content

Regarding trend quantification with the MK test, as found by Casas-Prat and Sierra (2010), the temporal trends are null or even negative (in a few offshore locations of the northern Catalan coast) when all wave directions are considered. In the northern Catalan coast, these negative trends may be partly related to the temporal evolution of events coming from the N, which tend to decrease. Figure 7 shows some of the most significant results, in which a few nodes have been deleted to better illustrate that there are no storms in these locations for such directions.

For all nodes, the trend in the E (most energetic) direction is not significant (not shown here). Therefore, the magnitude of the most severe storms will not tend to change. In contrast, increasing energy is expected for S storms, as illustrated in Fig. 7 (blue dots). This rise does not affect the entire Catalan coast but could be relevant locally. After a visual examination of the temporal evolution in E_S of S storms for some nodes in which trends have been detected, it is found that apart from a certain rise in magnitude, the positive trend is mostly related to an annual increase in the probability of storm occurrence. As shown in Sect. 4.3, this leads to a higher percentage of S storms. Figure 8 illustrates two examples (nodes 2 and 31) of this evolution in which events from the S are more common in the last decade than in the first one. For this direction, an annual lack of storms (zero energy) is not negligible. Therefore, as explained in Sect. 3.2, the probability of storm occurrence is incorporated. Figure 9 shows an example of the temporal trend, in which the final trend (continuous red line) can be compared with the trend of E_S when an S storm occurs (dashed red line). In addition, the 1000 bootstrapped samples of trends are plotted and the black dashed lines show the 95% confidence intervals. To compare the trends for different locations, these complex tendencies have been characterised

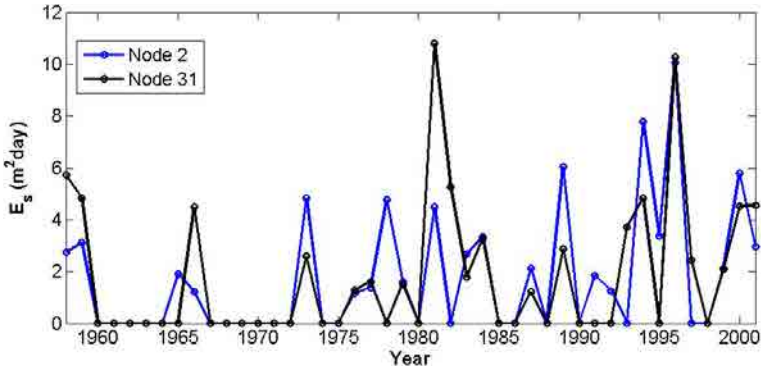

Fig. 8. Two examples of annual mean E_S temporal evolution for storm events coming from S.

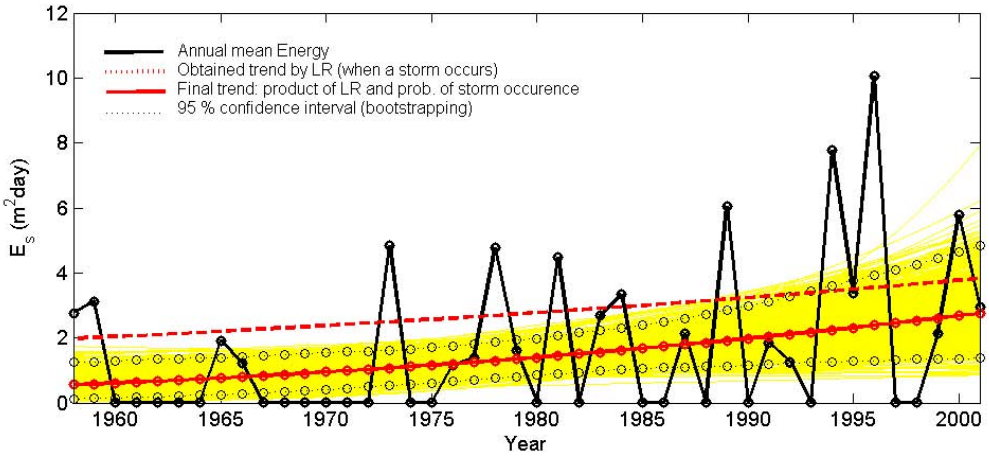

Fig. 9. An example of trend quantification of annual mean E_S from S (node 2, see Fig. 1). LR means linear regression.

by a single number: the mean rate of annual increase. This has been computed as the slope between E_S ($t = 1958$) and E_S ($t = 2001$) and is shown in Fig. 10 for S storms. Some of the nodes are marked with red dots to represent the locations in which a trend has been detected by the MK test (see Fig. 7). We can see that the majority of these nodes have most of the confidence interval within the positive area, which means that the E_S for S events are highly likely to increase. Moreover, the nodes with higher low confidence bounds are generally associated with the MK detection.

4.3 Trend analysis of wave directional frequency

Figure 11 shows the trend quantification of the S directional frequency of an example (node 31) as well as an extrapolation up to 2050. There is a considerable mean increase for this direction, but the confidence intervals cover a wide region, especially for the future prediction. This high uncertainty is due to the large inter-annual variability and the implicit reduction in data associated with the extreme analysis and the classification into sectors.

In Fig. 12, future projections for the mid-century (2050) are illustrated for all directions and compared with the 2010 projection (which represents the present situation). At locations with a considerable number of N events (e.g. node 2), this direction tends to decrease whereas a generalised increase in S frequency is detected at most locations. For example, for nodes 2 and 31, the S frequency is expected to at least double, in mean terms. In addition, the most energetic direction (E) does not significantly vary, except at some locations (e.g. node 31) for which the annual mean frequency tends to decrease (but not the energy, see Sect. 4.2). In Fig. 12, the marginal confidence bounds are complemented with 1000 bootstrapped samples of the future prediction, to visually integrate the interaction of uncertainty between the sectors.

4.4 Application to harbour agitation

As mentioned above, changes in wave direction can affect the agitation pattern inside harbours. The predominant storms on the Catalan coast are from the NE and the E. As a result,

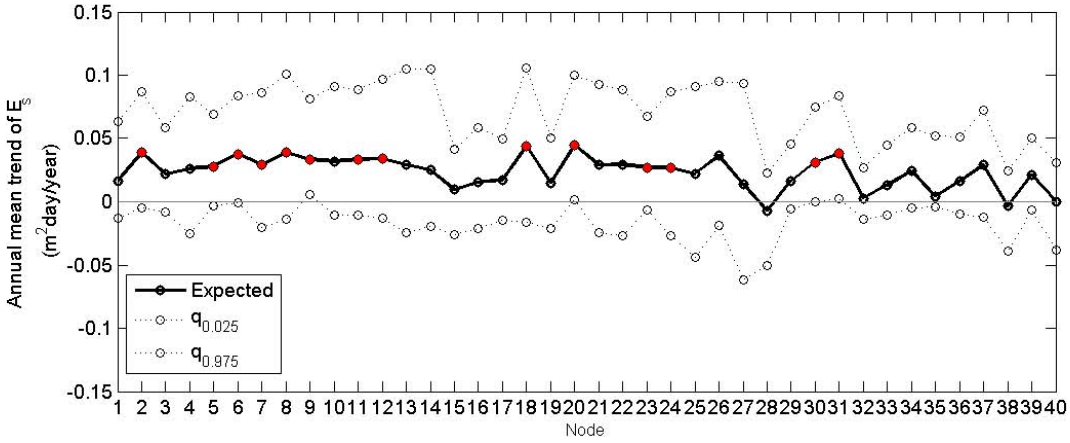

Fig. 10. Annual mean rate of increase/decrease of E_s (slope between E_s ($t = 1958$) and E_s ($t = 2001$)) of storm events coming from S for all nodes along the Catalan coast (for the time period 1958–2001). In addition, their 95% confidence intervals are added and those nodes with detected trend by Mann-Kendall (MK) test are marked in red.

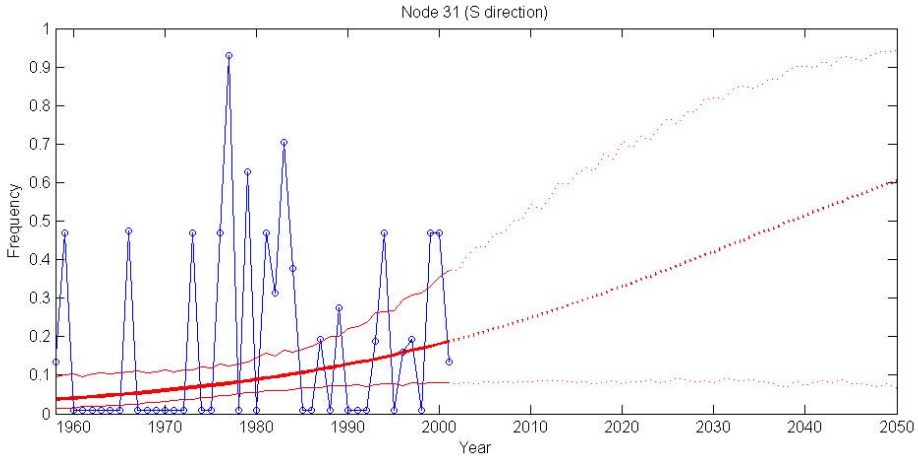

Fig. 11. Trend extrapolation of events coming from S in node 31. The figure shows the 95% confidence interval.

almost all Catalan harbours have entrances oriented towards the SW. Consequently, a rise in the number of southern wave storms could increase the waves in port berths, which would affect the safety and comfort of moored vessels. To illustrate this problem, the average agitation in the Tarragona Port (located close to node 30) was computed through a Boussinesq numerical model for the present conditions and the 2050 projections.

Figure 13 shows the plan of the Port and the surrounding coast. The existence of headlands and capes prevents the incidence of waves from the NE and SW in the Port. Therefore, only waves from the E, SE and S are considered in the analysis of agitation inside this port.

Figure 14 shows the agitation coefficient maps for the aforementioned three directions. The simulations were carried out with a peak wave period (T_p) of 10 s that can be considered typical for storm conditions. In fact, after performing a correlation between the mean period (T_m) and H_s, we found that $T_m = 3.92\sqrt{H_s}$, which means that $T_p = 10$ s corresponds to $H_s = 5$ m. The breakwater offers very good protection in the entire Port against E and SE waves (agitation coefficients below 0.2), although the wave penetration of SE waves is clearly higher. For S waves, the agitation coefficients increase dramatically in the entire Port, to reach values of approximately 0.4 in areas close to the port entrance. This means that high waves outside the port can affect port operations in different areas inside the harbour. The average agitation coefficients in the Port are 0.082 for E, 0.128 for SE and 0.230 for S.

Table 1 illustrates the changes in the average agitation coefficients for the 2010 and 2050 projections. Storm direction frequencies for node 30 indicate that in year 2050

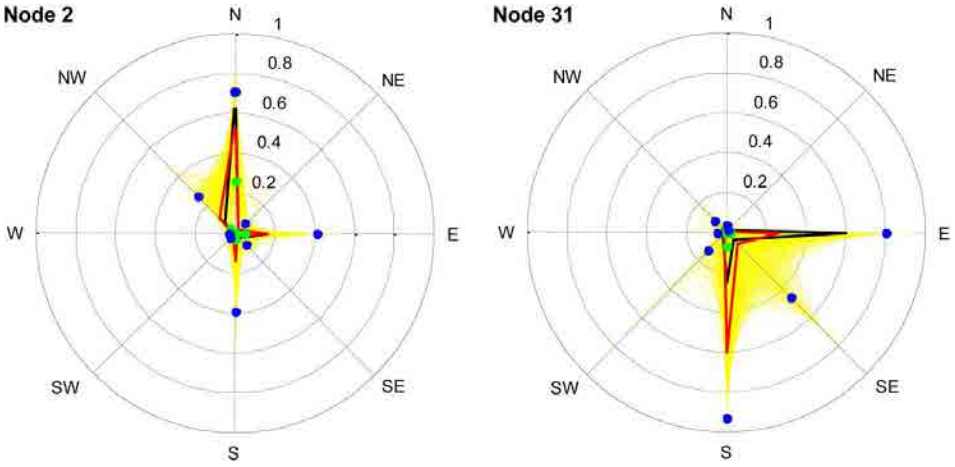

Fig. 12. Comparison between 2010 and 2050 projections (nodes 2 and 31, see Fig. 1). Black: 2010 annual mean frequency. Red: 2050 annual mean frequency. Yellow: bootstrapped 2050 projected sample. Green and blue dots: 95% marginal confidence intervals.

Table 1. Agitation coefficients (K_a) for the studied directions, and the frequency of storm presentation ($\hat{p}_i$) under projected present (2010) and future (2050) conditions.

Direction	K_a	$\hat{p}_i$ (2010)	$\hat{p}_i$ (2050)	$K_a \cdot \hat{p}_i$ (2010)	$K_a \cdot \hat{p}_i$ (2050)
E	0.082	0.44	0.10	0.036	0.008
SE	0.128	0.06	0.05	0.008	0.006
S	0.230	0.38	0.80	0.087	0.184
Global average K_a (95% conf. intervals)				0.131 (0.095, 0.180)	0.198 (0.102, 0.227)

the number of E storms will significantly decrease (from 44% to 10%), while storms from the S will dramatically increase (from 38% to 80%). If we take into account the average agitation coefficients in the entire Port for the three directions, we can derive an overall average agitation coefficient. This overall coefficient has a value of 0.131 for the present conditions and 0.198 for the 2050 projections. The respective 95% confidence intervals are (0.095, 0.180) and (0.102, 0.227). This represents a mean increase of about 50% in the average agitation inside the harbour due to storm waves, which could have severe consequences on harbour functionality by affecting loading, unloading and mooring operations, reducing port efficiency and increasing the economic costs for the users.

However, the uncertainty is high and the relative difference between 2010 and 2050 may range between −40% and 140%. Therefore, the results must be handled with care, even though they illustrate the potentially severe impact on port operations of changes in wave direction under storm conditions.

Fig. 13. Plan of the Tarragona Port and surrounding coast, showing that headlands prevent waves from NE and SW from reaching the port area.

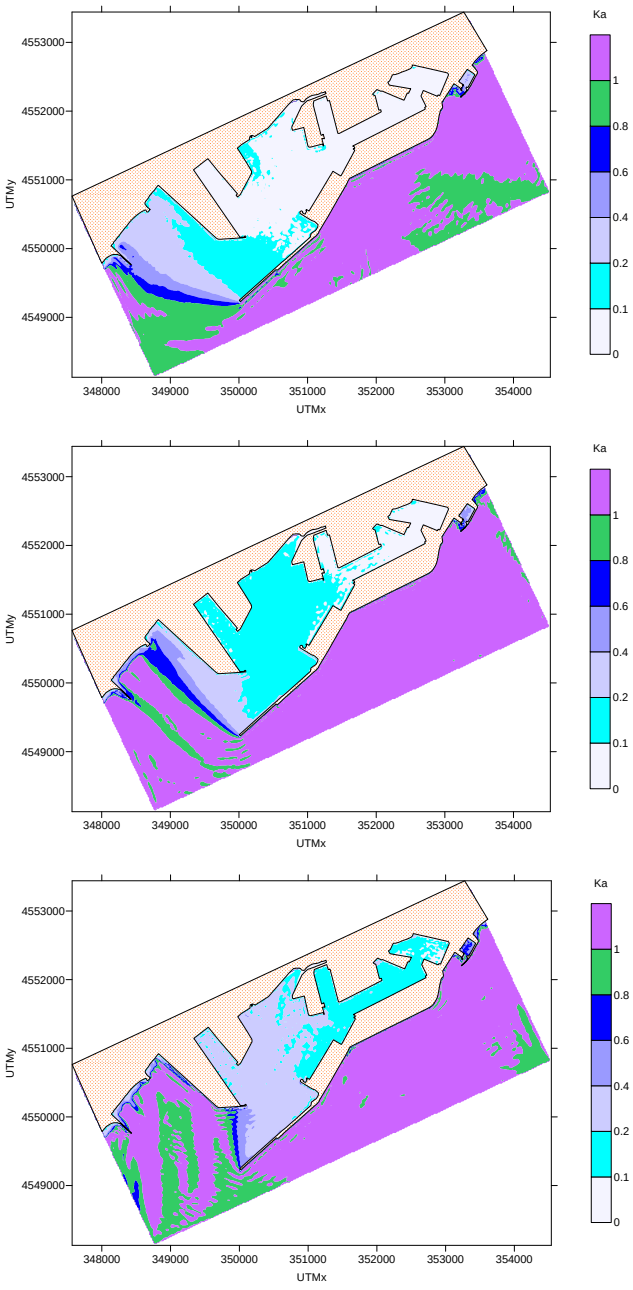

Fig. 14. Maps of agitation coefficients for E (top), SE (centre) and S (bottom) waves.

5 Conclusions

The Catalan coast has a variable wave climate in which both sea and swell conditions are generally present, depending on the fetch. The E direction, which is more closely related to mixed sea states, is the most frequent and energetic, with the exception of the northern part of the coast in which the N direction is more common (but milder than E).

Regarding the trend analysis of storm energy content, which is a representative parameter of wave storminess, the temporal trend that takes into account all directions is generally null for both annual mean and maximum values. Exceptionally, some negative trends are found for locations on the northern coast, which are partly associated with a decrease in E_s from the N. The energy of E storms has a null trend, but a significant positive trend is obtained for S storms, which is related to an increase in the magnitude of storms and in the probability of their occurrence. It was useful to separate the data into different wave directions, to detect trends that are not captured in an overall analysis. However, this classification reduces the number of data items in the analysis, somewhat increases the uncertainty, and adds the difficulty of dealing with a considerable number of zeros.

The trend in annual frequencies of wave directions has been assessed and consistent trends have been found with the storm energy content. The increase in S frequency is noteworthy. However, the uncertainty is large, which makes it difficult to build robust future predictions. Therefore, the application to the case study must be taken as a situation that may occur, but with a high level of uncertainty, as is partly quantified by the 95% confidence bounds. In addition, note that the choice of temporal model for the extrapolation of future projections produces a certain inherent uncertainty in the results, which is very difficult to evaluate. However, if no convincing alternative temporal pattern is known, simple trend shapes should be used according to the parsimony principle.

As an example of the potential implications of changes in the main wave direction during storms, the agitation in Tarragona Port (one of the most important ports on the Catalan coast) has been analysed through a Boussinesq-type numerical model. The comparison between present conditions and projections for 2050 (bearing in mind the large uncertainty that exists in these projections) indicates that the average agitation inside the Port under stormy conditions could be increased in mean terms by 50%. This would affect moored vessels and port operations, reduce port efficiency and increase costs for users. Therefore, the hazards of potential changes in wave direction during storms cannot be underestimated and should be taken into account in studies that analyse possible impacts of climate change.

In conclusion, the methods described above have served to evaluate the long-term tendency of wave climate parameters in stormy conditions, and to assess part of their uncertainty. These results are of course limited to the nature of the hindcast data. In addition, a relation between these possible future changes and (anthropogenic) climate change is plausible, but has not been proven. This is the “attribution” problem (Weisse and von Storch, 2010), which is very difficult to solve and should be the focus of future studies in the field.

Acknowledgements. The research was carried out in the frame of the EU project "Climate Change and Impact Research: The Mediterranean Environment (CIRCE)" (contract number TST5-CT-2007-036961) and the Spanish project "Vulnerabilidad, impactos y adaptación al cambio climático: estudio integrado sobre la agricultura, recursos hídricos y costas (ARCO)" (contract number 200800050084350). We are grateful to the *Organismo Público Puertos del Estado* (Spanish National Ports and Harbours Authority) for providing HIPOCAS data and to the *Xarxa d'Instruments Oceanogràfics i Meteorològics de la Generalitat de Catalunya* (XIOM, Catalan instrumental network) for buoy data. The first author is supported by an UPC PhD grant and the *Col·legi d'Enginyers de Camins, Canals i Ports – Catalunya* (Civil Engineering Association in Catalonia).

Edited by: J. Salat
Reviewed by: M. Marcos and another anonymous referee

References

Agresti, A.: Categorical data analysis, 2nd edn., Wiley, New York, USA, 734 pp., 2002.

Alvarez-Ellacuria, A., Orfila, A., Olabarrieta, M., Gómez-Pujol, L., Medina, R., and Tintoré, J.: An alert system for beach hazard management in the Balearic Islands, Coast. Manage., 37(6), 569–584, doi:10.1080/08920750903150662, 2009.

Bertotti, L. and Cavaleri, L.: The predictability of the "Voyager" accident, Nat. Hazards Earth Syst. Sci., 8, 533–537, doi:10.5194/nhess-8-533-2008, 2008.

Bingham, H. B.: A hybrid Boussinesq-panel method for predicting the motion of a moored ship, Coast. Eng., 40, 21–38, doi:10.1016/S0378-3839(00)00002-8, 2000.

Casas-Prat, M. and Sierra, J. P.: Trend analysis of the wave storminess: the wave direction, Adv. Geosci., 26, 89–92, doi:10.5194/adgeo-26-89-2010, 2010.

Chen, Y. and Liu, P.L.-F.: Modified Boussinesq equations and associated parabolic models for water wave propagation, J. Fluid Mech., 288, 351–381, doi:10.1017/S0022112095001170, 1995.

De Zolt, S., Lionello, P., Nuhu, A., and Tomasin, A.: The disastrous storm of 4 November 1966 on Italy, Nat. Hazards Earth Syst. Sci., 6, 861–879, doi:10.5194/nhess-6-861-2006, 2006.

Efron, B.: Bootstrap Methods: Another Look at the Jackknife, Ann. Stat., 7(1), 1–26, doi:10.1214/aos/1176344552, 1979.

Egozcue, J. J., Pawlowsky-Glahn, V., Mateu-Figueras, G., and Barceló-Vidal, C.: Isometric logratio transformations for compositional data analysis, Math. Geol., 35(3), 279–300, doi:10.1023/A:1023818214614, 2003.

Fisher, N. and Lee, A. J.: A correlation coefficient for circular data, Biometrica, 70, 327–332, doi:10.1093/biomet/70.2.327, 1983.

Gomis, D., Ruiz, S., Sotillo, M. G., Álvarez-Fanjul, E., and Terradas, J.: Low frequency Mediterranean sea level variability: The contribution of atmospheric pressure and wind, Global Planet. Change, 63, 215–229, doi:10.1016/j.gloplacha.2008.06.005, 2008.

González-Marco, D., Sierra, J. P., Fernández de Ybarra, O., and Sánchez-Arcilla, A.: Implications of long waves in harbor management: The Gijon port case study, Ocean Coast. Manage., 51, 180–201, doi:10.1016/j.ocecoaman.2007.04.001, 2008.

Guedes Soares, C., Carretero Albiach, J. C., Weisse, R., and Alvarez-Fanjul, E.: A 40 years hindcast of wind, sea level and waves in European waters, Proceedings of the 21st International Conference on Offshore Mechanics and Arctic Engineering, Oslo, Norway, 669–675, 2002.

Karambas, T. W. and Koutitas, C.: Resonant response of harbours to short-wave group, Maritime Engineering, 157, 163–170, doi:10.1680/maen.2004.157.4.163, 2004.

Kendall, M. G.: Rank Correlation Methods, Griffin, London, 1975.

Liste, M., Méndez, J., Losada, I., Medina, R., and Olabarrieta, M.: Variaciones hiperanuales de parámetros medios de oleaje en el litoral mediterráneo español en los últimos cinquenta años: efectos sobre la costa, IV Congreso de la Asociación Española de Climatología (AEC), 2004 (in Spanish).

Madsen, P. A., Murray, R., and Sørensen, O. R.: A new form of the Boussinesq equations with improved linear dispersion characteristics, Coast. Eng., 15, 371–388, doi:10.1016/0378-3839(91)90017-B, 1991.

Mann, H. B.: Nonparametric test against trend, Econometrica, 13, 245–259, 1945.

Marcos, M. and Tsimplis, M.: Coastal sea level trends in Southern Europe, Geophys. J. Int., 175, 70–82, doi:10.1111/j.1365-246X.2008.03892.x, 2008.

Martín-Fernández, J. A., Barceló-Vidal, C., and Pawlowsky-Glahn V.: Dealing with zeros and missing values in compositional data sets using nonparametric imputation, Math. Geol., 35(3), 253–278, doi:10.1023/A:1023866030544, 2003.

Mendoza, E. T. and Jiménez, J. A.: Factors controlling vulnerability to storm impacts along the Catalonian coast, in: Proceedings of the 29th International Conference on Coastal Engineering Lisbon, Portugal, 3087–3099, 2004.

Mendoza, E. T. and Jiménez, J. A.: Storm-induced beach erosion potential on the Catalonian coast, J. Coast. Res., Special Issue 48, 81–88, 2006.

Mestres, M., Sierra, J. P., Mösso, M., and Sánchez-Arcilla, A.: Sources of contamination and modelled pollutant trajectories in a Mediterranean harbour (Tarragona, Spain), Mar. Pollut. Bull., 60, 898–907, doi:10.1016/j.marpolbul.2010.01.002, 2010.

Monbaliu, J., Padilla Hernández, R., Hargreaves, J., Carretero, J. C., Weimin, L., Sclavo, M., and Gunther, H.: The spectral wave model, WAM adapted for applications with high spatial resolution, Coast. Eng., 41, 41–62, doi:10.1016/S0378-3839(00)00026-0, 2000.

Mösso, C., Mestres, M., Sierra, J. P., Sánchez-Arcilla, A., and Goodess, C.: Waves and surges in the Valencia Gulf. Variability rather than climate change, J. Coast. Res., Special Issue 56, 243–247, 2009.

Musić, S. and Nicković, S.: 44-year wave hindcast for the Eastern Mediterranean, Coast. Eng., 55, 872–880, doi:10.1016/j.coastaleng.2008.02.024, 2008.

Nadaoka, K. and Raveenthiran, K.: A phase-averaged Boussinesq model with effective description of carrier wave group and associated long wave evolution, Ocean Eng., 29, 21–37, doi:10.1016/S0029-8018(01)00024-5, 2002.

Nwogu, O.: An alternative form of the Boussinesq equations for nearshore wave propagation, J. Waterway Port C. Div., 119, 618–38, doi:10.1061/(ASCE)0733-950X(1993)119:6(618)), 1993.

Pawlowsky-Glahn, V. and Egozcue, J. J.: Compositional data and their analysis: an introduction (in compositional data analysis in the geosciences; from theory to practice), Geological Society, London, Special Publications, 264, 1–10, doi: 10.1144/GSL.SP.2006.264.01.01,, 2006.

Peregrine, D. H.: Long waves on a beach, J. Fluid Mech., 27, 815–882, doi:10.1017/S0022112067002605, 1967.

Ratsimandresy, A. W., Sotillo, M. G., Álvarez Fanjul, E., Carretero Albiach, J. C., Pérez Gómez, B., and Hajji, H.: A 44-year (1958–2001) sea level residual hindcast over the Mediterranean Basin, Phys. Chem. Earth, 33, 250–259, doi:10.1016/j.pce.2007.02.002, 2008a.

Ratsimandresy, A. W., Sotillo, M. G., Carretero Albiach, J. C., Álvarez Fanjul, E., and Haiji, H.: A 44-year high resolution ocean and atmospheric hindcast for the Mediterranean Basin developed within the HIPOCAS project, Coast. Eng., 55, 827–842, doi:10.1016/j.coastaleng.2008.02.025, 2008b.

Sánchez-Arcilla, A., González-Marco, D., and Bolaños, R.: A review of wave climate and prediction along the Spanish Mediterranean coast, Nat. Hazards Earth Syst. Sci., 8, 1217–1228, doi:10.5194/nhess-8-1217-2008, 2008.

Sierra, J. P., Sánchez-Arcilla, A., Egozcue, J. J., and Monsó, J. L.: Effect of Boussinesq-type equations on wave spectra propagation. Proceedings of the 21st International Conference on Coastal Engineering, Málaga, Spain, 350–362, 1988.

Soomere, T., Behrens, A., Tuomi, L., and Nielsen, J. W.: Wave conditions in the Baltic Proper and in the Gulf of Finland during windstorm Gudrun, Nat. Hazards Earth Syst. Sci., 8, 37–46, doi:10.5194/nhess-8-37-2008, 2008.

Sotillo, M. G., Ratsimandresy, A. W., Carretero, J. C., Bentamy, A., Valero, F., and González-Rouco, F.: A high-resolution 44-year atmospheric hindcast for the Mediterranean Basin: contribution to the regional improvement of global reanalysis, Clim. Dynam., 25, 219–236, doi:10.1007/s00382-005-0030-7, 2005.

Tomás, A., Méndez, F. J., Medina, R., Losada, I. J., Menéndez, M., and Liste, M.: Bases de datos de oleaje y nivel del mar, calibración y análisis: el cambio climático en la dinámica marina en España, IV Congreso de la Asociación Española de Climatología (AEC), 2004 (in Spanish).

Tsimplis, M., Marcos, M., Somot, S., and Barnier, B.: Sea level forcing in the Mediterranean between 1960 and 2000, Global Planet. Change, 63, 325–332, doi:10.1016/j.gloplacha.2008.07.004, 2008.

van Gelder, P. H. A. J. M., Mai, C. V., Wang, W., Shams, G., Rajabalinejad, M., and Burgmeijer, M.: Data management of extreme marine and coastal hydro-meteorological events, J. Hydraul. Res., 46(Extra Issue 2), 191–210, doi:10.1080/00221686.2008.9521954, 2008.

von Storch, H.: Misuses of Statistical Analysis in Climate Research, in: Analysis of Climate Variability: Applications of Statistical Techniques, edited by: Storch, H. V. and Navarra, A., Springer, New York,11–26, 1995.

WAMDI Group: Hasselman, S., Hasselman, K., Janssen, P. A. E. M., Komen, G. J., Bertotti, L., Lionello, P., Guillaume, A., Cardone, V. C., Greenwood, J. A., Reistad, M., Zambresky, L., and Ewing, J. A.: The WAM model – A third generation ocean wave prediction model, J. Phys. Oceanogr., 18, 1775–1810, 1988.

Weisse, R. and von Storch, H.: Marine Climate and Climate Change, in: Storms, Wind Waves and Storm Surges, Springer, Praxis Publishing, Chichester, UK, 2010.

Woo, S.-B. and Liu, P. L.-F.: Finite-element model for modified Boussinesq equations. II: Applications to nonlinear harbour oscillations, J. Waterway. Port C. Div., 130(1), 17–28, doi:10.1061/(ASCE)0733-950X(2004)130:1(17), 2004.

Paper B

Trend analysis of wave direction and associated impacts on the Catalan coast

M. Casas-Prat and J.P. Sierra

Climatic Change, **115**, 667–691, 2012.

ATENCIÓ ¡
Les pàgines 106 a 132 de la tesi contenen el “Paper B”, que es pot consultar a la web de l’editors

ATENCIÓN ¡

Las páginas 106 a 132 de la tesis el contienen “Paper B”, que puede consultarse en el web del editor

ATTENTION ¡

Pages 106 to 132 of the thesis are availables at the editor’s web

http://link.springer.com/article/10.1007%2Fs10584-012-0466-9

Paper C

Projected future wave climate in the NW Mediterranean Sea

M. Casas-Prat and J.P. Sierra

Journal of Geophysical Research: Oceans, **118**(7), 3548–3568, 2013.

JOURNAL OF GEOPHYSICAL RESEARCH: OCEANS, VOL. 118, 3548–3568, doi:10.1002/jgrc.20233, 2013

Projected future wave climate in the NW Mediterranean Sea

M. Casas-Prat[1,2] and J. P. Sierra[1,2]

Received 29 December 2012; revised 29 April 2013; accepted 5 May 2013; published 22 July 2013.

[1] Projected future regional wave climate scenarios at a high temporal-spatial scale were obtained for the NW Mediterranean Sea, using five combinations of regional-global circulation models. Changes in wave variables were analyzed and related to the variations of the forcing wind projections, while also evaluating the evolution of the presence of the different types of sea states. To assess the significance of the changes produced, a bootstrap-based method was proposed, which accounts for the autocorrelation of data and correctly reproduces the extremes. For the mean climate, relative changes of H_s up to $\pm 10\%$ were obtained, whereas they were around $\pm 20\%$ for the extreme climate. In mean terms, variations of H_s are similar to those associated with wind speed but are enhanced/attenuated, respectively, when fetch conditions are favorable/unfavorable. In general, most notable alterations are not in the H_s magnitude but rather in its direction. In this regard, during the winter season, it is interesting to note that the significant deviations between the results derived from the two global circulation models are larger than those between regional models. ECHAM5 simulated an enhanced west wind flow that is translated into more frequent W-NW waves, whereas the HadCM3Q3 global model gives rise to the east component, which contributes to a higher intensity and number of storms coming from such a direction and directly affects the wind-sea/swell distribution of coastal stretches that face east, like the Catalan coast. Different patterns of change were obtained during the summer when a common rise of NE-E waves was found.

Citation: Casas-Prat, M., and J. P. Sierra (2013), Projected future wave climate in the NW Mediterranean Sea, *J. Geophys. Res. Oceans*, *118*, 3548–3568, doi:10.1002/jgrc.20233.

1. Introduction

[2] Climate change has become a major concern due to its possible impact. The evidence of variation in cyclone activity [e.g., *Bengtsson et al*., 2009; *Ulbrich et al*., 2009]—and therefore in wind climate—is a warning to coastal communities as it will ultimately affect the wave climate, which, in turn, will impact the already threatened (and densely populated) coast.

[3] The Fourth Assessment Report (AR4) of the *Intergovernmental Panel on Climate Change* (*IPCC*) [2007], which mainly focused on sea level rise, highlighted a lack of information on the potential changes in regional wave climate [*Christensen et al*., 2007]. Besides sea level rise, a comprehensive assessment of potential climate change-driven impacts on the coastal zone must consider potential future changes in wave conditions, and therefore a greater understanding of wind waves in the climate system is required [*Hemer et al*., 2012a].

[4] Offering an initial overview without much computational effort, some authors have evaluated future wave-climate conditions through trend analysis of long, past time series [e.g., *Casas-Prat and Sierra*, 2012; *Hemer et al*., 2010; *Wang et al*., 2012]. However, despite being a good preliminary assessment, their results are limited to the trend assumptions involved. As such, there is a need for further analysis in which the greenhouse effect is explicitly accounted for.

[5] For different greenhouse emission scenarios based on social and economic hypotheses [*IPCC*, 2007], regional wave climate scenarios have been modeled using atmospheric climate projections available from regional circulation models (RCMs) [e.g., *Charles et al*., 2012; *Grabemann and Weisse*, 2008; *Hemer et al*., 2012b; *Lionello et al*., 2008a; *Wang et al*., 2010]. RCM output parameters (temperature, pressure, wind speed, etc.) are affected by different sources of uncertainty. As explained by *Déqué et al*. [2007], the greenhouse gas concentration of each emission scenario is just the initial source in the causal chain. Formulations, resolutions, and parameterizations used in the different RCMs (as well as the boundary conditions derived from the respective general circulation models (GCMs)) contribute to

[1]Laboratori d'Enginyeria Marítima, Universitat Politècnica de Catalunya · Barcelona Tech, Barcelona, Catalonia, Spain.
[2]Centre Internacional d'Investigació dels Recursos Costaners, Barcelona, Catalonia, Spain.

Corresponding author: M. Casas-Prat, Laboratori d'Enginyeria Marítima, Universitat Politècnica de Catalunya · Barcelona Tech, Barcelona, Catalonia, Spain 08034. (merce.casas@upc.edu)

©2013. American Geophysical Union. All Rights Reserved.
2169-9275/13/10.1002/jgrc.20233

additional uncertainty, and, lastly, the problem is further complicated because of the internal natural variability of simulated as well as actual climate. Based on a group of 16 transient experiments at the European scale, *Kjellström et al*. [2011] concluded that each of these factors contributes to the total uncertainty in a different way depending on the output variable analyzed and the season (uncertainty associated with RCM tends to be higher during the summer whereas uncertainty associated with GCM is higher in the winter). In the case of (wave-driving) wind speed, the emission scenario does not play an important role; instead, the choice of model, especially the GCM, is relevant [*Kjellström et al*., 2011; *Nikulin et al*., 2011].

[6] Therefore, in order to properly assess the wave climate change, it is necessary to consider several GCM-RCM realizations to cover as much of the uncertainty range as possible. Indeed, *Déqué and Somot* [2010] and *Donat et al*. [2010b] found that an ensemble is usually better than the "best" single model—if any exists—although it might be necessary to exclude outliers [*Donat et al*., 2010a]. Actually, it is far from clear which model is the "best" because model skill usually depends on both the analyzed output variables and the season [*Déqué et al*., 2005], and a better simulation of the observed climate does not prove that climate response is more reliable [*Déqué and Somot*, 2010].

[7] This study focuses on the Catalan coast, located in the NW part of the Mediterranean Basin (see Figure 1), which apparently is an area particularly exposed to climate change [*Ulbrich et al*., 2009]. Aiming to fill some of the existing gaps, this paper has three main goals: first, to provide the Catalan coast with detailed, high-resolution wave climate projections. To our knowledge, only the simulations of *Lionello et al*. [2008a] are available in the study area, which have a resolution of 50 km and 6 h and use just one RCM-GCM combination forced by A2 ("pessimistic") and B2 ("optimistic") greenhouse scenarios [*IPCC*, 2007]. The higher spatial and time resolution used in this study (25 km and 3 h) and the consideration of five different RCM-GCM realizations (forced by the increasingly used midline A1B scenario [*IPCC*, 2007]), respectively, allow us to better reproduce the complex regional wave climate features [*Sánchez-Arcilla et al*., 2008] and explore part of the aforementioned uncertainty caused by climate models.

[8] Second, in order to better assess the significance of the changes obtained, we propose a method to address the uncertainty derived from the data variability itself. Such variability is sometimes dismissed by using "standard" tests, which are not always suitable for the type of data involved (e.g., methods that assume independent and/or normally distributed data). The proposed methodology is a bootstrap-based method in which the modifications of *Cai and Davies* [2012] and *Pandey et al*. [2004] are jointly implemented, to account for, respectively, the autocorrelation present in the data and the poor representation of extremes by the classical bootstrapping.

[9] Third, to gain insight into the understanding of the atmosphere-wave climate system, the wave climate variations obtained are not merely described but are, in fact, discussed in relation to the latest studies on present and future wind climate. Besides the typical significant wave height (H_s) parameter, we address variations in the wave direction distribution, which seem to have an important role in the study area [*Casas-Prat and Sierra*, 2012] and possible changes in the wind-sea/swell distribution, as recently done by *Charles et al*. [2012].

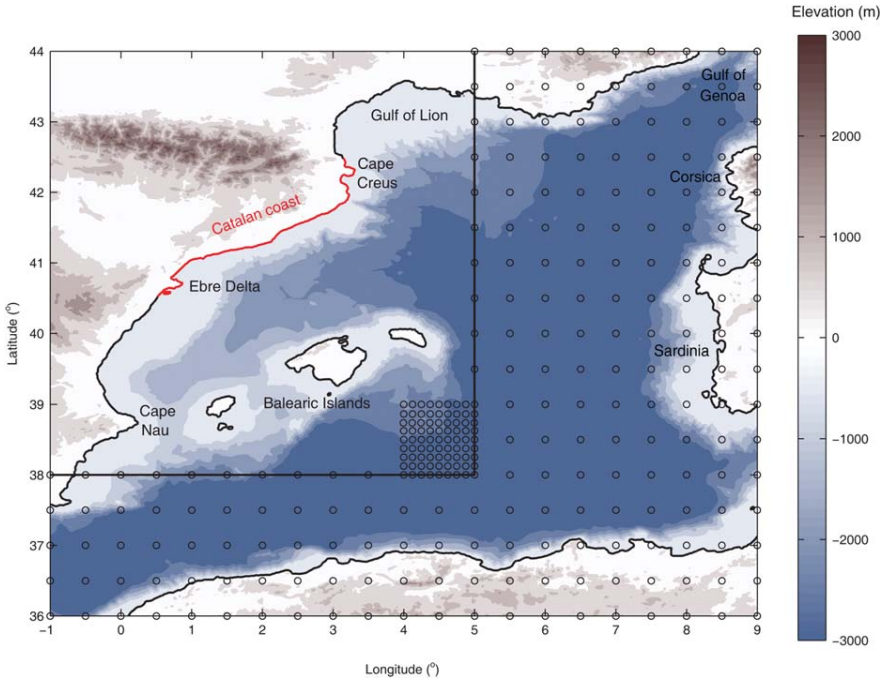

Figure 1. Situation of the Catalan coast in the study area. Circles indicate wave grid points of the two domains used in wave modeling (see section 3.1).

[10] The rest of the paper is structured as follows. Section 2 presents a review of wind climate in the study area. Sections 3 and 4 explain the methodology adopted with regard to wave modeling and uncertainty analysis. In sections 5 and 6, results are presented and discussed. Finally, section 7 presents a summary of conclusions.

2. Present and Future Wind Climate in the NW Mediterranean Sea: A Review

[11] To better understand changes in wave climate, it is important to first become acquainted with the expected changes of forcing wind patterns. This section gives an overview of the latest scientific knowledge regarding present (section 2.1) and future (section 2.2) wind (wave-forcing) climate in the NW Mediterranean Sea, where the Catalan coast is located.

2.1. Present Climate

[12] Extratropical cyclones are the dominant feature of midlatitudes [*Ulbrich et al*., 2009] as in the Mediterranean basin. They mainly form and grow via baroclinic instability, with the available potential energy being proportional to the variance of temperature in the troposphere [*Bengtsson et al*., 2009], which is highest during the winter season. In the Mediterranean Sea, there is a prominent maxima in the Gulf of Genoa (see Figure 1). Compared to northern Europe, Mediterranean events are normally shorter and less intense (with a typical radius of 500 km and average duration of 28 h according to *Lionello et al*. [2006]) and many subregional and mesoscale effects take place, producing a large spatial and seasonal variability [*Campins et al*., 2011]. The reduced scale, along with the peculiar features of the basin (complex orography, moisture of a relatively large mass of water), makes the Mediterranean climate more difficult to predict [*Ulbrich et al*., 2009]. It is therefore necessary to work at a higher spatial and temporal resolution compared to, for instance, the Atlantic Ocean [*Lionello et al*., 2002]. One example of a local feature is the Mistral wind (called *Mestral* in Catalonia), which consists of an intense and persistent NW wind often caused by a cyclone over the Gulf of Genoa, which is then channeled and intensified through the valleys between mountain ranges in the north side of the NW Mediterranean such as the Rhone Valley, or even through the Ebre Valley (see Figure 1). On the Catalan coast, it is also common to have east winds in stormy conditions (locally known as *Llevant* events), which are caused by either an anticyclone over northern Europe or a low-pressure area over Balearic Islands.

[13] During the summer, thermal and orographic effects play a greater role in the genesis and maintenance of cyclones. In the NW Mediterranean, apart from the Gulf of Genoa, there is another maxima in the number of cyclone centers over the Iberian Peninsula caused by temperature contrasts between land and sea [*Campins et al*., 2011]. During the warm period, the Mediterranean is also exposed to tropical systems [*Lionello et al*., 2002] as a result of being located in a transitional zone between humid mountains in the north and arid regions in the south, although these are not predominant events. Finally, spring and autumn can be considered as transitional periods between winter and summer contrasting patterns [*Campins et al*., 2011].

2.2. Future Climate

[14] It is very difficult to know exactly how the aforementioned atmospheric patterns will react to climate change due to the many competing processes that interact. With regard to extratropical cyclones and considering only their main forcing mechanism, the meridional temperature gradient, uncertainty arises from the fact that global warming is not expected to be homogeneous in either latitude or altitude. In the lower troposphere, stronger warming is expected to occur in polar regions, whereas in the higher troposphere it is expected at lower latitudes. This involves a decrease (increase) of such a gradient in the lower (upper) troposphere [*Weisse and Von Storch*, 2010]. Depending on the spatial extension of such temperature variations, the location of more unstable vertical stratification, linked to the preferred storm track locations, will vary [*Weisse and Von Storch*, 2010]. Many studies have found a consistent poleward shift of such a location [e.g., *Ulbrich et al*., 2009] which, at the European scale, would be translated into enhanced wind speeds over northern Europe, and a decrease in southern Europe [*Lionello et al*., 2008b; *Donat et al*., 2011] where the study area is located. *Nikulin et al*. [2011] concluded that such strengthening (weakening), in terms of gust winds, will occur approximately north (south) of 45°N, although locally there may be different signs of change. However, a recent study [*Scaife et al*., 2011], which used increased stratospheric resolution, concluded that this poleward shift was overestimated and will actually be about 10° further south than predicted in previous studies. In addition, despite not being the predominant factor, extratropical cyclones are also affected by sea surface temperature (SST) gradients, which affects their position and activity, and by concentration of water vapor in the atmosphere, which enhances their intensity [*Bengtsson et al*., 2006].

[15] As a result of these factors, most studies concur that there will be a decrease in the number of Mediterranean cyclones; however, there is a lack of consensus on whether the number of intense cyclones will increase or decrease [*Lionello et al*., 2002; *Pinto et al*., 2007], as summarized in the IPCC AR4 report. *Ulbrich et al*. [2009] pointed out that discrepancies between trends observed in studies are usually due to the different approaches used for defining an "extreme event." However, a recent study [*Ulbrich et al*., 2013] found that (for the IPCC A1B scenario), the total numbers of cyclones identified are largely similar between methods.

[16] The variation in wind direction remains even more uncertain. *Donat et al*. [2010a] analyzed changes in circulation weather types associated with (winter) European storminess using nine RCM-GCM combinations. For most of the simulations, they found that the predominant westerly flow over Europe will be significantly enhanced, whereas the cyclonic weather type (large cyclone located over central Europe associated with above-average wind speed over the Mediterranean Sea) is expected to decrease. Nevertheless, it is relevant to point out that, whereas East and SE flow remain unchanged or even decrease in most of the realizations, one GCM exhibited a contrasting pattern in which East and SE flows significantly tend to increase. Additionally, they found that the SW flow tends to decrease for the later GCM, whereas for many other GCMs it tends

to increase, although not being as statistically significant as the east flow decrease.

3. Wave Modeling

[17] We use the dynamical downscaling technique to project wave climate at a regional scale, as seen previously in other studies [e.g., *Charles et al*., 2012; *Grabemann and Weisse*, 2008; *Lionello et al*., 2008a]. In this section, we specify the adopted configuration of the model settings and the data sets used to run the wave model.

3.1. Model Settings

[18] Wave climate projections have been performed with the SWAN wave model [*Booij et al*., 1999] version 40.72ABCD following a downscaling-nesting procedure with two computational grids. The first includes the NW Mediterranean Sea with a resolution of 0.5° (see Figure 1) and assumes no waves entering the domain since wet boundaries are unknown. This artificial boundary does not significantly affect the area of interest (Catalan coast) because it includes the maximum fetch associated with the regional wave climate, which is about 600 km since the islands of Corsica and Sardinia are a barrier for most swell waves [*Sánchez-Arcilla et al*., 2008].

[19] The second nested domain (see Figure 1) has a spatial resolution of 0.125°—comparable to hindcast data in the zone—and includes the Balearic Islands. To properly account for their associated shadowing effects, a high spectral resolution is necessary [*Bolaños*, 2004]. In this study, relative frequency resolution is $\Delta f/f = 0.1$, where $0.04 \leq f \leq 1$ Hz, and directional bins are 10°.

[20] The computational time step of the nested simulation was set to 1 h (while 3 h for the coarse domain), although results have been stored every 3 h. Output consists of typical spectrum-integrated/derived variables: significant wave height H_s, peak wave period T_p and mean wave direction Θ_m.

3.2. Data Sets

[21] The bathymetry data used for the wave modeling is the GEBCO One Minute Grid (http://www.gebco.net/, accessed 2010), which, as the name indicates, has a spatial resolution of 1/60°.

[22] Wave forcing consists of high spatial-resolution (25 km), regional 10 m (nonstationary) wind projections undertaken within the context of the ENSEMBLES project, forced by the mid-line A1B emission scenario [*IPCC*, 2000]. Mean and maximum daily data are publicly available at http://www.ensembles-eu.org/ (accessed 2012) but the hourly time-resolution version of those simulations — necessary in order to properly reproduce regional wave climate in the study area (see section 2) — is stored locally. For this study, four European research institutes freely placed at our disposal their corresponding projections, forced by the following RCMs: HIRHAM5 (from *Danmarks Meteorologiske Institut*—DMI, see *Christensen et al*. [2007]), RACMO2 (from *Koninklijk Nederlands Meteorologisch Instituut*—KNMI, see *van Meijgaard et al*. [2008]), REMO (from *Max-Planck-Institut für Meteorologe*—MPI, see http://www.remo-rcm.de, accessed 2012) and RCA3 (from *Sveriges Meteorologiska och Hydrologiska Institut*—SMHI, see *Samuelsson et al*. [2011]). All projections were forced by the ECHAM5 general circulation model [*Roeckner et al*., 2003], and, for the RCA3 RCM, the configuration using HadCM3Q3 GCM [*Collins et al*., 2001] was also provided. For each RCM-GCM combination, two 30 year time slices were selected to project wave climate changes (as recommended by *Hemer et al*. [2011]): "present" (1971–2000) and "future" (2071–2100); except for MPI data, for which the first period is 1981–2010 (due to data availability). The five subsets of wind data are respectively named in this study as: HIR_E, RAC_E, REM_E, RCA_E, and RCA_H. As illustrated in Table 1, output time resolution is 3 h for RAC_E, RCA_E, and RCA_H, versus 1 h for HIR_E and REM_E. In all cases, the output is instantaneous except for REM_E, for which it is averaged over an 1 h time window. Actually, despite having the same (output) time resolution, every model has a slightly different (internal) computational time step (usually between 10 and 30 min). To homogenize the wave modeling realizations, a common time resolution of 3 h has been used to force the wave model. With regard to the spatial resolution, all models have a resolution of 25 km (see Table 1) but in the cases of RCA_E and RCA_H, a spatial average has been previously carried out in the atmospheric model. Therefore, their wind speed fields tend to underestimate extreme events [*Kriezi and Broman*, 2008].

[23] Finally, to explore the RCM-GCM bias, the projected wave climate for the present period is validated with the hindcast data of the HIPOCAS project [*Guedes Soares et al*., 2002] available for the same period of time. This wave data set has a time resolution of 3 h and a (variable) spatial resolution of 0.125° at nearshore areas whereas 0.5° offshore. Although some extreme events are underestimated by HIPOCAS data [*Casas-Prat and Sierra*, 2010a], it well represents the mean climate [*Ratsimandresy et al*., 2008].

4. Uncertainty Analysis of Projected Changes

[24] Let $\mathbf{x}(m)$ be the time series of the wave variables obtained by wave modeling (either H_s, T_p, or Θ_m, see section 3.1) for a certain wave grid point m considered ($m = 1, \cdots, M$, where M is the total number of wave grid points). For each $\mathbf{x}(m)$, some parameters have been calculated to characterize the wave climate, denoted in general as $\theta(m)$. The associated projected change, denoted as $\Delta\theta(m)$, is the "difference" between the value of $\theta(m)$ for the future scenario and the value of $\theta(m)$ for the present one. Quotes are used to indicate that the difference here refers to a general measure of comparison, and it does not necessarily represent the Euclidean distance between the two quantities. In fact, $\Delta\theta(m)$ is usually computed as the

Table 1. Subsets of 10 m Wind Data and Their (Output) Temporal and Spatial Resolution

Acronym	Institute	RCM	GCM	Δt (*h*)	Δx (km)
HIR_E	DMI	HIRHAM5	ECHAM5	1	25
RAC_E	KNMI	RACMO2	ECHAM5	3	25
REM_E	MPI	REMO	ECHAM5	1[a]	25
RCA_E	SMHI	RCA3	ECHAM5	3	25[a]
RCA_H	SMHI	RCA3	HadCM3Q3	3	25[a]

[a]The values have been obtained after averaging (see main text).

relative difference (except for those $\theta(m)$ expressed in terms of frequencies, where the absolute difference is used). In section 4.1, the estimated parameters are detailed.

[25] In the context of climate change, it is very important to perform an accurate uncertainty analysis of any projected changes. Even considering just one RCM-GCM combination with a certain emission scenario, there is a degree of uncertainty related to the data variability as each wave projection should be considered as a sample extracted from a large population. To achieve the second goal stated in section 1, rather than taking a deterministic approach, $\Delta\theta(m)$ is considered as a random variable, whose estimated value is that obtained from computed wave projections, $\Delta\hat{\theta}(m)$. To assess the significance of $\Delta\hat{\theta}$, a modified bootstrap method is used, combining (1) the method proposed by *Cai and Davies* [2012] and (2) the semiparametric approach of *Pandey et al*. [2003, 2004]. *Cai and Davies* [2012] proposed a model-free method adapted to time series, which are typically characterized by being autocorrelated, especially when time resolution is high (like in this study). The approach by *Pandey et al*. [2003, 2004] serves to overcome the deficiencies of bootstrapping as regards the correct estimation of extremes. In section 4.2, the basis of these two methods and how they are applied to this study are explained.

[26] Following the aforementioned bootstrapped method, a sample of projected changes $\Delta\hat{\theta}^*(m,j)$ (* means bootstrapped) is obtained for each parameter θ and each point m, where $j = 1, \cdots, n_{boot}$ and n_{boot} is the total number of bootstrapped samples (we choose $n_{boot} = 1000$ as recommended by *Park et al*. [2001]). The significance of $\Delta\hat{\theta}(m)$ is assessed by means of the null hypothesis $H_0 : \Delta\theta(m) = 0$. H_0 is rejected or, in other words, the estimated change is considered significant when the confidence intervals of $\Delta\hat{\theta}(m)$ do not include the zero. To account for the bias correction and center the sample $\Delta\hat{\theta}^*(m,j)$ around zero, as suggested by *Hall and Wilson* [1991], the confidence intervals are calculated as the $(\alpha/2)$ th and $(1-\alpha/2)$ th quantiles ($\alpha = 0.05$ is the confidence level) obtained from the sample $\Delta\hat{\theta}^*(m,j) - \Delta\hat{\theta}(m)$, instead of just $\Delta\hat{\theta}^*(m,j)$, where, as discussed earlier, $\Delta\hat{\theta}(m)$ is the estimated change of the original time series. Without this correction, the probability of accepting a false H_0 would increase, thereby decreasing the power of the test.

4.1. Parameters Estimated

[27] The parameters used to estimate future changes on wave conditions are divided into mean wave climate (median H_s, median T_p, frequencies of the directional sectors, frequencies of the type of sea states; see section 4.1.1) and extreme wave climate (50 year return value of H_s; see section 4.1.2).

4.1.1. Mean Wave Climate

[28] The median is a statistic that does not depend on the scale/distribution of the data and is robust in the sense that it is little affected by outliers. H_s and T_p are thus characterized using their respective median values, and $\Delta\theta$ is computed as the relative increase or decrease between present and future values. As for Θ_m, we have studied the frequency of the eight sectors centered in (coming from) north (N), northeast (NE), east (E), southeast (SE), south (S), southwest (SW), west (W), and northwest (NW) directions, with $\Delta\theta$ being the absolute difference between present and future frequencies. Note that the analysis of the directional frequencies is preferable to the average of Θ_m (calculated as the angle associated with the sum of the unit vectors described by each direction) since the latter does not always have a clear physical meaning. For example, in a hypothetical case with two predominant populations coming from north and east, respectively, the average direction would be NE, from which no waves would be coming.

[29] The wind-sea/swell distribution of waves is also assessed due to their different impact on the coastal beaches, typically corresponding to erosive versus regenerative processes. Despite the relatively short fetch in the study area compared to the open ocean, swell waves are present. But pure swell waves are rare [*García et al*., 1993] and are usually combined with growing wind sea, producing mixed sea states. In this study, we use the method presented by *Charles et al*. [2012], which is based on the inverse wave age A^{-1} (see equation (1)). If $A^{-1} < 0.15$, then waves are swell, whereas if $A^{-1} > 0.83$, they are wind-sea waves, with the mixed sea states falling in between. This categorization serves to estimate present and future occurrences associated with each type of wave climate. As for the directional frequencies, $\Delta\theta$ is computed as their absolute difference.

$$A^{-1} = \frac{W_{10}\cos\Delta\Theta}{C_p} \tag{1}$$

where $\Delta\Theta$ is the angle difference between wind and wave direction and $C_p = 1.56T_p$. This method is the same as the "wave age and wind/wave direction correlation method" presented by *de Farias et al*. [2012], although the latter is stricter about the difference between wave and wind direction (limited to 45° for wind-sea states versus 90° in *Charles et al*. [2012]). We adopt the more permissive version of the criterion; otherwise, very few wind-sea state cases would have been identified in our study area. We would like to point out that the aim of this study is not to precisely determine the present wind-sea/swell distribution—for which the complete frequency and directional spectrum would be necessary in order to apply a method of separation like those presented by *Portilla et al*. [2009]—but rather to determine their evolution caused by climate change.

4.1.2. Extreme Wave Climate

[30] As explained later in section 4.2, the inability of bootstrapping to correctly reproduce extremes is overcome by fitting a generalized pareto distribution (GPD, see equation (4)) to the tail of the distribution, following the approach of *Pandey et al*. [2003, 2004]. The extreme wave climate is therefore characterized by a parameter derived from the GPD model: the r-year return level of H_s, z_r (in this study $r = 50$), calculated by equation (2). As for the median of H_s and T_p, $\Delta\theta$ is calculated as the relative difference between present and future values.

$$z_r = u + \frac{\hat{\sigma}}{\hat{\xi}}\left[\left(\lambda_u^{-1}\left\{1 - \left[1 - \frac{1}{rn_y}\right]^{\beta^{-1}}\right\}\right)^{-\hat{\xi}} - 1\right] \tag{2}$$

where $\hat{\xi}$ and $\hat{\sigma}$ are the fitted GPD parameters (see equation (4)) obtained by the maximum likelihood method, n_y is the

number of observations per year (estimated as the total number of observations divided by the number of years), and $\lambda_u = 1 - F_E(u)$ is the threshold exceedance rate that can be estimated empirically as the proportion of observations above u (see section 4.2). The parameter β is the extremal index [see *Fawcett and Walshaw*, 2012], to account for the correlation between storms, normally present if only a threshold condition is imposed (no duration requirement, for instance).

[31] One important assumption of the GPD model is the independence between storms. This requirement is usually fulfilled by implementing, apart from the threshold establishment, some duration requirements based on experience and knowledge about wave physics [e.g., *Mendoza and Jiménez*, 2006], which makes it possible to detect dependent storms and combine them into a unique event. This approach works on a storm-by-storm basis and therefore implementing them for several scenarios, thousands of points (M) and n_{boot} samples (see section 4.2), as in this study, would be very time consuming. Instead, the coefficient β is involved in equation (2). For an independent process, $\beta = 1$ and as $\beta \to 0$ there is increasing dependence. The estimation of β is made as follows. For each original present model data set, β is estimated to fulfill $z_{50}\left(\hat{\beta}\right) = z_{50}^{\text{ind}}$ for each wave grid point m. The value z_{50} is obtained from equation (2) using all exceedances above u (and thus correlated), whereas z_{50}^{ind} (ind stands for "independent") is calculated using $\beta = 1$ while previously filtering out independent storms with the duration requirements defined by *Mendoza and Jiménez* [2006]. The results show that β has a mean value around 0.4–0.5, in the range of those obtained by *Fawcett and Walshaw* [2012].

4.2. Adopted Bootstrap Methodology

[32] The classical bootstrapping procedure (individual sampling allowing for repetition) is a robust, simple, straightforward method that has the advantage of being model free. In both older and more recent literature, it has been increasingly used in relation to computer science improvement. For the Catalan coast, *Casas-Prat and Sierra* [2010b] compared the confidence intervals of a temporal trend obtained by bootstrapping with a more complex Bayesian approach and found very similar results.

[33] However, this method was designed for independent and identically distributed data, and therefore it does not preserve the temporal dependence in the data. Bear in mind that, for example, when comparing the mean value of two autocorrelated samples, if the autocorrelation is not accounted for, unwarranted rejections of the null hypothesis are obtained [*Wilks*, 1997]. Different methodologies have been proposed in the last two decades to account for such autocorrelation or other (time) dependencies. The moving blocks bootstrap [*Wilks*, 1997] defines a block length, and, instead of resampling the data individually, at each iteration, an entire block is randomly selected from the original series. The choice of the block length depends on the data length and the strength and type of autocorrelation. *Park et al*. [2001] proposed the threshold bootstrap method, which, instead of using a constant block length, divides the data into chunks that include a certain number of cycles, with these being defined by crossing a selected threshold. In this methodology, both the threshold and number of cycles per chunk must be chosen. However, it has the advantage of splitting the data into "natural" cycles and therefore not producing unwanted discontinuities in the bootstrap data, as in the moving blocks bootstrap method. *Park et al*. [2001] also found that this method presents narrower confidence intervals for the mean and median estimators compared to the moving blocks bootstrap method.

[34] In this study, the classical bootstrap method is first modified based on *Cai and Davies* [2012], who recently developed a method that extends bootstrapping to nonstationary time series as well (e.g., having a temporal trend). The general idea is to divide the data into different groups classified according to the corresponding percentile bins. The bootstrap time series is built in a way that the "same" distribution of quantiles over time is reproduced, as detailed below. *Cai and Davies* [2012] also compared their method with the moving blocks bootstrap, obtaining results similar to the estimated parameters but with narrower confidence intervals.

[35] Let $\mathbf{x}(m) = \{x(1,m), x(2,m), x(3,m), \cdots, x(T,m)\}$, where T is the data (time) length, and n_q, a previously chosen number of quantiles to subsequently separate the data into bins (the choice of this parameter is discussed later in this section). Each single value $x(t,m)$ $(t = 1, \cdots, T)$, is then labeled as i, $x^i(t,m)$, if it belongs to the (i/n_q)-th quantile bin, i.e., i is the lowest value for which $x(t,m) < x_{i/n_q}(t,m)$, where $i = 1, \cdots, n_q$ $(x_1 = \infty)$. This classification allows us to divide the original data into groups of consecutive equal labels, e.g., $\{\{x^1(1,m)\}, \{x^2(2,m), x^2(3,m), x^2(4,m)\}, \{x^3(5,m), x^3(6,m)\}, \ldots, \{x^1(T-1,m), x^1(T,m)\}\}$. Following the same order of groups over time (in the example $\{\{1\},\{2\},\{3\},\cdots,\{1\}\}$), for each group i, the bootstrap values are randomly sampled among the pools of groups with the same label i (not necessarily having the same length as the original data group). This procedure is repeated until the total length of the original data is achieved (truncating at the end, if necessary), thus obtaining the bootstrap sample $\mathbf{x}^*(m) = \{x^*(1,m), x^*(2,m), x^*(3,m), \cdots, x^*(T,m)\}$ (for further details, see *Cai and Davies* [2012]). Repeating the entire procedure n_{boot} times, n_{boot} times series $\mathbf{x}^*(m)$ are obtained for each variable $\mathbf{x}(m)$.

[36] In order to take into account the spatial correlation of each $\mathbf{x}(m)$, as well as the cross correlation among the variables (e.g., cross correlation between H_s and T_p), instead of applying the method of *Cai and Davies* [2012] for each variable and wave grid point m separately, it is jointly implemented as follows. The method of *Cai and Davies* [2012] is only applied to a "representative" H_s time series, which consists of the spatial-average $H_s(t)$ time series, where the median is taken based on the entire set of wave grid points. Afterward, the same permutations are applied to each $\mathbf{x}(m)$ $(\forall m)$. This procedure is similar to the one of *Wilks* [1997]. He found that the simultaneous application of univariate resampling methods yields a powerful multivariate method in which the cross correlation is successfully captured by resampling, rather than through explicit modeling and estimation.

[37] In regard to selecting the number of quantiles, n_q, as recommended by *Cai and Davies* [2012], a sensitivity analysis is performed, and n_q is chosen as the maximum value

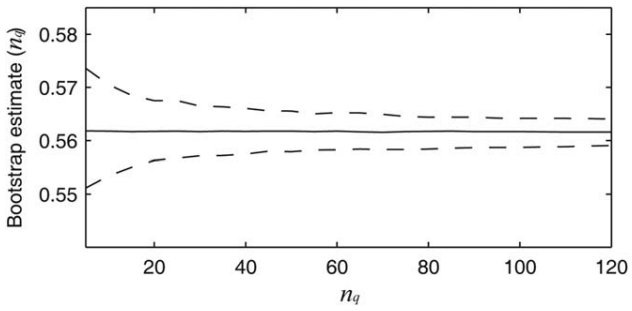

Figure 2. Bootstrap estimate of the median (H_s) as a function of n_q (for summer, RAC_E forcing).

after which the estimate of the statistic of interest and the corresponding bootstrap quantile ranges do not change significantly. In this study, we have used the aforementioned "representative" (spatial average) H_s as the statistic of interest. Based on the results obtained (see Figure 2), in which we use a random season (summer) and a random RCM (RAC_E), $n_q = 80$ is chosen.

[38] As previously mentioned, one important limitation of the bootstrap methodology is its inability to reproduce extreme events with reasonable values of n_{boot}. The reason is that a given random sample may not contain any extreme observations that are in the region of tail extrapolation [*Pandey et al*., 2003]. In order to study the extremes without increasing n_{boot} too much, which would entail a huge computational effort, this problem is overcome by using additionally the nonparametric approach of *Pandey et al*. [2003, 2004]. After obtaining the n_{boot} times series $\mathbf{x}^*(m)$ by the method of *Cai and Davies* [2012], their final distribution F_B is modeled as:

$$F_B(x|u) = \begin{cases} [1 - F_E(u)]F_P(x) + F_E(u) & \text{for } x > u \\ F_E(x) & \text{for } x \le u \end{cases} \quad (3)$$

where F_E is the empirical cumulative density function of $\mathbf{x}^*$ as obtained by *Cai and Davies* [2012] method, and F_P is the GPD, fitted to $\mathbf{x}^*$ above a certain threshold u (see section 4.1). In this study, $u = u(m)$ since stormy conditions near the coastline are not the same as those offshore. The 95th percentile is chosen, which gives $u \simeq 2$ m close to the Catalan coast, within the range of values recommended by the Spanish Harbor Authority for this area. For a generic variable x, the GPD model can be expressed as

$$F_P(x) = 1 - \left[1 + \xi\left(\frac{x-u}{\sigma}\right)\right]^{-1/\xi} \quad (4)$$

with σ and ξ being the scale and shape GPD parameters, respectively.

[39] Instead of using directly H_s, equation (4) is fitted to the $\ln H_s$ excesses, as recommended by *Ortego et al*. [2012]. Apart from taking into account the relative scale of H_s, *Ortego et al*. [2012] pointed out that with this transformation, they obtained a Weibull-type GPD function ($\xi < 0$), with the maximum $x_{sup} = -\sigma/\xi$ (see equation (4)), which is consistent with the fact that physical phenomena in the Earth system are naturally bounded and, in particular, ocean waves are limited by several factors: water depth, steepness of waves, maximum fetch distance, storm duration, etc. [*Ortego et al*., 2012].

[40] With this second modification, the adopted bootstrap method is no longer purely model free, but, since this only affects the tail of the distribution, it does not constitute a significant shortcoming, since previous studies related to wave climate [e.g., *Ortego et al*., 2012] have shown that this type of extreme data is well represented by a GPD function.

5. Results

[41] In this section, we present the obtained results, which are separated into present climate (see section 5.1) and climate change signals (see section 5.2). Special attention is paid to the winter season (sections 5.1.1 and 5.2.1), which is normally the most energetic season, although results for the summer are also provided (see sections 5.1.2 and 5.2.2). Winter is defined as the months of December-January-February, with summer comprising June-July-August, as is common in studies on the Mediterranean climate [e.g., *Giorgi and Lionello*, 2008].

[42] As mentioned in section 3.2, the present simulation of REM_E corresponds to the period 1981–2010, and therefore it differs from its future projection by 90 years instead of 100 like the other models. However, since the future changes are generally mild, this is not taken into account in the analysis of the results, since we do not consider this 10 year difference to be of major importance.

5.1. Review and Validation of the Present Climate

[43] A review of the present wave climate is made based on the simulated present period, highlighting both consistencies and disagreements obtained between models. A qualitative validation of the present climate is carried out by comparing with the HIPOCAS data (see section 3.2) and with previous studies.

5.1.1. Winter

[44] Modeled median H_s for the present climate is shown in the upper row of Figure 3 (the spatial pattern of the median T_p, not shown, is similar to that of the median H_s). The arrows correspond to the mean Θ_m and, for the sake of clarity, only arrows corresponding to one out of every three grid points are plotted. All realizations show a predominant mean NW-W direction (especially offshore), which agrees with the results of *Lionello et al*. [2008a], and can be explained by the predominant Mistral (NW) wind in the area during the winter season (see section 2.1 and Figure 4). Near the coast, however, as expected, the mean Θ_m tends to "turn" toward the coast, being within the range of E-SE-S-SW sectors. This area of coastline influence is primarily caused by the coastline orientation itself—producing fetch-limited conditions for (NW) seaward winds—and the large fraction of swell waves coming from the east sector [*Sánchez-Arcilla et al*., 2008].

[45] HIR_E model results are particularly different from the rest for the present climate, with the present median H_s being significantly larger than the other models and the present mean wave direction being less affected by the coastline orientation. This can be explained by the higher value of the median W_{10} in HIR_E model (see Figure 4) and therefore the greater presence of wind-sea waves

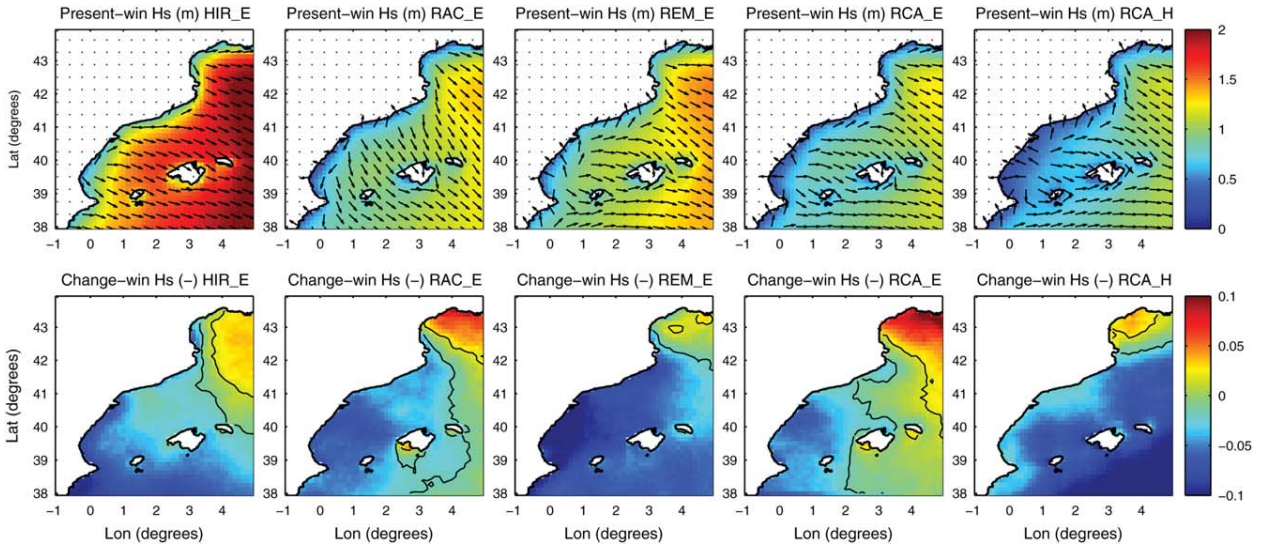

Figure 3. Estimated present (upper rows) and projected relative change (lower rows) of the median H_s (color maps) for winter, forced by the five RCM-GCM wind data sets. Arrows show the present mean wave direction, and thin black lines delimit areas of significant change.

associated with the aforementioned Mistral (seaward) wind pattern that counteracts (NE-E) swell waves. Comparison with the median H_s of the HIPOCAS data set (see Figure 5) and with the winter average H_s obtained by *Lionello et al*. [2008a] for the reference period confirms that HIR_E results represent an outlier and overestimate H_s in the study area. Regarding the (wave forcing) wind field, *Donat et al*. [2010b] and *Pryor et al*. [2012] obtained similar differences at the European and northern European scale, respectively, using similar RCM-GCM combinations. However, contrary to what seems to happen in the NW Mediterranean, *Pryor et al*. [2012] concluded that wind climate was better reproduced by HIRHAM5 RCM (RCM used in HIR_E configuration).

[46] With regard to the current directional distribution of waves, Figure 6 illustrates the corresponding eight directional sector frequencies (N, NE, E, SE, S, SW, W, and NW). Reasonable results are generally obtained from all models, with more or less the same patterns reproduced. Dominant Mistral wind events are clearly translated into a high value of NW wave occurrence with a maxima in the Gulf of Lion (up to 42%) and a second maxima in the Ebre Delta (around 25%, with values similar to rose diagrams of a nearshore buoy [*Bolaños et al*., 2009]). In the latter

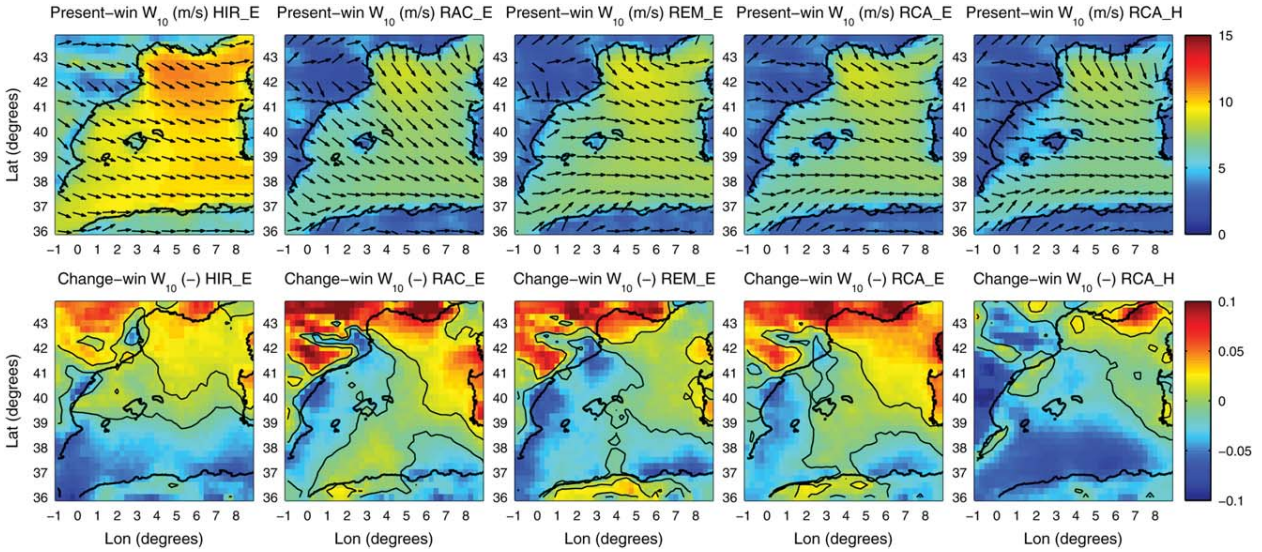

Figure 4. Estimated present (upper rows) and projected relative change (lower rows) of the median $W_{10}s$ (color maps) for winter corresponding to the five RCM-GCM wind data sets. Arrows show the present mean wave direction, and thin black lines delimit significant areas of change.

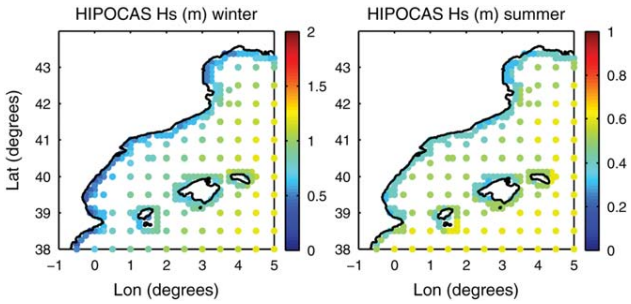

Figure 5. Median H_s for (left) winter and (right) summer calculated from HIPOCAS data set.

location, there is more variability among models and, for example, HIR_E exhibits a larger frequency that explains the NW direction of Θ_m near the coastline (see Figure 3). Note that in both the Gulf of Lion and the Ebre Delta, NW waves are fetch limited because wind blows from the land and therefore the large frequency of NW waves does not translate into a large H_s near the coastline. The second most frequent sector corresponds to north waves around Cape Creus and southward offshore (maximum frequencies ranging from 35% to 45%), which can be indirectly associated to the Mistral events too. Moving southward along the Catalan coast and in the north of the Cape Nau area, NE waves become more important because of the larger fetch associated with this direction. In between these two locations, the NE contribution is attenuated because of the shadow effect of the coastline orientation, which once again underscores the role of the coastline in the directional distribution of waves near the coast. Although the east flow is not the predominant one (see section 2.1), a notable proportion of east waves is encountered along most coastline stretches that face east (around 20% in the middle of the Catalan coast), which is more accentuated in RCA_H model. Finally, with regard to the whole south sector, SW waves are the most frequent, especially in the upper-middle Catalan coast (with a frequency up to 35%) whereas south waves are more important in the Ebre Delta. In general, the results obtained are qualitatively consistent with the analysis of hindcast data of *Casas-Prat and Sierra* [2012].

[47] The current frequencies associated to the types of sea states are illustrated in Figure 7. According to the classification used (see section 4.1), there is a predominance of wind-sea states in all models (with a frequency of up to 80%) throughout the domain offshore. Near the coastline, as expected, swell and mixed sea states gain importance. The patterns obtained by the models are consistent but some differences exist. With HIR_E model, wind waves are more frequent, which might be explained by the positive bias of the wind field seen in Figure 4 (which have a predominant fetch-limited NW component). On the contrary, RCA_H model has a higher occurrence of swell events between the Balearic Islands and the Iberian Peninsula, which is consistent with the higher simulation of east (sea-to-land) flow associated with this model (illustrated in Figure 6).

[48] Finally, in order to characterize the extreme wave climate, Figure 8 shows the present value of z_{50} corresponding to each model configuration (present climate in the upper row). The value z_{50} reaches values up to 7 m approximately, and it has a current spatial pattern similar to the median H_s. As seen with the median value, HIR_E overpredicts z_{50}, whereas values below the ensemble mean are obtained by RCA_E and RCA_H, which agrees with the wind underestimation of extremes of these models found by *Kriezi and Broman* [2008] (the differences associated to these last two models are more accentuated compared to the median H_s). Especially in terms of the number of storms (not shown), RCA_H is below the others.

5.1.2. Summer

[49] Compared to the winter season, summer is characterized by lower wave heights as shown in Figure 9 (upper row). Overestimation of H_s (and W_{10} too, see Figure 10) is also present for the HIR_E model. In general, mean Θ_m also has a predominant NW component, but it is not as (spatially) generalized as in the winter. As explained in section 2.1, apart from the Gulf of Genoa, in the summer there is a second important area of cyclogenesis over the Iberian Peninsula, which causes a SW-W wind flow, especially in the southwest part of the domain (see Figure 10), producing a larger median H_s there. This more energetic area in the south part of the domain is also captured in *Lionello et al*. [2008a] simulations, but their results show an average wave direction pointing south.

[50] The analysis of the directional frequencies of waves for the present period is shown in Figure 11. Maximum frequencies are associated with the NW direction being located at the Gulf of Lion (contrary to winter, HIR_E realization simulates less NW waves). As during winter, this is translated into a large concentration of north wave events around Cape Creus and offshore. The east sector is notably more frequent than in winter, being compensated by a lower presence of the south sector. In general, a large agreement is found among all models.

[51] Regarding the current distribution of the types of wave states (see Figure 12), there is a lower occurrence of wind-sea states compared to winter, being concentrated mainly in the NE zone. This is reasonable according to the milder wind conditions. Conversely, the presence of mixed sea states is more notable, especially in the midsouthern part of the domain.

[52] Figure 13 illustrates the estimation of the present z_{50} in the upper row. Maximum values of z_{50} are concentrated in the NE part of the domain, being up to 4 m approximately. Comparison between models shows a similar pattern of (over)underestimation as in winter.

5.2. Climate Change Signals

[53] In this section, the projected changes are presented, and, as in section 5.1, the agreement between models is assessed. In all figures, the thin black lines enclose the areas of statistically significant variations according to the methodology explained in section 4.

5.2.1. Winter

[54] The lower row of Figure 3 illustrates the projected future relative increase/decrease of the median H_s. Results show a common pattern of H_s reduction in most of the domain (up to 14%), whereas in the northern area we see the opposite, with a rise up to 15% (absolute maximum increase of 10 cm). *Lionello et al*. [2008a] found a similar projected change for the B2 greenhouse scenario with similar rates of change (for the A2 scenario they obtained

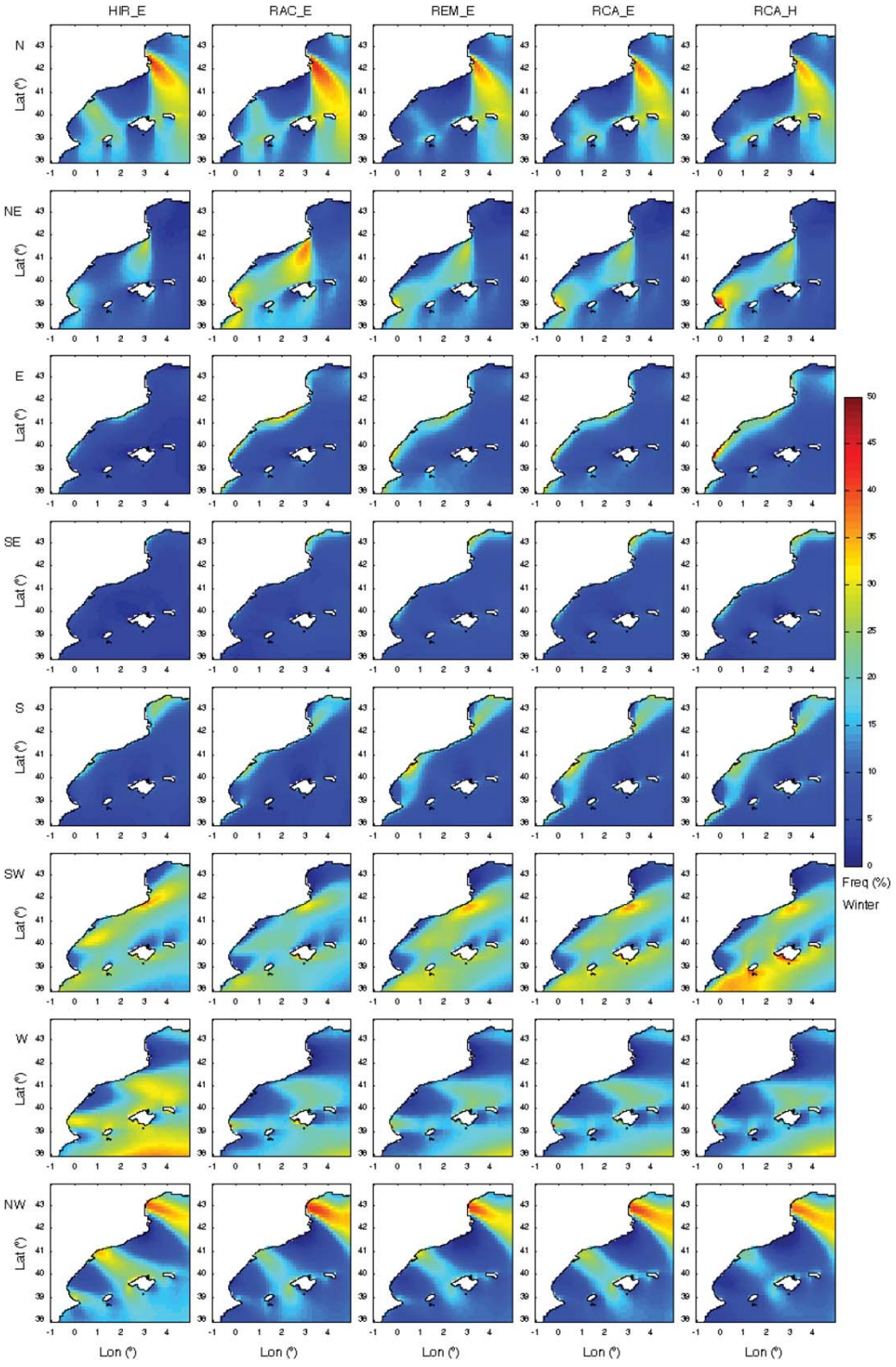

Figure 6. Estimated present frequency of each directional sector of waves for winter, obtained from the five (RCM-GCM) wind data sets.

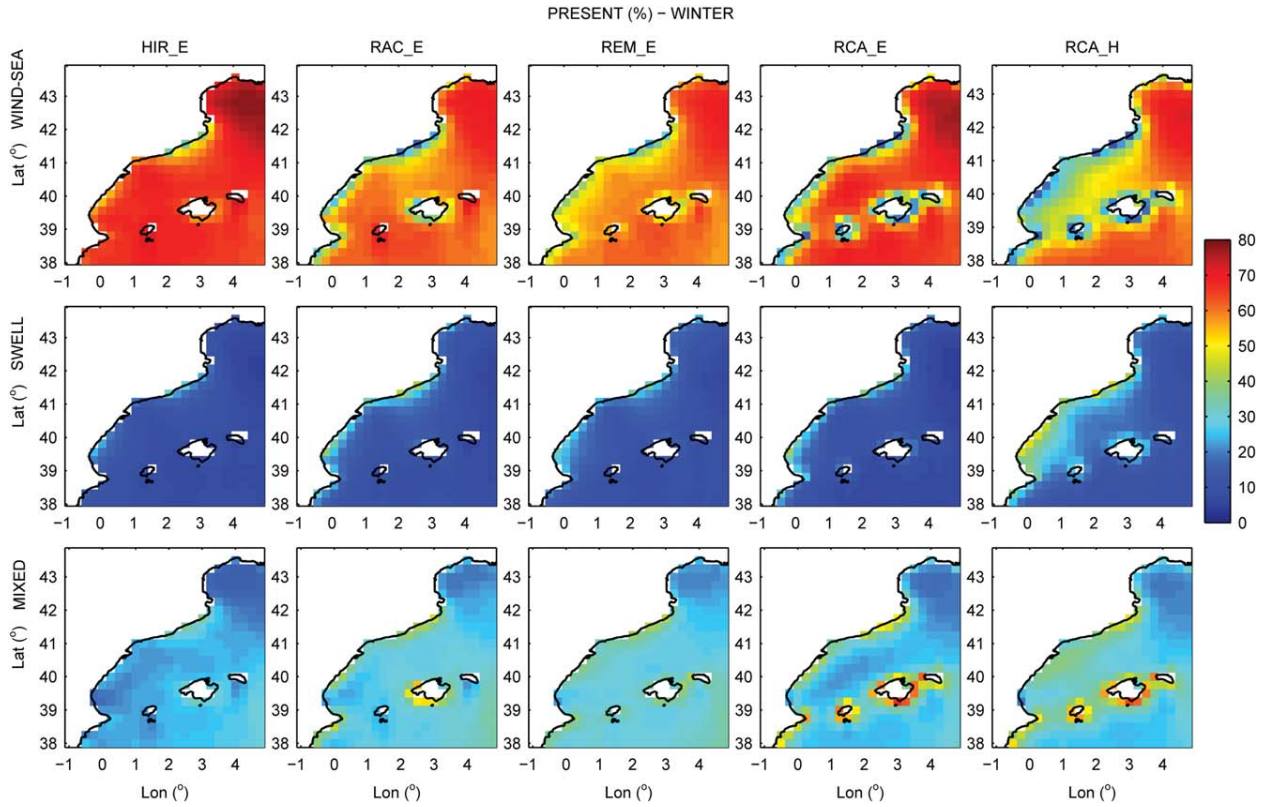

Figure 7. Estimated present distribution of wind-sea (upper row), swell (middle row), and mixed sea states (lower row) for winter.

negative rates all across the study area). A comparable increase is also observed in the wind fields (Figure 4), where the maximum rise is up to 18% (up to 0.5 m/s) but lower in average. The pattern of the predicted changes of the median T_p (not shown) is similar to that of H_s but has in general lower rates of increase/decrease, around $\pm 5\%$ (while around $\pm 10\%$ for the median H_s). Just for the last model (RCA_H), there are few narrow areas along the coast that faces east where the median T_p slightly increases, whereas the median H_s slightly decreases.

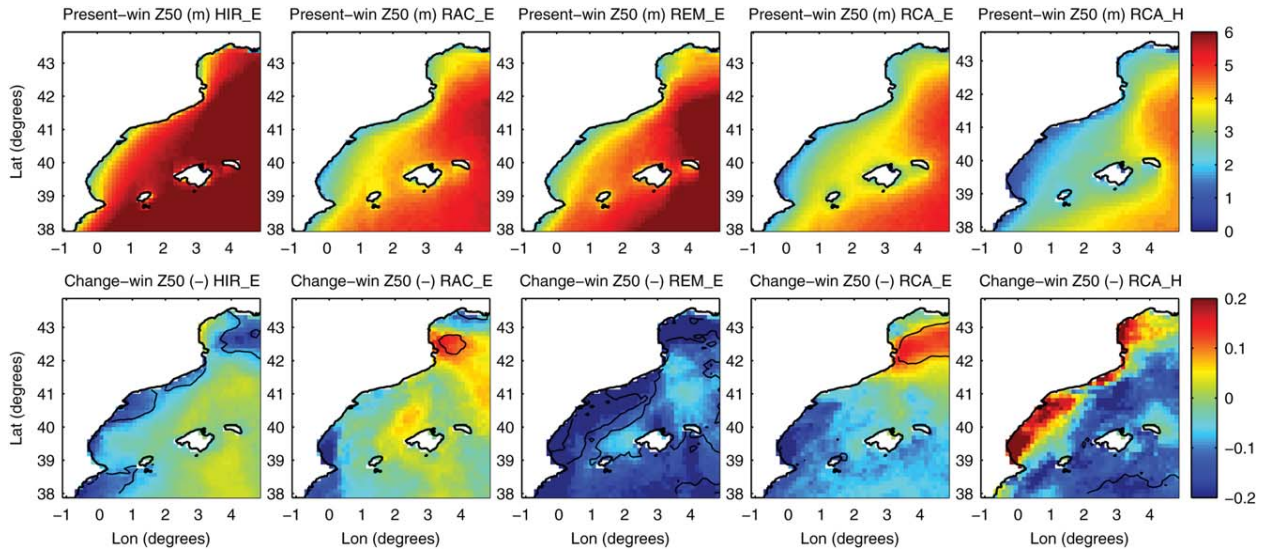

Figure 8. Estimated present (upper rows) and projected relative change (lower rows) of z_{50} for winter, forced by the 5 RCM-GCM wind data sets. Thin black lines delimit areas of significant change.

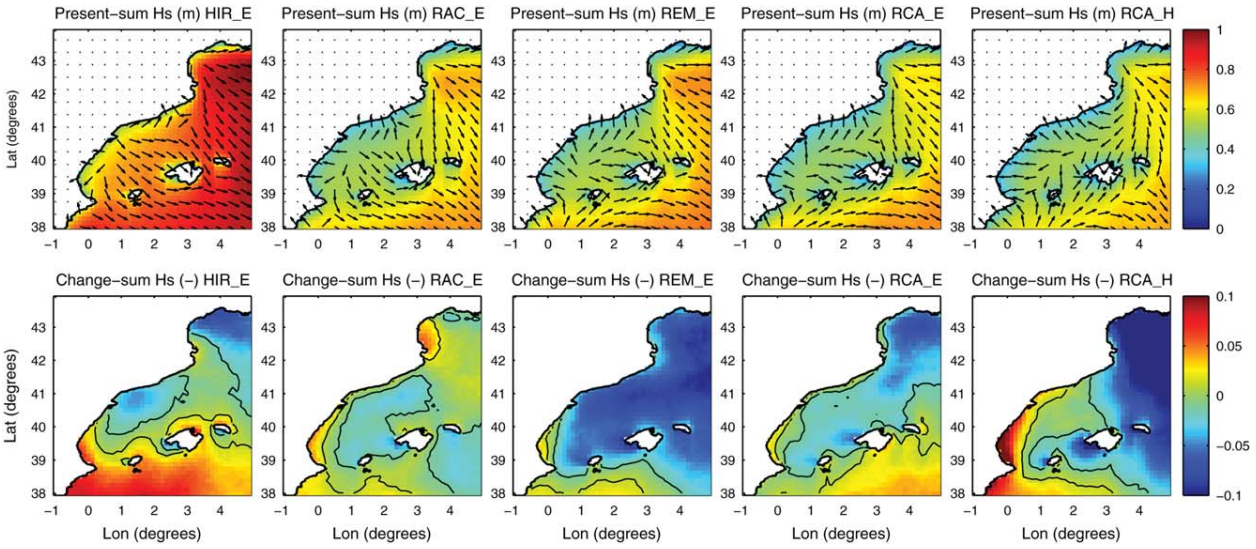

Figure 9. Same as Figure 3 but for summer.

[55] Regional variations between model realizations are observed in the size and intensity of the area of H_s increase in the northern segment but also in the location of the maximum decrease. In this regard, in the case of RCA_H (driven by HadCM3Q3 GCM), the maximum decrease occurs in the southeast segment of the domain but in the southwest in the other models (all are driven by the same ECHAM5 GCM). This discrepancy might be related to the increase of east flow associated with the RCA_H model as seen later on in this section. In all models, the median winter H_s along the Catalan coast is expected to decrease (up to 7%), which qualitatively agrees with previous results based on trend analysis [*Casas-Prat and Sierra*, 2012].

[56] The absolute predicted changes of directional frequencies are shown in Figure 14. Maximum absolute differences are about ±5%, but they might get higher in relative terms—e.g., up to 80% for East and NE directions and the RCA_H model. The most remarkable results lie in the difference between model realizations driven by ECHAM5 (HIR_E, RAC_E, REM_E, RCA_E) and HadCM3Q3 (RCA_H). In the former, there is a remarkable increase of NW and west frequencies (especially in the Gulf of Lion and Ebre Delta), up to 5% (35% in relative terms) and, to a lesser extent, a rise in the south and SW components (especially in the Ebre Delta and in the middle of the Catalan coast, respectively). In contrast, the RCA_H results show a significant increase of the whole east sector. In absolute terms, the maximum rise is about 6%, although it represents a maximum relative increase ranging from 77% to 117%. As discussed later in section 6, these discrepancies can be related with a different west-east wind flow simulation of the corresponding forcing GCMs.

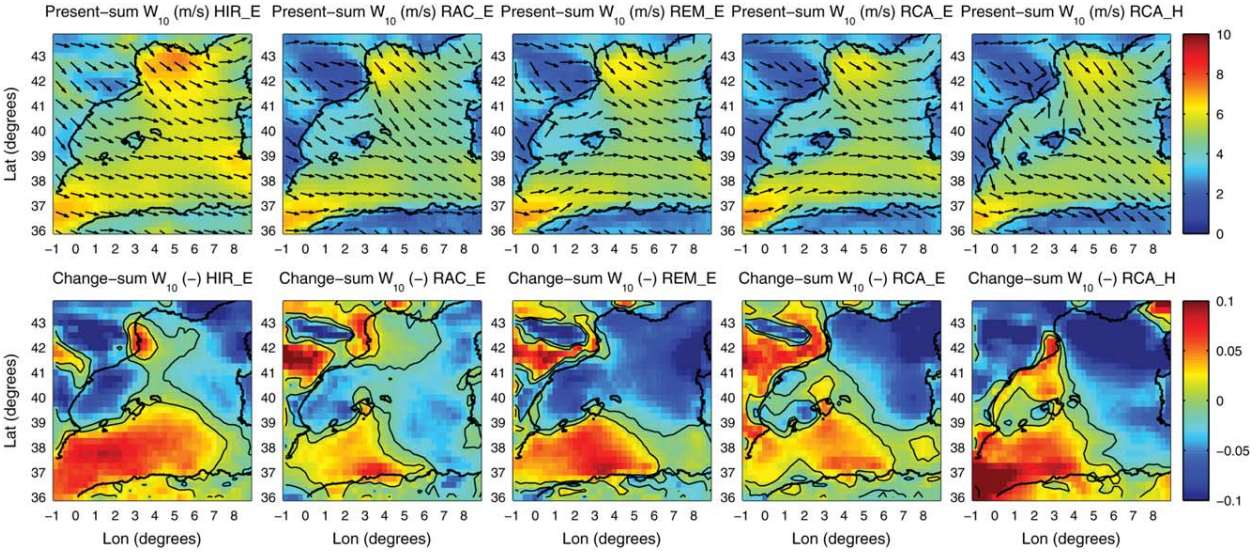

Figure 10. Same as Figure 4 but for summer.

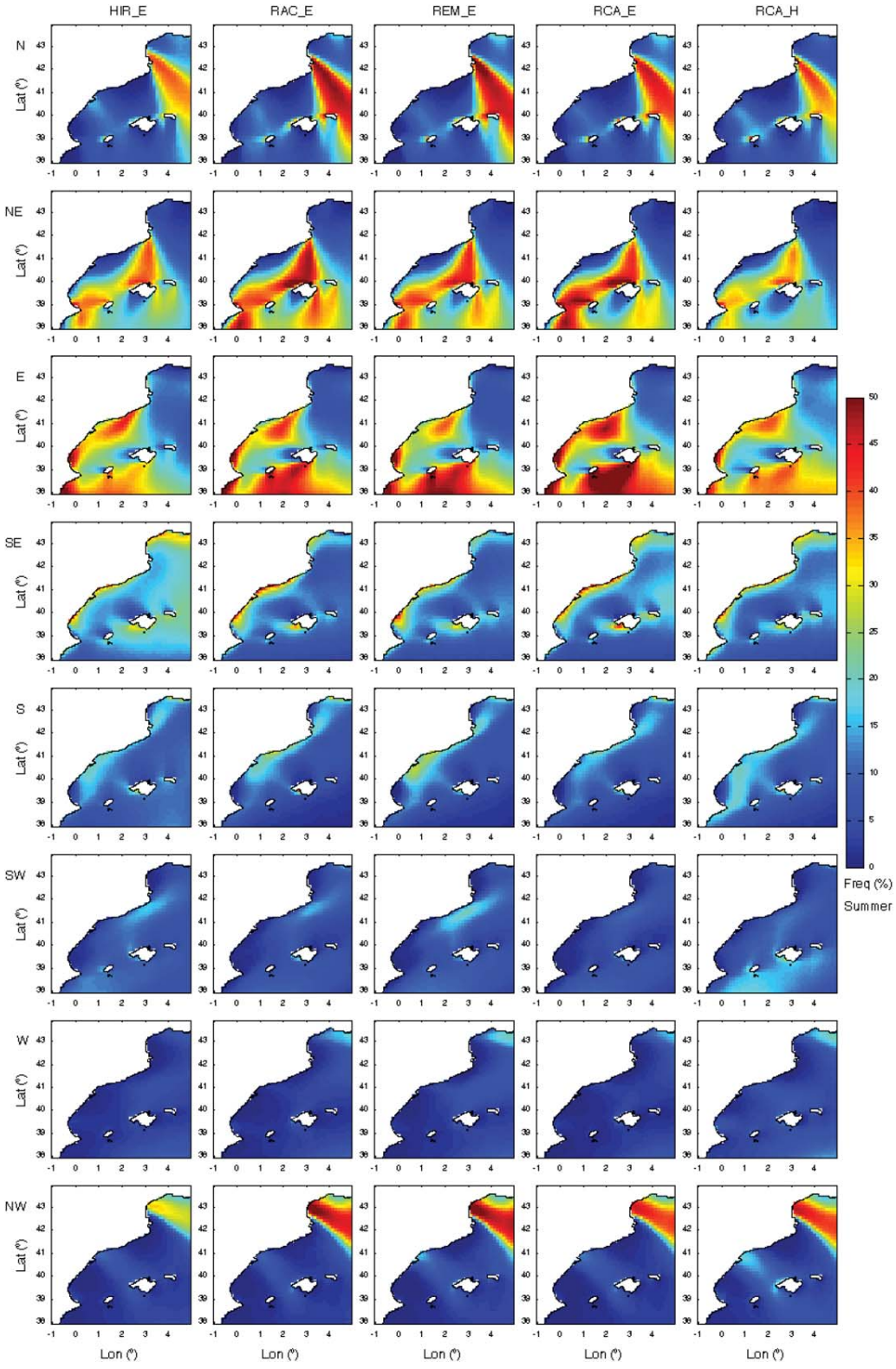

Figure 11. Same as Figure 6 but for summer.

[57] The aforementioned increase of NW wind/wave occurrence over the Gulf of Lion translates into a greater future predominance of wind-sea states in that location (see Figure 15) for all models driven by ECHAM5 except for HIR_E, which exhibits a different pattern of change, possibly due to the already positive bias of present wind-sea states (due to an overestimation of W_{10}). Meanwhile, a larger and more spatially extended rise in the occurrence of wind waves

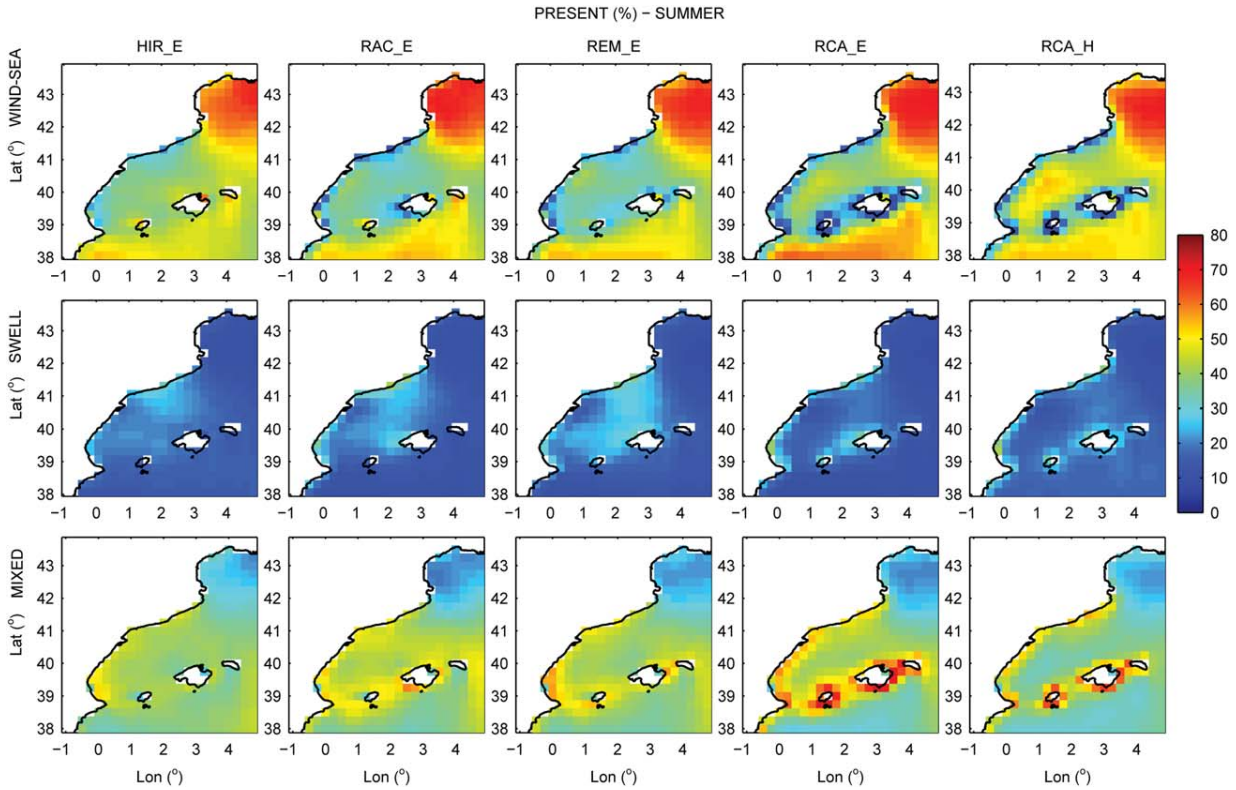

Figure 12. Same as Figure 7 but for summer.

is obtained offshore for RCA_H, whereas it drops along most coasts that face east. The increase of east flow associated to this GCM (see section 6) is expected to produce wind waves offshore that become mixed sea states when they get closer to the coast, due to the interaction with other wind waves generated there locally (note that pure swell is expected to decrease throughout the domain). Lastly, it is interesting to note the moderate rise of swell and mixed waves in RCA_E, REM_E, and RCA_E over the middle and southwest corner of the domain, which could be explained by the enhanced SW and south wave frequencies observed with these models, causing enhanced mixed waves (not pure wind waves, probably because SW winds are not expected to be very intense compared those coming from north).

[58] Finally, Figure 8 illustrates the relative change of z_{50} (lower row). Their magnitude is accentuated compared to the median H_s, with relative rises/drops around $\pm 20\%$ (in general, translated into maximum absolute changes

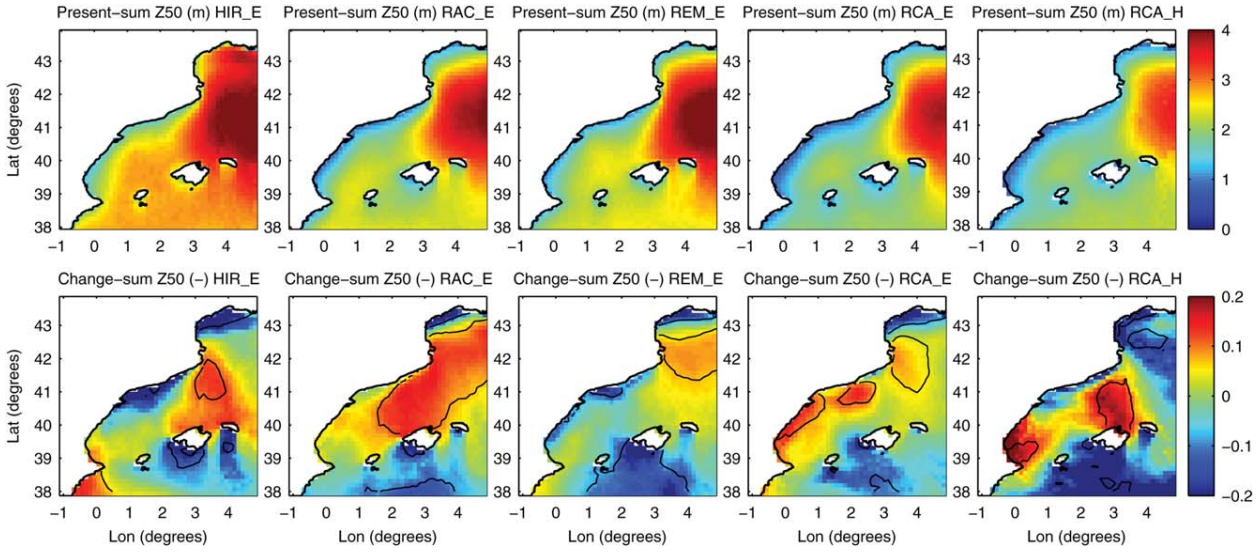

Figure 13. Same as Figure 8 but for summer.

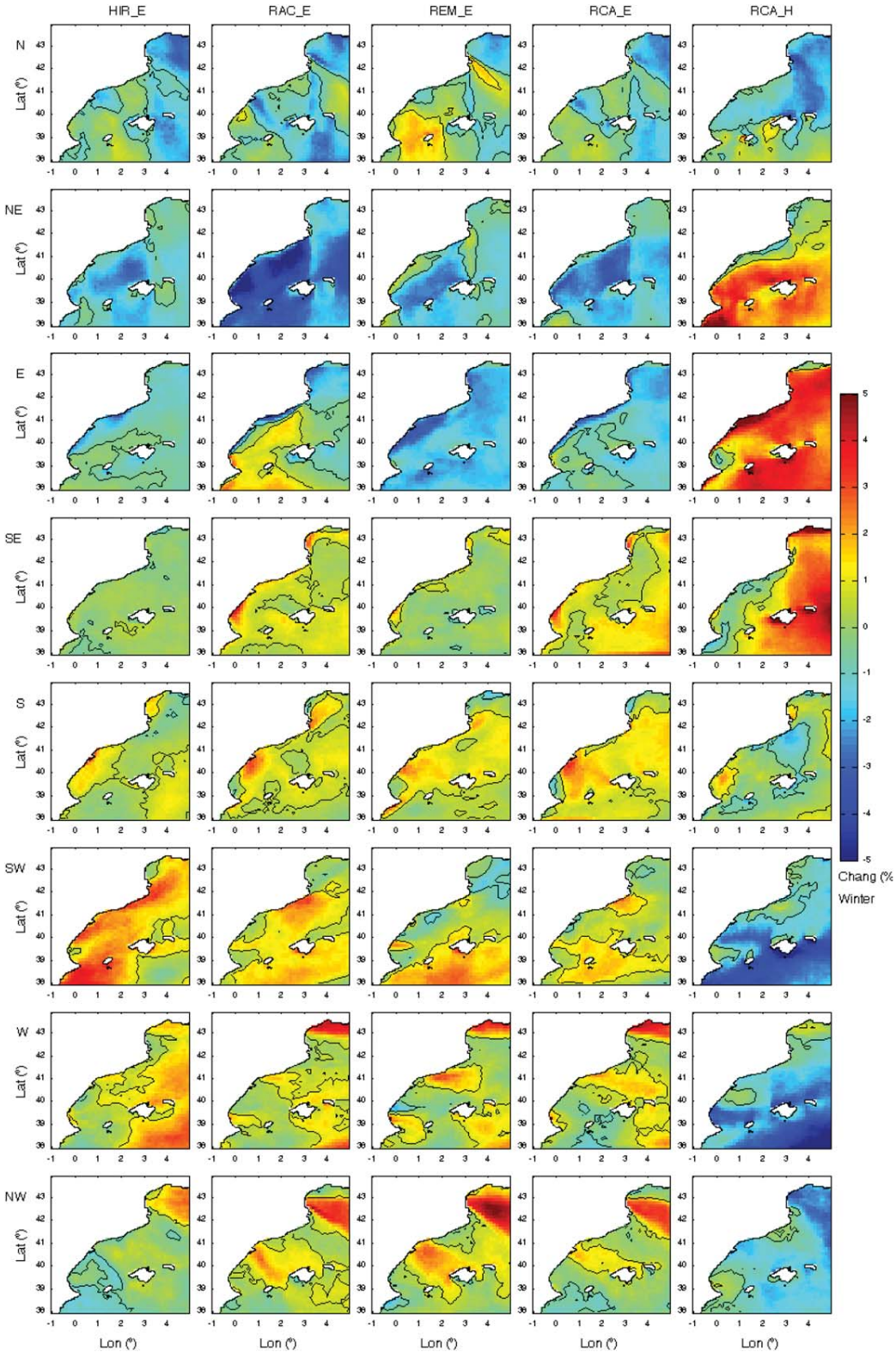

Figure 14. Projected absolute change of frequency of each directional sector of waves for winter, obtained from the five (RCM-GCM) wind data sets. Thin black lines delimit areas of significance change.

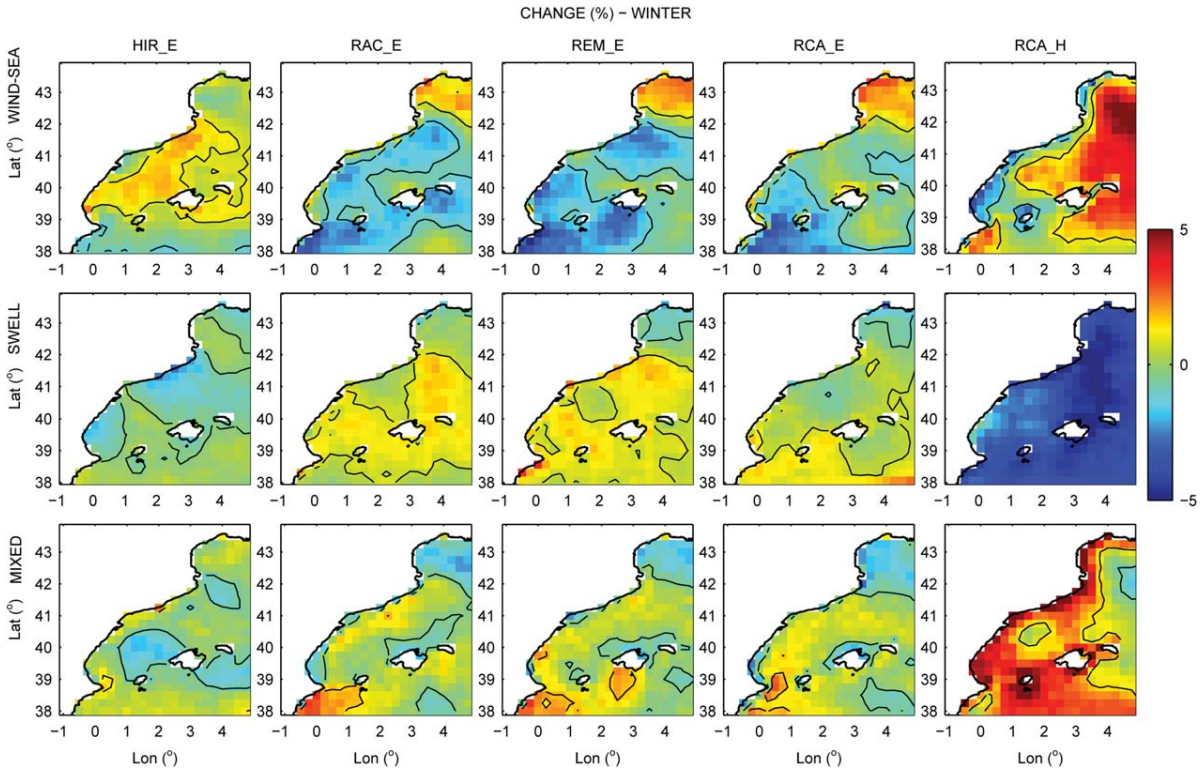

Figure 15. Projected absolute change of wind-sea, swell, and mixed sea states occurrence for winter. Thin black lines delimit areas of significant change.

<1 m—larger drops in REM_E case) and locally achieving maximum positive/negative rates of 64%/93%. A similar pattern is obtained for the relative change in total number of storms (not shown), but in this case the range is larger (±40%). However, it is difficult to derive a robust change because large differences are observed between models and the areas of statistically significant changes are less abundant compared to the mean climate. Such reduction of statistically significance was also observed by *Lionello et al.* [2008a] when analyzing the projected changes of the 10 year return value of H_s.

[59] The z_{50} projections could be grouped into: RAC_E and RCA_E, HIR_E and REM_E, and RCA_H. First, both RAC_E and RCA_E show an increase of z_{50} in the Gulf of Lion and Cape Creus area, consistent with the obtained increase of the median H_s, apparently related to Mistral wind events. But owing to the NW component of such wave-driving wind, extreme waves close to the coast from where the wind blows tend to be shorter due to fetch-limited conditions. In contrast, HIR_E and REM_E do not show any increase, while z_{50} tends to drop (especially in the latter case). Lastly, RCA_H (the one with the different GCM model) exhibits a very different pattern of change, with maximum increases located along most coastal stretches that face east. The reason is the enhanced east flow projected by this model (see section 3.1), which, in terms of H_s, is enhanced by favorable fetch conditions along such coasts, causing a rise of the number of east storms (not shown) over 50% along the Catalan coast. Nevertheless, these changes are not statistically significant.

5.2.2. Summer

[60] Predicted future changes in the median H_s in summer have a very different pattern compared to winter (see lower row of Figure 9). A general tendency to increase with a maximum of 15% (achieved in the case of RCA_H) is found in the southwest part of the domain—hardly affecting the Catalan coast—albeit with different intensities and local peculiarities among models. An increase in the average summer H_s was also found by *Lionello et al.* [2008a] for both the A2 and B2 scenarios (being B2 closer to our results, in terms of the location and expansion of the increase). Such a pattern of change is closely related to the wind (forcing) pattern (see Figure 10) in which, apart from rising in the southern part of the domain, there is an increase over land (in the NW part of the study area), which in most cases hardly contributes to wave generation. An opposite (negative) signal is simulated in the northeast corner, for which wind speed (and H_s) tends to decrease.

[61] Predicted changes in directional distribution during summer (see Figure 16) are substantial (up to 19% and 180% in absolute and relative terms, respectively) predominantly concentrated—in the positive sense—in the North, NE, and East sectors, and the SE to a lesser extent. Conversely, the south sector tends to decrease slightly, which would be explained by a lower thermal difference between land and sea in the future climate. Indeed, despite W_{10} rising in the south part of the domain, this is associated with a more NE component (not with the thermal SW flow), which subsequently translates into the wave climate. In contrast to winter, we observe a more similar response by

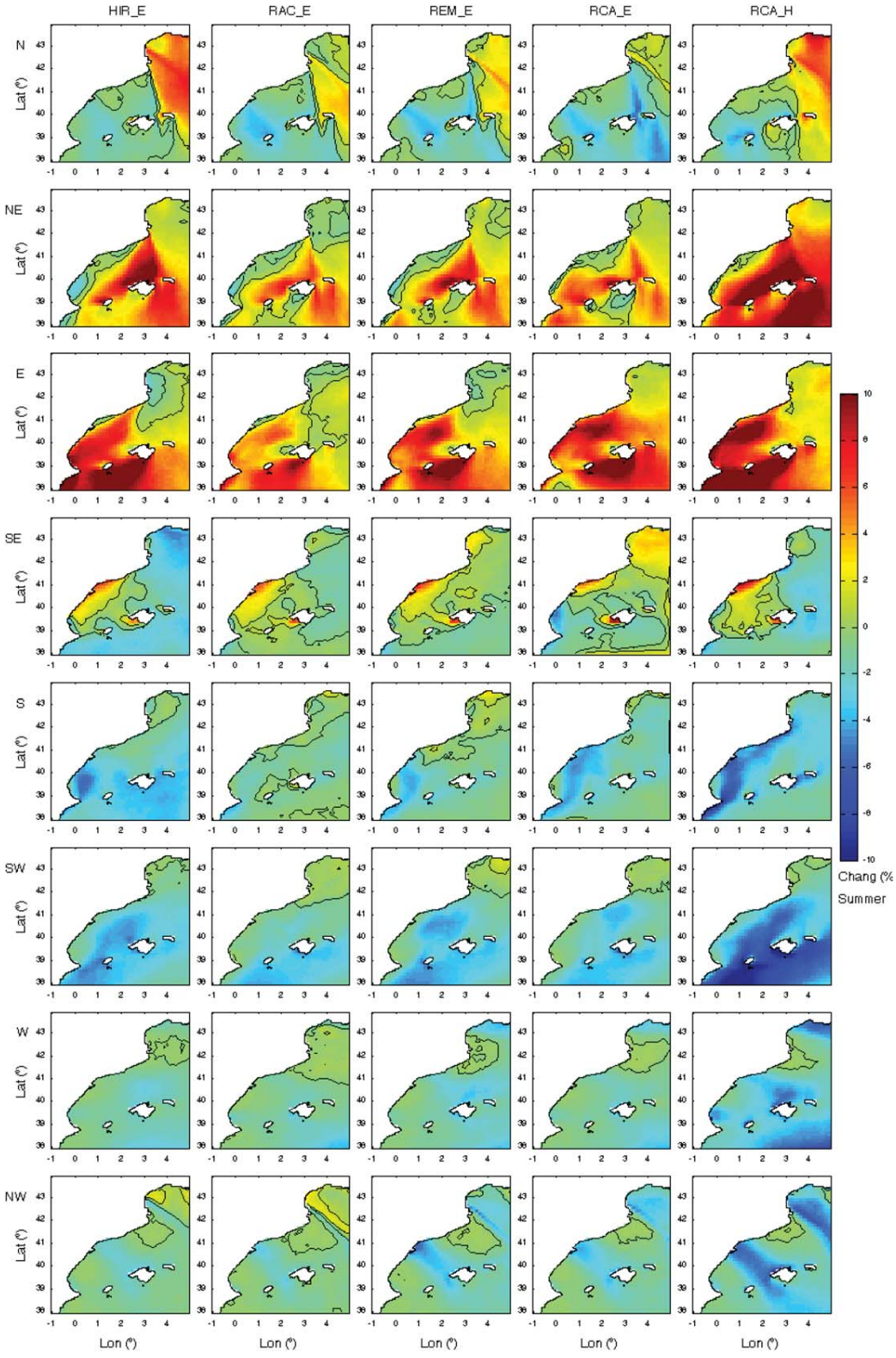

Figure 16. Same as Figure 14 but for summer.

the two families of GCMs, with the discrepancies due to both RCMs and GCMs.

[62] The decrease in the NW wave frequency translates into a decrease of wind-sea states in the Gulf of Lion (except for HIR_E, see Figure 17). There is a rise of wind (mixed) sea states south (north) of the Balearic Islands, which is possibly related to the increase of NE and East waves, as previously seen in Figure 11. The decrease of

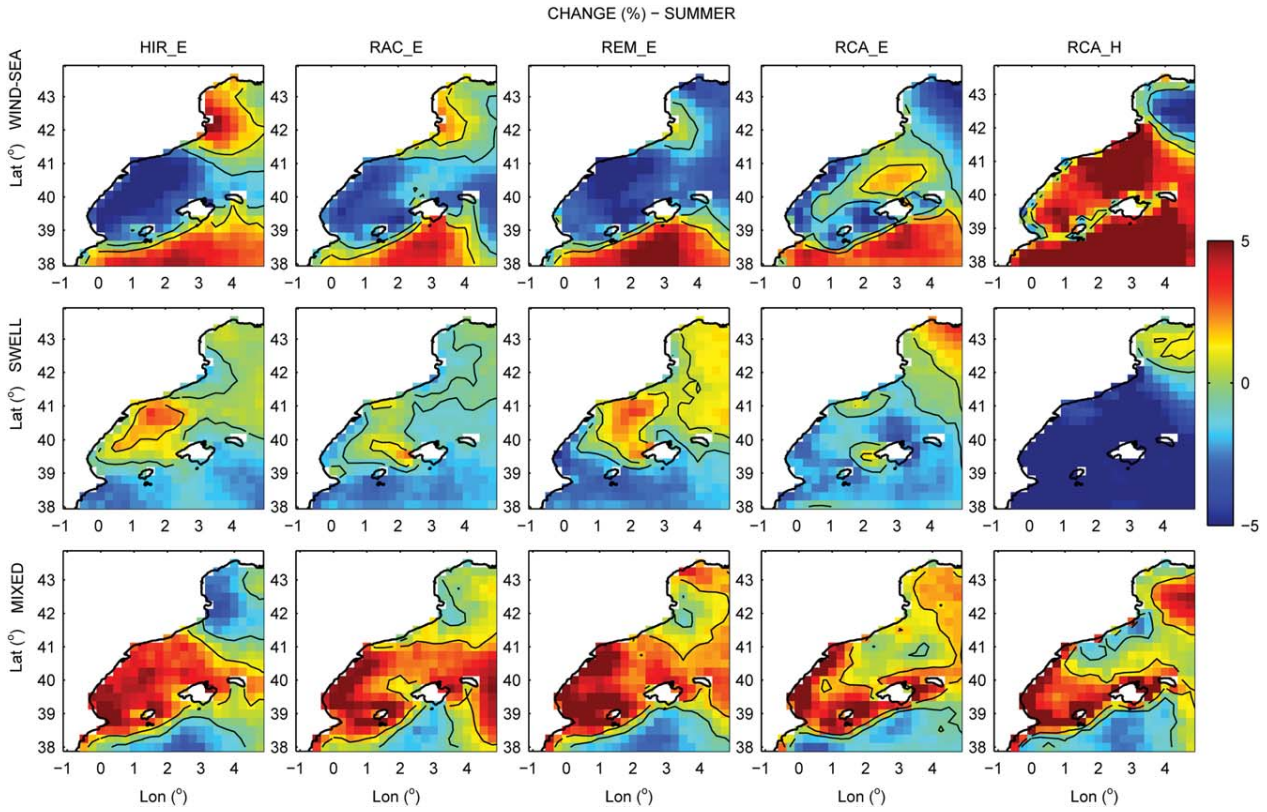

Figure 17. Same as Figure 15 but for summer.

mixed sea states (and swells) south of the Balearic Islands highlights the shadowing effect associated with such directions.

[63] Similar to what occurs in the winter, predicted changes of z_{50} (see lower row of Figure 13) are higher than for the median H_s: around ±20% in most locations (or even positive changes are found where the median H_s drops). Such relative changes are translated into maximum absolute changes of 0.50–0.90 m. In the direction analysis, all models showed an increase of the NE component (see Figure 16), which probably explains the rise in z_{50} in the NE area comprising the mainland and the Balearic Islands. However, the exact location and extension of such an increase varies between models. For example, whereas for RAC_E model, there is a notable increase of z_{50} along the midnorthern Catalan coast, REM_E only show an increase around Cape Creus. However, all models seem to coincide on a decrease to the south of the Balearic Islands.

6. Discussion

[64] In this section, we discuss and get into more detail about some of the interesting results presented in section 5. First, note that the rate of change of the median H_s is generally not proportional to the squared rate of change of the median W_{10} (which would be the case in a pure, fully developed wind-sea state). This indicates the presence of swell and mixed sea states and the complexity of sea waves, which can be fetch/duration limited due to the large temporal and spatial variability of wind fields in the study area [*Alomar*, 2012]. However, in stormy conditions, local wave generation is more important, and therefore the nonlinear relation $H_s \propto W_{10}^2$ might be more applicable, which might explain why increases in z_{50} are higher than in the median H_s field.

[65] With regard to the relation between H_s and T_p, results suggest that the proportionality $T_p \propto \sqrt{H_s}$ will broadly remain applicable in the future, and therefore the projected relative change of T_p can be mostly approximated as the square root of the relative change of H_s, even though the aforementioned complexity of the wave climate. Bear in mind that $T_p \propto \sqrt{H_s}$ is based on fetch limited wave growth, and therefore it is reasonable that it remains applicable in general in the study area, where fetches are short compared to the open ocean, and therefore no abrupt changes in the wind-sea/swell distribution are found. However, this might not be always appropriate. As shown in the recent study of *Hemer et al*. [2013], projected positive changes of T_p can be found in large areas where H_s does not increase, due to the extended influence of enhanced wave generation propagating as swell across the global ocean.

[66] The analysis of the eight directional sector frequencies has served to highlight the differences between projected changes simulated by different GCMs. These results are consistent with the findings of *Donat et al*. [2010a] (see section 2.2). In an ensemble mean, they found a significant increased frequency of westerly wind flow (relative change of 16%) and less frequent easterly flow (−27%), which was confirmed by all models except HadGEM (a model with

many similarities to HadCM3Q3, the one used in RCA_H) in which the whole easterly flow sector rose. As expected, relative differences in the directional frequencies of winds translate into waves, but they are more accentuated when fetch configuration is favorable. In the Catalan coast, these two GCM responses would lead to an increase of waves coming from either East or S-SW, entailing completely different coastal impacts. *Casas-Prat and Sierra* [2012] showed that an increase of the south sector (found in the trend analysis of hindcast data) would have an impact on most harbors along such a coast. On the other hand, more frequent east waves could produce more problems related with beach erosion.

[67] It is difficult to determine the exact origin of the discrepancies between the two GCMs, which are generally higher than those between RCMs, especially in winter wind field projections [*Kjellström et al*., 2011] and their corresponding (wind-driven) wave projections, as seen in this study. The latitude limit between the strengthening/weakening of wind speed in HadCM3Q3 appears to be at a higher latitude compared to ECHAM5 according to the wind projections analyzed in this study. That coincides with the results of *Donat et al*. [2010b], which, using a model similar to HadCM3Q3, showed that the pattern of change in the pressure field—decrease (increase) of pressure over northern (southern) Europe—is shifted northward compared to other models. Therefore, the pressure gradient (which controls the geostrophic wind) is also shifted northward for this model.

[68] It is also hard to conclude which GCM is more reliable in terms of the projected changes in wind climate and, consequently, in wave climate. In this study, just two GCMs are used, and a larger sample would definitely be necessary to derive a robust conclusion. From this study, we cannot say that the HadCM3Q3 represents an outlier because all the other realizations were produced with the same ECHAM5 GCM. In a single model analysis basis, *Bengtsson et al*. [2006] found that ECHAM5 model can produce a good representation of extratropical storms. Moreover, *Ulbrich et al*. [2008] found that, among 16 GCMs, ECHAM5 is one of the models closest to the ensemble average, both in terms of representation of present climate and of climate change signal. However, they did not include a GCM similar to HadCM3Q3 in the analysis. In addition, although the differences encountered between future projections of ECHAM5 and a similar model to HadCM3Q3, *Donat et al*. [2010a] found that they both reproduce the current characteristic climatological pressure patterns that are relevant for central Europe better than other GCMs. Therefore, given the uncertainty, projections obtained by both GCMs in this study should be considered as equally feasible.

[69] Future Mediterranean climate is generally associated with a weakening of storms, which is reflected in this study with a major H_s reduction during winter. However, results obtained in this study suggest a probable increase in wind intensity in the Gulf of Genoa, which is close to the 45°—latitude limit encountered by *Nikulin et al*. [2011] between areas of increased/decreased storm intensity (see section 2.2)—leading to higher waves locally. In absolute terms, such an increase in wind speed (and consequently on wave height) is not as important as those found in some areas in northern Europe (up to 5 m/s [*Nikulin et al*., 2011]). However, as pointed out by *Donat et al*. [2011], small changes in climate conditions can lead to a considerable increase of risk.

7. Conclusions

[70] This study provides regional future wave climate projections for the end of the century for the NW Mediterranean Sea obtained using five combinations of RCM-GCM (four RCM and two GCM). Although results from different models have been compared, instead of averaging the results in an ensemble projection, they have been analyzed separately remarking both their agreements and discrepancies. Some studies suggest that an ensemble mean is better than a single model [e.g., *Donat et al*., 2010a], but we would like to point out that such an ensemble has to be done with caution, in order not to cancel out contrasting patterns. In this study, the winter wave projections should be at least separated between those corresponding to the two GCMs, before calculating an ensemble average for being used, for instance, for further impact assessment.

[71] Evolution of waves in the future climate has been analyzed in terms of mean and extreme climate for winter and summer seasons using the following variables: significant wave height (H_s), peak period (T_p), and mean wave direction (Θ_m). Mean climate has been characterized by the median of H_s and T_p, the frequency of the eight directional sectors N, NE, E, SE, S, SW, W, NW and by the frequencies of the types of wave states; and the 50 year return period of H_s (z_{50}) has been used to inspect the extremes.

[72] Although models simulate similar patterns for the present period, important differences have been obtained in projected changes between the two GCMs in the winter season, which can be explained by the differences already present in wind projections [*Kjellström et al*., 2011]. Projected wave climate realizations mostly differ in the directional distribution. HadCM3Q3 predicts a greater frequency of NE-E-SE waves, whereas the opposite is predicted with the ECHAM5 model, in which the S-SW and N-NW components tend to increase. This discrepancy is translated into the distribution of the type of sea states: swell/wind-sea/mixed. The increased frequency of NE-E-SE waves in HadCM3Q3 produces more wind-sea states offshore and more mixed sea states near the coastal zones that face east. Such differences are not observed in the median H_s but in z_{50}, as well as the number of storms coming from east.

[73] In general, as expected, changes in wave climate mirror changes in (forcing) wind speed, but they are attenuated or enhanced according to the fetch configuration. For instance, although Mistral events have a tendency to increase in the Gulf of Lion, its short fetch limits the growth of the waves near the coast (this is especially important for extremes). Changes of the median H_s are lower than squared changes of W_{10}, highlighting the presence of swell and mixed sea states, despite the relatively short fetches compared to the open ocean. There is a general decrease of the median H_s in most of the domain, which corresponds to a decrease of W_{10} in the majority of the Mediterranean area. However, at high latitudes near the Gulf of Genoa, the increase of the W_{10} median causes a rise

of the median H_s in the NE corner of the wave model domain. All models agree with this tendency, although each realization differs in magnitude/extension. Such a degree of agreement is not maintained in the extreme climate in which there is more variability among models. In addition, we must be aware of the possibility of having higher values of W_{10} (and thus H_s) compared to those predicted by the models used in this study, since, as mentioned in section 2.2, atmospheric models with increased stratospheric resolution (still not available at a regional scale) have shown that the poleward shift of storms might be more southward [*Scaife et al*., 2011].

[74] Variations of T_p largely mirror the variations of H_s, with its rate of change approximately the square root of those of H_s because fetches in the study area are relatively short, and no abrupt changes in the wind-sea/swell distribution are found.

[75] Wave climate during the summer clearly shows different patterns compared to winter, which is reasonable due to the different processes involved in the atmosphere, such as those caused by thermal effects like the land-sea temperature gradients. During this season, the median H_s tends to rise in the south part of the domain, which once again is explained by an increase of W_{10} there. With regard to directions, there is consistency between both different RCMs and different GCMs, supporting the conclusion of *Déqué et al*. [2005] that uncertainties among climate models depend on the season studied (apart from the variable). They all project an increase in both the NE-E waves, which in turn produce an increase of mixed sea states north of the Balearic Islands and the wind-sea component south of the islands (except in the HadCM3Q3 GCM, where wind-sea states also increase to the north, probably because NE waves increase is more notable in this area/model). Indeed, the increase of NE, which can be partly associated with storm events caused by the Genoa area of cyclogenesis, produces an increase of z_{50} north of the Balearic Islands, which was not captured in the analysis of the median H_s.

[76] In general and for both studied seasons, maximum rates of projected H_s changes are around $\pm 10\%$ for mean conditions (median H_s) versus $\pm 20\%$ for extreme climate (z_{50}).

[77] **Acknowledgments.** This research was carried out within the framework of the Spanish project "Vulnerabilidad, impactos y adaptación al cambio climático: estudio integrado sobre la agricultura, recursos hídricos y costas (ARCO)" (contract 200800050084350), during the Ph.D. program of the lead author, who is currently on a grant from the *Ministerio de Educación* (Spanish Ministry of Education). Said author also acknowledges the support received from the *Col·legi d'Enginyers de Camins, Canals i Ports - Catalunya* (Civil Engineering Association in Catalonia). The authors gratefully acknowledge the research centers and institutions that have freely and disinterestedly provided us with the atmospheric climate projection data sets used in this study: *Danmarks Meteorologiske Institut* (DMI, Denmark)—special thanks to Ole B. Christensen, Neil Mackellar and Fredrik Boberg; *Koninklijk Nederlands Meteorologisch Instituut* (KNMI, Netherlands)—special thanks to Erik van Meijgaard; *Max-Planck-Institut für Meteorologie* (MPI, Germany)—special thanks to Daniela Jacob and Alberto Elizalde; *Sveriges Meteorologiska och Hydrologiska Institut* (SMHI, Sweden)—special thanks to Erik Kjellström and Barry Broman. We are also grateful to the *Organismo Público Puertos del Estado* (Spanish Ports and Harbors Authority) for providing HIPOCAS (wave and atmospheric) data that served to validate the results and to GEBCO for the One Minute Grid bathymetry data available at http://www.gebco.net. We also want to thank Maribel Ortego (UPC) and Raimon Tolosana-Delgado (UPC) for their constructive comments regarding the uncertainty analysis; Marcel Zijlema (TU Delft), for his advice about the SWAN wave model; and Federico Jerez (UPC) and Josep Maria Jordana (UPC), for their helpful assistance during the implementation of the wave model in parallel mode in the ALIEN cluster (of the Civil Engineering School at UPC).

References

Alomar, M. (2012), Improving wave forecasting in variable wind conditions. The effect of resolution and growth rate for the Catalan coast, PhD thesis, 193 p., Univ. Politècnica de Catalunya, Barcelona.

Bengtsson, L., K. I. Hodges, and E. Roeckner (2006), Storm tracks and climate change, *J. Clim.*, *19*(15), 3518–3543.

Bengtsson, L., K. I. Hodges, and N. Keenlyside (2009), Will extratropical storms intensify in a warmer climate?, *J. Clim.*, *22*(9), 2276–2301.

Bolaños, R. (2004), Tormentas de oleaje en el Mediterráneo: Física y Predicción [in Spanish], PhD thesis, Universitat Politècnica de Catalunya. Barcelona, 184 pp.

Bolaños, R., G. Jordà, J. Cateura, J. Lopez, J. Puigdefabregas, J. Gomez, and M. Espino (2009), The XIOM: 20 years of a regional coastal observatory in the Spanish Catalan coast, *J. Mar. Syst.*, *77*(3), 237–260.

Booij, N., R. C. Ris, and L. H. Holthuijsen (1999), A third-generation wave model for coastal regions: 1. Model description and validation, *J. Geophys. Res.*, *104*(C4), 7649–7666.

Cai, Y., and N. Davies (2012), A simple bootstrap method for time series, *Commun. Stat. Simul. Comput.*, *41*(5), 621–631.

Campins, J., A. Genovés, M. A. Picornell, and A. Jansà (2011), Climatology of Mediterranean cyclones using the ERA-40 dataset, *Int. J. Climatol.*, *31*, 1596–1614.

Casas-Prat, M., and J. P. Sierra (2010a), Trend analysis of wave storminess: Wave direction and its impact on harbour agitation, *Nat. Hazards Earth Syst. Sci.*, *10*(11), 2327–2340.

Casas-Prat, M., and J. P. Sierra (2010b), Trend analysis of the wave storminess: The wave direction, *Adv. Geosci.*, *26*(D), 89–92.

Casas-Prat, M., and J. P. Sierra (2012), Trend analysis of wave direction and associated impacts on the Catalan coast, *Clim. Change*, *115*(3), 667–691.

Charles, E., D. Idier, P. Delecluse, M. Déqué, and G. Cozannet (2012), Climate change impact on waves in the Bay of Biscay, France, *Ocean Dyn.*, *62*(6), 831–848.

Christensen, J., et al. (2007), Regional climate projections, Solomon, S., D. Qin, M. Manning, Z. Chen, M. Marquis, K.B. Averyt, M. Tignor and H.L. Miller (eds.) in *Climate Change 2007: The Physical Basis. Contribution of Working Group I to the Fourth Assessment Report of the Intergovernmental Panel on Climate Change*, pp. 847–940, Cambridge Univ. Press, United Kingdom and New York.

Collins, M., S. F. B. Tett, and C. Cooper (2001), The internal climate variability of HadCM3, a version of the Hadley Centre coupled model without flux adjustments, *Clim. Dyn.*, *17*, 61–81.

de Farias, E. G. G., J. A. Lorenzzetti, and B. Chapron (2012), Swell and wind-sea distributions over the mid-latitude and Tropical North Atlantic for the period 2002–2008, *Int. J. Oceanogr.*, *2012*, 1–8.

Déqué, M., and S. Somot (2010), Weighted frequency distributions express modelling uncertainties in the ENSEMBLES regional climate experiments, *Clim. Res.*, *44*(2-3), 195–209.

Déqué, M., et al. (2005), Global high resolution versus limited area model climate change projections over Europe: Quantifying confidence level from PRUDENCE results, *Clim. Dyn.*, *25*, 653–670.

Déqué, M., et al. (2007), An intercomparison of regional climate simulations for Europe: Assessing uncertainties in model projections, *Clim. Change*, *81*, 53–70.

Donat, M., G. Leckebusch, J. Pinto, and U. Ulbrich (2010a), European storminess and associated circulation weather types: Future changes deduced from a multi-model ensemble of GCM simulations, *Clim. Res.*, *42*(1), 27–43.

Donat, M. G., G. Leckebusch, S. Wild, and U. Ulbrich (2010b), Benefits and limitations of regional multi-model ensembles for storm loss estimations, *Clim. Res.*, *44*(2-3), 211–225.

Donat, M. G., G. C. Leckebusch, S. Wild, and U. Ulbrich (2011), Future changes in European winter storm losses and extreme wind speeds inferred from GCM and RCM multi-model simulations, *Nat. Hazards Earth Syst. Sci.*, *11*(5), 1351–1370.

Fawcett, L., and D. Walshaw (2012), Estimating return levels from serially dependent extremes, *Environmetrics*, *23*(3), 272–283.

García, M. A., A. Sánchez-Arcilla, J. P. Sierra, J. Sospedra, and J. Gómez (1993), Wind waves off the Ebro Delta, NW Mediterranean, *J. Mar. Syst.*, *4*, 235–262.

Giorgi, F., and P. Lionello (2008), Climate change projections for the Mediterranean region, *Global Planet. Change*, *63*, 90–104.

Grabemann, I., and R. Weisse (2008), Climate change impact on extreme wave conditions in the North Sea: An ensemble study, *Ocean Dyn.*, *58*, 199–212.

Guedes Soares, C., R. Weisse, J. C. Carretero, and E. Alvarez (2002), A 40 years hindcast of wind, sea level and waves in European waters, paper presented at OMAE 2002: 21st International Conference on Offshore Mechanics and Arctic Engineering, Oslo, Norway.

Hall, P., and S. R. Wilson (1991), Two guidelines for bootstrap hypothesis testing, *Biometrics*, *47*(2), 757–762.

Hemer, M. A., J. A. Church, and J. R. Hunter (2010), Variability and trends in the directional wave climate of the Southern Hemisphere, *Int. J. Climatol.*, *30*, 475–491.

Hemer, M. A., X. L. Wang, R. Weisse, and the COWCLIP Team (2011), WCRP-JCOMM workshop on coordinated global wave climate projections, Tech. Rep. 1581, Switzerland.

Hemer, M. A., X. L. Wang, R. Weisse, and V. R. Swail (2012a), Advancing wind-waves climate science, *Bull. Am. Meteorol. Soc.*, *93*(6), 791–796.

Hemer, M. A., K. L. McInnes, and R. Ranasinghe (2012b), Climate and variability bias adjustment of climate model-derived winds for a southeast Australian dynamical wave model, *Ocean Dyn.*, *62*(1), 87–104.

Hemer, M. A., Y. Fan, N. Mori, A. Semedo, and X. L. Wang (2013), Projected change in wave climate from a multi-model ensemble, *Nat. Clim. Change*, *3*, 471–476.

IPCC (2000), Summary for policymakers. Emissions Scenarios. A Special Report of Working Group III of the Intergovernmental Panel of Climate Change.

IPCC (2007). An assessment of the Intergovernmental Panel of Climate Change. Synthesis Report.

Kjellström, E., G. Nikulin, U. Hansson, G. Strandberg, and A. Ullerstig (2011), 21st century changes in the European climate: Uncertainties derived from an ensemble of regional climate model simulations, *Tellus A*, *63*(1), 24–40.

Kriezi, E. E., and B. Broman (2008), Past and future wave climate in the Baltic Sea produced by the SWAN model with forcing from the regional climate model RCA of the Rossby Centre, paper presented at US/EU-Baltic International Symposium, Tallin, Estonia.

Lionello, P., F. Dalan, and E. Elvini (2002), Cyclones in the Mediterranean region: The present and the doubled CO2 climate scenarios, *Clim. Res.*, *22*, 147–159.

Lionello, P., P. Malanotte-Rizzoli, and R. Boscolo (2006), *Mediterranean Climate Variability*, 421 pp., Elsevier, Amsterdam.

Lionello, P., S. Cogo, M. B. Galati, and A. Sanna (2008a), The Mediterranean surface wave climate inferred from future scenario simulations, *Global Planet. Change*, *63*, 152–162.

Lionello, P., U. Boldrin, and F. Giorgi (2008b), Future changes in cyclone climatology over Europe as inferred from a regional climate simulation, *Clim. Dyn.*, *30*, 657–671.

Mendoza, E. T., and J. A. Jiménez (2006), Storm-induced beach erosion potential on the Catalonian coast, *J. Coast. Res.*, *SI 48*, 81–88.

Nikulin, G., E. Kjellström, U. Hansson, G. Strandberg, and A. Ullerstig (2011), Evaluation and future projections of temperature, precipitation and wind extremes over Europe in an ensemble of regional climate simulations, *Tellus A*, *63*(1), 41–55.

Ortego, M. I., R. Tolosana-Delgado, J. Gibergans-Báguena, J. J. Egozcue, and A. Sánchez-Arcilla (2012), Assessing wavestorm hazard evolution in the NW Mediterranean with hindcast and buoy data, *Clim. Change*, *113*(3–4), 713–731.

Pandey, M. D., P. H. A. J. M. Van Gelder, and J. K. Vrijling (2003), Bootstrap simulations for evaluating the uncertainty associated with peaks-over-threshold estimates of extreme wind velocity, *Environmetrics*, *14*(1), 27–43.

Pandey, M. D., P. H. A. J. M. Van Gelder, and J. K. Vrijling (2004), Dutch case studies of the estimation of extreme quantiles and associated uncertainty by bootstrap simulations, *Environmetrics*, *15*(7), 687–699.

Park, D. S., Y. B. Kim, K. I. Shin, and T. R. Willemain (2001), Simulation output analysis using the threshold bootstrap, *Eur. J. Oper. Res.*, *134*(1), 17–28.

Pinto, J. G., U. Ulbrich, G. C. Leckebusch, T. Spangehl, M. Reyers, and S. Zacharias (2007), Changes in storm track and cyclone activity in three SRES ensemble experiments with the ECHAM5/MPI-OM1 GCM, *Clim. Dyn.*, *29*(2-3), 195–210.

Portilla, J., F. J. Ocampo-Torres, and J. Monbaliu (2009), Spectral partitioning and identification of wind sea and swell, *J. Atmos. Oceanic Technol.*, *26*, 2107–122.

Pryor, S. C., R. J. Barthelmie, N. E. Clausen, M. Drews, N. MacKellar, and E. Kjellström (2012), Analyses of possible changes in intense and extreme wind speeds over northern Europe under climate change scenarios, *Clim. Dyn.*, *38*(1-2), 189–208.

Ratsimandresey, A. W., M. G. Sotillo, E. Alvarez-Fanjul, J. Carretero-Albiach, B. Perez-Gomez, and H. Hajji (2008), A 44-year (1958–2001) sea level residual hindcast over the Mediterranean Basin, *Phys. Chem. Earth*, *33*, 250–259.

Roeckner, E., et al. (2003), The atmospheric general circulation model ECHAM5. Model description, Tech. Rep. 349, Hamburg.

Samuelsson, P., et al. (2011), The Rossby Centre Regional Climate model RCA3: Model description and performance, *Tellus A*, *63*(1), 4–23.

Sánchez-Arcilla, A., D. González-Marco, and R. Bolaños (2008), A review of wave climate and prediction along the Spanish Mediterranean coast, *Nat. Hazards Earth Syst. Sci.*, *8*, 1217–1228.

Scaife, A. A., et al. (2011), Climate change projections and stratospheretroposphere interaction, *Clim. Dyn.*, *38*(9-10), 2089–2097.

Ulbrich, U., J. G. Pinto, H. Kupfer, G. C. Leckebusch, T. Spangehl, and M. Reyers (2008), Changing Northern Hemisphere storm tracks in an ensemble of IPCC climate change simulations, *J. Clim.*, *21*(1-2), 1669–1679.

Ulbrich, U., G. C. Leckebusch, and J. G. Pinto (2009), Extra-tropical cyclones in the present and future climate: A review, *Theor. Appl. Climatol.*, *96*(1-2), 117–131.

Ulbrich, U., et al. (2013), Are greenhouse gas signals of Northern Hemisphere winter extra-tropical cyclone activity dependent on the identification and tracking algorithm?, *Meteorol. Z.*, *22*, 1, 61–68.

van Meijgaard, E., L. van Ulft, W. van de Berg, F. Bosveld, B. van den Hurk, G. Lenderink, and A. Siebesma (2008), The KNMI regional atmospheric climate model RACMO, version 2.1, Tech. Rep. 302. Koninklijk Nederlands Meteorologisch Instituut: Bilt

Wang, X. L., V. R. Swail, and A. Cox (2010), Dynamical versus statistical downscaling methods for ocean wave heights, *Int. J. Climatol.*, *30*, 317–332.

Wang, X. L., Y. Feng, and V. R. Swail (2012), North Atlantic wave height trends as reconstructed from the twentieth century reanalysis, *Geophys. Res. Lett.*, *39*, L18705, doi:10.1029/2012GL053381.

Weisse, R., and H. Von Storch (2010), *Marine Climate and Climate Change. Storms, Wind Waves and Storm Surges*, 200 pp., Praxis Publishing, Chichester, U. K.

Wilks, D. K. (1997), Resampling hypothesis tests for autocorrelated fields, *J. Clim.*, *10*, 65–82.

Paper D

A physical-based statistical method for modeling ocean wave heights

M. Casas-Prat, X.L. Wang and J.P. Sierra

Ocean Modelling,
doi: http://dx.doi.org/10.1016/j.ocemod.2013.10.008, 2013.

Accepted Manuscript

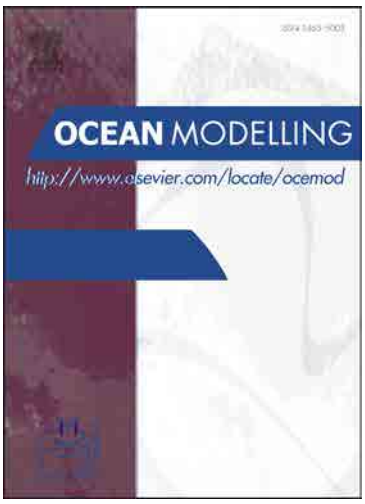

A physical-based statistical method for modeling ocean wave heights

Mercè Casas-Prat, Xiaolan L. Wang, Joan P. Sierra

PII: S1463-5003(13)00189-3
DOI: http://dx.doi.org/10.1016/j.ocemod.2013.10.008
Reference: OCEMOD 863

To appear in: *Ocean Modelling*

Received Date: 31 May 2013
Revised Date: 25 October 2013
Accepted Date: 30 October 2013

Please cite this article as: Casas-Prat, M., Wang, X.L., Sierra, J.P., A physical-based statistical method for modeling ocean wave heights, *Ocean Modelling* (2013), doi: http://dx.doi.org/10.1016/j.ocemod.2013.10.008

This is a PDF file of an unedited manuscript that has been accepted for publication. As a service to our customers we are providing this early version of the manuscript. The manuscript will undergo copyediting, typesetting, and review of the resulting proof before it is published in its final form. Please note that during the production process errors may be discovered which could affect the content, and all legal disclaimers that apply to the journal pertain.

ACCEPTED MANUSCRIPT

A physical-based statistical method for modeling ocean wave heights

Mercè Casas-Prat[a,b], Xiaolan L. Wang[c], Joan P. Sierra[a,b]

[a] *Laboratori d'Enginyeria Marítima, Universitat Politècnica de Catalunya · Barcelona Tech, Jordi Girona 1-3 D1, Barcelona, Catalonia, Spain*

[b] *Centre Internacional d'Investigació dels Recursos Costaners, Jordi Girona 1-3 D1, Barcelona, Catalonia, Spain*

[c] *Climate Research Division, Science and Technology Branch, Environment Canada, 4905 Dufferin Street, Toronto, Ontario, Canada*

Abstract

This study proposes a computationally inexpensive statistical method for modeling ocean wave heights, focusing particularly on modeling wave heights in near-shore areas. A multiple linear regression is used to predict significant wave heights (H_s) using predictors derived from the sea level pressure (SLP) field, including the use of squared SLP gradients to represent geostrophic winds. One time step lagged H_s is also included as a predictor, which could be interpreted as the first order derivative in the spectral energy balance governing equation. Further, based on the frequency/directional dispersion theory of waves, the swell component is accounted for by using a set of selected principal components derived from the squared SLP gradient vectors (including magnitudes and directions). The effect of non-Gaussian (non-negative) variables is also assessed by applying two types of transformation to the data.

The proposed method is evaluated and shown to have good skills for the study area (Catalan coast). This method can be used to project possible future wave climate change for use in coastal impact assessment studies. It is used in this study to project the wave climate for the study area that corresponds to 5 sets of regional climate model (RCM) atmospheric projections, which were made by different RCMs forced by the same global circulation model (GCM), or by the same RCM forced by two GCMs. For the season analyzed (winter), the results show that the uncertainty due to using different GCMs to drive the same RCM is greater than that due to using different RCMs driven by the same GCM.

Keywords: climate change, statistical downscaling, wave height, Mediterranean Sea

1. Introduction

Nowadays, climate change is a hot research topic because of its possible impacts on our society and on the environment in the near future. The greenhouse effect might contribute

*Corresponding author. *Telephone*: +34 93 4017405. *Email address*: merce.casas@upc.edu (Mercè Casas-Prat)

ACCEPTED MANUSCRIPT

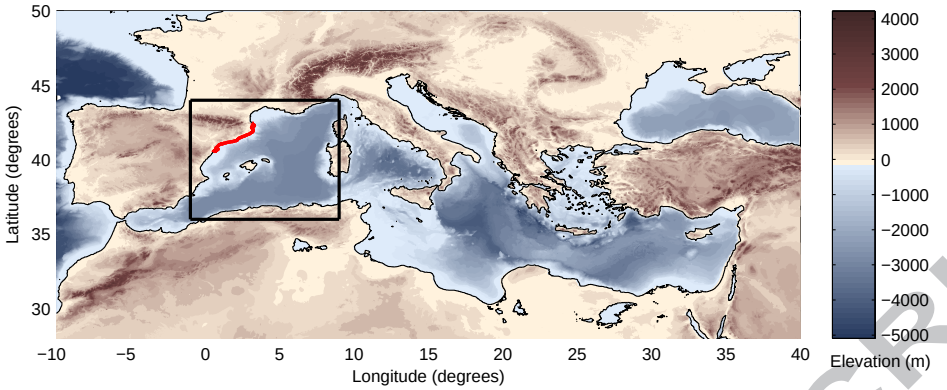

Figure 1: Situation of the Catalan coast (red) within the study area (black square) and the Mediterranean Sea

not only to an increase of the global temperature, but also to changes in the atmospheric pressure and wind patterns at both global and regional scales, affecting the frequency and intensity of storms at a given location (e.g. Bengtsson et al., 2006, 2007, 2009; Weisse and von Storch, 2010). Changes in any characteristics of storms will affect ocean wave climate both locally (wind-sea) and remotely (swell waves). This might produce several coastal impacts such as a possible increase of coastal erosion, inundation, structure failure, decrease of harbour operability, etc. (e.g. Casas-Prat and Sierra, 2012; Hemer, 2009; Slott et al., 2006; Zacharioudaki and Reeve, 2011). In this context, the IPCC (2000) established different greenhouse gas emission scenarios. Several regional and global circulation models (RCMs and GCMs) have been developed and used to project changes in the atmosphere patterns (temperature, pressure, wind, precipitation, etc.) and to estimate the sea level rise corresponding to these scenarios. However, even in the IPCC fourth assessment report (IPCC, 2007) limited attention has been paid to wave climate projections, especially on regional scales that are essential to perform coastal impact assessment.

Average population densities are significantly higher in the near-coastal zone than inland areas (Small and Nicholls, 2003). Thus, evaluating the impact of climate change on coastal areas where wave climate plays an important role, is of great importance. To infill this gap, in the recent years some studies have been carried out to project future wave climate conditions using numerical wave models forced by surface winds as simulated in RCMs and GCMs. Some examples are: Mori et al. (2010), Hemer et al. (2013b,a) and Semedo et al. (2011, 2013) at the global scale and Lionello et al. (2008), Grabemann and Weisse (2008), Charles et al. (2012), Hemer et al. (2012) and Casas-Prat and Sierra (2013) at a regional scale. This approach, named "dynamical downscaling" is very time-consuming; and many combinations have to be taken into account in order to consider all the sources of uncertainty (greenhouse scenario, inter-model variability... see Déqué et al. 2007 for more details). Thus, statistical downscaling approaches have been developed as an alternative for making projections of wave

ACCEPTED MANUSCRIPT

climate (e.g. Callaghan et al., 2008; Camus et al., 2011; Gunaydin, 2008; Mori et al., 2013; Wang and Swail, 2006; Wang et al., 2010). This method is based on building an empirical relationship between atmospheric variables and wave climate parameters using observations or reanalysis data, and assumes that this relationship will hold under the projected future climate conditions. Although the physical processes are notably simplified with a more or less simple relationship, if the main wave features are properly captured, comparable (or even better) results can be obtained when compared to dynamical downscaling (Wang et al., 2010). Apart from the significant reduction of required computational time and memory, the statistical approach has the advantage of being flexible regarding the selection of the forcing variable(s). For example, one can use atmospheric variables that are well simulated by climate models, such as sea level pressure, as predictors to project ocean waves (Wang et al., 2010); whereas for a numerical wave modeling one has to use the 10-m wind data, although they are usually not as well simulated by climate models (e.g. McInnes et al., 2011).

Wang and Swail (2006) and Wang et al. (2010) used a multiple linear regression to represent the relationship between the predictand, significant wave height (H_s), and two SLP-based predictors that mainly represent local wave generation. They obtained reasonably good results at the global and the North Atlantic scales but the swell component of waves is insufficiently represented in their model. Wang et al. (2012) recently developed a more skillful model which accounts for the swell component by using the principal components (PCs) of the aforementioned SLP-based predictors and lagged values of the predictand. In this study, we aim to improve the representation of swell in the model, focusing on modeling (deep water) near-shore regional waves with finer spatial (0.125°) and temporal (3 h) resolutions that are suitable for studying regional coastal impacts of climate change and adaptation. Based on the work of Wang and Swail (2006), Wang et al. (2010) and Wang et al. (2012), we develop a new approach taking into account the physical theory of directional and frequency decomposition of swell waves (e.g. Holthuijsen, 2007). The new model is then applied to 5 sets of projections of the atmosphere by four different RCMs (forced by one or two GCMs; see Table 1), to explore the inter-model variability and to project future changes in wave climate, as done by Casas-Prat and Sierra (2013) with dynamical downscaling.

The study area is situated in the NW Mediterranean Sea, focusing on the Catalan coast (highlighted in red in Fig. 1 and 2). The new method is therefore adapted to the features of this zone, providing the area with a range of wave projections that are of sufficiently high spatial and temporal resolutions for coastal impact assessments in the context of climate change. In general, we aim to develop a computationally inexpensive method of general applicability. Thus, our method can easily be adapted for use in other regions.

The remainder of this paper is structured as follows. Section 2 describes the main features of the atmospheric and wave climate of the study area, and Section 3, the datasets used to calibrate and validate the statistical model and to project the future wave climate conditions in this area. Section 4 describes how the statistical method is developed and applied to the study area. Along with some discussion, Section 5 presents the results of model evaluation, and future wave projections are discussed in Section 6. Finally, Section 7 summarizes the main conclusions of this study, along with some discussion.

ACCEPTED MANUSCRIPT

2. Study area

Although we focus on the wave climate along the Catalan coast, in order to account for swell waves (see Section 2.2), a larger domain (than merely the Catalan sea area) is considered as the "study area", which is illustrated with a black square in Fig 1 and shown enlarged in Fig. 2. In determining the boundaries of this study area, we consider: 1) the maximum fetch affecting the Catalan coast and 2) the shadow effects produced by the Balearic islands (more details in Section 2.2). We will produce therefore wave climate projections for the whole study area (not only for the Catalan coast). However, the results are less reliable/accurate for grid points near the domain boundaries, especially those that are close to the Gibraltar strait, since no exchange with the Atlantic Ocean is considered in the datasets used.

Having a better knowledge of the main aspects of atmospheric and (corresponding) wave climate is important to better design the statistical model, and to properly interpret the modeling results. Therefore, a review of those aspects has been undertaken and is presented in the subsections below.

2.1. Atmospheric climate

Several reviews and studies have been carried out in the recent years in order to better describe the characteristics of the complex Mediterranean climate (e.g. Bolle, 2003; Campins et al., 2011; Lionello et al., 2006; Nissen et al., 2010). Like other areas in a similar latitude, the Mediterranean region is a transitional zone with a large environmental meridional gradient between humid mountains in the North and hot and arid regions in the South and is affected by both tropical and mid-latitude systems (Campins et al., 2011; Lionello et al., 2006). However, the presence of a relatively large and deep mass of water makes the Mediterranean quite unique (Bolle, 2003), ranging its orography from depths to altitudes of the order of 5000 m and being communicated to the Atlantic through the Gibraltar strait. This water mass not only represents a heat reservoir and source of moisture for land areas but is also a source of energy that can be transformed into cyclone activity (Lionello et al., 2006). According to Nissen et al. (2010), 69% of the wind storms are caused by cyclones (low pressure systems) located in the Mediterranean region while the remaining 31% have their origin in the North Atlantic or Northern Europe.

Although forced by planetary scale patterns, the complexity of the basin (e.g. sharp orography) produces many subregional and mesoscale features with a large spatial and seasonal variability (Campins et al., 2011). Winter and summer have contrasting patterns because of the different cyclogenetic mechanisms taking place (Campins et al., 2011). Therefore, statistical analysis of climate data should be preferably performed for each season separately. During summer, cyclones/heat-lows are short-lived, weak and shallow, mainly caused by thermal contrasts and orographic effects (Campins et al., 2011). On the contrary, during winter, cyclones are well-developed depressions and tend to be deeper, longer-lived, more mobile and intense. Spring and autumn can be considered as transitional seasons between both extremes (Campins et al., 2011). Their different physical origins turn into different spatial distributions of low pressure system centres as well. Although the Gulf of Genoa

ACCEPTED MANUSCRIPT

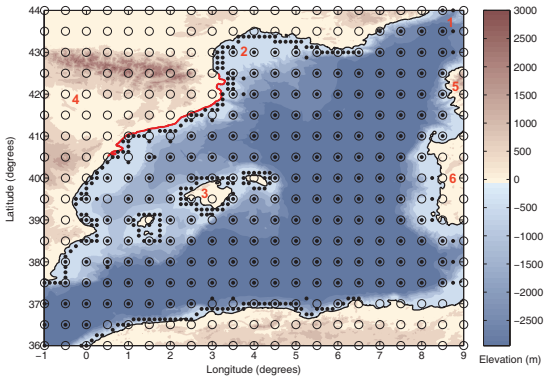

Figure 2: Study area (in red contour line the Catalan coast) and datasets (dots: H_s grid, circles: SLP grid). Red numbers are used to indicate geographical units for spatial reference: Gulf of Genoa (1), Gulf of Lion (2), Balearic Islands (3), Iberian Peninsula (4), Corsica (5), Sardinia (6)

area (located in the top-right corner of our study area, see Fig. 2) exhibits a preferred area for cyclogenesis during the whole year, many summer low pressure systems develop over land (e.g. Sahara and Iberian Peninsula) indicating that thermal heating over land plays an important role in the genesis and maintenance of such depressions. During winter, cyclones are located mainly over the sea with a clear maximum in the Genoa area (one of the areas with highest wind activity) and the Cyprus area (Eastern Mediterranean), the two locations of the maximum number of cyclone centres (Campins et al., 2011; Nissen et al., 2010). These lower pressure areas located in the Gulf of Genoa produce a dominant NW wind field over the study area, causing the well-known regional Mistral (NW) wind, which is strengthened by the channelling effect of, for example, the Ebre valley (south of Catalan coast) and Rhone valley (in the Gulf of Lion).

Owing to such smaller scale processes, Mediterranean cyclones/heat-lows have significantly shorter lifespans and smaller spatial scales than the extra-tropical Atlantic ones, with 65% of them being at a subsynoptic scale. Their typical radius and average lifespan is about 500 km and 28 h, respectively (excluding the shortest ones), whereas cyclones in the Atlantic have radius of the order of 1000–2000 km and normally last 3-3.5 days (Lionello et al., 2006). This change of scale makes evident that when working in an area like the Mediterranean we have to work with a smaller spatial scale than compared to the open ocean. According to Lionello et al. (2006), for studying the Mediterranean basin, the grid cell size should be at most 50 km. They also pointed out that the spatial resolutions used for most of the existing global climate simulations cannot resolve adequately the Mediterranean basin.

2.2. Wave climate

All the aforementioned characteristics of the atmospheric pressure and wind variations have a clear influence on the wave climate. Ocean waves are generated by the combined effect of atmospheric storminess condition and fetch. Fetch modulates the effectiveness of storms in generating waves, making some storms more effective in producing waves (Lionello and

ACCEPTED MANUSCRIPT

Sanna, 2005). For instance, although the Mistral wind is very important in Catalonia, it does not significantly contribute to the Catalan extreme wave climate because of the shoreline orientation. Instead, Catalan coastal events are dominated by storm events coming from NE-E (Casas-Prat and Sierra, 2010b), in which larger fetches coincide with stronger winds (Sánchez-Arcilla et al., 2008). Therefore, apart from the complex spatial and time variability of wind fields, waves in the Catalan coast are also affected by short fetches (up to about 600 km since Corsica and Sardinia islands can be considered as a barrier from waves coming from E), shadow effects caused by Balearic Islands for waves coming from S and SE, and complex bathymetry with deep canyons close to the coast (especially in the Northern Catalan coast) (Sánchez-Arcilla et al., 2008). This again emphasizes the need of using a high spatial resolution climate model in this area. Although the fetches are short, the swell component is important in the Catalan coast. Using the circular correlation coefficient (Fisher and Lee, 1983) between wind and wave direction, Casas-Prat and Sierra (2010a) pointed out that, except for the northern Catalan coast where a larger proportion of storms are locally generated by N winds, mixed sea states are dominant along the coast.

The Catalan coast wave climate is therefore dominated by low-to-medium winds with occasional strong events (maximum wind recorded was 25 m/s (Bolaños et al., 2009)). In the last twenty years, a maximum H_s close to 6 m with T_p of about 14 s has been recorded in the Ebre delta (Southern Catalan coast) whereas the associated mean values are, respectively, 0.8 m and 5 s (Bolaños et al., 2009). The mean duration of wave storms is estimated to be below 24h, defined using the Peak Over Threshold method with a threshold of 2 m and considering certain duration requirements to separate independent storms (Bolaños et al., 2009).

3. Data

The data used in the present study can be divided into two groups. The first is used to calibrate and validate the statistical model (Section 3.1), whereas the second serves to project future wave climate (Section 3.2).

3.1. Calibration and validation

The 44-year (1958-2001) wave and atmospheric hindcast database from the European HIPOCAS project (Guedes Soares et al., 2002) is used to calibrate and validate the statistical model (see Section 4.5). The atmospheric variables are taken from the output of the Regional Circulation Model REMO (Jacob, accessed 2012), forced by the global NCEP reanalysis data (Kalnay et al., 1996). The waves were simulated using the WAM model (The WAMDI Group, 1988). Although real measurements (with buoys, wave gauges, radars...) are usually more reliable, they do not have enough spatial and temporal coverage for the purpose of this study.

The HIPOCAS database has been validated for wind, wave and sea-level parameters (Musić and Nicković, 2008; Sotillo et al., 2005; Ratsimandresy et al., 2008a; Ratsimandresy et al., 2008b). HIPOCAS data underestimates to some extend extreme events (Ratsimandresy et al., 2008b), which might be attributable to numerical inertia. Certainly, taking into

ACCEPTED MANUSCRIPT

account the complex Mediterranean climate, this dataset would benefit from an observation-based correction, as recently done by Minguez et al. (2011) and Martinez-Asensio et al. (2013). However, Ortego et al. (2012) did not find statistical evidence of wave storm magnitude bias between HIPOCAS data and buoy observations in the southern Catalan coast. Ratsimandresey et al. (2008b) found that HIPOCAS data generally reproduces mean values quite well. Therefore, the HIPOCAS data is suitable to calibrate and validate our statistical model in this study. In particular, we use the sea level pressure (SLP) and the significant wave height (H_s) from this database. These data have a temporal resolution of 1h and 3h, respectively, and the spatial resolution is 0.5° for SLP and varies from 0.125° to 0.5° for H_s (the later illustrated with dots in Fig 2).

3.2. Future projections

Once the coefficients of the model are estimated and evaluated, the statistical model is applied to 5 datasets of SLP projections obtained from climate models in order to obtain their corresponding H_s fields. As detailed in Table 1, these 5 sets of SLP projections were respectively simulated using 4 different RCMs: HIRHAM5 (Christensen et al., 2007), RACMO2 (van Meijgaard et al., 2008), REMO, and RCA3 (Samuelsson et al., 2011). Such regional high spatial-resolution projections (25 km) were developed within the context of the ENSEMBLES project forced by the mid-line A1B emission scenario (IPCC, 2007). The high temporal resolution (1h-3h) version of those simulations were freely put at our disposal by 4 European research institutes (see Table 1). The ECHAM5 GCM (Roeckner et al., 2003) simulations were used as lateral boundary conditions for all four RCMs; and the HadCM3Q3 GCM (Collins et al., 2001) simulations were also used as lateral boundary conditions for a second set of projections by the RCA3 (Table 1).

For each available set of RCM projections, two 30-year time slices (as recommended by Hemer et al., 2011) were selected: the period 1971-2000 (or 1981-2010 for MPI data) is chosen to represent the "present" (or baseline) climate, and the period 2071-2100, to represent "future" climate. The availability of different sets of projections by different RCMs forced with the same GCM, or by the same RCM forced with different GCMs, serves not only to obtain robust estimates of changes in H_S but also to explore the inter-model variability, which tends to be higher than those between emission scenarios (Déqué et al., 2007; Wang and Swail, 2006).

All the SLP data used in this study are interpolated onto the same lat.-long. grid of 0.5° resolution (shown as circles in Fig 2), using the same 3-hourly time steps.

4. Method

The statistical method we develop in this study is inspired by the previous work of Wang and Swail (2006), Wang et al. (2010) and Wang et al. (2012). In this section, we describe the new methodological developments in comparison with these previous studies. First, we review the related regression model for simulating ocean waves in Subsection 4.1, to provide the context of the new method we propose here. Then, we explain the new aspects of the proposed method in Subsections 4.2, 4.3 and 4.4. Finally, we describe the calibration, evaluation in Subsection 4.5.

ACCEPTED MANUSCRIPT

Table 1: Subsets of SLP data used to project H_s

Acronym	RCM	GCM	$\Delta t(h)$
HIR_E	HIRHAM5	ECHAM5	1
RAC_E	RACMO2	ECHAM5	3
REM_E	REMO	ECHAM5	1
RCA_E	RCA3	ECHAM5	3
RCA_H	RCA3	HadCM3Q3	3

4.1. The related regression models

Multivariate regression models have been used to represent the relationship between H_s and atmospheric variables to simulate H_s (e.g. Wang and Swail, 2006; Wang et al., 2010). Although these are statistical/empirical methods, the physics of ocean waves are considered in the selection of the appropriate predictors. Ocean waves are generated by air-pressure fluctuations, which are almost entirely caused by surface winds (Holthuijsen, 2007). However, the present-day climate models represent several atmospheric (such as sea level pressure) fields much better than the surface (10-m) wind fields, as pointed out by Wang et al. (2010). For that reason, Wang and Swail (2006), Wang et al. (2010), and Wang et al. (2012) used anomalies of sea level pressure (SLP) and of squared SLP spatial gradients as predictors for H_s, instead of using surface wind speeds. The base of this method is that H_s is closely related to squared wind speed at the surface level in a fully developed sea state (e.g. Janssen et al., 2002), while geostrophic winds at the sea level are closely related to spatial gradients of SLP and are good proxy for surface winds. However, this alternative approach is hardly possible in dynamical modeling of waves, because dynamical wave models are driven by surface winds.

The regression model used in Wang and Swail (2006) and Wang et al. (2010) is of the form:

$$\hat{H}_s(t,m) = \hat{a}(m) + \hat{a}_P(m)\, P(t,m) + \hat{a}_G(m)\, G(t,m) \tag{1}$$

where m and t are respectively the location and time index ($m = 1, 2, ..., M$; $t = 1, 2, ..., T$), and P and G denote anomalies of sea level pressure (SLP) and of squared SLP spatial gradient, respectively. Here and throughout this article, $\hat{X}$ denote an estimate of X. Wang and Swail (2006) and Wang et al. (2010) applied this model to simulate seasonal mean or 12-hourly H_s in the global oceans and in the North Atlantic, respectively, with spatial resolution of 2°.

Recently, Wang et al. (2012) extended the set of predictors in model (1), adding the principle components (PCs) of $P(t,m)$ and of $G(t,m)$ over a domain that is larger than the wave field in question to represent the swell component of waves, as well as p-lagged dependent variables, $H_s(t-p,m)$, to account for serial correlation in the predictand (dependent variable) H_s. They also proposed a data adaptive Box-Cox transformation procedure to diminish the departure of H_s and SLP gradients from a normal distribution. They have

ACCEPTED MANUSCRIPT

shown that their new model is more skillful, resulting in less biased simulations of 6-hourly H_s, than model (1).

The methodological developments we propose below include physical and statistical aspects. On the physical aspects, we modify the way to account for swell waves by using the term Δ_{sw} as defined later in section 4.2, and the way to account for serial correlation in H_s using the term Δ_t defined later in section 4.3. Thus, our new model is of the form:

$$\begin{aligned}\hat{H}_s(t,m) =& \hat{a}(m) + \hat{a}_P(m)\, P(t,m) + \hat{a}_G(m)\, G(t,m) \\ &+ \Delta_{\text{sw}}(t,m) + \Delta_t(t,m)\end{aligned} \tag{2}$$

The last term makes the statistical model more coherent with ocean wave physics, because it can be interpreted as a discrete approximation of the first order derivative that appears in the spectral energy balance governing equation (e.g. Holthuijsen, 2007). Such temporal dependence is especially important for high temporal resolution data as in the present study. In fact, it is closely related to the large autocorrelation found in the 3-hourly H_s time series. More details about the inclusion of this term are given in Section 4.3.

On the statistical aspects, we take into account the data scale and explore the effects of deviation from the Gaussian distribution assumption in the multiple linear regression analysis by transforming the data in different ways, as detailed below in Section 4.4.

Since different regimes dominate in different seasons (see Section 2.1), waves in different seasons should be modeled, separately. In this study, we focus on the winter (most energetic) season, which is defined here as December-January-February.

4.2. Inclusion of swell

Swell waves are waves propagating across the ocean, after being generated remotely during a storm. As explained in Section 2.2, the Catalan coast is often affected by an important swell component coming from E. Ignoring swell waves would lead to a significant underestimation of H_s.

The initially random wave field generated in a storm propagates while disintegrating in several more regular waves because of the frequency and directional dispersion phenomena (Munk et al., 1963). The low-frequency waves travel faster than high-frequency ones causing the frequency dispersion. Moreover, despite having a predominant forcing wind direction, waves also propagate at other directions around the predominant one, producing the directional dispersion. Due to these dispersion effects, the swell energy spectrum is narrower in both frequency and direction space, and swell waves are much lower than those initially generated in the storm (as illustrated in Fig. 3). Holthuijsen (2007) pointed out that ocean waves barely lose energy outside storms because the waves are not steep enough to break and therefore the reduction of H_s is solely due to dispersion, without involving dissipation. However, swell dissipation has been observed across oceans, which might be attributed to air-sea friction or underwater processes (Ardhuin et al., 2009). Such dissipation increases with fetch (and therefore it is very important in large oceans) and mostly affects steep (short) waves (with higher frequencies). This explains why swell waves are usually long waves. Our study

ACCEPTED MANUSCRIPT

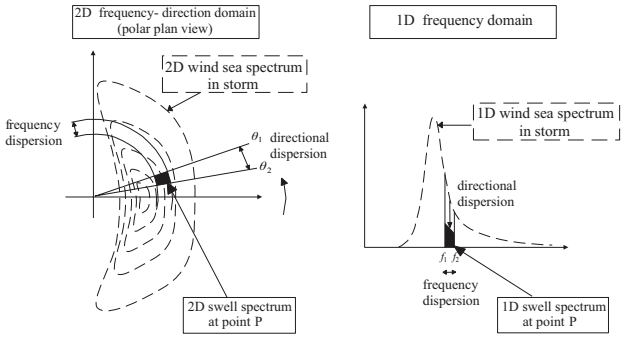

Figure 3: The transformation by frequency and directional dispersion of a wind-sea spectrum into a swell spectrum within the frequencies (f_1, f_2) and directions (θ_1, θ_2) at a geographic location P (from Holthuijsen, 2007); courtesy of Leo H. Holthuijsen

area does not have long fetches. Therefore, we do not explicitly account for dissipation; we only consider typical periods of swell waves, as shown later in this section.

At any generation location m_0, according to Rayleigh wave theory, H_s can be expressed as a function of the original wind-sea density spectrum $E(t, f)$:

$$\begin{aligned} H_s(t, m_0) &= 4\left[\int\int E(t, f)D(\theta)\mathrm{d}f\mathrm{d}\theta\right]^{1/2} \\ &= 4\left[\int E(t, f)\mathrm{d}f\right]^{1/2} \end{aligned} \tag{3}$$

where θ is the angle deviation from the main direction, and $D(\theta)$, the directional spreading function, whose integral over the whole range of directions is 1. $D(\theta)$ can be expressed as (Denis and Pierson, 1953):

$$D(\theta) = \frac{2}{\pi}\, cos^2(\theta) \tag{4}$$

where $-90° \leq \theta \leq 90°$.

As illustrated in Fig. 3, a swell wave train that is generated at location m_0 and is associated with frequency bin (f_1, f_2) and directional bin (θ_1, θ_2) will arrive at point m_P after a certain time lag δ. The swell wave height H_{sw} is described by:

$$\begin{aligned} H_{\mathrm{sw}}(t + \delta, m_{\mathrm{P}}) &= 4\left[\int_{f_1}^{f_2}\int_{\theta_1}^{\theta_2} E(t, f)D(\theta)\mathrm{d}f\mathrm{d}\theta\right]^{1/2} \\ &= 4\left[\int_{\theta_1}^{\theta_2} D(\theta)\mathrm{d}\theta \int_{f_1}^{f_2} E(t, f)\mathrm{d}f\right]^{1/2} \end{aligned} \tag{5}$$

ACCEPTED MANUSCRIPT

Here, $\delta = d/C_g$ is the time needed by the wave train to travel from location m_0 to location m_P (over a distance d) at the associated average group velocity C_g. Following Eq. (3) and (5), $H_{\mathrm{sw}}(t+\delta, m_{\mathrm{P}})$ can be rewritten as a portion of $H_0(t, m_0)$ as follows:

$$H_{\mathrm{sw}}(t+\delta, m_P) = [K_f\, K_\theta]^{1/2}\, H_0(t, m_0) \tag{6}$$

where K_f and K_θ are the coefficient of reductions due to frequency and directional dispersion, respectively. They can be expressed as:

$$K_f = C \int_{f_1}^{f_2} \tilde{E}(x)\mathrm{d}x \tag{7}$$

$$K_\theta = \int_{\theta_1}^{\theta_2} D(\theta)\mathrm{d}\theta \tag{8}$$

where $\tilde{E}(x)$ denotes the normalized density spectrum, and C is chosen to satisfy:

$$C \int \tilde{E}(x)\mathrm{d}x = 1 \tag{9}$$

with $x = f/f_{peak}$, and f_{peak} being the peak frequency. Considering a JONSWAP spectrum, $\tilde{E}(x)$ has a constant shape described by:

$$\tilde{E}(x) = x^{-5} \exp\left[\frac{5}{4}(1-x^{-4})\right] \gamma^{\exp[-\frac{1}{2}(\frac{x-1}{\sigma})^2]-1} \tag{10}$$

where we consider the average values of $\gamma = 3.3$, $\sigma = 0.07$ for $f \leq f_{peak}$, and $\sigma = 0.09$ otherwise (Holthuijsen, 2007). Since H_0 is assumed to be proportional to G, we have:

$$H_{\mathrm{sw}}(t+\delta, m_P) \propto [K_f\, K_\theta]^{1/2}\, G^0(t, m_0) \tag{11}$$

Superscript ^{0} is used above to denote the original variable (before subtracting the baseline climate). To compute K_f and K_θ we selected 4 frequency and 5 directional bins as detailed in Table 2, assuming $T_{peak} = 1/f_{peak} = 10$ s (representative T_{peak} of stormy conditions, which have a greater contribution to swell). Frequency limits are chosen to cover typical periods of swell in this area, which are 7–12 s (Sánchez-Arcilla et al., 2008). Note that due to the simplification of the statistical method and the resolution of the H_s grid, it does not make sense to consider smaller bins. In other words, it is meaningless to consider two frequency bins whose associated times to propagate typical fetches through the study area differ by less than 3 h (the temporal resolution of H_s data).

Therefore, at point m_P and time t, the total swell wave height H_{sw}^c is the combined contribution of $n_f = 4$ frequency bins of different swell wave trains coming from different locations m_0^l ($l = 1, 2, ..., n_0$, where n_0 is the total number of grid points of influence) generated at time $t - \delta^{k,l}$, where $k = 1, ..., n_f$. Thus,

ACCEPTED MANUSCRIPT

Table 2: Frequency and directional bins and their associated coefficients of reduction

a. Frequency bin (x)	K_f	b. Directional bin (θ)	K_θ
(0.72, 0.83)	0.04	(-90°, -54°)	0.05
(0.83, 1)	0.29	(-54°, -18°)	0.26
(1, 1.25)	0.40	(-18°, 18°)	0.38
(1.25, 1.67)	0.17	(18°, 54°)	0.26
		(54°, 90°)	0.05

$$H^c_{sw}(t, m_P) \propto \sum_{l=1}^{n_0} \sum_{k=1}^{n_f} \sqrt{K_f^k \, K_\theta^{k,l}} \, G^0(t - \delta^{k,l}, m_0^l). \tag{12}$$

Note that $\delta^{k,l}$ is influenced by the distance between each pair of points and the group velocity C_g of the wave train associated with the k^{th} frequency bin. Therefore, the coefficient of reduction due to directional dispersion $K_\theta^{k,l}$ depends on both the indices l and k because θ is determined by the difference between the angle formed by the line between points m_0^l and m_P and the direction of wind, i.e. the direction of the SLP gradient, at time $(t - \delta^{k,l})$ and point m_0^l.

The gist of this approach is to find the n_0 points of influence. This depends on the topography (land or sea) of the region, and on the direction of surface winds (which varies with time). Therefore, in a general case, any point could depend almost on any other point in the domain as a function of the atmospheric forcing driver at a certain time before. To simplify the problem, the following method is proposed to find the points of influence.

First, we use principal component analysis to obtain the first N leading PCs of the squared SLP gradient (G) fields, namely, a small number of important subspaces that contain most of the dynamics of the SLP gradient fields (von Storch and Zwiers, 2002). In order to retain the information of wind direction, which plays an important role in the propagation of swell waves, we first decompose G^0 into $G^0_x = G^0 \cos\theta_w$ and $G^0_y = G^0 \sin\theta_w$, where θ_w is the direction of the SLP gradient (i.e. geostrophic wind). Then, we form the T-by-$2M$ matrix $\mathbf{G}_{xy} = [\mathbf{G}_x, \mathbf{G}_y]$, with G_x and G_y being the anomalies of G^0_x and G^0_y, respectively. We decompose $\mathbf{G}_{xy}$ into PCs and empirical orthogonal functions (EOFs). The ith leading PC, $\mathrm{PC}_i(t)$, represents the temporal evolution (over time period $t = 1, 2, ..., T$) of the ith spatial pattern, $\mathrm{EOF}_i(j)$ ($i = 1, 2, ..., \min\{T, 2M\}$; here $T > 2M$, thus, $i = 1, 2, ..., 2M$). Each of the EOFs here is a vector of length $2M$, with the first half ($j = 1, 2, ..., M$) describing the spatial pattern of G_x (i.e., the U component of wind over locations $m = 1, 2, ..., M$), and the second half ($j = M + 1, M + 2, ..., 2M$), the pattern of G_y (i.e., V component of wind over locations $m = 1, 2, ..., M$). The product of $\mathrm{PC}_i(t)$ and $\mathrm{EOF}_i(j)$ is the i-th leading component of $\mathbf{G}_{xy}$, denoted as $\mathbf{G}_{xy,i}$. Then,

ACCEPTED MANUSCRIPT

$$\mathbf{G}_{xy} = \sum_{i=1}^{2M} \mathbf{G}_{xy,i}. \tag{13}$$

Note that the directions of the gradient associated with each EOF are "constant" while its magnitude varies over time. We write "constant" in quotes because depending on the phase of each pattern, the direction may vary 180°, with the waves generated for each case being in completely opposite directions and affecting a different part of the domain. To account for this variation, we further divide the PC_i into their positive and negative phases:

$$\mathrm{PC}_i^+ = \begin{cases} \mathrm{PC}_i & \text{if } \mathrm{PC}_i > 0 \\ 0 & \text{otherwise} \end{cases}$$
$$\mathrm{PC}_i^- = \begin{cases} \mathrm{PC}_i & \text{if } \mathrm{PC}_i < 0 \\ 0 & \text{otherwise} \end{cases} \tag{14}$$

Secondly, for each chosen leading pattern EOF_i ($i = 1, 2, ..., N$, with $N < 2M$) and each phase, we calculate the set of n_0 points of influence from which swell waves may arrive to a certain point m_P. As described in Eq. (4), waves can be generated and propagated within a sector ±90° around the wind direction. Specifically, for each target point m_P, a point m is considered as one of influence (m_0) if the imaginary straight line between points m_P and m is within the sector comprising ±90° around the direction defined by $\mathbf{G}_{xy,i}$ at point m and does not cross any coastline (i.e., it is not interfered by any land obstacle). To account for refraction effects that would make those waves travelling near coast turning towards it, a certain angle tolerance level (5°) is used so that wave trains that travel very close to the coast are not accounted for. Obviously, this method simplifies the real world situation, in which wave direction can be further modified by local phenomena like diffraction.

Different from Wang et al. (2012), we do not include the leading PCs of SLP anomalies in this study; and we include the leading PCs of $\mathbf{G}_{xy}$ in a different way, namely in the term Δ_{sw}, to account for swell wave trains, which is detailed below in this section.

Figure 4 shows an example of the n_0 selected points of influence for a wave grid point m and for the first leading pattern EOF_1, which explains 36% of the variability in $\mathbf{G}_{xy}$ and can be associated with a typical Mistral event (see Section 2.1).

With the above decomposition procedures, the term $\Delta_{\mathrm{sw}}(t, m)$ in Eq. (2) can be approximated by

ACCEPTED MANUSCRIPT

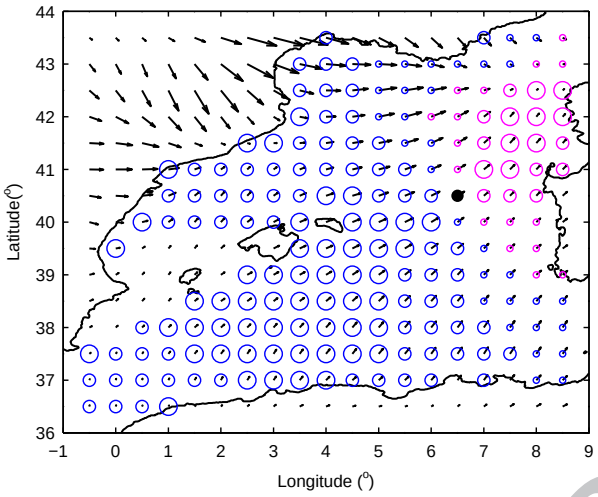

Figure 4: Example of the n_0 points of influence (circles) selected for the target wave grid point m_P (black dot). The blue (purple) circles correspond to the positive (negative) phase of the first atmospheric pattern EOF_1. Arrows illustrate the corresponding gradient direction associated to the positive phase of EOF_1 (i.e. when $PC_1 > 0$). The circle size denotes the directional dispersion associated to each point m_0, making use of the $n_\theta = 5$ directional bins but joining those with the same absolute value as follows: large circles ($|\theta|$ =0°–18°), medium circles ($|\theta|$ =18°–54°)) and small circles ($|\theta|$ =54°–90°) (see Table 2b)

$$\Delta_{\mathrm{sw}}(t,m) = \sum_{i=1}^{N} \hat{a}^{+,i}_{\mathrm{EOF}}(m) \underbrace{\sum_{l=1}^{n_0^i} \sum_{k=1}^{n_f} \sqrt{K_f^k \, K_\theta^{l,i}} \, \mathrm{PC}_i^+(t-\delta^{k,l}) G_{\mathrm{EOF}i}(m_0^l)}_{[*]} + \\ + \sum_{i=1}^{N} \hat{a}^{-,i}_{\mathrm{EOF}}(m) \underbrace{\sum_{l=1}^{n_0^i} \sum_{k=1}^{n_f} \sqrt{K_f^k \, K_\theta^{l,i}} \, \mathrm{PC}_i^-(t-\delta^{k,l}) G_{\mathrm{EOF}i}(m_0^l)}_{[*]}, \quad (15)$$

where $G_{\mathrm{EOF}i}$, the gradient field associated with the pattern $\mathrm{EOF_i}$, is defined as:

$$G_{\mathrm{EOF}i}(m) = \sqrt{\mathrm{EOF_i}^2(m) + \mathrm{EOF_i}^2(m+M)} \quad (16)$$

where $m = 1, 2, ..., M$. For each t, m and i, the term $[*]$ above is a known value. Therefore, we only need to estimate the $2N$ coefficients, $\hat{a}^+_{\mathrm{EOF}}(m,i)$ and $\hat{a}^-_{\mathrm{EOF}}(m,i)$, along with coefficients $\hat{a}$, $\hat{a}_P$ and $\hat{a}_G$ in Eq. (2), through multivariate linear regression analysis.

We consider the first 30 leading PCs ($N = 30$) as potential predictors to be included in the term Δ_{sw}. As in Wang et al. (2012), we also use the F test to determine the optimal set of predictors for each wave grid point m. Only the potential predictors that significantly (at

ACCEPTED MANUSCRIPT

5% level) reduce the sum of square error (SSE) of the regression fit are chosen and included. The F test is implemented in both forward and backward iteration modes, considering all the possible combinations. At each iteration, one predictor is added/subtracted and we compare the SSE of the larger model, SSE_l, with SSE of the smaller one, SSE_s (they just differ by one predictor), using the following F statistic:

$$F = \frac{\mathrm{SSE}_s - \mathrm{SSE}_l}{\mathrm{SSE}_l/(L_{\mathrm{eq}} - k_p)} \tag{17}$$

where k_p is the number of free parameters in the larger model, and the effective sample size (von Storch and Zwiers, 2002) L_{eq} is defined as

$$L_{\mathrm{eq}} = \frac{L}{1 + 2\sum_{j=1}^{J-1}\left(1 - \frac{j}{L}\right)\rho(j)} \tag{18}$$

with $\rho(j)$ being the j-order autocorrelation of the larger model residual series $\varepsilon = H_s - \hat{H}_s$, and L being the sample size. Here, J is chosen so that only $\rho(j) > 0.1$ are accounted for in the estimation of L_{eq}.

4.3. Inclusion of lagged dependent variable

Ocean wave generation is not an instantaneous process. Even if having a constant blowing wind, H_s gradually increases over a certain period of time until a fully developed wave field is formed. In a real case, in which wind speed constantly varies in magnitude and direction, a fully developed wave field is not always achieved. Therefore, in general, H_s depends on both the wind condition and the previous sea state. This explains why H_s is a highly autocorrelated variable, especially when the time step of the data is small like in the present study (3h). In this study, we only consider lag-1 dependent variable $H_s(t-1, m)$, which is different from Wang et al. (2012), but is in agreement with the wave action density balance governing equation and is found to be sufficient for the study area. That is,

$$\Delta_t(t, m) = \hat{\alpha}^{r^*}(m)\, \hat{H}_s^{r^*-1}(t-1, m). \tag{19}$$

Here, $\hat{\alpha}$ is estimated (after the set of predictors is selected for the target point m; see Section 4.2) using an iterative procedure with r^* iterations. At the start of the iteration ($r = 0$), $\Delta_t = 0$; and for $r > 0$,

$$\begin{aligned} \hat{H}_s^r(t, m) = {} & \hat{a}^r(m) + \hat{a}_P^r(m)\, P(t, m_s) + \hat{a}_G^r(m)\, G(t, m_s) \\ & + \Delta_{\mathrm{sw}}^r(t, m) + \hat{\alpha}^r(m)\, \hat{H}_s^{r-1}(t-1, m). \end{aligned} \tag{20}$$

We conduct 20 iterations, which we find is usually enough to reach convergence. The iteration with the lowest root mean square error (RMSE) is chosen and denoted as $\hat{H}_s^{r^*}$. Typically, r^* is around 4. $H_s(t = 0, m) = 0$ is assumed when applying Eq. (19) to simulate H_s.

ACCEPTED MANUSCRIPT

4.4. Data scale

One important assumption in regression analysis is that the residuals ($\varepsilon(t) = H_s(t) - \hat{H}_s(t)$ in this case) are Gaussian distributed. This assumption is violated here, because in theory $H_s(t)$ are non-negative data, which are obviously non-Gaussian. The consequences of such violation could tender the model performance, even resulting in nonsense values such as $\hat{H}_s < 0$.

To evaluate the effects of violation of the Gaussian assumption on the model performance, and to improve the model performance, we explore two options for transforming the positive data (actually, both G and H_s are all positive values): i) the log transformation (noted as $\mathrm{tr}^{\ln}$ in Table 4), which has been used by others (e.g. Casas-Prat and Sierra, 2010a; Ortego et al., 2012); and ii) the Box-Cox power transformation (noted as $\mathrm{tr}^{\mathrm{bc}}$ in Table 4 and Eq. (21) (Sakia, 1992), which also includes the log transformation as a special case (the case of $\lambda = 0$) and has recently been applied by Wang et al. (2012):

$$\mathrm{tr}^{\mathrm{bc}}(X) = \begin{cases} \ln(X) & \text{if } \lambda = 0 \\ (X^{\lambda} - 1)/\lambda & \text{otherwise} \end{cases} \tag{21}$$

where X denotes a variable of positive values. The parameter λ is chosen so that the departure of X from a Gaussian distribution is minimized.

As detailed in Table 4 (settings 6-8), we apply these transformations to the predictand (H_s) alone, and to both H_s and the non-Gaussian predictor G (before calculating the anomalies and deriving the principal components, but after calculating the direction of the SLP gradient). The resulting model performance is compared later in Section 5.

4.5. Model calibration and performance measures

The statistical model is calibrated and validated with HIPOCAS data (1958–2001) (see Section 3.1), which is split into two non-overlapping subsets: 1971-2000 for model calibration, and 1958-1970 for evaluation of model performance.

We use the HIPOCAS data for the period 1971-2000 (calibration period) to calibrate the statistical model, namely, to estimate the unknown parameters in Eq. (2), including $\hat{a}$, $\hat{a}_P$, $\hat{a}_G$, $\hat{a}^{+,i}_{\mathrm{EOF}}$, $\hat{a}^{-,i}_{\mathrm{EOF}}$ and $\hat{\alpha}^{it^*}$ (see Eqs. (2), (15) and (19) and Figure 5). This 30-year period is also chosen as the baseline period to derive the climate model simulated baseline climate for use to infer projected future changes in H_s (see Section 3.2).

Then, we use the HIPOCAS data for the period 1958-1970 (validation period) to evaluate the performance of the above calibrated statistical model. The validation considers the following three aspects: i) overall model performance, ii) model skill for a range of different quantiles of wave heights, and iii) model errors in modeling waves along the Catalan coast. Note that all anomalies in this study are relative to the climatological mean field of the baseline period (1971-2000).

Firstly, as an overall measure of model performance, we calculate the classical correlation coefficient (r) between the HIPOCAS and statistically predicted H_s (H_s and $\hat{H}_s$ respectively) at each wave grid points, obtaining a map that shows the spatial distribution of the model performance (see Section 5).

ACCEPTED MANUSCRIPT

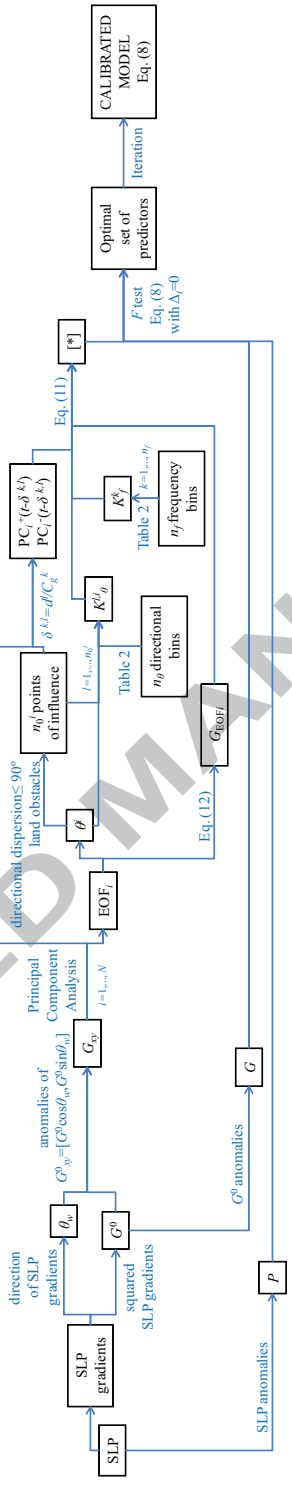

Figure 5: Model calibration flowchart

ACCEPTED MANUSCRIPT

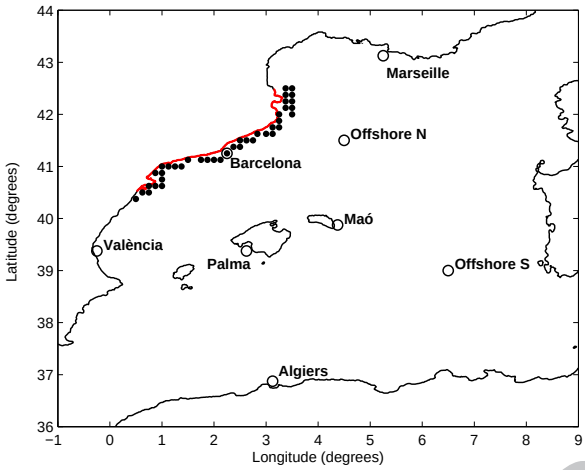

Figure 6: Main locations used to validate the model. Circles: selected nodes to compare PSS and FBI. Dots: nodes near the Catalan coast

Table 3: Contingency Table used to calculate PSS and FBI indices (H_s: observed H_s, $\hat{H}_s$: predicted H_s). Adapted from Lin and Wang (2011)

	$H_s \geq H_{s,q}$	$H_s \leq H_{s,q}$
$\hat{H}_s \geq H_{s,q}$	a (hits)	b (false alarms)
$\hat{H}_s < H_{s,q}$	c (misses)	d (correct negatives)

As in Lin and Wang (2011), the model skill is also measured by the Pierce skill score (PSS) and the frequency bias index (FBI):

$$\mathrm{PSS}\,(q) = \frac{a}{a+c} - \frac{b}{b+d}, \tag{22}$$

$$\mathrm{FBI}\,(q) = \frac{a+b}{a+c}, \tag{23}$$

where $q = [0.1, 0.2, 0.8, 0.9, 0.95, 0.975, 0.99]$ are the quantiles of H_s for which the model prediction skill is evaluated, and a, b, c, and d are as defined in Table 3, with $a+b+c+d = L$. A higher PSS value indicates a higher model skill. For a perfect model, $c = b = 0$ and PSS$= 1$ (the maximum PSS value). FBI measures the model bias. For an unbiased model, FBI$= 1$. So, the closer the FBI is to unity, the less biased the model is. An FBI value that is greater (smaller) than unity indicates overestimation (underestimation) by the model.

The PSS and FBI are calculated for all wave grid points but are only shown and inter-compared for 8 selected locations, including 6 notably populated coastal nodes (Marseille, Barcelona, Maó, Palma, València and Algiers) to represent spatial heterogeneities of the wave climate (also within areas of available high spatial resolution data) and 2 offshore locations (simply referred to as Offshore N and Offshore S; see Figure 6).

ACCEPTED MANUSCRIPT

Table 4: The 8 model settings evaluated in this study(see text for further explanation).

Setting	P	G	PC	$PC^{\pm}$	Δ_{t}	Δ_{sw}	$\mathrm{tr}^{\mathrm{ln}}(H^0)$	$\mathrm{tr}^{\mathrm{ln}}(G^0)$	$\mathrm{tr}^{\mathrm{bc}}(H^0)$	$\mathrm{tr}^{bc}(G^0)$
1	x	x								
2	x	x	x							
3	x	x		x						
4	x	x		x	x					
5	x	x			x	x				
6	x	x			x	x	x			
7	x	x			x	x	x	x		
8	x	x			x	x			x	x

Finally, since this study focuses on the Catalan coast, we also calculate and use the relative error (RE) of $\hat{H}_s$ associated with $q = [0.5, 0.95, 0.99]$ for the 40 near-coast locations (black dots shown in Figure 6) to analyze the behaviour of the model in this near-coast area.

5. Evaluation of the proposed model

We evaluate the 8 model settings detailed in Table 4. These include two groups of settings: Setttings 1-5 compare different combinations of predictors, with Setting 5 being the method proposed and used in this study; whereas Settings 6-8 are for exploring the effect of transforming the data on the model performance.

Setting 1 uses just P and G as potential predictors, corresponding to model (1). Settings 2 and 3, instead of using the term Δ_{sw} developed in this study, involve just the simultaneous PCs (i.e., PCs at time t) of $\mathbf{G}_{xy}$, with and without separating the PCs into their positive and negative phases, respectively, in addition to the local predictors in Eq. (1). Setting 4 adds the temporal dependence of H_s (term Δ_t, see Section 4.3) into Setting 3. Setting 5 corresponds to Eq. (2) and represents the method developed and used in this study. Based on the swell frequency/directional bin decomposition and the selection of points of influence, all associated swell wave trains with their corresponding time lags are considered in the term Δ_{sw} (see Section 4.2) as well as the temporal dependence of H_s in the term Δ_t.

The map of correlation between the HIPOCAS and statistically predicted H_s fields is shown in Figure 7 for Settings 1-5. It can be seen that the correlation skill improves from Setting 1 to Setting 2, and to Setting 5, with Setting 5 having the best skill in terms of correlation.

In general, Setting 5 is also more skillful and less biased than Settings 1-4 for predicting H_s. To illustrate this, the PSS and FBI scores, which serve to measure the model performance as a function of H_s magnitude, are shown in Figures 8 and 9 for the 8 selected locations shown in Figure 6. Setting 5 is more skillful (higher PSS) and less biased than Settings 1-3 for all magnitudes of H_s; it is comparable to Setting 4 for predicting higher waves but it is more skillful than Setting 4 in predicting lower waves (Figs. 8-9). In general, all model settings over-predict smaller waves and under-predict higher waves (Fig. 9).

ACCEPTED MANUSCRIPT

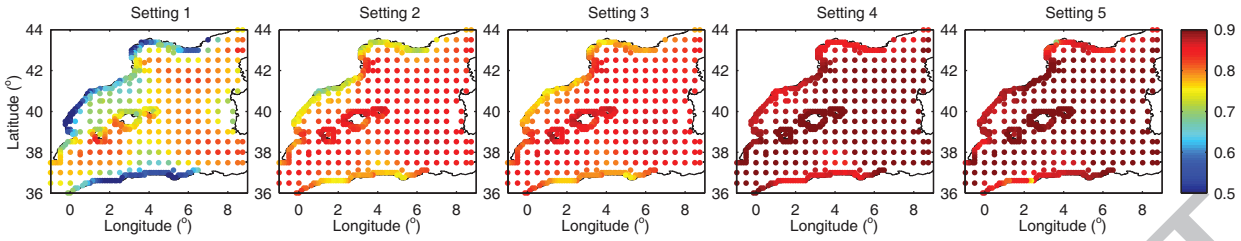

Figure 7: Correlation coefficient of all locations for model Settings 1, 2, 3, 4 and 5

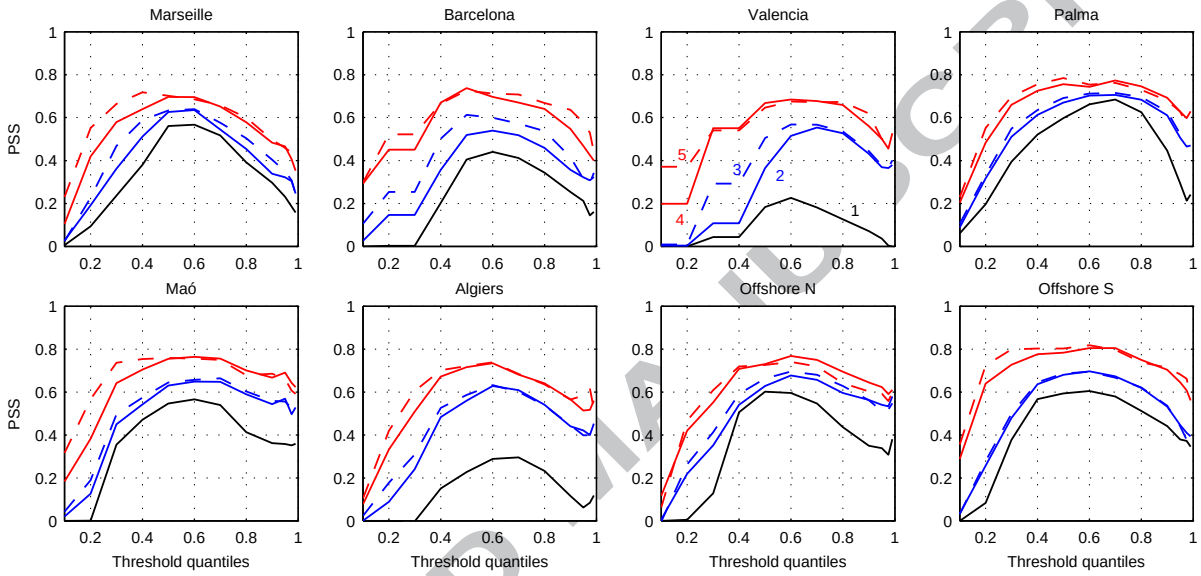

Figure 8: PSS for selected locations (see Figure 6) for model Settings 1 (solid black), 2 (solid blue), 3 (dashed blue), 4 (solid red) and 5 (dashed red).

For grid points along the Catalan coast, Figure 10 shows the relative error, RE, of predicting the 50th, 95th and 99th percentiles of H_s. In general, all model settings tend to moderately over-predict medium waves (up to about 20%) but notably underpredict extreme waves (up to about 38% for the 99th percentiles) except for 99th percentiles for the northern nodes. Nevertheless, Setting 5 nearly always has the smallest relative errors for the near-shore grid points.

Next, we describe the model performance and the differences among the model settings in a little more detail.

The simplest model, Setting 1, which involves only two local predictors P and G (with G being the most important predictor), achieves reasonably good r scores for offshore locations (around 0.8); but it poorly predicts H_s at near-shore locations, with r dropping down to around 0.5. This pattern is also observed in the PSS plots (Figure 8, black curves), showing higher PSS values for the two offshore locations than for near-shore locations (such as Algiers, Barcelona, and Valencia). Along the Catalan coast, the r score is slightly higher in the

ACCEPTED MANUSCRIPT

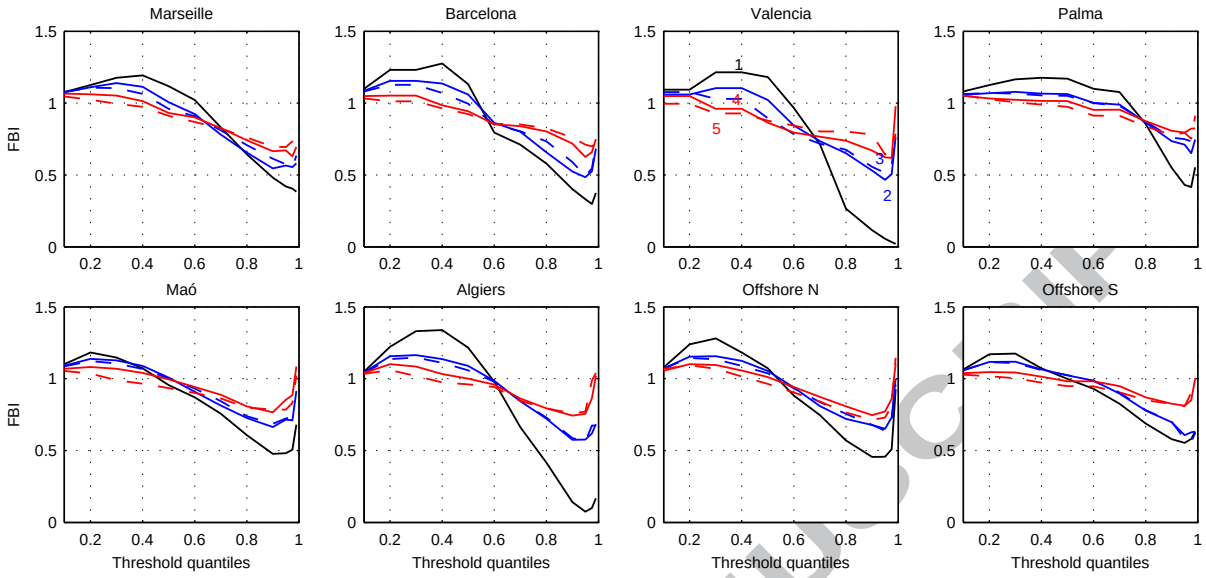

Figure 9: FBI for selected locations(see Figure 6) for model Settings 1 (solid black), 2 (solid blue), 3 (dashed blue), 4 (solid red) and 5 (dashed red).

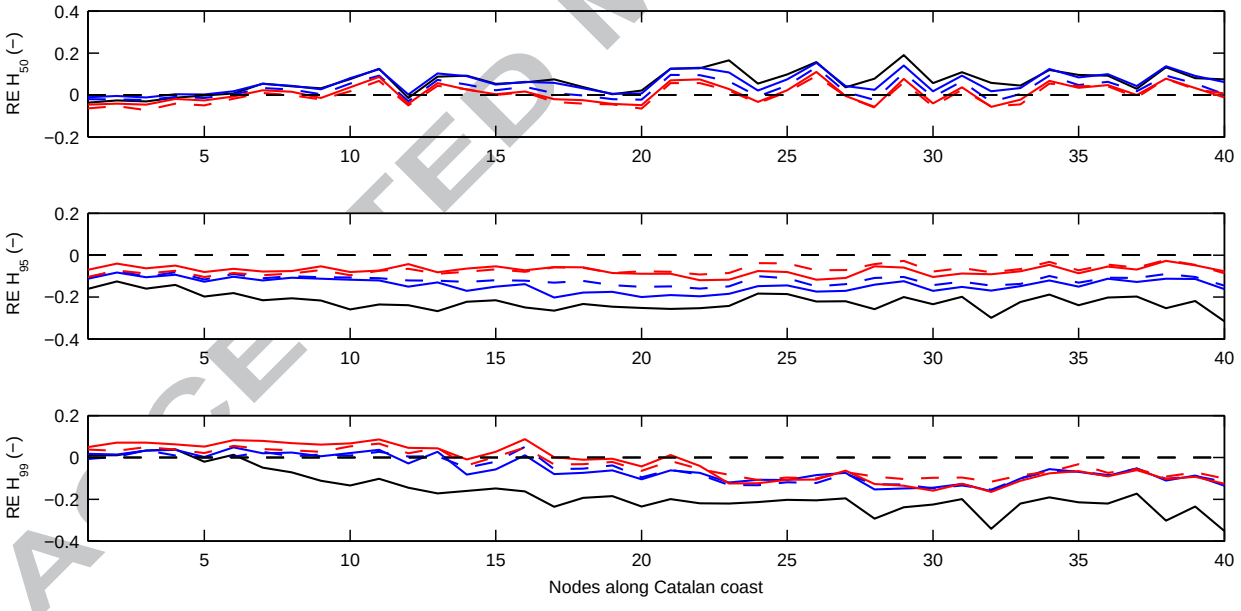

Figure 10: Relative error for nodes along the Catalan coast (numbered from North to South, see Figure 6), for model Settings 1 (solid black), 2 (solid blue), 3 (dashed blue), 4 (solid red) and 5 (dashed red).

ACCEPTED MANUSCRIPT

Northern part, which can be explained by the greater presence of locally generated waves (Casas-Prat and Sierra, 2010b). Differences in RE among the model settings are smaller for the nodes in the most Northern Catalan coast where the r scores are also relatively larger.

With the addition of the 30 leading PCs as potential predictors (Setting 2), the r score largely improves everywhere, especially at the near-shore locations ($r > 0.7$). The better model performance is also reflected in the PSS and FBI scores (Figures 8 and 9, solid blue curves). The absolute value of RE along the Catalan coast is considerably reduced, especially for extreme waves (Fig. 10). These results highlight the importance of the inclusion of predictors that can account for swells, in addition to the local predictors P and G. It is particularly important to account for swell components in predicting H_s near the coast. This is probably due to the fact that the direction of swells is restricted by the coastline orientation.

The separation of positive and negative phases of PCs (Setting 3) further increases the r score everywhere ($r > 0.75$), which emphasizes the (expected) assymmetric contribution to waves at a certain location by different phases of a certain atmospheric pattern. This is also associated with larger PSS values, especially for coastal locations like Barcelona or Valencia (see Figure 8), lower model biases (Fig. 9), and smaller absolute RE values along the Catalan coast. However, the improvement in model performance from Setting 2 to Setting 3 is much smaller than that from Setting 1 to Setting 2, which is reflected in all skill measures.

The next significant improvement is achieved by the inclusion of the lag-1 dependent variable $H_s(t-1)$, i.e., the term Δ_t in Eq. (2), as a predictor to predict $H_s(t)$ (Setting 4). The average r score is now around 0.85, with values around 0.9 being seen at many locations (Fig. 7). This is also associated with greater model skill (larger PSS values) and lower biases (FBI values to closer to unity; see solid red curves in Figures 8 and 9). The average RE (in absolute value) along the Catalan coast is 4.3% for the median H_s, 14% for the 95th percentile, and 16% for the 99th percentile, which is reasonably good in the context of H_s prediction.

Being the most complex model among the firt group of model settings, Setting 5 includes the term Δ_{sw} as defined in Section 4.2 to further improve representation of swell waves. As summarized earlier, Setting 5 performs the best among Settings 1-5, although the improvement over Setting 4 is small in general. In fact, the small difference between the results of Settings 4 and 5 might be explained by the relatively short fetches of the study area and, consequently, the small impact of assuming no time lag δ between the origin of swell waves and their propagation to the point of interest as in Settings 3 and 4. In the open ocean where fetches are considerably larger, the difference might be more remarkable. Along the Catalan coast, the improvement of Setting 5 over Setting 4 is more noticeable. As shown in Figs. 8-9, Setting 5 is more skillful than Setting 4 in predicting smaller waves, although it is comparable to Setting 4 for predicting higher waves. Compared to Setting 4, the average absolute RE decreases by 4%, 55% and 50% for, respectively, the 50th, 90th, and 99th (see the dashed red curves in Figure 10). Thus, we choose to focus on Setting 5 in the subsequent analysis.

The second group of model settings (Settings 6-8) are compared in Figures 11-14. They involve the same set of potential predictors as does Setting 5, but with a transformation

ACCEPTED MANUSCRIPT

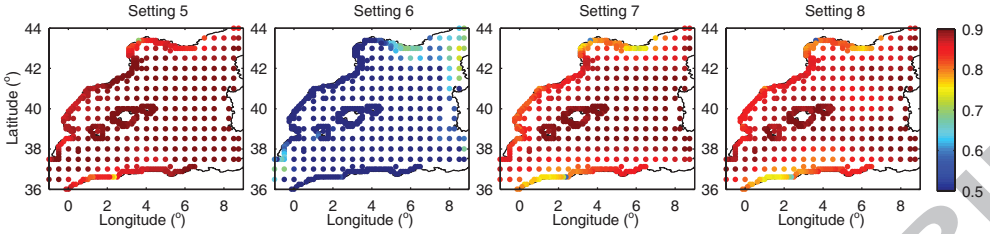

Figure 11: Correlation coefficient of all locations for model Settings 5, 6, 7 and 8

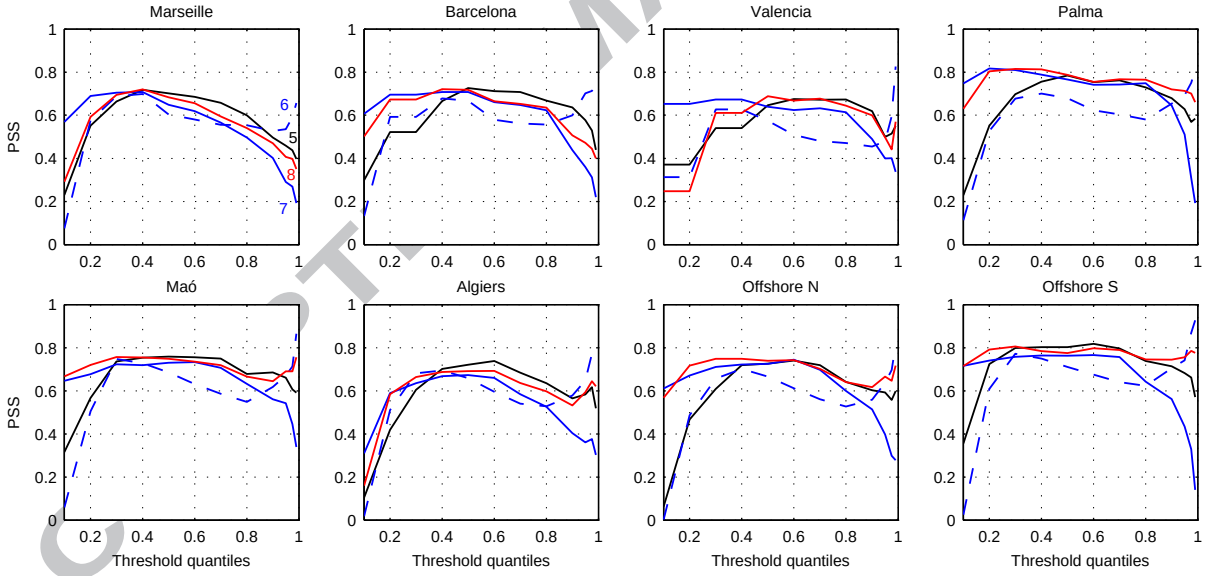

Figure 12: PSS for selected locations (see Figure 6) for model Settings 5 (solid black), 6 (dashed blue), 7 (solid blue) and 8 (solid red).

ACCEPTED MANUSCRIPT

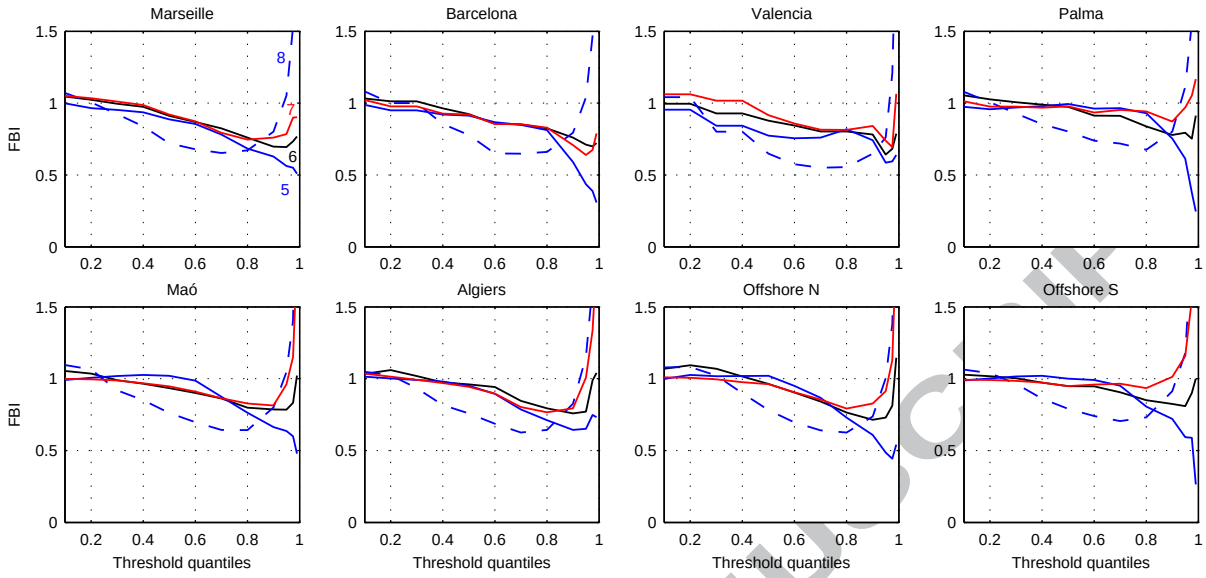

Figure 13: FBI for selected locations (see Figure 6) for model Settings 5 (solid black), 6 (dashed blue), 7 (solid blue) and 8 (solid red).

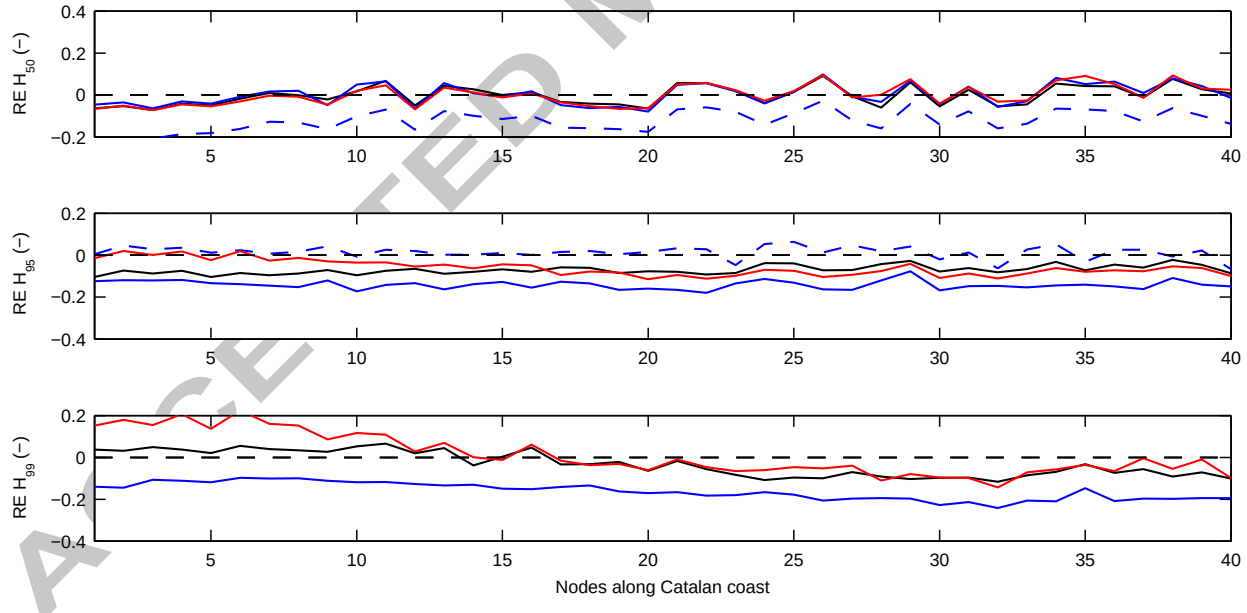

Figure 14: Relative error for nodes close to the Catalan coast, from North—lower values—to South—larger values—(see Figure 6), for model Settings 5 (solid black), 6 (dashed blue), 7 (solid blue) and 8 (solid red).

ACCEPTED MANUSCRIPT

applied to the wave heights H^0 and/or the squared SLP gradients G^0, to explore the effect of transforming the non-negative data on model performance, as explained in Section 4.4. Actually, predictions of wave heights using model Settings 1-5 could be negative (which is unphysical), because the positive characteristic of wave heights was not accounted for in these settings.

In Setting 6, log-transformation is applied only to the predictand, but in Setting 7, it is also applied to the squared SLP gradients before they are used to derive all potential predictors (including the local G and the PCs of G fields). Finally, Setting 8 is similar to Setting 7 but a Box-Cox transformation is applied instead of the log-transformation. Note that any transformation is always applied to the original (positive) variable, before obtaining the corresponding anomalies (see Section 4.1).

In terms of the r score, adding log-transformation to the predictand without applying any transformation to the predictors deteriorates the model performance (see Settings 5 and 6 in Fig. 11). The reason is probably the following. With the log transformation, the additive model (2) turns into a product of exponential terms, which, in the case of any perturbation in the forcing fields and/or estimation error, results in exaggerated and unrealistic $\hat{H}_s$ values. This entails a large over-prediction of extreme H_s as shown in Figure 13 (dashed blue curves). Note that the RE values of the 99th percentile is not shown in Figure 14, because they are greater than 0.4 and fall out of the y-axis limit. On the contrary, medium waves are under-predicted, with negative RE values being associated with median H_s along the Catalan coast (see dashed blue curves in Figs. 13-14). This lower performance might also be related to the loss of proportionality between H_s and squared pressure gradients due to the transformation of H_s.

As shown in Figs. 11-13, applying the log-transformation to both the predictand and the squared SLP gradients (Setting 7) is much better than transforming the predictand alone (Setting 6), but is generally still not as good as without any transformation (Setting 5). However, it is interesting to point out that for low waves (up to the 40th percentile), Setting 7 is better than Setting 5. Note that the main reason for applying a transformation is the non-Gaussianity of the residuals caused by the non-Gaussianity of the variables involved in the model. Such deviation from Normal distribution is more pronounced in the lower quantiles. Positive variables have a relative scale and are lower bounded whereas Gaussian variables are free to range from $-\infty$ to $+\infty$. Therefore, it makes sense to obtain a larger improvement in predicting the lower quantiles.

Finally, replacing the log-transformation with a Box-Cox transformation improves the prediction skill for medium-to-high waves but slightly worsens the skill for low waves (compare Settings 7 and 8 in Fig. 12). For low waves, the PSS curve of Setting 8 (solid red curve in Figure 12) is closer either to Setting 5 or to Setting 7, depending on the location; it is closer to Setting 7 at locations where the λ value is close to zero, but closer to Setting 5 otherwise. The estimate λ value for H_s is 0.29, 0.11, 0.24, 0.16, 0.06, 0.16, 0.07, and 0.11 for Marseille, Barcelona, Valencia, Palma, Maó, Algiers, Offshore N, and Offshore S, respectively, which are within the range of values λ estimated for this region by Wang et al. (2012). At the locations with lower λ values, the PSS of Setting 8 tends to be closer to that of Setting 7, which is reasonable since Box-Cox transformation with $\lambda = 0$ is log trans-

ACCEPTED MANUSCRIPT

formation. In terms of PSS, Setting 8 seems to be the best option for offshore deep water locations, but it is not clearly better for coastal nodes. Setting 8 substantially over-predicts extreme waves, showing larger positive RE values associated with the 99th H_s percentile at the Northern Catalan coast (see Figure 14).

The above results of model performance evaluation suggest that the model Setting 5 is the best option for Catalan coast. Thus, we will use it to make projections of future wave climate in the next section.

6. Future wave climate projections

The calibrated statistical model is then applied to obtain H_s that correspond to each of the 5 simulated SLP datasets described in Section 3.2. To diminish biases in the climate model simulations, the simulated SLP fields, denoted as $P^s(t,m)$, are adjusted as follows:

$$P^a(t,m) = \frac{\sigma^r(m)}{\sigma^s(m)}\left(P^s(t,m) - \overline{P^s}(m)\right) + \overline{P^r}(m), \tag{24}$$

where superscript ^{r} denotes the reference climate (i.e., obtained from the HIPOCAS data in this study), and $\overline{X}$, the climatological mean (over the baseline period 1971-2000) of variable X. The $\sigma^s(m)$ and $\sigma^r(m)$ are the standard deviation field of $P^s(m)$ and $P^r(m)$, respectively. Thus, $P^a(t,m)$ are the simulated SLP fields that have been adjusted to have the observed baseline climate $P^r(m)$ and variation scale $\sigma^r(m)$.

The above adjustments are performed for each of the 5 sets of SLP simulations. These adjusted SLP fields, $P^a(t,m)$, are then used to derive the predictors, including $P(t,m)$, $G(t,m)$, and their PCs and anomalies (see Section 4 for the details). These predictors are then fed into the calibrated statistical model to obtain the corresponding H_s.

To investigate how these adjustments affect the estimated changes in H_s between future and present, and to show the actual model biases and inter-model variability, simulations of H_s without these adjustments are also conducted and compared with those obtained with the adjustments.

Despite the shortcoming of having a few values $\hat{H}_s < 0$, Setting 5 is selected to make H_s projections because it presents the best skill for the Catalan coast area, the focus of this study. Firstly, these projections are carried out with the predictors derived from the unadjusted model data. Their biases are assessed by comparing the projected H_s for the present-day (baseline period) climate with the corresponding value of the HIPOCAS data (see Figure 15). Secondly, the predictors derived from the adjusted model data are also used to obtain the H_s projections, which are then used to assess uncertainty in wave projections.

To explore the mean wave climate, projected changes in the median H_s are estimated. We chose to use a percentile-type parameter to avoid the effects of negative H_s. Regarding the extreme wave climate, we analyze the 50-year return value of H_s, which was computed as in Casas-Prat and Sierra (2013) using a Generalized Pareto Distribution model.

Figures 16 and 17 show the median H_s projected using Setting 5, with the predictors being derived before and after applying the adjustments to the model data, respectively. The upper panels show the present-day climatological values; whereas the lower panels show

ACCEPTED MANUSCRIPT

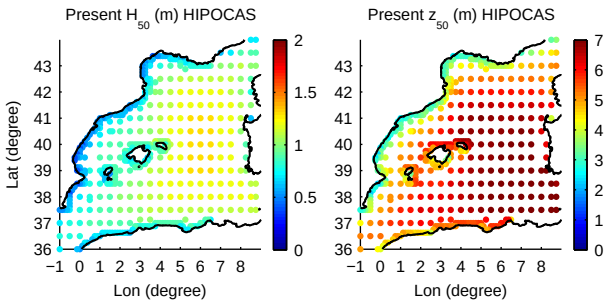

Figure 15: The median (left) and 50-year return value (right) of H_s obtained from HIPOCAS data for the present (baseline) period.

the projected changes in future climates that are expressed as a portion of the present-day climatological value. Each column corresponds to one of the five sets of model simulations (see Section 3.2).

As shown in Figure 16, HIR_E model has a clear positive bias (overestimation of projected H_s). The other models show more similar present-day wave climates, which have much smaller positive biases. When forced by the same GCM ECHAM5, all four RCMs (HIR_E, RAC_E, REM_E, RCA_E) project future changes that share a common tendency for H_s to increase in the NE part of the domain (up to 10%). An increase is projected for the area near the Gulf of Genoa, suggesting an increase in future cyclone activity in this important cyclogenesis area in the Mediterranean (see Section 2.1). This is consistent with the projected increase in mean gust of gust event days in winter (October-March) reported by Schwierz et al. (2010), who analyzed CHRM (a RCM) simulations with the ECHAM5 and HadCM3/HadAM3 lateral boundary conditions. In the SW part of the domain, H_s tends to decrease (up to 10%) but the extent of decrease varies between RCMs. HIR_E projects a more pronounced decrease; whereas the REM_E and RCA_E models project much more limited decreases. Similar patterns of projected mean wave climate were obtained by Casas-Prat and Sierra (2013) using dynamical downscaling. However, they simulated the area of increase (in the NE part of the domain) closer to the Catalan coast.

On the other hand, RCA_H (which is forced by the HadCM3Q3 global model) projects a general decrease of H_s (up to 10%) over the entire domain (especially in the SE part). Close to the east-facing coasts, H_s reduction is smaller and in some stretches it tends to remain the same or even to slightly increase. This spatial pattern of change is in agreement with what is projected by global models as presented in the study of Donat et al. (2010) and by the regional dynamical downscaling of Casas-Prat and Sierra (2013). Donat et al. (2010) found an increase of E flow for a model similar to HadCM3Q3 but a tendency of the increased W flow for those forced by the ECHAM5 global model. The existing differences between the two global atmospheric models in the E-W flow patterns translate into the H_s field, especially for those coastline stretches (such as the Catalan coast) where the fetch limitation related to this direction is relevant.

After the simulated SLP data being adjusted to have the observed baseline climate and

ACCEPTED MANUSCRIPT

variation scale, the bias for the present-day median H_s (see Figure 17) almost disappears completely, as would be expected. The adjustments also affect the projected changes in H_s; they attenuate the projected relative changes in general (especially for models driven by ECHAM5), although the pattern of change is maintained. It is not possible to know which projected changes are more reliable, because any type of statistical adjustments has its own limitations. In particular, such adjustments cannot account for any feedback (e.g., how changes in ocean waves may affect changes in SLP) that may exist in the real world.

Similarly, Figures 18 and 19 show the present-day climate and projected changes of the 50-year return value of H_s (z_{50}). The model bias patterns (compare upper panels of Fig. 18 with right panel of Fig. 15) are similar to those for the median H_s, showing in general significant HIR_E overestimation and moderate or low overestimation by the other models. The projected future changes (Fig. 18, lower panels) vary more between models than for the median H_s, as similarly found by Casas-Prat and Sierra (2013). These results are reasonable because extreme values are normally exposed to a larger uncertainty. Along the Catalan coast, there is a general tendency for z_{50} to decrease or remain constant, except in the northern coast where models RCA_E and HIR_E project an increase. The maximum rate of change is around $\pm 20\%$ (larger than for the median H_s) which in agreement with the non-linear relation between H_s and wind for wind-sea states, typically present in stormy conditions, as pointed out by Casas-Prat and Sierra (2013). Very similar spatial patterns and magnitudes of change were obtained by Casas-Prat and Sierra (2013) for the models REM_E and RCA_E. On the contrary, the projected change that they obtained for RCA_H differed from the present study, obtaining a notable increase of z_{50} along almost all E-facing coasts.

The adjustments to the simulated SLP data reduce the current z_{50} but not necessarily the model bias. For example, among the five sets of RCM-GCM simulations, HIR_E has the largest positive bias before the adjustments, but it has a negative bias after the adjustments.

As for the median H_s, after applying the adjustments (Fig. 19), the magnitude of change in the z_{50} is slightly reduced, but to much lesser extent than for the median H_s. Indeed, the projected changes of z_{50} are barely the same (compare Figs. 18 and 19).

7. Summary and discussion

This study proposes a statistical method to model near-shore H_s, at a 3 h and 25 km resolution. This high spatial-temporal resolution is suitable for coastal impact analysis although a complete assessment would have to involve additional wave parameters, such as wave direction (Reguero et al., 2011).

A multivariate regression model is used to represent the relationship between the predictand, H_s, and SLP-derived predictors. The local SLP gradient and its squared value (a proxy of the geostrophic wind energy) are used to account for the local wave generation. This study illustrates that the local predictors (P and G) alone (Setting 1), as used in Wang et al. (2010), are not sufficient to properly model H_s in near shore areas where the coastline orientation seems to enhance the role of swell waves. Similar to the findings by Wang et al. (2012), a large improvement is achieved in this study by adding the leading PCs of

ACCEPTED MANUSCRIPT

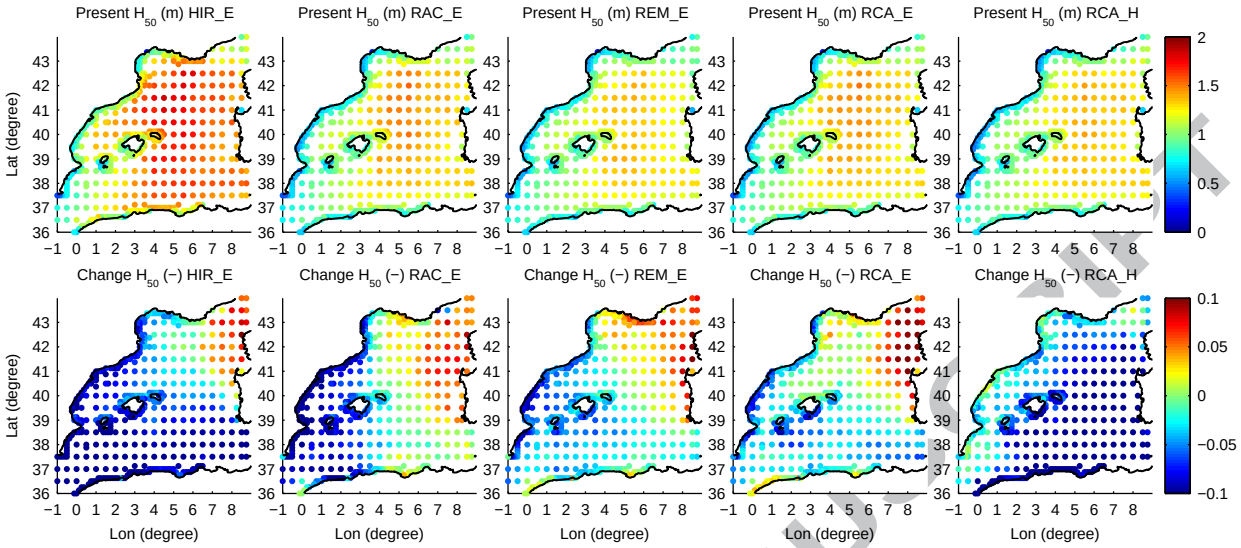

Figure 16: The present-day climate (upper panels) and future relative change (lower panels) of the median H_s obtained using Setting 5 without any adjustment to the simulated SLP data.

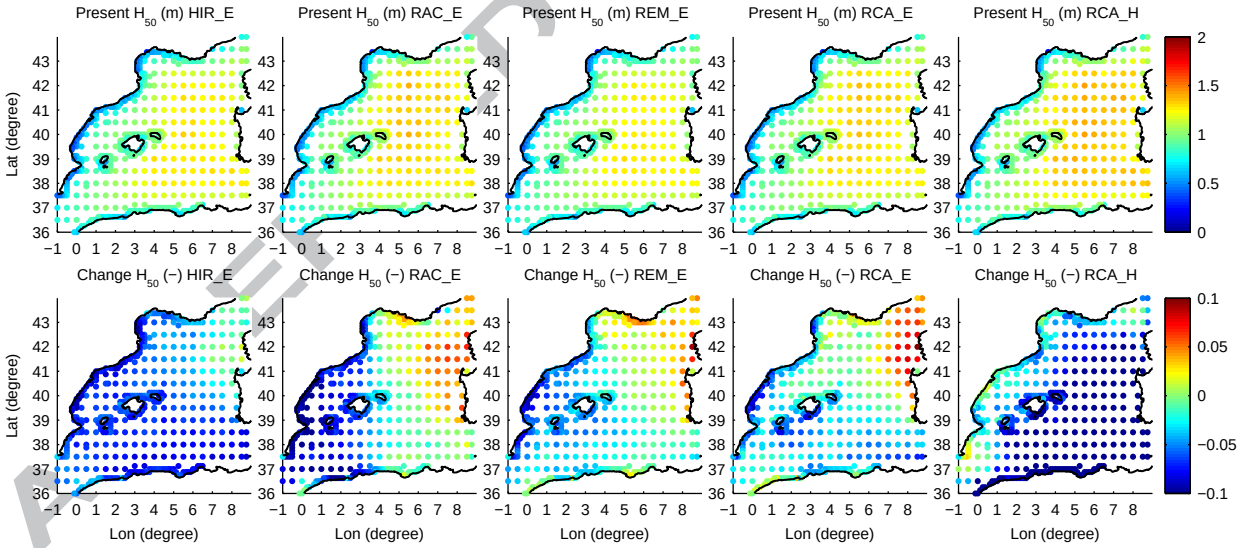

Figure 17: Same as Figure 16 but with the simulated SLP data being adjusted to the observed baseline climate and variation scale.

ACCEPTED MANUSCRIPT

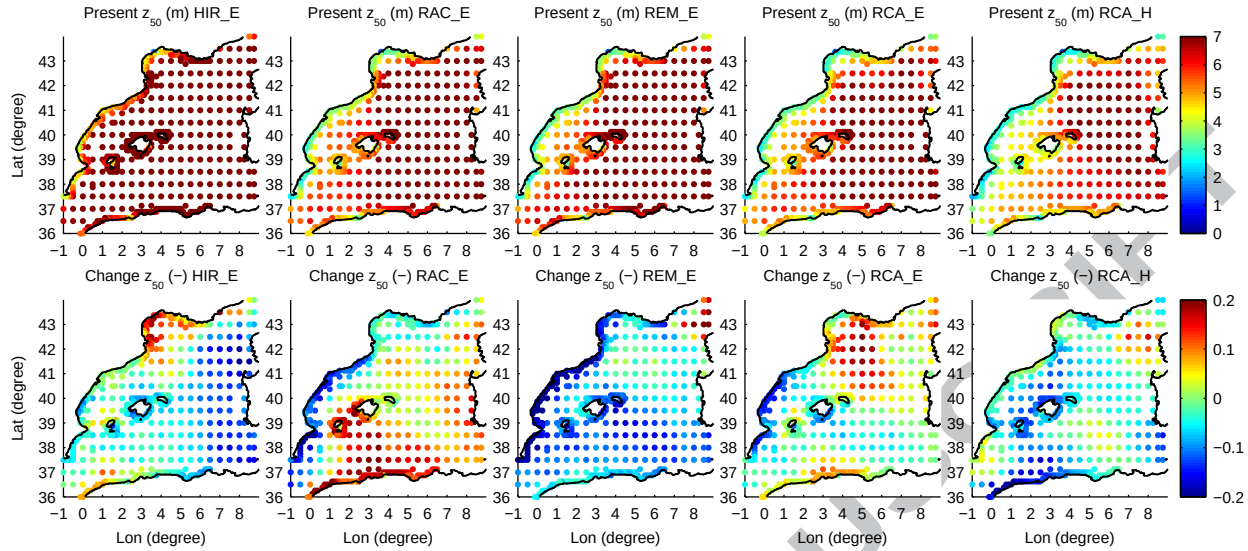

Figure 18: The present-day climate (upper panels) and future relative changes (lower panels) of the 50-year return value of H_s obtained using Setting 5 without any adjustment to the simulated SLP data.

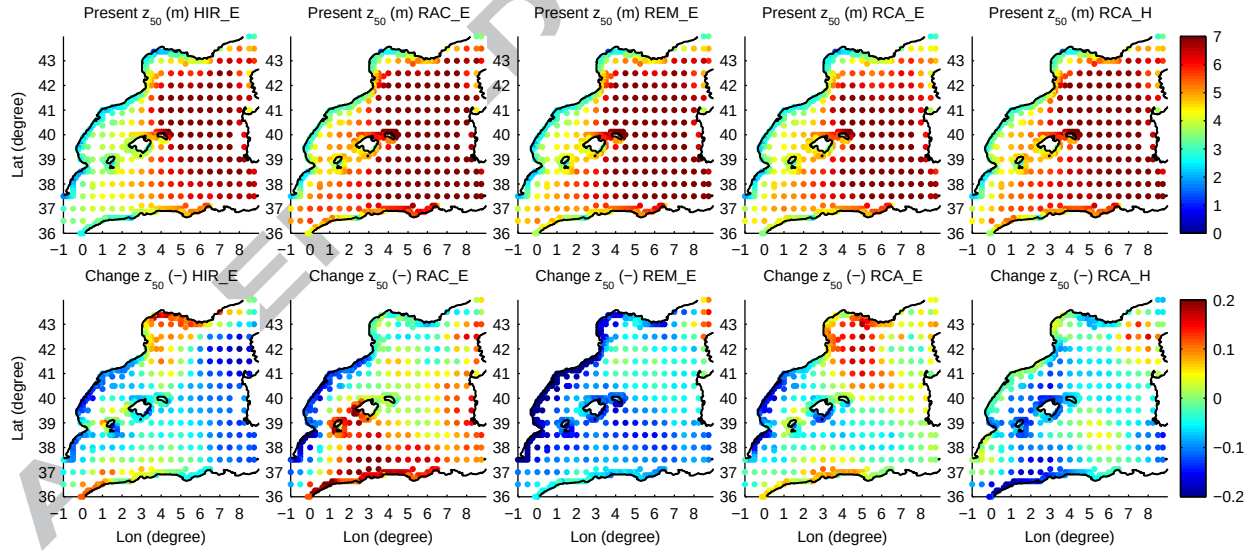

Figure 19: Same as Figure 18 but with the simulated SLP data being adjusted to the observed baseline climate and variation scale.

ACCEPTED MANUSCRIPT

SLP gradient fields (in this study including magnitudes and directions) to account for swell waves (Settings 2 and 3) and adding the lagged H_s to account for the temporal dependence (Setting 4).

Since this study aims to improve the performance in modeling H_s in the near shore areas, where good representation of the swell component is particularly important, special focus has been given to the swell term. The proposed method (Setting 5) uses the PCs derived from the squared SLP gradient vectors (including magnitudes and directions). By retaining the geostrophic wind direction information and separating between its positive and negative phase, this approach enables the detection of swell wave trains affecting each wave grid location. The time lag between the wave generation area and the propagated swell at the point of interest is also considered. Based on the directional/frequency dispersion of waves, each swell train is finally weighted as a function of the considered frequency bin and the deviation of the swell wave train propagation from the forcing wind direction at the origin. Results show that, in the study area (especially in the near shore areas), the model performs better with this swell representation approach. The improvement is not very pronounced though, which might be attributable to the short fetches of the study area. More pronounced improvement can be expected if this method is used to model H_s in near shore areas with larger fetches (and therefore swell waves travelling longer distances). Meanwhile, the proposed PCs sign decomposition and swell train detection approach could be adapted to model wave direction together with H_s in a future study.

To overcome the problem of having non-Gaussian (non-negative) variables (whereas linear regression assumes normal residuals), we have tried a couple of methods to transform the non-negative predictors. The results show that transformation of the predictand (H_s) alone (Setting 6) worsens the model skill, because it distorts the relationship between H_s and the squared SLP gradient fields (as discussed in the Auxiliary Material of Wang et al., 2012). The log-transformation (Setting 7) improves the results for low-to-medium waves, and the Box-Cox transformation (Setting 8), for medium-to-high waves, especially at offshore locations.

The proposed method models H_s in the study area reasonably well and thus is suitable to project future wave climate in this area. Thanks to the low computationally cost, it can be used to explore the uncertainty associated with several factors such as atmospheric models, greenhouse scenarios, and internal variability. In addition, since the method is based on general (deep water) wave physics, it can also be tuned and applied to other areas, even to coastal regions bounded by large oceans. In the latter case, just a slight increase in the computational cost is expected in the first step of model calibration, which would not affect the model performance and applicability to project the associated future wave scenarios.

In this study, we have explored the inter-model variability and bias using five sets of RCM projections of the atmosphere (Table 1), which has been also investigated in the recent dynamical downscaling study of Casas-Prat and Sierra (2013). We have also explored how a bias adjustment can affect the projections. In general, the same pattern of change (between present-day and future projections) is found but the projected changes are slightly attenuated when the simulated SLP data are adjusted to have the reference (HIPOCAS) climate and variation scale. In this study, the adjustment is based on the mean climate but

ACCEPTED MANUSCRIPT

it would be interesting to see how other approaches (e.g. quantile-macthing adjustments) might affect the future projections.

The two GCMs seem to project two different patterns of wave climate change, which is also reported by Casas-Prat and Sierra (2013) and might be related to the differences in the W-E flow generated by each GCM as pointed out in the study of Donat et al. (2010). Moreover, these atmospheric differences are accentuated in the wave climate because of the fetch configuration. Projections forced by ECHAM5 show a general decrease of the median H_s, except for the Genoa area (NE corner) where H_s tends to increase (up to 10%). Projections derived by HadCM3Q3 show a larger decrease of the median H_s offshore, with a slight increase in some east-facing coastline stretches. Using dynamical downscaling, Casas-Prat and Sierra (2013) obtained similar patterns of change but with the area of H_s increase in the four sets of ECHAM5-driven projections (Table 1) being closer to the Catalan coast.

As similarly found by Casas-Prat and Sierra (2013), our results indicate that, for the studied winter season, the variability caused by using different RCM's is much lower than the one caused by the different GCM's. However, differences among RCM's become larger for the z_{50}, showing sometimes contrasting patterns of future changes (e.g. increase/decrease in z_{50} at the Northern Catalan coast) (This is also seen in the results of Casas-Prat and Sierra (2013)). Differences between projections obtained in this statistical downscaling study and those of dynamical downscaling study of Casas-Prat and Sierra (2013) become larger when looking at the extremes, as would be expected, but still seems to be lower than the inter-model variability.

The statistical model developed in this study can be applied to climate model simulations of the atmosphere to simulate historical wave climate. The resulting historical wave climate can then be compared with an observation or reanalysis dataset, to assess the collective skill of the statistical model and the related climate model in representing historical wave climate. The statistical model can also be applied to projections of the atmosphere by multiple climate models for multiple emission scenarios. The results can be analyzed to comprehensively quantify inter-model and inter-scenario uncertainties. With the emerging of high resolution projections of the atmosphere by high resolution climate models (such as CMIP5 simulations), it would be also interesting to see if the RCM downscaling step is still necessary in this case. These are interesting topics for future research.

Acknowledgments

This research was carried out within the frame of the Ph.D program of the first author during her visiting research stay in Climate Research Division of Environment Canada, which was funded by the *Ministerio de Educación* (Spanish Ministry of Education). The first author also acknowledges the support received by the *Col·legi d'Enginyers de Camins, Canals i Ports* (Civil Engineering Association in Catalonia).

The authors are grateful to the *Organismo Público Puertos del Estado* (Spanish Ports and Harbors Authority) for providing HIPOCAS (wave and atmospheric) data that served to calibrate and validate the statistical model.

ACCEPTED MANUSCRIPT

We also gratefully acknowledge the research centers and institutions that have freely and disinterestedly provided us with the atmospheric climate projections datasets used in this study to project the future wave climate: *Danmarks Meteorologiske Institut*(DMI, Denmark) — special thanks to Ole B. Christensen, Neil Mackellar and Fredrik Boberg; *Koninklijk Nederlands Meteorologisch Instituut* (KNMI, The Netherlands) — special thanks to Erik van Meijgaard; *Insitut für Meterologie* (MPI, Germany) — special thanks to Daniela Jacob and Alberto Elizalde; *Sveriges Meteorologiska och Hydrologiska Institut* (SMHI, Sweden) — special thanks to Erik Kjellström and Barry Broman.

References

Ardhuin, F., Chapron, B., Collard, F., 2009. Observation of swell dissipation across oceans. Geophysical Research Letters 37, 1–5.

Bengtsson, L., Hodges, K.I., Esch, M., Keenlyside, N., Kornblueh, L., Luo, J.J., Yamagata, T., 2007. How may tropical cyclones change in a warmer climate? Tellus A 59, 539–561.

Bengtsson, L., Hodges, K.I., Keenlyside, N., 2009. Will Extratropical Storms Intensify in a Warmer Climate? Journal of Climate 22, 2276–2301.

Bengtsson, L., Hodges, K.I., Roeckner, E., 2006. Storm Tracks and Climate Change. Journal of Climate 19, 3518–3543.

Bolaños, R., Jordà, G., Cateura, J., Lopez, J., Puigdefabregas, J., Gomez, J., Espino, M., 2009. The XIOM: 20 years of a regional coastal observatory in the Spanish Catalan coast. Journal of Marine Systems 77, 237–260.

Bolle, H., 2003. Mediterranean Climate: Variability and Trends. Springer.

Callaghan, D.P., Nielsen, P., Short, A., Ranasinghe, R., 2008. Statistical simulation of wave climate and extreme beach erosion. Coastal Engineering 55, 375–390.

Campins, J., Genovés, A., Picornell, M.A., Jansà, A., 2011. Climatology of Mediterranean cyclones using the ERA-40 dataset. International Journal of Climate 31, 1596–1614.

Camus, P., Cofiño, A.S., Mendez, F.J., Medina, R., 2011. Multivariate Wave Climate Using Self-Organizing Maps. Journal of Atmospheric and Oceanic Technology 28, 1554–1568.

Casas-Prat, M., Sierra, J.P., 2010a. Trend analysis of the wave storminess: the wave direction. Advances in Geosciences 26, 89–92.

Casas-Prat, M., Sierra, J.P., 2010b. Trend analysis of wave storminess: wave direction and its impact on harbour agitation. Natural Hazards and Earth System Sciences 10, 2327–2340.

Casas-Prat, M., Sierra, J.P., 2012. Trend analysis of wave direction and associated impacts on the Catalan coast. Climatic Change 115, 667–691.

Casas-Prat, M., Sierra, J.P., 2013. Projected future wave climate in the NW Mediterranean Sea. Journal of Geophysical Research: Oceans 118. doi:10.1002/jgrc.20233.

Charles, E., Idier, D., Delecluse, P., Déqué, M., Cozannet, G., 2012. Climate change impact on waves in the Bay of Biscay, France. Ocean Dynamics 62, 831–848.

Christensen, O.B., Drews, M., Christensen, J.H., Dethloff, K., Ketelsen, K., Hebestadt, I., Rinke, A., 2007. Technical report 06-17 The HIRHAM Regional Climate Model Version 5 (β). Technical Report.

Collins, M., Tett, S.F.B., Cooper, C., 2001. The internal climate variability of HadCM3, a version of the Hadley Centre coupled model without flux adjustments. Climate Dynamics 17, 61–81.

Denis, M.S., Pierson, W.J., 1953. On the motions of ships in confused seas. Society of Naval Architects and Marine Engineers 61, 280–357.

Déqué, M., Rowell, D.P., Lüthi, D., Giorgi, F., Christensen, J.H., Rockel, B., Jacob, D., Kjellström, E., De Castro, M., Van Den Hurk, B., 2007. An intercomparison of regional climate simulations for Europe: assessing uncertainties in model projections. Climatic Change 81, 53–70.

Donat, M., Leckebusch, G., Pinto, J., Ulbrich, U., 2010. European storminess and associated circulation

ACCEPTED MANUSCRIPT

weather types: future changes deduced from a multi-model ensemble of GCM simulations. Climate Research 42, 27–43.
Fisher, N.I., Lee, A.J., 1983. A correlation coefficient for circular data. Biometrica 70, 327–332.
Grabemann, I., Weisse, R., 2008. Climate change impact on extreme wave conditions in the North Sea: an ensemble study. Ocean Dynamics 58, 199–212.
Guedes Soares, C., Weisse, R., Carretero, J.C., Alvarez, E., 2002. A 40 years hindcast of wind, sea level and waves in European waters, in: Proceedings of OMAE 2002: 21st International Conference on Offshore Mechanics and Arctic Engineering, Oslo, Norway. pp. 669–675.
Gunaydin, K., 2008. The estimation of monthly mean significant wave heights by using artificial neural network and regression methods. Ocean Engineering 35, 1406–1415.
Hemer, M.A., 2009. Identifying Coasts Susceptible to Wave Climate Change. Journal of Coastal Research 56, 228–232.
Hemer, M.A., Fan, Y., Mori, N., Semedo, A., Wang, X.L., 2013a. Projected change in wave climate from a multi-model ensemble. Nature Climate Change 3, 471–476.
Hemer, M.A., Katzfey, J., Trenham, C., 2013b. Global dynamical projections of surface ocean wave climate for a future greenhouse gas emission scenario. Ocean Modelling 70.
Hemer, M.A., McInnes, K.L., Ranasinghe, R., 2012. Climate and variability bias adjustment of climate model-derived winds for a southeast Australian dynamical wave model. Ocean Dynamics 62, 87–104.
Hemer, M.A., Wang, X.L., Weisse, R., COWCLIP, T., 2011. WCRP-JCOMM Workshop on Coordinated Global Wave Climate Projections. Technical Report 1581. Switzerland.
Holthuijsen, L.H., 2007. Waves in oceanic and coastal waters. Cambridge University Press.
IPCC, 2000. IPCC Special report. Emissions scenarios. Technical Report.
IPCC, 2007. IPCC Synthesis Report. Technical Report.
Jacob, D., accessed 2012. The regional model - remo. URL: http://www.remo-rcm.de/The-Regional-Model-REMO.1267.0.html.
Janssen, P.A.E.M., Doyle, J.D., Bidlot, J., Hansen, B., Isaksen, L., Viterbo, P., 2002. Impact and feedback of ocean waves on the atmosphere. Advanced Fluid Mechanics I, 155–197.
Kalnay, E., Kanamitsu, M., Cistler, R., Collins, W., Deaven, D., Gandin, L., Iredell, M., Saha, S., White, G., Woollen, J., Zhu, Z., Chelliah, M., Ebisuzaki, W., Higgins, W., Janowiak, J., Mo, K., Ropelewski, C., Wang, J., Leetma, A., Reynolds, R., Jenne, R., Joseph, D., 1996. The NCEP/NCAR Reanalysis Project. Bulletin of the American Meteorological Society 77, 437–471.
Lin, A., Wang, X.L., 2011. An algorithm for blending multiple satellite precipitation estimates with in situ precipitation measurements in Canada. Journal of Geophysical Research 116, 1–19.
Lionello, P., Cogo, S., Galati, M.B., Sanna, A., 2008. The Mediterranean surface wave climate inferred from future scenario simulations. Global and Planetary Change 63, 152–162.
Lionello, P., Malanotte-Rizzoli, P., Boscolo, R., 2006. Mediterranean climate variability. Elsevier.
Lionello, P., Sanna, A., 2005. Mediterranean wave climate variability and its links with NAO and Indian Monsoon. Climate Dynamics 25, 611–623.
Martinez-Asensio, A., Marcos, M., Jorda, G., Gomis, D., 2013. Calibration of a new wind-wave hindcast in the Western Mediterranean. Journal of Marine Systems 121–122, 1–10.
McInnes, K.L., Erwin, T.A., Bathols, M., 2011. Global climate model projected changes in 10 m wind speed and direction due to anthropogenic climate change. Atmspheric science letters 12, 325–333.
Minguez, R., Espejo, A., Tomas, A., Mendez, F.J., Losada, I.J., 2011. Directional calibration of wave reanalysis databases using instrumental data. Journal of Atmospheric and Oceanic Technology 28, 1466–1485.
Mori, N., Shimura, T., Yasudaa, T., Masea, H., 2013. Multi-model climate projections of ocean surface variables under different climate scenarios—Future changes of waves, sea level and wind. Ocean Engineering 71, 122–129.
Mori, N., Yasuda, T., Mase, H., Tom, T., Oku, Y., 2010. Projection of Extreme Wave Climate Change under Global Warming. Hydrolofical Research Letters 4, 15–19.
Munk, W.H., Miller, G.R., Snodgrass, F.E., Barber, N.F., 1963. Directional recording of swell from distant

ACCEPTED MANUSCRIPT

storms. Philosophical transactions of the Royal Society London A 255, 505–584.
Musić, S., Nicković, S., 2008. 44-year wave hindcast for the Eastern Mediterranean. Coastal Engineering 55, 872–880.
Nissen, K.M., Leckebusch, G.C., Pinto, J.G., Renggli, D., Ulbrich, S., Ulbrich, U., 2010. Cyclones causing wind storms in the Mediterranean: characteristics, trends and links to large-scale patterns. Natural Hazards and Earth System Science 10, 1379–1391.
Ortego, M.I., Tolosana-Delgado, R., Gibergans-Báguena, J., Egozcue, J.J., Sánchez-Arcilla, A., 2012. Assessing wavestorm hazard evolution in the NW Mediterranean with hindcast and buoy data. Climatic Change 113, 713–731.
Ratsimandresy, A.W., Sotillo, M.G., Alvarez-Fanjul, E., Carretero-Albiach, J., Perez-Gomez, B., Hajji, H., 2008a. A 44-year (19582001) sea level residual hindcast over the Mediterranean Basin. Physics and Chemistry of the Earth 33, 250–259.
Ratsimandresy, A.W., Sotillo, M.G., Carretero Albiach, J.C., Álvarez Fanjul, E., Hajji, H., 2008b. A 44-year high-resolution ocean and atmospheric hindcast for the Mediterranean Basin develped within the HIPOCAS project. Coastal Engineering 55, 827–842.
Reguero, B.G., Losada, I.J., Mendez, F.J., 2011. Variability of multivariate wave climate in Latin America and the Caribbean. Global and planetary change 100, 70–84.
Roeckner, E., Bäuml, G., Bonaventura, L., Brokopf, R., Esch, M., Giorgetta, M., Hagemann, S., Kirchner, I., Kornblueh, L., Manzini, E., Rhodin, A., Schlese, U., Schulzweida, U., Tompkins, A., 2003. The atmospheric general circulation model ECHAM5. Model description. Technical Report 349. Hamburg.
Sakia, R.M., 1992. The Box-Cox transformation: a review. The Statistician 41, 169–178.
Samuelsson, P., Jones, C.G., Willén, U., Ullerstig, A., Gollvik, S., Hansson, U., Jansson, C., Kjellström, E., Nikulin, G., Wyser, K., 2011. The Rossby Centre Regional Climate model RCA3: model description and performance. Tellus A 63, 4–23.
Sánchez-Arcilla, A., González-Marco, D., Bolaños, R., 2008. A review of wave climate and prediction along the Spanish Mediterranean coast. Natural Hazards and Earth System Science 8, 1217–1228.
Schwierz, C., Köllner-Heck, P., Zenklusen Mutter, E., Bresh, D.N., Pier-Luigi, V., Wild, M., Schär, C., 2010. Modelling European winter wind storm losses in current and future climate. Climatic Change 101, 484–514.
Semedo, A., Beherens, A., Bengtsson, L., Günther, H., Sterl, A., Weisse, R., 2011. Impact of a Warmer Climate on the Global Wave Field, in: 12th International Workshop on Wave Hindcasting and Forecasting and 3rd Coastal Hazards Symposium, Kohala Coast, Hawaii.
Semedo, A., Weisse, R., Behrens, A., Sterl, A., Bengtsson, L., Günther, H., 2013. Projection of global wave climate change towards the end of the 21st century. Journal of Climate doi:10.1175/JCLI-D-12-00658.1.
Slott, J.M., Murray, A.B., Ashton, A.D., Crowley, T.J., 2006. Coastline responses to changing storm patterns. Geophysical Research Letters 33, 1–6.
Small, C., Nicholls, R.J., 2003. A Global Analysis of Human Settlement in Coastal Zones. Journal of Coastal Research 19, 584–599.
Sotillo, M.G., Ratsimandresy, A.W., Carretero, J.C., Bentamy, a., Valero, F., González-Rouco, F., 2005. A high-resolution 44-year atmospheric hindcast for the Mediterranean Basin: contribution to the regional improvement of global reanalysis. Climate Dynamics 25, 219–236.
The WAMDI Group, 1988. The WAM Model - A Third Generation Ocean Wave Prediction Model. American Meteorological Society 18, 1775–1810.
van Meijgaard, E., van Ulft, L., van de Berg, W., Bosveld, F., van den Hurk, B., Lenderink, G., Siebesma, A., 2008. The KNMI regional atmospheric climate model RACMO, version 2.1. Technical Report 302.
von Storch, H., Zwiers, F.W., 2002. Statistical analysis in climate research. Cambridge University Press.
Wang, X.L., Feng, Y., Swail, V.R., 2012. North Atlantic wave height trends as reconstructed from the Twentieth Century Reanalysis. Geophysical Research Letters 39, 1–6.
Wang, X.L., Swail, V.R., 2006. Climate change signal and uncertainty in projections of ocean wave heights. Climate Dynamics 26, 109–126.
Wang, X.L., Swail, V.R., Cox, A., 2010. Dynamical versus statistical downscaling methods for ocean wave

ACCEPTED MANUSCRIPT

heights. International Journal of Climatology 30, 317–332.
Weisse, R., von Storch, H., 2010. Marine Climate and Climate Change. Storms, wind waves and storm surges. Springer ed., Praxis Publishing, Chichester, UK.
Zacharioudaki, A., Reeve, D.E., 2011. Shoreline evolution under climate change wave scenarios. Climatic Change 108, 73–105.

ACCEPTED MANUSCRIPT

Paper E

Analysis of potential impacts on coastal areas due to changes in wave conditions

J.P. Sierra and M. Casas-Prat

Submitted to *Climatic Change*.

Manuscript
Click here to download Manuscript: Impacts_v26.doc
Click here to view linked References

Analysis of potential impacts on coastal areas due to changes in wave conditions

J.P. Sierra[1,2] and M. Casas-Prat[1,2]

J.P. Sierra, Laboratori d'Enginyeria Marítima, Universitat Politècnica de Catalunya BarcelonaTech, Barcelona, Catalonia, Spain (joan.pau.sierra@upc.edu).

M. Casas-Prat, Laboratori d'Enginyeria Marítima, Universitat Politècnica de Catalunya BarcelonaTech, Barcelona, Catalonia, Spain (merce.casas@upc.edu).

[1]Laboratori d'Enginyeria Marítima, Universitat Politècnica de Catalunya BarcelonaTech, Jordi Girona 1-3, Mòdul D1, Campus Nord, 08003 Barcelona, Catalonia, Spain.

[2]Centre Internacional d'Investigació dels Recursos Costaners (CIIRC), Jordi Girona 1-3, Mòdul D1, Campus Nord, 08003 Barcelona, Catalonia, Spain.

Corresponding author: joan.pau.sierra@upc.edu
Phone: +34 934016467
Fax: +34 934011861

ABSTRACT

This study examined the main physical processes related to coastal and port engineering that could be altered by future changes in wave parameters as a consequence of climate change. To estimate the order of magnitude of the potential changes in these processes, several assumptions and simplifications were made and, in most cases, they were assessed by using simple, empirical state-of-the-art expressions. The studied processes were grouped in three categories according to whether they affect beaches, harbors or coastal structures in general. The changes in these processes were estimated as a function of the deepwater variations of the main wave parameters: wave height (H_0), wave period (T) and wave direction (θ_0). A moderate range of variation was assumed for these parameters at deep water (±10% or ±20% in H_0 and its square root in T, and ±10º in θ_0), taking into account recent studies of future wave projections. The results indicated that potential changes in wave height would strongly affect overtopping discharge, stability and scouring of rubble-mound structures and, to a lesser extent, siltation, wave transmission and longshore sediment transport. Changes in wave direction would affect longshore sediment transport in particular and, at a lower magnitude, processes related to port operability (agitation and siltation). Siltation is the only process affected significantly by changes in T alone.

Keywords: Wave impact, coastal dynamics, harbors, coastal structures, beaches, climate change

1. Introduction

Climate change has become a major focus of attention of the scientific community because of its potential hazards and impacts on our environment in the near future. In coastal areas, one of the best-known consequences of the greenhouse effect and the resulting global warming is sea-level rise (SLR), mainly due to melting of ice sheets and thermal volume expansion (e.g. Pritchard and Vaughan 2007). Despite the great uncertainty regarding future SLR, numerous studies have estimated its impacts on coastal areas (e.g. Stive 2004; Nicholls et al. 2007; Nicholls and Cazenave, 2010).

Although coastal vulnerability assessments focus mainly on SLR, other nonclimatic drivers (e.g. socioeconomic change) that can significantly interact with climate change are often ignored, despite being essential for climate and coastal management policy development (Nicholls et al. 2008). In addition, SLR is not the only physical process of concern to coastal communities. As pointed out by various authors (e.g. Bengtsson et al. 2006; Weisse and von Storch 2010), the greenhouse effect and the complex interactions of atmospheric processes may produce changes in near-surface wind and pressure patterns, which, in turn, can affect the pattern of another important coastal driver: the wave field.

Numerous studies have reported that changes in ocean wave climate are detectable (e.g. Aumann et al. 2008; Wang et al. 2009). Evidences suggest that the number, intensity and location of storms will change (e.g. Wang et al. 2004; Bengtsson et al. 2006; Lionello et al. 2008). Most of these studies have focused on changes in wave height, whereas little attention has been paid to changes in wave direction or wave period. These two parameters must not be neglected. Even in a situation of constant wave

storminess magnitude, rotation of the mean wave direction may have severe consequences because most beach and harbor defense structures were designed assuming a permanent directional distribution of waves. This situation can become critical because a large percentage of coasts are already eroding (e.g. Sánchez-Arcilla et al. 2011). Moreover, a higher frequency of coastal storms in the same direction as the harbor mouth could influence port operations by causing increased agitation (Casas-Prat and Sierra, 2012) and siltation. In addition, changes in wave period would affect propagation processes such as shoaling, refraction and diffraction, and therefore they could modify sediment transport patterns or wave penetration into harbors.

In recent years, a number of studies have analyzed the potential impacts on specific coastal areas of wave changes due to climate change, focusing in particular on coastal erosion (e.g. Zacharioudaki and Reeve 2011; Casas-Prat and Sierra 2012) and harbor operability (Casas-Prat and Sierra 2010, 2012).

This paper provides an overview of the main impacts that changes in sea wave patterns produced by climate change can have on coastal areas and infrastructures. These impacts are analyzed simply and generically, and the expected effects on different processes are roughly quantified (obtaining orders of magnitude) as a guideline for coastal impact assessment. Effects on other maritime areas of interest such as navigation and offshore structures are not analyzed. Moreover, the effect of SLR is not taken into account, although the combination of SLR with changes in sea wave patterns can enhance some negative impacts on coastal areas.

In Section 2, we identify the main physical coastal processes that can be affected by changes in the wave field and describe the followed methodology to quantify such affectation. In Section 3, we present the results thus obtained for each process. Finally, in Section 4, along with a discussion and inter-comparison of the results we present the conclusions of this study.

2. Methodology

Changes in wave parameters can be studied by focusing mainly on the mean climate or the extreme climate. Both are important because they affect different processes and, as a consequence, they produce diverse impacts. Table 1 presents the processes identified and analyzed in this study, being their relationship with mean and extreme wave climates qualitatively indicated as high, low or none. The study focuses on the impacts produced by these processes as a result of variations in the following wave parameters: significant wave height (H), peak wave period (T) and mean wave direction (θ). The effect of climate change on each system affected is assessed in terms of the relative variation of each process studied (using the measured parameter given in Table 1), which is compared with the change of the respective driving wave parameters at deep water (denoted with the subscript "0" for H and θ; based on the linear wave theory we assume that T remains the same as waves propagate). The study therefore assesses physical impacts without examining socioeconomic or ecological effects.

The studied processes are grouped in two categories—beaches and harbors—according to the coastal environment affected. A third kind of system—coastal structures—is studied separately because the processes analyzed there affect both coasts and harbors

and therefore cannot be assigned to just one of the other groups. Overtopping and scouring, for example, are problems that can affect either harbor breakwaters or coastal seawalls.

For the sake of simplicity, effects due to wave changes are analyzed assuming that only one wave parameter is altered at a given time. However, since both H_0 and T depend on wind speed (whose magnitude is predicted to vary in the future climate), both parameters are expected to change together often, particularly in areas where swell does not prevail. For this reason, in this study we consider that both parameters vary simultaneously as a result of wind influence. Nevertheless, Hemer et al. (2013) found that T can increase while H remains the same in areas where the swell component is important. Therefore, we examine the impacts due to variations in *i*) H_0 and T together, *ii*) T alone and *iii*) θ_0 alone (see Table SM1). Indeed, the three parameters could all change together, such that their effects would superimpose nonlinearly, but this is not assessed in the present study.

The range of variation of H_0 is based on the work of Hemer et al. (2013), who projected maximum variations (at the global scale) in the mean H_0 of 10% by the end of the century. This rate, however, is expected to be higher in regard to the extreme wave climate due to the nonlinear relation between wave height and wind speed. Casas-Prat and Sierra (2013), for instance, obtained changes in the 50-year return period of H_0 of up to 20% on the Catalan coast by 2100, but a lower maximum expected change in the median H_0 (around 10%). Taking into account these results, the maximum variation of wave height due to climate change considered in this study is ±20% for extreme waves and ±10% for mean wave climate. Given that, we assume that T varies at a rate equal to the square root of the (relative) wave height change (see Eqs. 1 and 2) because, for fully developed seas, H_0 is proportional to the square of wind speed while T is proportional to wind speed (Resio et al. 2002).

$$H_{0F} = \kappa H_{0P} \tag{1}$$

$$T_F = \sqrt{\kappa} T_P \tag{2}$$

where κ is the ratio between future and present wave height. In this study, $0.8 \leq \kappa \leq 1.2$ (extreme waves) or $0.9 \leq \kappa \leq 1.1$ (mean wave climate), and the subscripts F and P indicate future and present conditions, respectively. The variation of T alone (just Eq. 2) is only considered for those processes mainly affected by the mean wave climate (and therefore $0.9 \leq \kappa \leq 1.1$) because swell events are not the dominant feature during storm conditions.

Meanwhile, the variations due to θ are assessed as:

$$\theta_{0F} = \theta_{0P} + \Delta\theta_0 \tag{3}$$

where θ is measured as the angle between the wave front and the shoreline or structure orientation and $\Delta\theta$ is the variation between present and future conditions. A distinction is also made between processes controlled by the mean wave climate and those driven by extreme wave conditions. In the former case, maximum values of $\Delta\theta_0$ are limited to

±10º as obtained by Hemer et al. (2013). In the latter case, the worst condition for the beach or structure, i.e. perpendicular incidence of the waves, is considered for both present and future situations (therefore, $\theta_{0P} = 0º$ and $\Delta\theta_0 = 0º$). Table SM1 summarizes the cases considered in this study to evaluate the effect of changes in the wave conditions.

The rate of change of the analyzed processes is computed analytically where possible, as a function of the rate of change κ. For several processes, however, this simple approach cannot be followed and it is necessary to compute the rate of change as a function of present/future wave parameters (see Supplementary Information).

2.1. Potential impacts on beach dynamics

It is well accepted that changes in ocean wave climate (location, frequency, direction and severity of ocean storms) will bring about changes in the locations and magnitudes of coastal erosion and accretion in the future (Stive at al. 2002). Additionally, with future changes in wave climate and water levels, coastal flood risk will increase, affecting the sustainability of coasts worldwide (Nicholls et al. 2007). In this paper, we examine the potential impacts of wave changes on sandy coasts, focusing on variations in both longshore sediment transport (LST) and cross-shore sediment transport (CST), as well as the flooding caused by the wave-induced run-up.

As waves approach the coast, they break and generate a long-shore current which moves beach material in parallel to the coast causing the LST. This process, driven by the mean wave climate, controls the long term beach dynamics and the patterns of erosion and accretion. We analyze the impact of wave changes on this process in terms of the volume variation of sediment (per unit length and unit time, ΔV_l), which is governed by alongshore gradients in LST rates (see Supplementary Information).

On the contrary, CST and beach flooding are mainly forced by the extreme wave climate, being relevant at event or seasonal time scales. CST governs the short term beach dynamics and encompasses both offshore and onshore transport. The impact on CST is assessed by means of the wave contribution to the storm erosion potential (*ER*), as defined by Jiménez et al. (2012). In turn, waves contribute to beach inundation due to the wave run-up, the uprush of water from wave action which is the combination of the wave set-up and the wave swash caused by waves breaking in the nearshore. The impact is assessed in terms of the distance flooded *d*.

2.2. Potential impacts on ports

Besides coasts, ports are the infrastructure most likely to be affected by changes in wave climate. Changes in wave conditions can affect the wave height pattern within harbors, as shown by Casas-Prat and Sierra (2010, 2012) for some ports on the Catalan coast. In this paper, we analyze the impact on two processes that are very important for port operability: agitation and siltation. Episodic extreme waves may affect these processes but the analysis is centered in the (persistent) mean wave climate, that controls the common (long-term) operational problems.

The agitation within a harbor depends not only on the wave parameters but also on port features and the surrounding environment: geometry, bathymetry, reflectivity of structures, etc. In other words, agitation is case-specific and each harbor has its own pattern. Because of the numerous factors involved, agitation cannot be simplified or estimated using a single formula. As a consequence, more complex tools such as numerical models, which require a large amount of case-specific information (e.g. harbor layout), must be used to study agitation. It is therefore impossible to obtain results that can be generalized and applied to all harbors. Nevertheless, in order to roughly estimate how changes in wave parameters can affect port agitation, we analyze wave propagation under changing wave parameters in a port with a simplified geometry (see Supplementary Information). Such agitation is assessed by the mean wave height due to agitation inside the port (H_a)

In addition, many ports throughout the world suffer from considerable siltation, which entails expensive maintenance dredging. Winterwerp (2005) described the siltation rate as a function of a number of processes: horizontal entrainment, tidal filling, fresh/salt-driven density currents, warm/cold density currents and sediment-induced density currents. The siltation produced by any of these processes is basically affected by the sediment availability outside the harbor and the water movements that can mobilize such sediment towards the inside. In this study, we focus on the second aspect only considering the wave influence and therefore neglecting other effects.. We assess the siltation in terms of the (wave) sediment carrying capacity, S_W, i.e. the amount of suspended sediment that can be transported by waves. We consider therefore the sediment that could potentially enter the harbor given certain wave conditions, assuming unlimited supply of sediment. Such wave conditions are derived from the wave height fields near the harbor entrance obtained with the simulations previously carried out to evaluate the agitation problem. Once the wave conditions that can potentially move the sediment are determined, S_W is calculated (see Supplementary Information).

2.3. Potential impacts on coastal structures

We also examine the potential impacts of changes in wave parameters on a series of processes related to coastal structures: stability, overtopping, scouring, wave reflection and wave transmission. These processes can affect structures located either on coasts or in harbors and are principally controlled by the extreme wave climate, except for the last two, for which the mean wave climate is also relevant. In order to compute the impact associated to each process for present and future conditions, additional parameters are involved in the computation, basically those related with the structure layout (the followed methodology is detailed in Supplementary Information).

The first process studied is structure stability. We consider the stability of common rubble-mound breakwaters, whose design is based on the computation of the weight (W) of the armor units in the primary cover layer. In this case, instead of studying the direct impact on structure stability, we assess the necessary changes in the dimensioning of the structure, i.e. in terms of W. We use an empirical formula (see Supplementary Information) formula, in which W depends on the design wave height at the structure toe (H_s), obtained from extreme wave climate analysis.

Another analyzed process is structure overtopping. Overtopping occurs when the wave run-up obtained under extreme wave conditions exceeds the structure freeboard. The amount of allowable overtopping depends on the function of the particular structure. Certain functions—such as berth for vessels, roadways, storage areas or buildings located just behind the breakwater—put restrictions on the allowable overtopping discharge (Burchart and Hughes 2003). This discharge depends mainly on the water level and the nearshore wave height, although only the latter is considered in this study. A number of methods are available to predict the overtopping of particular structures. For the purposes of this paper—illustrating potential impacts rather than making precise computations—we consider that empirical methods are suitable to obtain the overtopped discharge (q) (see Supplementary Information).

Scouring, the removal of granular bed material by hydrodynamic forces in the vicinity of coastal structures, is another process analyzed here. This phenomenon can lead either to partial damage or, in some cases, to the complete failure of all or portions of a structure (Burchart and Hughes 2003) and is particularly sensitive to extreme waves. To compute the scouring at the toe of a rubble-mound breakwater we use an empirical expression (see Supplementary Information) that serves to estimate the scour depth (S).

In addition, when a wave encounters an obstacle such as a coastal structure, part of the wave energy is diverted and propagated in another direction causing wave reflection. This reflected wave can transport energy to unwanted areas, such as the interior of a harbor (increasing the agitation within it) or a beach (producing more erosion). Therefore, changes in reflected wave heights can cause adverse effects in coastal areas that must be foreseen. This process is sensitive to both mean and extreme wave climates. Empirical equations have been developed from laboratory research and are employed here to assess the impact of changes in wave parameters on wave reflection, which are measured with the reflected wave height (H_r).

Finally, when waves interact with a structure, a portion of their energy may pass over and through the structure, generating waves behind it. This process is known as wave transmission. Like in wave reflection, both the mean and extreme wave climates are important in the study of this process, which is performed using the transmitted wave height (H_t). Wave transmission is particularly important in low-crested structures, especially rubble-mound ones, which have greater porosity. These structures are commonly employed in coastal defense projects, so predicting of the amount of energy transmitted behind them is crucial to their design (van der Meer et al. 2005). To compute wave transmission we use also en empirical expression (see Supplementary Information)

3. Results

3.1. Changes in wave height and period

In this Section, we analyze the changes in the processes mentioned in Section 2 produced by variations of H_0 and T by a factor of κ and $\kappa^{1/2}$ respectively (cases i and ii of Table SM1). Figure 1 and 2 show the results concerning the mean and extreme wave climate, respectively, when H and T vary together. In the case of coastal structures, they are divided into coastal and port environments, which typically have different dimensions and configurations (see Supplementary Material). Variable P in the y-axis

denotes generically "parameter estimated", being different for each process (see Table 1).

Figure 1a compares the results obtained for LST, agitation and siltation. Siltation and agitation exhibit, respectively, the largest and lowest range of variation, falling LST in between.

Siltation is very sensitive to changes in H and T. The ratio of future and present S_W is considerably larger than κ, ranging from -37% to +35%. On the other hand, the other relevant process related to port operability (agitation) show in average a rate of increase/decrease similar to κ. A 10% increase(decrease) in H_0 (and the corresponding decrease in T) yields, on average, a 12%(13%) increase(decrease) in H_a. For both siltation and agitation, these changes are averages over the 240 simulations performed. In some particular cases, the decrease and the increase reach greater values.

Eroded beach volume caused by LST varies by a factor of $\kappa^{5/2}$ (see Supplementary Information). For the analyzed range of change ($0.9 < \kappa < 1.1$), this means that the ratio of future and present ΔV_l varies between -22% and +27% (Figure 1a).

In Figure 1b, the changes in the reflection and transmission wave heights due to changes in H_0 and T for mean wave climate are shown separately for coastal and harbor structures. The variations in H_r are practically the same as those in the incident wave height because the reflection coefficient K_r (the rate between incident and reflected H) does not significantly vary as a function of H and T. Differences between the two types of structure are barely noticeable. In contrast, for H_t, the rate of variation depends on the environment considered. H_t undergoes smaller changes (-10% to 12%, similar to those of H_r) for port structures (-15% to +20% for coastal ones) due to the greater freeboards and the assumption that such structures are impermeable and allow a low transmission of wave energy.

When T changes alone (case ii of Table SM1) the analysis of the processes controlled by the mean wave climate indicates that only siltation is significantly affected (-15% to +17%). The other processes experience variations at a rate lower than 3% ($\leq \kappa^{1/2}$).

Figure 2a sets against results corresponding to beach processes driven by extreme wave climate (CST and flooding) and structure overtopping, stability and scouring. CST and beach flooding have the lower rate of variation, especially CST that varies by a factor of $\kappa^{1/4}$ (see Supplementary Information): 20% increase in H_0 causes a 5% increase in ER. Therefore, although the change of extreme H_0 is supposed to be higher than the mean H_0, changes in CST are expected to be lower than changes in LST, in terms of the parameters studied.

The flooded distance varies linearly with respect to relative variations of H_0. Therefore, the potential impacts on coastal flooding due to higher and longer waves are of the same order as the ratio of increase in wave height (κ), although their main effect will probably be to enhance the consequences of storm surges and SLR.

Concerning stability, we see that the ratio between the necessary weight of a rubble-mound structure under future and present conditions is slightly greater for coastal structures than for port breakwaters (Figure 2a). On average, a 20% increase in H_0

would require stones up to 87% (coastal structures) or 72% (port breakwaters) heavier. If the same units were kept in the armor layer of the breakwater, they might be moved from their original position or even removed from their location, thereby generating instability and eventually the destruction of the breakwater due to the increase of H. On the contrary, waves with a 20% smaller H_0 would need blocks up to 52% (coasts) or 48% (ports) lighter, so the stability of the structure would be increased in this case.

Figure 2a also presents the average ratio between future and present overtopping, the process that mostly varies with changes in the extreme H (and T). Increases of 10% and 20% (in H_0) can induce, respectively, overtopping discharges 67% and 159% greater than the present values in the case of costal structures and 96% and 249% greater in the case of port breakwaters. Although coastal structures have lower freeboards, the ratio of overtopping is greater for port structures probably because coastal structures are located in shallower waters and the largest waves—those which produce the largest overtopping discharges—break before reaching such structures. The large sensitivity of overtopping to H_0 increases will be particularly critical in structures that already have overtopping problems. Moreover, in the context of climate change, we must take into account that these potential changes will most likely be accompanied by SLR, which in turn will reduce the crest freeboard of coastal structures, further increasing overtopping discharges.

Scouring is the last process plotted in Figure 2a. As expected, it will be lower(greater) for future lower(greater) H and T. It has been found that this variation is greater (in relative value) as the ratio between water depth and wave period (or wave length) increases (see Figure SM4). This can be explained by the fact that, for relatively large depths—typically associated with ports rather than with coastal structures—the absolute value of scouring is low (see Supplementary Material) and, therefore, even small absolute variations can give rise to large rates of variation. Consequently, changes in scouring between future and present conditions are greater for port breakwaters (+75% and -52%) than for coastal structures (+47% and -38%).

Finally, Figure 2b shows the same processes as Figure 1b but affected by extreme wave climate. Apart from a larger range of variation ($0.8< \kappa<1.2$), there are differences in the wave climate for the present situation, that obviously consider more energetic waves than for the mean wave climate (see Supplementary Material). These variations barely affect the pattern of change of H_r, that varies at the similar rate as the incident wave height. In the case of H_t, however, different results are obtained compared to the mean wave climate. In average, port structures undergo larger changes in H_t. This could be explained by the fact that, because these structures are located at greater depths, they are exposed to higher waves and, as a consequence, greater amounts of wave energy are transmitted to the lee side of the structure. By contrast, coastal structures are located in shallower waters and the largest waves break before reaching the structure. From Figure 2b we can derive that a 20% decrease in H_0 can cause decreases of up to 30% (coasts) or 33% (ports) in H_t while a 20% increase in H_0 can give rise to increases of up to 33% (coasts) or 39% (ports) in H_t.

3.2. Changes in wave direction

In this section the processes that suffer from variations in the wave direction are assessed (case iii of Table SM1). They are those affected by the mean wave climate:

LST, agitation, siltation, wave reflection and wave transmission. As seen later on, the least affected are the last two processes whereas the largest variations are encountered for LST (for nearly perpendicular waves).

In Figure 3 the variations in LST rates are plotted as a function of $\Delta\theta_0$ for different angles for the present conditions (θ_{0P}). We can see that, for a given value of $\Delta\theta_0$ and for waves with less oblique incidence ($\theta_{0P} < 45º$), the smaller the value of θ_{0P}, the greater the changes in LST rates (the smallest variations are obtained for $\theta_{0P} = 45º$). On the contrary, for highly oblique waves ($\theta_{0P} > 45º$), the larger the value of θ_{0P}, the greater the changes, but these changes are less pronounced than in the case of $\theta_{0P} < 45º$. Note that, for a 45º angle, any change in wave direction produces only small relative changes in LST rates because LST rates have their highest values at this angle. On the contrary, for 90º/0º angles (incidence parallel/perpendicular to the shoreline), the present LST rate is zero, so the relative changes (according to Eq. SM8) would be infinite. As explained in Supplementary Information, these variations in LST rates coincide with the changes in beach volume.

Figure 4a shows how changes in agitation are conditioned to θ_{0P}. For a given value of $\Delta\theta_0$, the waves with the most direct incidence towards the mouth of the harbor (positive θ_{0P}) are associated with the largest changes in the agitation coefficients. In general, a 10º decrease in wave angle entails a decrease of up to 22% in the average H_a, while a 10º increase in wave angle entails an increase of up to 20% in H_a. Note that these variations are higher than the ones obtained when varying the wave height and period.

Figure 4b presents for the same cases considered for Figure 4a, how siltation is affected by changes in wave direction. A singular pattern for high negative angles (less incidence towards the mouth) is obtained, since siltation increases in value at a greater rate than for positive angles. This is probably due to the lower absolute values of siltation obtained for large negative angles, because a small increase in absolute magnitude can cause large increases in relative value.

A similar analysis is performed in order to estimate the changes on wave reflection. We found that variations in K_r (and therefore in H_r) are negligible, with values lower than 0.2%. With also relatively similar low rates, the ratio of H_t ranges from 0% to 1.4% for coastal structures, while this value is negligible (< 0.1%) for port structures. The angle of wave attack has no or only marginal influence on K_t for rubble-mound breakwaters (the most common type), as pointed out by van der Meer et al. (2005). Therefore, for rubble-mound structures it can be assumed that H_t does not change if the wave direction at the structure varies. Nevertheless, since we are assuming changes in deepwater wave direction, we must account for changes in the propagated wave height from deep water to the structure due to the different wave direction, which leads to the aforementioned slight changes.

6. Discussion and conclusions

The main objective of this paper was first to identify the physical processes in coastal areas most affected by changes in wave parameters, and second, to analyze the degree of dependence of these processes on the corresponding driving wave parameters. We have therefore reviewed the main physical processes relevant to coastal/port engineering that could be altered by future variations in wave climate as a consequence of climate

change. An order of magnitude of the changes in these processes has been estimated as a function of the variations (at deep water) in the main wave parameters that control wave propagation: wave height (H_0) and period (T) together, due to their close relationship, T alone (changes generated by the swell influence) and wave direction (θ_0). A moderate range of variation is assumed for these parameters (±10% or ±20% in H for mean and extreme wave climate, respectively, its square root in T and ±10º in θ). As mentioned above, H, T and θ could change simultaneously, so their impact would be superimposed in a nonlinear way not estimated in this study.

Due to the complexity of the analyzed processes, a number of simplifications and assumptions has been made in order to perform this study. Therefore, results shown in Table 2 should be taken as an indication and properly calibrated for the zone where the impact assessment is carried out. Nevertheless, the results still give us a general idea of the most affected physical coastal processes given a future wave climate change scenario which can be very useful in the prioritization of further detailed coastal impact studies

From Table 2, we conclude that changes in H_0 and T will strongly affect overtopping discharge, stability and scouring of rubble-mound structures and, to a lesser extent, siltation, wave transmission, LST and port agitation. Beach flooding and wave reflection would change at the same rate as wave height, while CST would change at lower rates than wave height.

The changes in wave period alone affect significantly port siltation (-15% to +17%) in agreement with the general understanding that long period waves increase suspended sediment concentration transported by waves (Zhang et al 2009), while the other processes vary at a lower rate than T itself ($\leq \pm 3\%$).

As for the wave period, the variations produced by changes in wave direction have been studied only in processes dominated by the mean wave climate. Among these processes, the one most affected by potential changes in wave direction is the LST rate, which could undergo huge variations in magnitude. Processes related to port operability (agitation and siltation) are also sensitive to changes in wave direction. By contrast, the effects of changes in wave direction on wave reflection and wave transmission are almost negligible in magnitude.

The main conclusion of this study is that plausible changes in wave conditions due to climate change could greatly affect both harbors and coasts due to the nonlinear relations governing the processes studied. In the case of harbors, increases in wave height could force port authorities to make large investments to reinforce breakwaters against instability or to increase their freeboard to limit overtopping discharge. Moreover, berms or other defense methods could become necessary to reduce structure scouring that could result in damage, or even destruction of, breakwaters. Finally, other possible consequences of changes in wave conditions (in particular, wave direction) could make it necessary to design new structures or even make major changes to port layout (at considerable economic cost) in order to avoid excessive siltation or agitation within the harbor.

Modifications in wave conditions could involve major changes in beach dynamics due to significant variations in LST rates and, consequently, the need to take major coastal

defense measures (e.g. beach fills, new coastal structures). As in the case of ports, coastal defense structures could be affected by instability, overtopping and scouring. This could make it necessary to reinforce these structures or build berms to prevent them from being damaged or collapsing. It might also be necessary to increase the freeboard of seawalls in order to protect maritime promenades or seaside infrastructure (roads, railways, buildings) from overtopping. All of these measures would obviously entail considerable costs.

Since even small changes in wave climate can lead to large impacts on coastal processes, it is necessary to raise awareness among coastal and port authorities and other stakeholders about the potential impacts of climate change on coastal areas. These impacts include not only those caused by SLR but also those driven by wave climate. The identification of potential future vulnerabilities and risks can facilitate the process of designing appropriate adaptation responses.

Finally, we want to stress that our impact assessment has only involved physical parameters. To perform an integrated assessment of these impacts and the risk associated to coastal areas, it would be necessary to take socioeconomic aspects into account (e.g. Arnell et al. 2004; Nicholls et al. 2008) that would also facilitate the inter-comparison between different impacts.

Aknowledgements
This research was carried out in the frame of the European project CIRCE (contract number TST5-CT-2007-036961) and the Spanish project ARCO (contract number 200800050084350). The second author is currently enjoying a PhD grant from the Spanish Ministry of Education.

References

Arnell NW, Livermore MJL, Kovats S, Levy PE, Nicholls R, Parry ML, Gaffin SR (2004) Climate and socio-economic scenarios for global-scale climate change impact assessments: characterizing the SRES storylines. Global Environmental Change 14:3-20

Aumann H, Ruzmaikin A, Teixeira J (2008) Frequency of severe storms and global warming. Geophys Res Lett 35:L19805

Bengtsson L, Hodges KI, Roeckner E (2006) Storm tracks and climate change. J Climate 19:3518-3543

Burchart HF, Hughes SA (2003). Coastal Engineering Manual. Part VI, Chapter V: Fundaments of design. USACE, p. 316

Casas-Prat M, Sierra JP (2010) Trend analysis of wave storminess: wave direction and its impact on harbour agitation. Nat Hazard Earth Syst Sci 10:2327-2340.

Casas-Prat M, Sierra JP (2012) Trend analysis of wave direction and associated impacts on the Catalan Coast. Clim Change 115:667-691

Casas-Prat M, Sierra JP (2013) Projected future wave climate in the NW Mediterranean Sea. J Geophys Res Oceans 118, doi:10.1002/jgrc.20233

Hemer MA, Fan Y, Mori N, Semedo A, Wang XL (2013) Projected change in wave climate from a multi-model ensemble. Nat Clim Change, doi;10.1038/NCLIMATE1791

Jiménez JA, Sancho-García A, Bosom E, Valdemoro HI, Guillén J (2012) Storm-induced damages along the Catalan coast (NW Mediterranean) during the period 1958-2008. Geomorphology 143-144:24-33

Lionello P, Cogo S, Galati MB, Sanna A (2008) The Mediterranean surface wave climate inferred from future scenario simulations. Glob Planet Change 63:152–162

Nicholls RJ, Cazenave A (2010) Sea-level rise and its impact on coastal zones. Science 328:1517-1520

Nicholls RJ, Wong PP, Burkett V, Woodroffe CD, Hay J (2008) Climate change and coastal vulnerability assessment: scenarios for integrated assessment. Sustainability Science 3:89-102

Nicholls RJ, Wong PP, Burkett VR, Codignotto JO, Hay JE, McLean RF, Ragoonaden S, Woodroffe CD (2007) Coastal systems and low-lying areas. Climate change 2007: impacts, adaptation and vulnerability. In: Parry ML, Canziani OF, Palutikof JP, van der Linden PJ, Hanson CE (eds), Contribution of Working Group II to the Fourth Assessment Report of the Intergovernmental Panel on Climate Change. Cambridge University Press, Cambridge, pp. 315–356

Pritchard HD, Vaughan DG (2007) Widespread acceleration of tidewater glaciers on the Antarctic Peninsula. J Geophys Res 112:F03S29

Resio DT, Bratos SM, Thompson EF (2002) Meteorology and wave climate, in Coastal Engineering Manual, Part II, Chapter 2, 72 p.

Sánchez-Arcilla A, Mósso C, Sierra JP, Mestres M, Harzallah A, Senouci M, El Raey M (2011) Climate drivers of potencial hazards in Mediterranean coasts. Reg Environ Change 11:617–636

Stive MJF (2004) How important is global warming for coastal erosion? Clim Change 64:27–39

Stive MJF, Aarninkhof SGJ, Hamm L, Hanson H, Larson M,Wijnberg KM, Nicholls RJ, Capobianco M (2002) Variability of shore and shoreline evolution. Coast Eng 47:211–235

Van der Meer JW, Briganti R, Zanuttigh B, Wang B (2005) Wave transmission and reflection at low-crested structures: design formulae, oblique wave attack and spectral change. Coast Eng 52:915-929

Wang X, Swail V, Zwiers F, Zhang X, Feng Y (2009) Detection of external influence on trends of atmospheric storminess and northern oceans wave heights. Clim Dyn 32(2):189–203

Wang X, Zwiers F, Swail V (2004) North Atlantic ocean wave climate change scenarios for the twenty-first century. J. Climate 17:2368-2383

Weisse R, von Storch H (2010) Marine climate and climate change. Storms, wind waves and storm surges. Springer, Praxis Publishing, Chichester, UK

Winterwerp JC (2005) Reducing Harbor Siltation. I: Methodology. J Waterw Port Coast Ocean Eng 131:258-266

Zacharioudaki A, Reeve DE (2011) Shoreline evolution under climate change wave scenarios. Clim Change 108:73-105

Tables

System affected	Process	Impact	Measured parameter	Mean wave climate	Extreme wave climate
Beaches	Longshore sediment transport	Erosion/accretion	Volume variation ΔV_l	H	L
	Cross-shore sediment transport	Erosion/accretion	Erosion rate ER	L	H
	Wave set-up	Flooding	Distance flooded d	N	H
Harbors	Wave propagation within the harbor	Agitation	Wave height H_a	H	L
	Sediment transport close to the harbor	Siltation	Sediment carrying capacity S_{*w}	H	L
Coastal structures	Wave action	Instability	Block weight W	N	H
		Overtopping	Discharge q	L	H
		Scouring	Scour depth S	L	H
	Wave reflection	Erosion/accretion, agitation	Reflected wave height H_r	H	H
	Wave transmission	Erosion/accretion, agitation	Transmitted wave height H_t	H	H

Table 1. Analyzed processes, their impacts, measurement parameter, and their relationship (H, high; L, low; N, none) to mean and extreme wave climates

Process / Impact	Domain	H_{s0} (±20%) & T (±10%) [H_{s0} (±10%) & T (±5%)]	T (±5%)	Direction (-10º to +10º)
LST rate	Coasts	[-23% to +27%]	-2.3% to +1.1%	-296.4% to +264.8%
CST rate	Coasts	-5% to +5%	-	-
Flooding	Coasts	-20% to +20%	-	-
Agitation (Hs)	Ports	[-13% to +12%]	-3% to +2%	-22% to +20%
Siltation	Ports	[-37% to +35%]	-15% to +17%	-24% to +21%
Stability (block) weight)	Coasts	-52% to +87%	-	-
	Ports	-48% to +72%	-	-
Overtopping discharge	Coasts	-73% to +159%	-	-
	Ports	-83% to +249%	-	-
Scouring	Coasts	-38% to +47%	-	-
	Ports	-52% to +75%	-	-
Wave reflection	Coasts	-19% to +19% [-10% to +10%]	+1.8% to -1.9%	<0.2%
	Ports	-19% to +19% [-10% to +10%]	+1.4% to -1.5%	<0.2%
Wave transmission	Coasts	-30% to +33% [-15% to +20%]	-1.7% to +2%	0% to +1.4%
	Ports	-33% to +39% [-10% to +12%]	-0.2% to +0.2%	0% to +1.4%

Table 2. Range of variation in different processes due to changes in wave height and period and wave direction. In brackets values corresponding to mean wave climate

Figures

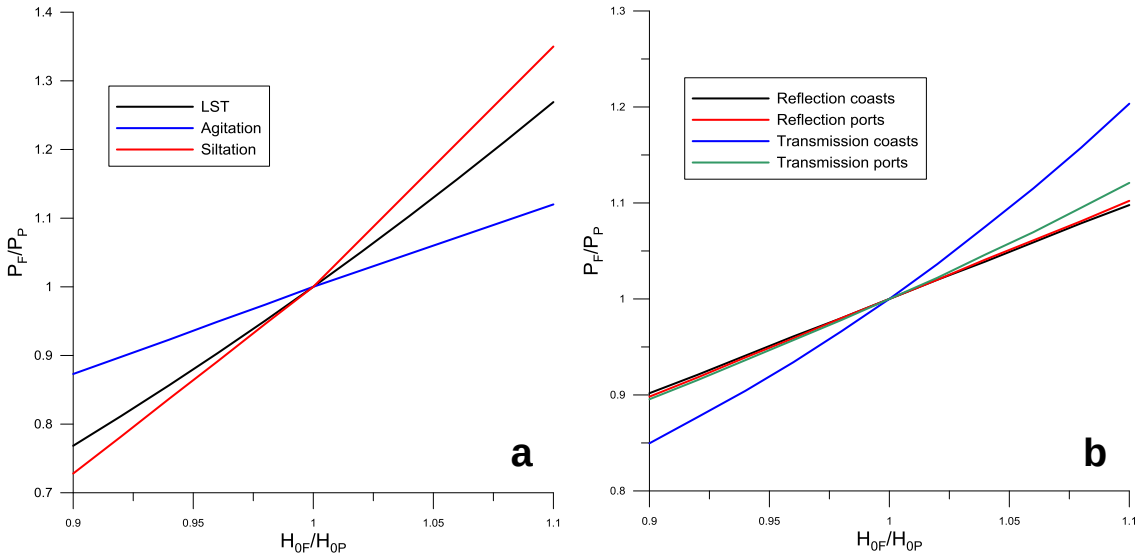

Figure 1. Changes in processes driven by mean wave climate due to variations in wave height and period. a: LST, agitation and siltation. b: Reflection and transmission (the vertical axis measures the ratio of future and present values of the assessed parameters, see Table 1)

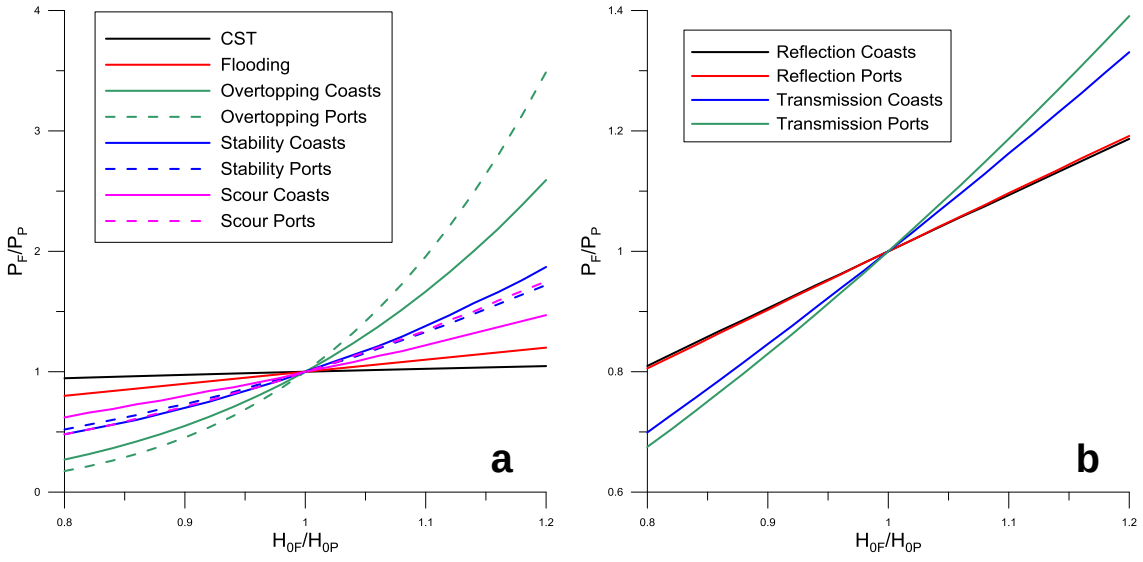

Figure 2. Changes in processes driven by extreme wave climate due to variations in wave height and period. a: CST, flooding, overtopping, stability and scouring. b: Reflection and transmission (the vertical axis measures the ratio of future and present values of the assessed parameters, see Table 1)

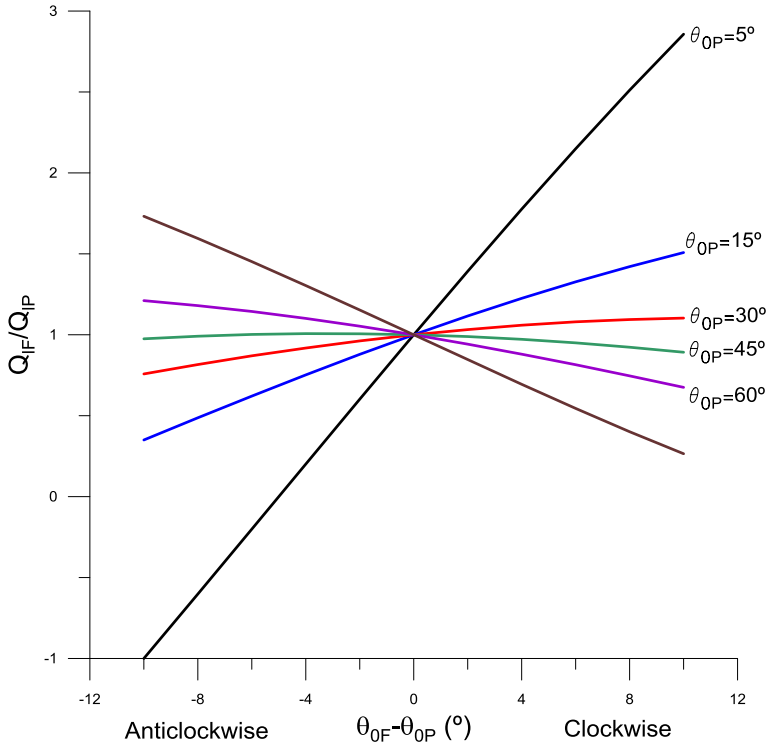

Figure 3. Changes in longshore sediment transport rates as a function of changes in wave direction

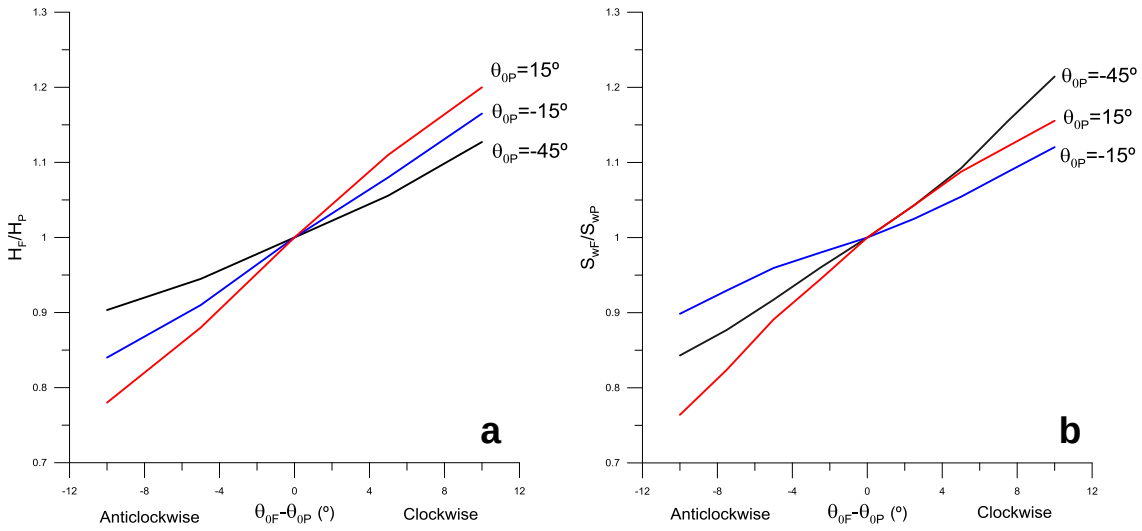

Figure 4. a: Changes in wave height within the harbor due to variations in wave angle. b: Changes in the siltation rate due to variations in wave angle. In both cases changes are estimated for different present angles

The supplementary material details the methodology, hypothesis and assumptions used in our study. Four supplementary figures are included, and three supplementary tables.

1. Methodology

Table SM1 summarizes the cases considered in this study to evaluate the effect of changes in the wave conditions. The rate of change of the analyzed processes is computed analytically where possible, as a function of the rate of change of H_0 (κ). However, this simple approach cannot always be followed (especially in the case of wave direction changes), being necessary to involve specifically the present/future (deep water) wave parameters (H_{0P}, T_P, θ_{0P}, H_{0F}, T_F, θ_{0F}) and not just their corresponding rate of change. With the aim of being representative, we consider a range of values that covers most of the wave climates that occur in the world (near coastal zones). On the basis of the projected present (global) wave climate of Mori et al. (2010), to evaluate the impact caused by changes in H_0 and/or T, five values of H_{0P} are selected for the mean climate (from 1 to 5 m at intervals of 1 m) and ten for the extreme climate (3 to 12 m at intervals of 1 m). To assign a value to T_P, we follow the recommendations of the Spanish Port Authority, which state that $T = kH^{0.5}$, where k is a value that usually ranges from 4 to 8. We consider five values of k (k = 4, 5, 6, 7 and 8) and, therefore, for each H_{0P}, five corresponding values of T_P are adopted. Concerning the impact of the wave direction, 35 different values of θ_{0P} are selected (from -85º to +85º at intervals of 5º), except for agitation and siltation processes, where the asymmetry derived from the orientation of the harbor mouth is taken into account, as explained in Section 1.2. All of these parameters are defined in deep water (denoted with the subscript "0" for those changing during the wave propagation: H and θ), so in cases where the assessment of the analyzed impact requires values for intermediate or shallow waters (defined with the subscript "s" since they are normally a function of the impacted structure layout), waves are propagated until the point where the coastal process is computed. This is done using linear wave theory and considering bottom contours that are straight and parallel to the shoreline. During this propagation, we assume that waves break when $H = 0.6h$ (Thornton and Guza 1983), where h is the water depth.

As explained below, in the case of port agitation and siltation, the propagation of waves within a harbor is very complex and very difficult to assess in a simple way due to the number of physical processes involved in wave propagation: shoaling, refraction, diffraction and reflection. In order to account for such processes, the impact on port agitation and siltation is performed by using a Boussinesq-type numerical model. The settings of the model and selected simulations are described in Section 1.2.1.

1.1. Beach dynamics

1.1.1. Impact of longshore sediment transport (LST)

One of the expressions most widely used to estimate LST is the CERC formula (SPM, 1984):

$$Q_l = \frac{KP_l}{(\rho_s - \rho) g (1-n)} \tag{SM1}$$

where Q_l is the LST rate, P_l is the longshore energy flux, ρ_s is the sediment density, ρ is the water density, g is the acceleration due to gravity and n is the sediment porosity (≈ 0.4). According to SPM (1984):

$$P_l \approx 0.05\rho g^{3/2} H_0^{5/2} (\cos\theta_0)^{1/4} \sin 2\theta_0 \tag{SM2}$$

By substituting (SM2) in (SM1), we obtain:

$$Q_l = \frac{0.05K\rho g^{1/2} H_0^{5/2} (\cos\theta_0)^{1/4} \sin 2\theta_0}{(\rho_s - \rho)(1-n)} \tag{SM3}$$

If, in the future, deepwater wave height and period change together and the wave direction remains the same, from Eq. (SM3) we obtain:

$$\frac{Q_{lF}}{Q_{lP}} = \frac{H_{0F}^{5/2}}{H_{0P}^{5/2}} \tag{SM4}$$

Assuming that the future wave height varies from the present height by a factor of κ, from Eq. (1) it follows:

$$\frac{Q_{lF}}{Q_{lP}} = \kappa^{\frac{5}{2}} \tag{SM5}$$

The long-term beach dynamics is governed by gradients in LST rates. Using a simple approach and neglecting nonlinear effects, the increase in volume (per unit length and unit time) between two points 1 and 2 separated by a distance Δx is:

$$\Delta V = \frac{Q_{l2} - Q_{l1}}{\Delta x} \tag{SM6}$$

Assuming that the wave height and period change in the same proportion along the entire stretch of coast analyzed—an acceptable assumption at local scales such as single beaches—we have:

$$\frac{\Delta V_F}{\Delta V_P} = \frac{Q_{lF2} - Q_{lF1}}{Q_{lP2} - Q_{lP1}} = \frac{\kappa^{5/2} Q_{lP2} - \kappa^{5/2} Q_{lP1}}{Q_{lP2} - Q_{lP1}} = \kappa^{5/2} \tag{SM7}$$

To estimate variations in LST due to changes in T alone, we use an expression equivalent to SM2, extracted from SPM (1984):

$$P_l \approx \frac{1}{32} c\rho g H_0^2 \sin 2\theta_0 \tag{SM8}$$

where c is the wave celerity. From here:

$$\frac{Q_{lF}}{Q_{lP}} = \frac{c_F}{c_P} = \frac{L_F}{T_F}\frac{T_P}{L_P} \tag{SM9}$$

where L is the wave length. Operating:

$$\frac{Q_{lF}}{Q_{lP}} = \frac{L_{0F}\tanh\left(\frac{2\pi h}{L_F}\right)}{T_F}\frac{T_P}{L_{0P}\tanh\left(\frac{2\pi h}{L_P}\right)} = \frac{\frac{gT_F^2}{2\pi}\tanh\left(\frac{2\pi h}{L_F}\right)}{T_F}\frac{T_P}{\frac{gT_P^2}{2\pi}\tanh\left(\frac{2\pi h}{L_P}\right)} \tag{SM10}$$

where L_0 is the deepwater wave length. Since the variations in T are small (±5%) we can assume that:

$$\frac{\tanh\left(\frac{2\pi h}{L_F}\right)}{\tanh\left(\frac{2\pi h}{L_P}\right)} \approx 1 \tag{SM11}$$

and SM10 becomes:

$$\frac{Q_{lF}}{Q_{lP}} \approx \frac{T_F^2}{T_F}\frac{T_P}{T_P^2} = \frac{T_F}{T_P} = \kappa^{\frac{1}{2}} \tag{SM12}$$

Finally, we analyze the modification of the LST rate due to changes in the wave direction. Starting from Eq. (SM3), and given that $H_{0F} = H_{0P}$, we have:

$$\frac{Q_{lF}}{Q_{lP}} = \frac{(\cos\theta_{0F})^{1/4}\sin 2\theta_{0F}}{(\cos\theta_{0P})^{1/4}\sin 2\theta_{0P}} \tag{SM13}$$

Table SM2 summarizes these changes for the six cases analyzed.

As shown in Eq. (SM7) for the case of changes in H and T, for changes in T or θ the ratio of variation of Q_l coincides with the ratio of variation of ΔV.

1.1.2. Impact of cross-shore sediment transport (CST)

The impact on CST is assessed by means of the wave contribution to the storm erosion potential, *ER*, which is given by the following expression (Jiménez et al. 2012):

$$ER = \left(\frac{H_0}{T}\right)^{0.5}\tau \tag{SM14}$$

where τ is storm duration. Although storm duration is a parameter that may be different in the future, we are not evaluating its variation in this paper. Therefore, from Eqs. (1) and (2) we obtain:

$$\frac{ER_F}{ER_P} \approx \left(\frac{H_{0F}}{T_F}\right)^{0.5}\left(\frac{T_P}{H_{0P}}\right)^{0.5} = \frac{\kappa^{\frac{1}{2}}}{\kappa^{\frac{1}{4}}} = \kappa^{\frac{1}{4}} \tag{SM15}$$

1.1.3. Coastal flooding

Mase (1989) presented a predictive equation for the maximum run-up (R_{max}) of irregular waves on smooth, impermeable beaches based on laboratory data, that we use to perform our analysis:

$$\frac{R_{\max}}{H_0} \approx 2.32\xi_0 \tag{SM16}$$

where H_0 is the deepwater significant wave height and ξ_0 is the surf similarity parameter, given by:

$$\xi_0 \approx \tan\beta\left(\frac{H_0}{L_0}\right)^{-\frac{1}{2}} \tag{SM17}$$

where tanβ is the beach slope.

The impact on the coastal area due to run-up is determined by the surface flooded. The distance flooded (d) with respect to the shoreline is:

$$d = \frac{R_{\max}}{\tan\beta} \tag{SM18}$$

By substituting Eqs. (SM16) and (SM17) in Eq. (SM18) and assuming linear theory, we obtain:

$$d = 2.32H_0\left(\frac{H_0}{L_0}\right)^{-\frac{1}{2}} = 2.9\frac{H_0^{\frac{1}{2}}}{T^{-1}} = 2.9TH_0^{\frac{1}{2}} \tag{SM19}$$

By introducing the rate of change κ from Eqs. (1) and (2) in Eq. (SM19), we can derive the relationship between present (d_P) and future (d_F) flooded distances due to wave run-up:

$$\frac{d_F}{d_P} = \frac{H_{0F}^{\frac{1}{2}}T_F}{H_{0P}^{\frac{1}{2}}T_P} = \kappa^{\frac{1}{2}}\kappa^{\frac{1}{2}} = \kappa \tag{SM20}$$

Thus, flooded distance varies linearly with respect to relative variations of H.

1.2. Ports

1.2.1. Port agitation

In order to roughly estimate how changes in wave parameters can affect port agitation, we analyze wave propagation under changing wave parameters in a rectangular port (similar in shape to many western Mediterranean marinas) with simple bathymetry (straight, parallel bottom contours). The analysis involves a number of simulations with a Boussinesq-type numerical model, employed in previous studies (González-Marco et al. 2008; Casas-Prat and Sierra 2010, 2012), from which we can compute the spatial average of the significant wave height within the port (H_a) for present and future conditions and consequently the ratio between H_a and H_0, i.e., the agitation coefficient (K_a). Figure SM1 shows the geometry of the port and the convention adopted for wave directions.

Since the assumed potential changes take place in deep water, it is necessary to propagate waves from deep water to the limit of the simulation domain (located very close to the main breakwater). To take into account the variability that this can introduce in the results, three different depths are considered for the outer limit of the simulation domain: 10 m, 15 m and 20 m. Moreover, we assume that the whole harbor is dredged at the same depth as the outer breakwater.

Apart from κ it is necessary to explicitly involve the (deep water) wave conditions for the present/future to carry out the propagation until the boundary domain and afterwards the simulation with the numerical model to obtain H_a. Since agitation is mainly affected by the mean wave climate, as stated in Section SM1, five different wave heights are used (H_{0P} = 1, 2, 3, 4 and 5 m). T is obtained as $T = kH^{0.5}$ where k is a value that usually ranges from 4 to 8. However, to generate a reasonable number of numerical simulations, in this case we just use the central value of $k = 6$. Moreover, each wave height and period combination is run for four different directions (the same for present and future conditions): -60º, -30º, 0º and 30º (see Figure SM1 for sign criteria). All these combinations represent a total of 240 simulations that are performed with the numerical model. To evaluate the impact of the changes in H and/or T, H_a and K_a are computed by averaging, for each wave height and period variation, the respective quantities obtained for the four directions and the three depths considered. Figure SM2 shows an example of the spatial pattern of agitation coefficients obtained with two wave climate configurations.

A similar procedure is followed to analyze changes in agitation caused only by changes in wave direction. For the three depths analyzed, nineteen directions (from -55º to 25º, at intervals of 5º) are considered, each simulated with the combination of five wave heights (from 1 to 5 m at intervals of 1 m) and periods (those corresponding to $k = 6$).
A total of 255 simulations are therefore run to evaluate the effects of wave direction. For each $\Delta\theta_0$ considered (-10º, -5º, 0º, 5º and 10º), a final average for values corresponding to all θ, H and h considered with the corresponding $\Delta\theta_0$ is performed to obtain the final associated values of H_a and K_a. Note that in this case, future and present

deepwater wave heights are the same and therefore changes in future agitation coefficients directly translate into variations in H inside the port, i.e. $H_{aF}/H_{aP} = K_{aF}/K_{aP}$. Figure SM3 shows how the spatial pattern of K_a changes with wave direction.

The fact that the selected range of wave directions is not centered around 0º and does not comprise very large values can be explained by harbor design criteria. Harbor mouths are usually oriented in such a way as to provide shelter against the most frequent waves. As a result, we can expect that large positive values of wave incidence would be very infrequent.

1.2.2. Siltation

The siltation is assessed in terms of the sediment carrying capacity that, given infinite sediment availability, can be interpreted as the amount of suspended sediment that can potentially enter and silt the port. Dou et al. (1995) suggested a sediment carrying capacity (S_*) formula for combined waves and currents:

$$S_* = S_{*c} + S_{*w} \tag{SM21}$$

where S_{*c} and S_{*w} are the sediment carrying capacities due to currents and waves, respectively. In this study we only consider the effect of waves, so the term S_{*c} is neglected. We calculate S_{*w} as a function of the wave conditions at the surrounding of the harbor mouth since they are the ultimately responsible of the sediment transport towards the harbor. These wave conditions cannot be properly estimated by simple analytical methods owing to the complex local processes involved such as diffraction. For this reason we make use of the simulations previously carried out with the Boussinesq-type numerical model for the study of the agitation inside the harbor. Once these wave conditions are determined we use the expression proposed by Zhang et al. (2009) for waves outside the surf zone (like those typically encountered in the entrance of the harbor):

$$S_{*_w} = \beta_1 \frac{\gamma\gamma_s}{(\gamma_s - \gamma)} \frac{f_w H_{rms}^3}{T^3 g^2 h \omega \sinh^3(kh)} \tag{SM22}$$

where β_1 is a dimensionless coefficient, γ the specific density of sea water, γ_s the specific density of sediment particles, g the acceleration of gravity, h the water depth, ω the settling velocity, f_w the friction factor, k the wave number and H_{rms} the root-mean-square wave height ($H_{rms} = H^{1/2}$). The ratio between future and present sediment carrying capacities is therefore:

$$\frac{S_{*wF}}{S_{*wP}} = \frac{H_{sF}^{3/2}}{T_F^3 \sinh^3(k_F h)} \frac{T_P^3 \sinh^3(k_P h)}{H_{sP}^{3/2}} \tag{SM23}$$

In this study, H_s is the average of the significant wave heights in the surroundings of the harbor mouth (shaded area in Figure SM1).

1.3. Coastal structures

In order to compute the measured parameter for each analyzed process for present and future conditions, values must be assigned to additional parameters involved in the computation. As seen below, empirical formulas for those processes affecting coastal structures are typically obtained as a function of the wave climate at the depth of the structure toe. Therefore, this water depth (h) must be specified. In the case of structures located in coastal areas, six values are taken (from 2 to 12 m at intervals of 2 m). In the case of harbor rubble-mound breakwaters, nine depths are used (from 8 to 40 m at intervals of 4 m, because vertical breakwaters are recommended over rubble-mound breakwaters at greater depths [PPEE, 2009]).

Moreover, parameters related to structure dimensions—such as crest width (B), structure freeboard (R_c) and structure slope (α)— are also used. For B and R_c, different values are selected depending on the type of structure. Coastal defense structures usually have widths of 2 to 15 m (Lamberti et al. 2005), so seven crest widths (from 2 to 14 m at intervals of 2 m) are considered for these structures. In the case of harbor breakwaters, looking at a number of breakwater sections, we conclude that the most common range of crest widths is from 6 to 30 m, so nine crest widths are selected to perform the computations (from 6 to 30 m at intervals of 3 m). When the structure freeboard (R_c) is needed, three values are considered for coastal structures (0.6, 0.8 and 1 times H) and three for harbor structures (1, 1.2 and 1.4 times H) to allow wave transmission and overtopping while also taking into account that PPEE (2009) establishes a value of 1.5 for rubble-mound structures without overtopping. Finally, we use four values of α (0.33, 0.4, 0.5 and 0.66), which cover the range recommended by PPEE (2009).

1.3.1. Structure stability

To study the effects of wave parameter changes on structure stability we use Hudson's (1961) formula, which computes the necessary weight of the armor layer blocks (W) in a rubble mound structure:

$$W = \frac{g\rho_s H_s^3}{K_D (S_r - 1)^3 \cot\alpha} \tag{SM24}$$

where ρ_s is the density of the stones, K_D is a stability coefficient that depends on the shape and roughness of the armor units and their degree of interlocking, S_r is the ratio between the densities of the stones and the water, α is the structure slope angle measured from the horizontal, and the subscript s indicates that the wave parameters are computed at the structure location.

If the wave conditions change, the necessary weight of the blocks in the future will be:

$$\frac{W_F}{W_P} = \left(\frac{H_{sF}}{H_{sP}} \right)^3 \tag{SM25}$$

Since we assume that the modification in wave conditions is produced in deep water, we have to translate these variations to the point where the structure is located. According to the linear theory, with bottom contours that are straight and parallel to the structure, and normal wave direction, we have:

$$H_s = \sqrt{\frac{c_{g0}}{c_{gs}}} H_0 \tag{SM26}$$

where c_g is group celerity.

In the event of changes in H and T, by substituting Eq. (SM26) in Eq. (SM25) and taking into account Eqs. (1) and (2), we find that the ratio between the necessary weight of a rubble-mound coastal structure under future and the present conditions is:

$$\frac{W_F}{W_P} = \kappa^{\frac{15}{4}} \left(\frac{c_{gsP}}{c_{gsF}} \right)^{\frac{3}{2}} \tag{SM27}$$

1.3.2. Structure overtopping

For a rubble-mound structure, the following equation (Pullen et al. 2007) is employed:

$$\frac{q}{\sqrt{gH_s^3}} = 0.2 \exp\left(-2.3 \frac{R_c}{H_s \gamma_f \gamma_\beta} \right) \tag{SM28}$$

where q is the overtopping discharge (in $m^3/s/m$), H_s the significant wave height at the structure, R_c is the crest freeboard, γ_f is a roughness factor (1 for smooth structures and decreasing values as structure roughness increases) and γ_β is an obliquity factor (1 for perpendicular wave attack and lower values as obliquity increases). Assuming the worst condition—perpendicular wave attack ($\gamma_\beta = 1$)—and an impermeable rubble-mound structure with two layers ($\gamma_f = 0.55$), Eq. (SM28) is transformed into:

$$\frac{q}{\sqrt{gH_s^3}} = 0.2 \exp\left(-4.18 \frac{R_c}{H_s} \right) \tag{SM29}$$

From the ratio between future and present conditions, we obtain:

$$\frac{q_F}{q_P} = \sqrt{\frac{H_{sF}^3}{H_{sP}^3}} \exp\left[-4.18 R_c \left(\frac{1}{H_{sF}} - \frac{1}{H_{sP}} \right) \right] \tag{SM30}$$

where H_{sF} and H_{sP} are computed using Eq. (SM26).

1.3.3. Structure scouring

According to Summer and Fredsøe (2000), scouring at the toe of a rubble-mound breakwater can be computed by:

$$\frac{S}{H_s} = \frac{f(\alpha)}{\left[\sinh\left(\frac{2\pi h_s}{L_s}\right)\right]^{1.35}} \tag{SM31}$$

$$f(\alpha) = 0.3 - 1.77\exp\left(-\frac{\tan\alpha}{15}\right) \tag{SM32}$$

where S is scouring, h_s is the depth at the structure toe, L_s is the wave length, and tan α is the structure slope. Then, the ratio between future and present scouring will be:

$$\frac{S_F}{S_P} = \frac{H_{sF}}{\left[\sinh\left(\frac{2\pi h_s}{L_{sF}}\right)\right]^{1.35}} \frac{\left[\sinh\left(\frac{2\pi h_s}{L_{sP}}\right)\right]^{1.35}}{H_{sP}} \tag{SM33}$$

Considering Eq. (1) and (SM26), we derive:

$$\frac{S_F}{S_P} = \kappa^{\frac{5}{4}} \frac{c_{gsP}^{\frac{1}{2}}}{c_{gsF}^{\frac{1}{2}}} \frac{\left[\sinh\left(\frac{2\pi h_s}{L_{sP}}\right)\right]^{1.35}}{\left[\sinh\left(\frac{2\pi h_s}{L_{sF}}\right)\right]^{1.35}} \tag{SM34}$$

This expression is computed for a number of cases (ratios of variation of wave heights) as a function of the present relative depth (h_s/L_{sP}). Figure SM4 summarizes the results and shows that scouring will be lower(greater) for future lower(greater) wave heights and periods. The greatest decreases and increases in scouring is found in the limit of deep water ($h_s/L_{sP} = 0.5$).

1.3.4. Impacts on wave reflection

The degree of wave reflection is defined by the reflection coefficient (K_r), which is the ratio between the reflected wave height (H_r) and the incident wave height (H_i).

Laboratory research (Seelig and Ahrens 1981; Seelig 1983; Allsop and Hettiarachchi 1988) has indicated that the reflection coefficient for most forms of structures is given by:

$$K_r = \frac{a\xi^2}{b + \xi^2} \tag{SM35}$$

where a and b are coefficients whose values mainly depend on structure geometry and ξ is the surf parameter or Iribarren number (Battjes 1974), which can be computed as:

$$\xi = \frac{\tan\alpha}{\left(\frac{2\pi H_s}{gT^2}\right)^{0.5}} \tag{SM36}$$

where tan α is the seaward slope of the structure. According to Sorensen and Thompson (2002), for rubble-mound structures $a = 0.6$ and $b = 6.6$, while for vertical structures a value of $K_r = 0.9$ may be used.

To assess the variation of the reflection coefficient due to changes in wave parameters, we substitute Eq. (SM36) in (SM35) and, making the ratio between present and future conditions, we obtain the following expression:

$$\frac{K_{rF}}{K_{rP}} = \kappa \frac{41.4H_{sP} + g\tan^2\alpha T_P^2}{41.4H_{sF} + g\tan^2\alpha T_F^2} \tag{SM37}$$

where the wave heights at the structure toe must be computed using Eq. (SM26). Once the ratio between reflection coefficients is estimated, the ratio between future and present reflected wave height (which is the parameter used to assess this process) can be easily computed.

1.3.5. Impacts on wave transmission

The amount of energy transmitted is commonly defined by a wave transmission coefficient K_t, which is the ratio between the transmitted wave height H_t and the incident wave height H_i.

One of the expressions most widely used to compute wave transmission for a low-crested structure was proposed by D'Angremond et al. (1996):

$$K_t = -0.4\frac{R_c}{H_s} + \delta\left(\frac{B}{H_s}\right)^{-0.31}\left(1 - e^{-0.5\xi}\right) \tag{SM38}$$

where R_c is the crest freeboard, B is the crest width of the structure, ξ is the surf parameter (see Eq. SM36) and δ is a constant whose value is 0.64 and 0.80, respectively, for permeable and impermeable structures. In this study, we assume that port structures are impermeable ($\delta = 0.80$) because they need to prevent wave energy from entering the harbor. However, because many coastal defense structures do not have a core and are rather permeable, and to cover a wider range of options, we consider these structures to be permeable ($\delta = 0.64$).

Due to the dependence of K_t on several parameters, a direct ratio between present and future conditions cannot be obtained. To analyze the influence of changes in wave height on wave transmission, the present K_t is computed with Eq. (SM38) and (SM26) for all cases described previously. For each of these parameter combinations, the future

K_t is also obtained and the ratio between future and present conditions is computed. The average of all the ratios is then calculated in order to estimate the variation between future and present conditions. In Table SM3, the variation of the transmission coefficients and transmitted wave heights (H_t is the parameter used to assess the process) due to changes in wave period and height is shown for coastal and port structures and for mean and extreme wave climate.

Supplementary References

Allsop NWH, Hettiarachchi SSL (1988) Reflections from coastal structures, Proceedings of the 21st International Conference on Coastal Engineering, Torremolinos, Spain, pp 782-794

Battjes JA (1974) A computation of set-up, longshore currents, run-rp and overtopping due to wind-generated waves, Ph.D. thesis, Delft University of Technology, The Netherlands

D'Angremond K, van der Meer JW, de Jong RJ (1996) Wave transmission at low crested structures. Proceedings of the 25th International Conference on Coastal Engineering, Orlando, FL, USA, pp 2418-2427.

Dou GR, Dong FW, Dou XB (1995) Sediment transport capacity of tidal currents and waves. Chinese Sci Bull 40:1096-1101

González-Marco D, Sierra JP, Fernández de Ybarra O, Sánchez-Arcilla A (2008) Implications of long waves in harbour management. The Gijon Port case study. Ocean Coast Manage, 51:180-201

Hudson RY (1961) Laboratory investigation of rubble mound breakwaters. Trans Am Soc Civil Eng 126, Pt IV.

Lamberti A, Archetti R, Kramer M, Paphitis D, Mosso C, Di Risio M (2005) European experience of low crested structures for coastal management. Coast Eng 52:841-866

Mase H (1989) Random Wave Runup Height on Gentle Slope. J Waterw Port Coast Ocean Eng 115:649–661

Mori N, Yasuda T, Mase H, Tom T, Oku Y (2010) Projection of extreme wave climate change under global warming. Hydrol Res Lett 4:15-19

PPEE (2009). ROM 1.0-09. Recommendations for the project design and construction of breakwaters (Part 1: Calculation and project factors. Climate agents). Puertos del Estado, Madrid, Spain, 520 p.

Pullen T, Allsop NWH, Bruce T, Kortenhaus A, Schüttrumpf H, van der Meer JW (2007) EurOtop wave overtopping of sea defences and related structures – Assessment Manual, p. 193

Seelig WN (1983) Wave reflection from coastal structures, Proceedings Coastal Structures '83, Arlington, VA, USA, pp 961-973

Seelig WN, Ahrens JP (1981) Estimation of wave reflection and energy dissipation coefficients for beaches, revetments and breakwaters, Technical Paper 81-1, U.S. Army Engineer Waterways Experiment Station, Vicksburg, MS, USA

Sorensen R, Thompson EF (2002). Harbour Hydrodynamics, in Coastal Engineering Manual, Part II, Chapter 7, 91 p.

SPM (1984) Shore Protection Manual. 4th ed., 2 Vol, U. S. Army Engineer Waterways Experiment Station, U. S. Government Printing Office, Washington, DC

Summer BM, Fredsøe J (2000) Experimental study of 2D scour and its protection at a rubble mound breakwater. Coast Eng 40:59-87.

Thornton EB, Guza RT (1983) Transformation of wave height distribution. J Geophys Res 88:5925-5938

Zhang Q-E, Yan B, Wai OWH (2009) Fine sediment carrying capacity of combined wave and current flows. Int J Sed Res 24:425-438

Supplementary Tables

Case	Mean wave climate	Extreme wave climate
i) H and T vary	$0.9H_{0P} < H_{0F} < 1.1H_{0P}$ $0.95T_P < T_F < 1.05T_P$ $\theta_{0F} = \theta_{0P}$	$0.8H_{0P} < H_{0F} < 1.2H_{0P}$ $0.9T_P < T_F < 1.1T_P$ $\theta_{0F} = \theta_{0P}$
ii) T varies	$H_{0F} = H_{0P}$ $0.95T_P < T_F < 1.05T_P$ $\theta_{0F} = \theta_{0P}$	-
iii) θ varies	$H_{0F} = H_{0P}$ $T_F = T_P$ θ_{0P} - 10º < θ_{0F} < θ_{0P} + 10º	-

Table SM1. Cases studied to evaluate the impacts caused by changes in the wave conditions

Angle variation $\Delta\theta$	**Present angle** θ_{0P}					
	5º	**15º**	**30º**	**45º**	**60º**	**75º**
-15º	196.4%(1)	-100%	-40.7%	-8.9%	25.9%	104.2%
-10º	0.0%(1)	-65.0%	-24.2%	-2.5%	21.1%	73.2%
-5º	-100.0%	-31.3%	-10.5%	0.5%	12.3%	37.8%
-2º	-39.8%	-12.1%	-3.8%	0.6%	5.3%	15.3%
2º	39.2%	11.6%	3.2%	-1.1%	-5.8%	-15.3%
5º	96.4%	27.7%	7.0%	-3.8%	-15.2%	-38.1%
10º	185.7%	50.8%	10.3%	-10.8%	-32.5%	-73.5%
15º	264.8%	68.5%	9.8%	-20.6%	-51.0%	-

Table SM2. Variation (%) of beach volume due to LST ($\Delta V_F/\Delta V_P$) as a function of changes in wave direction; (1) indicates that transport is in the opposite direction

	Coasts Mean C.		**Ports Mean C.**		**Coasts Extreme C.**		**Ports Extreme C.**	
H_{0F}/H_{0P}	K_{tF}/K_{tP}	H_{tF}/H_{tP}	K_{tF}/K_{tP}	H_{tF}/H_{tP}	K_{tF}/K_{tP}	H_{tF}/H_{tP}	K_{tF}/K_{tP}	H_{tF}/H_{tP}
0.80					0.87	0.70	0.84	0.68
0.85					0.91	0.77	0.88	0.75
0.90	0.94	0.85	0.995	0.90	0.94	0.85	0.92	0.83
0.95	0.97	0.92	0.997	0.95	0.97	0.92	0.96	0.91
1.00	1.00	1.00	1.00	1.00	1.00	1.00	1.00	1.00
1.05	1.025	1.09	1.008	1.06	1.03	1.08	1.04	1.09
1.10	1.09	1.20	1.02	1.12	1.06	1.16	1.08	1.19
1.15					1.08	1.24	1.12	1.29
1.20					1.11	1.33	1.16	1.39

Table SM3. Variation in transmission coefficients and wave heights due to changes in wave period and wave height

Supplementary Figures

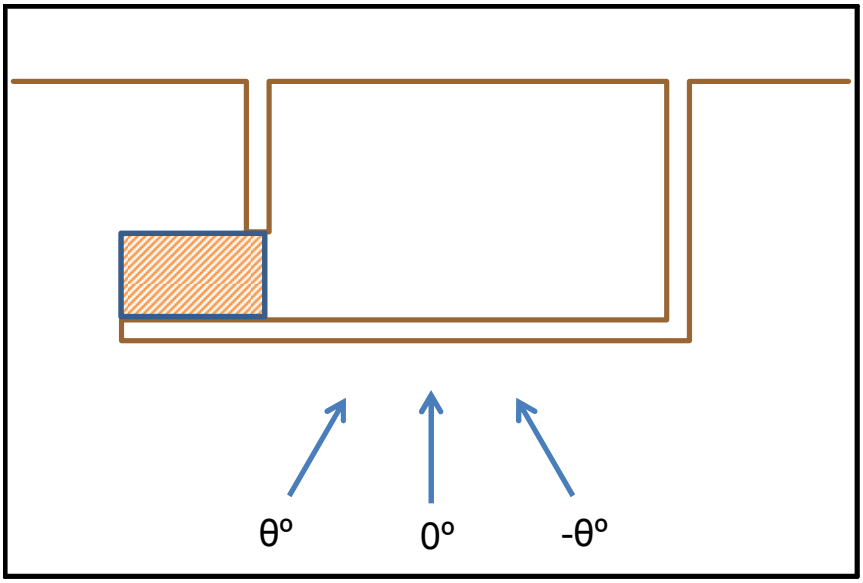

Figure SM1. Sketch of the harbor used to study agitation and siltation. The incident wave directions (θ) are defined in deep water. The shaded area around the mouth of the harbor indicates the zone where the wave parameters have been computed to assess the sediment carrying capacity.

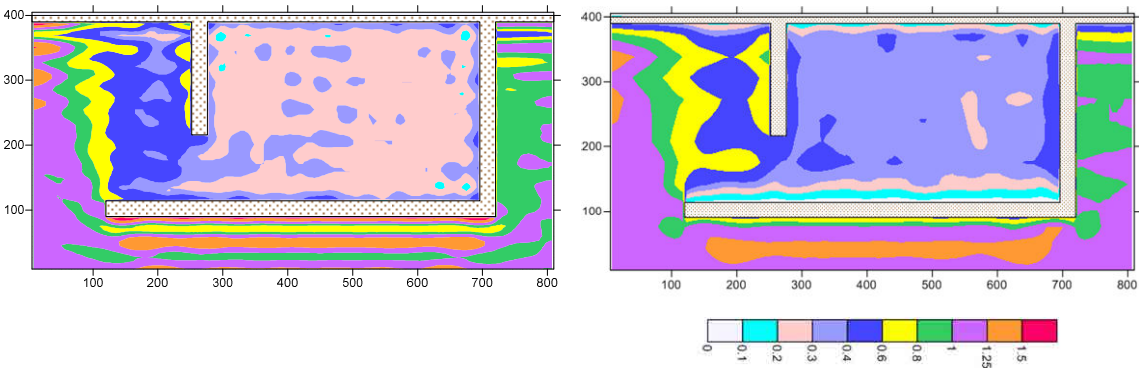

Figure SM2. Example of variation of the agitation coefficient with wave height and period. $H_0 = 2$ m and $T = 8.5$ s (left), $H_0 = 4$ m and $T = 11.4$ s (right). Wave direction is perpendicular to the breakwater

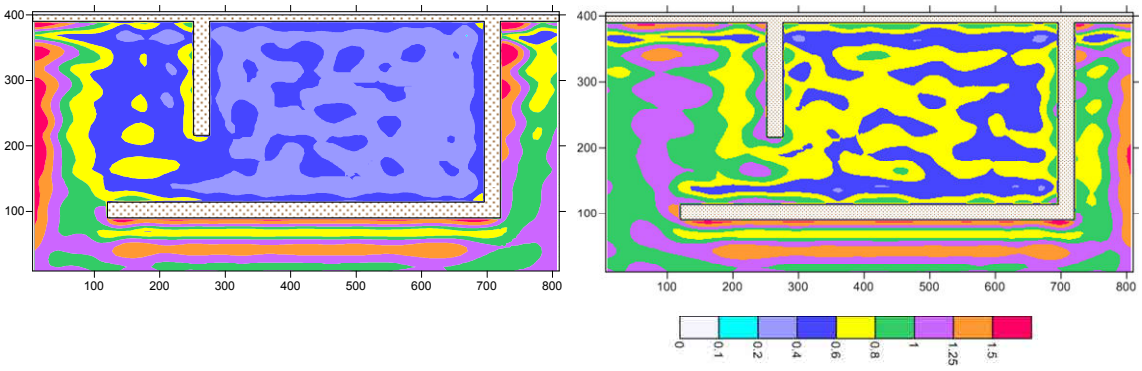

Figure SM3. Example of variation of the agitation coefficient with wave direction. $\theta_{0P} = -30^{\circ}$ (left), $\theta_{0P} = 30^{\circ}$ (right). Both simulations were carried out for $H_0 = 3$ m and $T = 10.4$ s

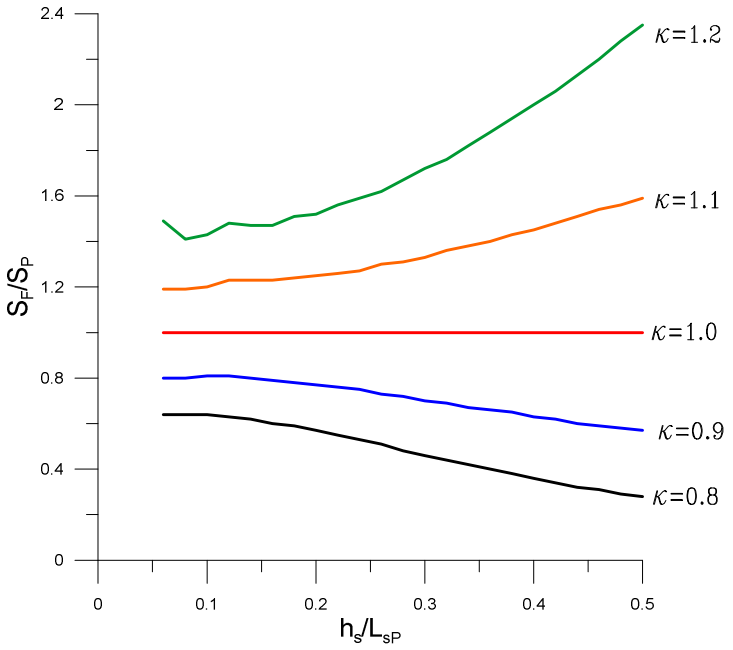

Figure SM4. Changes in scouring due to variations in wave height and period. Changes are estimated for different ratios of change (κ) as a function of present relative depth (h_s/L_{sP})

ATENCIÓ ¡
Les pàgines 106 a 132 de la tesi contenen el “Paper B”, que es pot consultar a la web de l’editors

ATENCIÓN ¡

Las páginas 106 a 132 de la tesis el contienen “Paper B”, que puede consultarse en el web del editor

ATTENTION ¡

Pages 106 to 132 of the thesis are availables at the editor’s web

http://link.springer.com/article/10.1007%2Fs10584-012-0466-9